Investigating blood vessel heterogeneity and maturation with a round-up approach employing iPSC-derived endothelial and vascular accessory cells in custom perfusion microfluidic devices

Chesnais, François

Awarding institution:
King's College London

Investigating blood vessel heterogeneity and maturation with a round-up approach employing iPSC-derived endothelial and vascular accessory cells in custom perfusion microfluidic devices.

Thesis submitted for the degree of Doctor of Philosophy

François Chesnais

Supervisors: Dr. Lorenzo Veschini

Professor Agamemnon Grigoriadis

Professor Trevor Coward

Centre for Oral, Clinical and Translational Sciences

Faculty of Dentistry, Oral & Craniofacial Sciences

King's College London

September 2022

Acknowledgments

I would like to acknowledge and give my warmest thanks to my supervisors who made this work possible. First, my biggest appreciation goes to Dr. Lorenzo Veschini without whom nothing would have been possible. Thank you for all the guidance academically and personally, I am forever grateful. I would like to thank Professor Trevor Coward for the precious help and advice and all the team at the Academic Centre of Reconstructive Sciences. I would like to extend my gratitude to Professor Agamemnon Grigoriadis for his support and kindness. An immense thank you to my PhD panel and Professor Lucy Di-Silvio for their unvaluable guidance.

For their contributions in the work produced in this thesis I would like to thank Hassan Farah at King's College London for his technical assistance and kindness; Professor Catherine Verfaillie and Dr. Manoj Kumar at KU Leuven for their continuous support and for providing precious stem cells; Dr. Davide Danovi, Dr. Rocio Sancho, Dr. Sergio Pedraza-Arevalo, Matteo Battilocchi and Erin Roy from the Centre for Gene Therapy and Regenerative Medicine at King's College London for their help with projects including the access to imaging facility, *in vivo* experiments, pancreatic project and their participation in the elaboration of manuscripts; James Glazier and his group from Indiana University for the project on mathematical modelling and simulations.

I am extremely thankful for all the students I had the opportunity to supervise and work with during these years. I would like to thank Juliette Le Caillec and Amy Taylor for their help in developing the co-culture system. I thank profusely Jordan Joel, Kerushan Thomas and Sima Shakib for their contribution to the Lab-on-chip project. I would also like to thank Eyad Elbahtety and Carlos Araujo Muro for their work on the stem cell-derived models. Special thanks goes to Jonas Hue for his unvaluable help in the different projects and to Elena Engstler, Ruby Stokes and Marco Branco for their participation in the development of image analysis pipelines.

I would also like to thank the friends I made at King's college London for all the fun moments and the support. Special thanks to Raveena Bhondi, Alessandro Maffei, Leanne Cleaver, Sherry Nasab, Aize Pellon, Maria Gonzalez, Matt Blakeley, Polis Charalambous, Lydia Kim, Ben Walters, Giovanni Gonnella, Martina Mifsud, Abby Weston and Anneliese Jarman,

Finally, I am deeply grateful to my friends and family for their moral support throughout these four years. To my mum and dad for their endless support and reassurance and to my brother, sister and close family for your continuous encouragements.

Abstract

Creation of biomimetic *in vitro* systems recapitulating tissue physiology requires developing technologies to recreate the tissue microenvironment including appropriate blood vessels and perfusion. Blood vessels and endothelial cells (ECs) exhibit a variety of specialised functions, reflected in a remarkable phenotypical heterogeneity. Here, we first describe the creation of tools to study this EC heterogeneity at the single cell level and characterise EC behaviour in different populations of arterial, venous and microvascular ECs. We implement high content imaging to decipher heterogeneity in terms of proliferation, junctional status and Notch signalling pathway. The information extracted are key to a better understanding of the molecular mechanisms involved in EC and blood vessel specialisation. To recapitulate this functional heterogeneity and obtain mature populations of vascular cells for future tissue engineering purposes, we then describe the differentiation of stem cell-derived vascular cells. By implementing and refining existing protocols, we report the creation of mature populations of ECs, pericytes and fibroblasts and study their functional ability to create mature blood vessels *in vitro*. Following the characterisation and derivation of vascular cells, we focus on the elaboration of microfluidic devices for the generation of functional blood vessels.

Current Lab-on-chip (LOC) technology allows creating very complex *in vitro* systems allowing passive tissue perfusion and generation of capillary-like structures. However, these systems cannot recreate the physiologic microenvironment including continuous perfusion and physiologic sheer and normal stresses to blood vessel walls, key determinants of vascular homeostasis and ultimately adequate tissue functions. We present a new scalable 3D printing-based workflow to manufacture Lab-on-chip devices at microfluidic scales enabling creation of complex and continuously perfusable LOC devices. Our workflow from design to manufacture is significantly less expensive and more flexible than current technologies. We employ 3D printing to accelerate the prototyping and manufacture of vasculature-on-chip systems and refine an organotypic system to create capillaries with organ-specific endothelial cells and stromal cells. We also design a custom perfusion system to introduce a physiologic continuous perfusion in our device. This allows the validation of our tailored design for the perfusion of self-assembled microvascular networks and the study the maturation of blood vessels over time in a flow-dependent manner. We envision that this technology will empower fast prototyping, manufacture and validation of novel *in vitro* systems of increasing complexity including interconnected multi-tissue systems.

List of publications

- **Chesnais, F.**, Hue, J., Roy, E., Branco, M., Stokes, R., Pellon, A., Le Caillec, J., Elbahtety, E., Battilocchi, M., Danovi, D., Veschini, L., 2022a. High-content image analysis to study phenotypic heterogeneity in endothelial cell monolayers. J. Cell Sci. 135, jcs259104. https://doi.org/10.1242/jcs.259104

- **Chesnais, F.**, Joel, J., Hue, J., Shakib, S., Di-Silvio, L., Grigoriadis, A.E., Coward, T., Veschini, L., 2022b. Continuously perfusable, customisable and matrix-free vasculature on a chip platform (preprint). Bioengineering. https://doi.org/10.1101/2022.08.02.499348

- **Chesnais, F.**, Sego, T.J., Engstler, E., Battilocchi, M., Danovi, D., Glazier, J.A., Veschini, L., 2022c. A spatialised agent-based model of NOTCH signalling pathway in Endothelial Cells predicts emergent heterogeneity due to continual dynamic phenotypic adjustments (preprint). Cell Biology. https://doi.org/10.1101/2022.08.06.503043

List of presentations

- May 2022: "Custom 3D-printed Lab-on-chip devices to study blood vessel formation and maturation using iPSC-derived vascular cells". (**Chesnais F.**, Veschini L.) EMBO Workshop: Building networks: engineering in vascular biology, Barcelona, Spain (Poster presentation)

- Dec 2020: "Custom 3D-printed Lab-on-chip devices to study blood vessel formation and maturation using iPSC-derived vascular cells". (**Chesnais F.**, Coward T. Veschini L.) World Biomaterials congress, Glasgow, Scotland, online (Oral presentation)

Table of Contents

List of figures

List of tables

Abbreviations

µm: micrometre

(v)FR: (volumetric) Flow rate

2D: two dimensions

3D: three dimensions

3DP: Three-dimensional printing

ABS: Acrylonitrile butadiene styrene

AC: Anastomosis channel

ANOVA: Analysis of variance

BBB: Blood brain barrier

bFGF: basic Fibroblast Growth Factor (FGF2)

BM: Basement membrane

BMP4: Bone Morphogenic Protein 4

CAD: Computer assisted design

CD (31): Cluster of differentiation (31)

cDNA: complementary Deoxyribonucleic Acid

CFD: Computational fluid dynamics

CNS: Central nervous system

CNTL: Control

COL1A1: Collagen type 1, alpha 1

CVS: Cardiovascular system

DAPI: 4′,6-diamidino-2-phenylindole

DAPT: Difluorophenyl acetamido-propanamido phenylacetate

DLP: Digital Light processing

DMEM: Dulbecco's modified eagle medium

E9.5: embryonic day (E) 9.5

ECFC-Endothelial cell forming colony

ECM: Extracellular Matrix

ECPT: Endothelial cell profiling tool

EDM: Endothelial Differentiation Medium

EDTA: Ethylenediamidtetraacetic acid

EGF: Epidermal growth factor

EGM2: Endothelial Growth Medium 2

FB: Fibroblast

FBS: Foetal bovine serum

FDM: Fused deposition modelling

GFP: Green fluorescent protein

HAoEC: Human aortic endothelial cell

HCAEC: Human coronary artery endothelial cell

HCMEC: Human cardiac microvascular endothelial cell

HDF: Human dermal fibroblasts

HDMEC: Human dermal microvascular endothelial cell

hESCs: (human) Embryonic Stem Cells

HGF: Hepatocyte growth factor

HPMEC: Human pulmonary microvascular endothelial cell

HSaVEC: Human saphenous vein endothelial cell

HUVEC: Human umbilical vein endothelial cell

iPSCs: induced Pluripotent Stem Cells

KO serum: Knockout serum

LOC (device): Lab-on-a-chip (device)

LWC: Lab-on-chip to world connection

MACS: Magnetic activated cell sorting

mm: millimetre

MMP: Matrix metalloproteinase

MSC: Mesenchymal stem cell

NICD: Notch intracellular domain

NSP: Notch signalling pathway

OVAA: Organotypic Vasculogenic/Angiogenic assay

PC: Pericyte

PCL: polylactocaprone

PDGF: Platelet-derived growth factor

PDMS: Polydimethylsiloxane

RFP: Red fluorescent protein

RNA: Ribonucleic Acid

RT-qPCR: Reverse-Transcription quantitative Polymerase Chain Reaction

SFig.: Supplementary Figure

SLA: Stereolithography

STL: Standard tessellation language

TGFB: Transforming growth factor beta

UV: Ultraviolet

v/a/L/ECs: venous/arterial/lymphatic Endothelial Cells

VEGF: Vascular Endothelial Growth Factor

VoC: Vasculature-on-chip

vSMC: vascular Smooth muscle cell

Glossary

<u>Anastomosis</u>: in the context of blood vessels, anastomosis refers to the merging of two existing vessels, often coming from sprouting.

<u>Angioblasts</u>: Vascular progenitors formed in the embryo that will give rise to endothelial cells

<u>Angiocrine</u>: Angiocrine signalling refers to the secretion of molecules from blood vessels to stimulate organ growth, function or repair.

<u>Angiogenesis</u>: Formation of new blood vessels from existing blood vessels via the selection, migration and maturation of endothelial cells.

<u>Basement membrane</u>: Sheet of extracellular matrix formed between epithelial tissues such as the endothelium and connective tissues.

<u>Biomimetic</u>: Biomimetism refers to the creation of structures or objects to resemble natural designs.

<u>Embryoid body</u>: Three-dimensional aggregates of stem cells, often used to recapitulate developmental processes.

Intussusceptive angiogenesis: Creation of new blood vessels by splitting of an existing blood vessel.

Mesoderm: The mesoderm is one of the three germ layers formed in the embryo and will give rise to the heart and skeletal muscles, connective tissues, the digestive tract, red blood cells and tubules of the kidneys.

Microfluidics: Refers to the study of fluid dynamics in micro-channels and miniaturised systems.

Microphysiological system: Microphysiological systems, or organ-on-chips, consist in a miniaturised and integrated platform aimed at connecting multiple types of tissues often under dynamic culture to recreate human physiology and create complex *in vitro* systems.

Organoids: Self-organised three-dimensional aggregates of cells, often derived from stem cells, with the aim of recreating specific environment and mimic micro-anatomy.

Paracrine: Cell communication process in which cells signal to neighbouring cells to induce a change in behaviour.

Perivascular cells: Cells that compose the layers around blood vessels, mainly pericytes and smooth muscle cells, with a role in blood vessel homeostasis and function.

Stem cell: Cells in the body that are undifferentiated or partially differentiated and can give rise to various types of cells while keeping their proliferative status.

Stromal cell: Type of cell composing the connective tissue.

Vasculogenesis: Formation of de novo blood vessels via aggregation and differentiation of angioblasts to form primitive blood vessel networks.

"en face" immunostaining: Technique used to study the endothelial cell monolayer in blood vessels by splitting the blood vessel and mounting the endothelium flat.

Chapter 1: Introduction

The cardiovascular system is the first functional organ in the embryo, essential for the development of every tissue in the body (Carmeliet, 2003). Blood vessels form a spread-out network, supplying organs with nutrients and oxygen, removing waste and enabling a permanent immune surveillance (Potente et al., 2011). Given that fundamental role, dysregulation in blood vessel formation is linked to a range of disorders including inflammatory diseases, cancer progression, metabolic impairment and hypertension (Carmeliet, 2003). As cardiovascular and ischemic diseases prevalence keep going up in an aging population, the need for tissue engineered vascular grafts has been steadily growing over the years but still faces problems such as thrombosis and occlusion. Furthermore, primary arterial endothelial cells dedifferentiate *in vitro*, making it hard to use them for clinical applications or tissue engineering purposes.

Understanding fundamental mechanisms of vascular development and maturation is paramount to develop novel therapeutic strategies. At the same time, reproducing these mechanisms *in vitro* will enable recreating a vascular system which in turn is a key to create tissues from stem cells *in vitro*.

The main aim of this study is to create models of functionally mature artificial vascular networks as a scalable platform for tissue engineering purposes. To achieve an adequate model of vascular system *in vitro*, key aspects must be investigated.

First, this project will explore the conditions necessary for the function of blood vessels by studying mechanisms involved in blood vessel heterogeneity, in two and three dimensions *in vitro*. These experiments will then help to define experimental conditions required to differentiate stem cells into mature and functional endothelial and mural cells.

Then, we will investigate the optimal conditions to create perfusable vascular networks *in vitro* using custom made Lab-on-chip devices and investigate perfusion-dependent and perfusion independent mechanisms of vascular maturation.

This project will increase our understanding over the molecular and cellular mechanisms of vasculogenesis and vascular maturation and deliver novel Lab-on-chip devices to grow mature perfusable vascular networks in *vitro.*

1- **<u>Blood vessels and the cardiovascular system</u>**

The circulatory system is a closed, hierarchically organised network composed of arteries, arterioles, capillaries, venules and veins. Arteries transport oxygenated blood from the heart and are subject to a high pressure whereas veins bring the blood back to the heart and face lower pressure. Capillaries and small blood vessels are composed exclusively of an endothelial cell (EC) layer whereas bigger vessels are covered with mural cells, pericytes for intermediate vessels and smooth muscle cells (SMC) for bigger vessels. The cardiovascular system is responsible for several vital function such as nutrients and gas exchange, immune surveillance or organ development.

a. **Macro and micro anatomy of blood vessels**

The vascular system is formed by an interconnected network of blood vessels of different origins, morphology, and function. Highly oxygenated blood is carried from the heart into big arteries that divide into smaller arterioles leading to the different capillary beds as seen in Fig. 1.1. The blood depleted in nutrient and oxygen is then collected in venules transported via bigger (collecting) veins to the lungs.

Anatomically, big arteries and veins share a common organisation. The innermost layer is the endothelium, supported by its basement membrane, forming the tunica intima (Milutinović et al., 2019). The tunica media is composed of several layers of vascular smooth muscle cells (vSMCs) and a composition of circular elastic fibres such as collagen and other proteoglycans (Tellides and Pober, 2015). The outer layer of big vessels is the tunica adventitia, formed by connective tissue (fibroblasts, progenitors, immune cells), extracellular matrix (ECM) components and fibres, vasa vasorum as well as lymphatic vessels and nerves (Milutinović et al., 2019; Waller et al., 1992). Although structurally similar, the walls from blood vessels can vary in composition. The presence of mural cells (or perivascular cells), composed of pericytes, smooth muscle cells, stellate cells and astrocytes, depends on the type of blood vessel and the hemodynamic forces it witnesses.
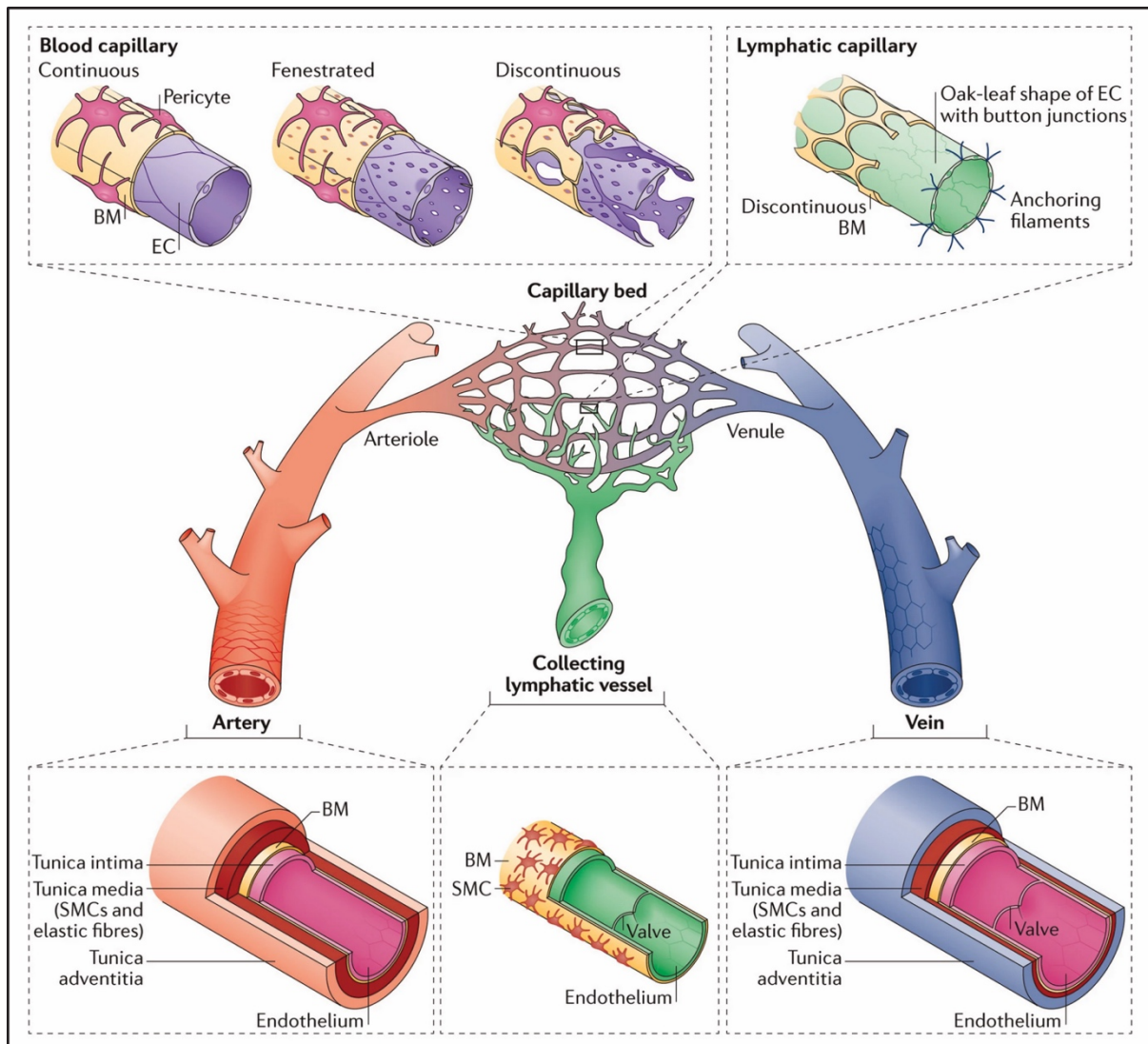
Figure 1.1: Architecture and morphology of the vasculature (Potente and Mäkinen, 2017). The vascular tree is composed of hierarchical network of arteries (red) interconnected by a capillary bed to veins (blue), also linked to the open lymphatic system (green). Larger arteries and veins are composed of a layer of endothelial cells (endothelium), a basement membrane (BM) and layers of perivascular cells (Smooth muscle cells and pericytes) and elastic fibres. Lymphatic vessels are covered by fewer perivascular cells and possess valves like the veins. Capillary beds are heterogeneous depending on the organ, with continuous, fenestrated or discontinuous morphologies in relation to their specific function.

Small capillaries are composed of ECs only, with a thin basement membrane and the presence of few or no pericytes. These capillary beds also differ morphologically depending on the organ (Aird, 2007a, 2007b). Blood vessel capillary from organs without secretory functions such as the brain or the skin possess continuous junctions and basement membrane to selectively control trans-endothelial transport (Augustin and Koh, 2017). On the other side, ECs from organs with an essential role in secretion or filtration such as the liver, bone marrow or kidney display discontinuous or fenestrated endothelium (Fig. 1.1)(Aird, 2007a; Augustin and Koh, 2017; Potente and Mäkinen, 2017).

Larger vessels experience higher hemodynamic forces than capillaries (for example 66 cm/sc peak velocity and 11 cm/sec mean velocity in the human ascending aorta against 26 and 13 cm/sec in the vena cava)(Gabe et al., 1969), with the need to reinforce the vessel structure. Small vessels such as venules and some capillaries are covered by pericytes only. Pericytes have a role in vessel stabilisation (playing a role in VE-Cadherin expression in ECs through the interaction with Tie2 and angiopoietins), maturation, flow regulation and contractility as well as trans-endothelial transport (Armulik et al., 2011, 2010; Hall et al., 2014; Hellstrom et al., 1999; Lindahl et al., 1997). In the lymphatic system, the layer of pericytes is replaced by a layer of SMCs, whose contractile phenotype promotes the movement of fluid back into the venous circulation. The unidirectional flow in the lymphatic system as well as in the venous system is ensured by the presence of valves, created in the lumen by stromal cells and EC migration (Geng et al., 2017; Tatin et al., 2013).

b. Function of the vascular system

During development, the cardiovascular system remodels quickly to adapt to its environment and becomes the first functional organ due to its central role in maintaining homeostasis, remove waste and promote organ development. Proper development of blood vessels is crucial for the development of organs due to the limited diffusion of oxygen. In adults, the vascular tree is mostly quiescent, and its structure is fixed, but it can rapidly remodel in response to stimuli to restore homeostasis in hypoxic or ischemic tissues.

One of the main functions of the vascular system is to supply nutrients and solutes to all organs and to remove metabolic waste. To do so, blood vessels in the intestine pick up the nutrients from the digestion and will deliver it throughout the body. Capillaries in intestinal villi are characterised by an extreme ability to absorb nutrients via large trans-endothelial transport, making the epithelial diffusion of nutrients very efficient (Pappenheimer and Michel, 2003). This rapid nutrient exchange is increased by the highly vascularised villi, their morphology to increase surface contact as well as the polarisation of specialised capillaries and telocyte populations through VEGFA (Vascular endothelial growth factor A) signalling (Bernier-Latmani et al., 2022). Once the blood is filled with nutrients from the intestinal villi, it is rapidly delivered to organs.

The other main role of the vascular system consists in enabling rapid gas exchange to maintain organ homeostasis. Blood coming from the venous system is passed through the capillary beds in the lung, enabling direct diffusion of O_2 and CO_2. The vascular-epithelial barrier in the lung

has a unique architecture to increase surface contact. This intimate cellular crosstalk is specified early in development and results from close endothelium/lung epithelium angiocrine signalling (Augustin and Koh, 2017; Lazarus et al., 2011; White et al., 2007, p. 9).

As observed in the lung or intestine development, blood vessel formation is key to organ's development and regeneration (Augustin and Koh, 2017; Rafii et al., 2016). This angiocrine function is highly specific to the micro-environment of different organs. For example, this crosstalk has been extensively described in the bone vasculature where specialised vessel subtypes are essential for osteogenesis (Kusumbe et al., 2014; Ramasamy et al., 2016). In long bones, a specific vessel subtype expressing high levels of endomucin has been characterised as mediating growth of the bone vasculature and maintaining homeostasis for the development of bones. A follow-up study has deciphered this mechanisms as an endothelial cell-specific Notch pathway activity promoting osteogenesis (Ramasamy et al., 2014). This phenomenon has also been described in regeneration, with inductive signals coming from the endothelium in the liver (Ding et al., 2010) or the bone marrow for haematopoiesis (Itkin et al., 2016).

The closed vasculature system is also responsible for the removal and transport of different wastes. In the kidney, several populations of ECs contribute to the filtration processes and podocytes function as well as the water reabsorption process (Jourde-Chiche et al., 2019). In the central nervous system, recent studies on the lymphatic system have highlighted its central role in protein waste removal in relation to dementia onset (Nedergaard and Goldman, 2020).

At the centre of blood vessel function is the ability of the endothelium to be a semi-permeable barrier, enabling the transport of fluid, proteins and molecules in a controlled manner. This exchange is permitted by the structure of capillary beds, with thin monolayer of ECs in direct contact with stromal cells (Bendayan, 2002). As described above, the permeability differs in between organs due to the EC morphology, but it is regulated everywhere by both passive diffusion of solutes and active transport of macromolecules. Dysregulation of this machinery is associated with many diseases, for example disruption of the blood brain barrier (BBB) during development has been described as a cause of autism spectrum disorder (Tărlungeanu et al., 2016).

Along with its role for homeostasis, blood vessel and the endothelium monolayer have a central role in immune cell trafficking. Leucocytes in the circulation invade organs via the attachment and trans-endothelial migration mainly in post-capillary venules (Aird, 2007a; Butcher, 1991). This interaction is mediated by selectins expressed by leucocytes and different adhesion molecules and junctional proteins expressed by ECs (ICAM-1/VCAM-1,intercellular/vascular cell adhesion molecule-1, PECAM-1/CD31, Platelet/endothelial cell adhesion molecule 1 or

VE-Cadherin, Vascular endothelium Cadherin)(Arif et al., 2021; Muller et al., 1993). This rapid phenomenon involving the release of cytokines to attract circulating leucocytes is fundamental to mediate inflammation and immune response. The regulation of this trafficking is crucial to maintain immune surveillance and has been linked with the onset of atherosclerosis (Roy et al., 2022) and studied as potential target to fight different inflammatory conditions (Winneberger et al., 2021).

2- <u>Development of blood vessels: vasculogenesis, angiogenesis and arteriogenesis</u>

a. Embryonic development of the vasculature

The formation of primitive blood vessels starts with the differentiation of ECs from early precursors in the embryo that proliferate and form primitive networks. In mice, early blood vessel development starts around E6 with the differentiation of haemangioblasts from primitive streak mesodermal progenitors (Fig. 1.2)(Suburo and D'Amore, 2006). This specific progenitor is a subpopulation of mesodermal cells expressing brachyury (T) and KDR (Kinase insert domain Receptor, also known as Vascular endothelial growth factor receptor 2)(Huber et al., 2004). Independently, haemangioblasts will form in the yolk sac to form blood islands, composed of hematopoietic progenitors, endothelial cells and mural cells (Risau and Flamme, 1995). These blood islands will then form the primitive vascular plexi that will undergo remodelling and expansion as explained thereafter.

After formation for the primitive vascular network in the yolk sac, the latter will expand in the embryo to reach every developing organ and link with the heart and primitive blood vessels. At E8, the yolk sac is fully vascularized along with the formation of the first aorta (Drake and Fleming, 2000), and contains all of the blood cell progenitors, but the circulation is still not fully functional (McGrath et al., 2003; Palis and Yoder, 2001). In parallel, the yolk sac haemangioblasts are responsible for the primitive haematopoiesis giving rise solely to immature erythrocytes as described in figure 1.2. Definitive haematopoietic stem cells will be formed later and give rise to all haematopoietic lineages by migrating to the foetal liver and postnatally in the marrow.
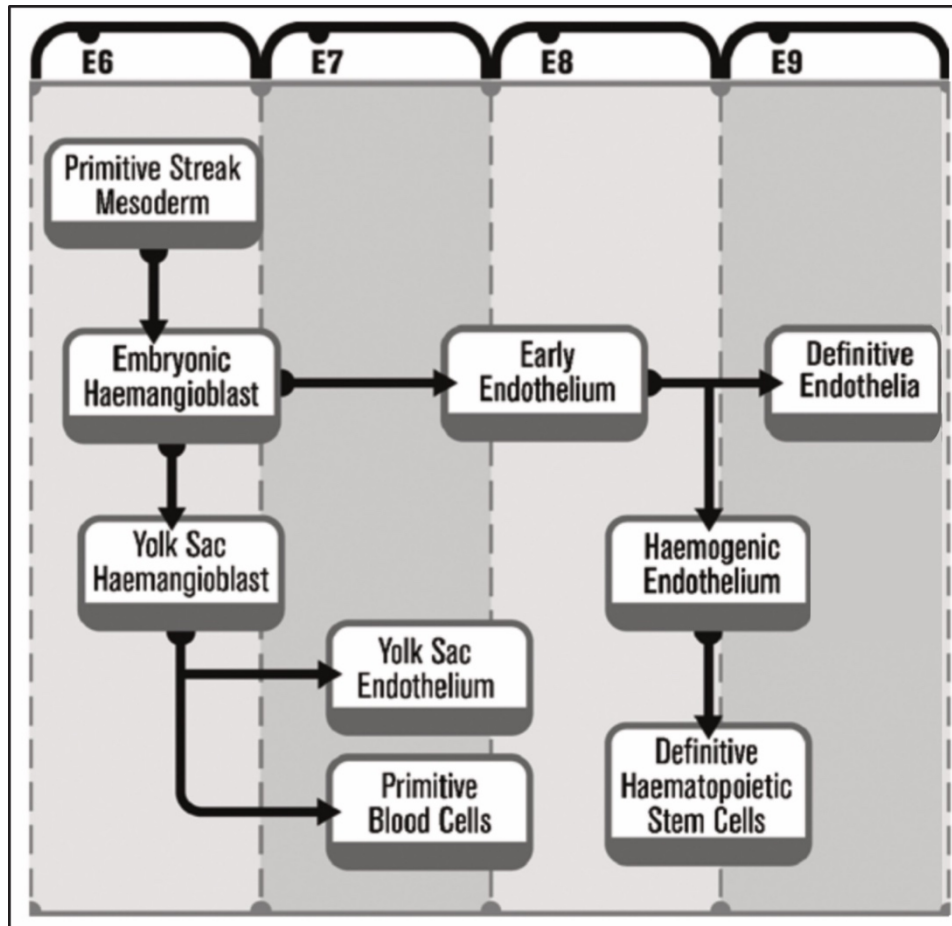
Figure 1.2: Timetable of the blood vessel development in the early mouse embryo. (Suburo and D'Amore, 2006). Blood vessel development starts in the early embryonic days (E6: Embryonic day 6) with the formation of angioblasts from the primitive streak mesoderm. At E7, the yolk sac endothelium is formed in parallel to primitive haematopoiesis. At E8, the primitive circulation is established from the early endothelium along with the formation of the heart and gives rises to the definitive haematopoietic stem cells through the formation of hemogenic endothelium and to the definitive vasculature at E9.

Between E8 and E8.5, a primitive circulation is established along with the formation of the heart and somitogenesis, with red blood cells being found outside the yolk sac only around E8.5 (somite pairs 4 to 8)(Drake and Fleming, 2000; Hirota et al., 1985; McGrath et al., 2003). Between E8.5 and E10, the vascular system will mature, invading the embryo and enabling red blood cells to circulate, to reach a closed loop around E10.5 (McGrath et al., 2003) in relation with the formation of cardiac chambers (Ji et al., 2003).

b. Vasculogenesis, angiogenesis and arteriogenesis

The first blood vessels in the embryo are formed by vasculogenesis, which is the process of *de novo* formation of blood vessels from endothelial precursors, giving rise to the dorsal aorta and the cardinal vein (Cleaver and Melton, 2003). The cells, located in primitive blood islands, that will form the first blood vessels are called angioblasts. These angioblasts arise from the

paraxial, cardiogenic or head mesoderm and are generated in the first stages of development to create primitive chords and plexi, prior to the onset of blood flow (Fig. 1.3A). On the molecular level, several pathways have been implicated in the mesodermal induction into angioblasts. The local microenvironment is especially responsible for the secretion of FGF-2 (Fibroblast growth factor 2), necessary for their differentiation (Cox and Poole, 2000). Studies on endothelial cell progenitors have reported the role of Hedgehog signalling (Vokes et al., 2004), VEGF signalling through its several receptors (Carmeliet et al., 1996; Shalaby et al., 1997), neuropilins (Kawasaki et al., 1999) and TGF-β (Dickson et al., 1995) in the early formation of blood vessel via vasculogenesis. Following this molecular determination, primitive plexi are then extended and remodelled to supply the different organs and enable their growth.

Sprouting angiogenesis is the primary mechanism by which primitive vascular plexi expand (Fig1.3B) and it is finely regulated by the balance between pro and anti-angiogenic factors. The main molecules involved in endothelial differentiation, survival and proliferation as well as blood vessel maturation and integrity are the vascular endothelial growth factors (VEGF)(Ferrara, 2002). The chief inducers of sprouting angiogenesis are VEGF family members (VEGFA-D and Placental Growth Factor PGF) which act though their receptors (VEGFR1-4) and co-receptors (Neuropilin 1 and 2). Due to their central role, genetic disruption of any of these factors has been linked to developmental vascular defects including vasculogenesis, angiogenesis, lymphangiogenesis and vascular maturation (Crawford and Ferrara, 2009; Ebos and Kerbel, 2011; Ferrara, 2002; Staton et al., 2007).

During angiogenic sprouting, specific cells from a capillary are selected as tip cells which are responsible for initiation and extension of a new sprout (Fig 1.4). Tip cells specification is induced by angiogenic factors such as molecules from the VEGF family, the FGF (Fibroblasts growth factor) family, PDGF (Platelet derived growth factor) or HGF (Hepatocyte growth factor) and modulated by intracellular signalling and EC-EC crosstalk via NOTCH and other juxtacrine signalling molecules. The tip cell is selected following the receipt of biochemical cues, specially VEGFA and Notch signalling (Gerhardt et al., 2003; Hellström et al., 2007), and will migrate in the direction of the pro-angiogenic gradient.
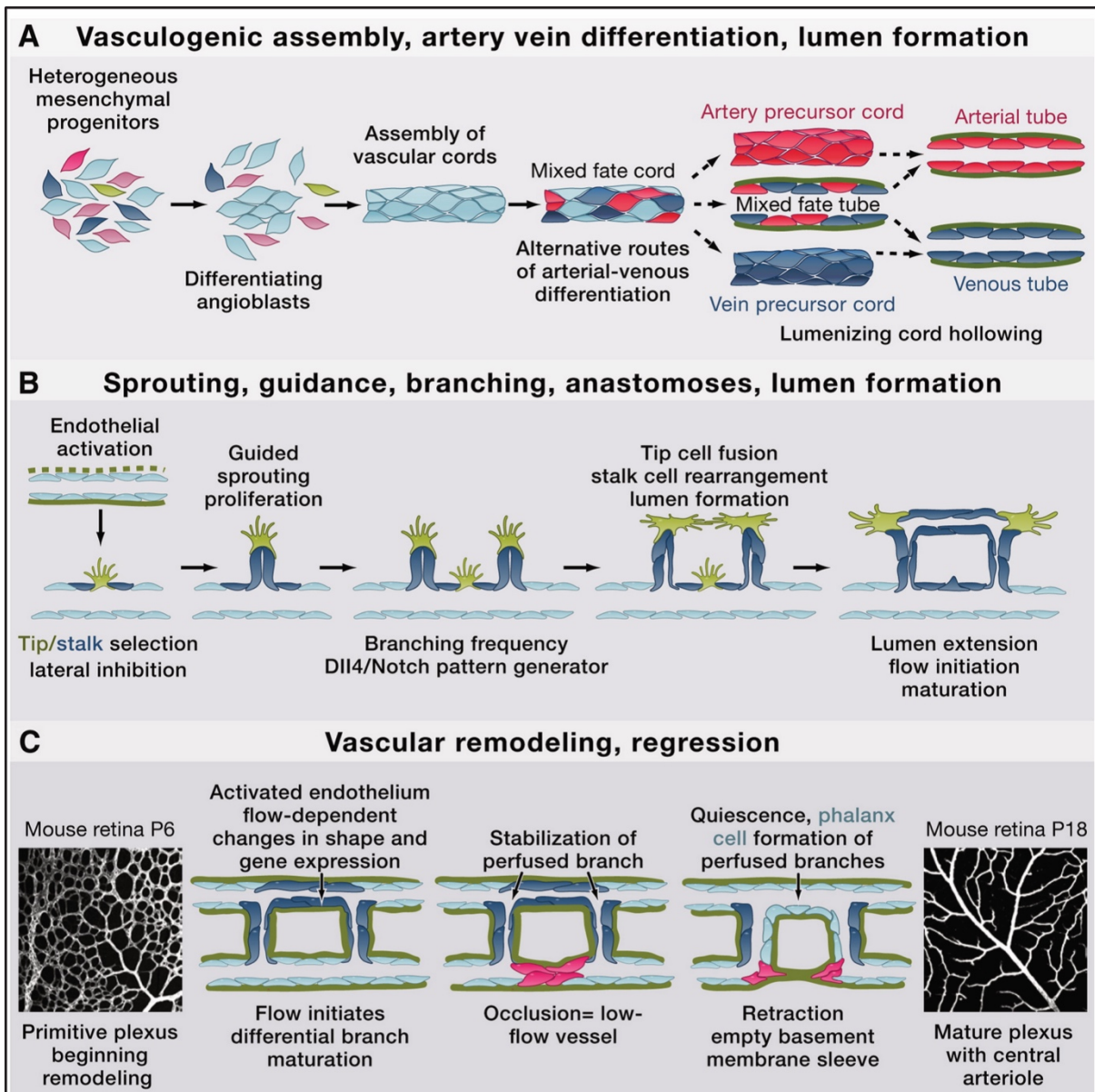
Figure 1.3: Schematic of blood vessel formation (Potente et al., 2011). A) Vasculogenesis and tube formation from angioblast followed by lumen acquisition in parallel of arteriovenous specification. B) Temporal formation of vessel via endothelial sprouting, tip cell selection, branching lumen formation and vessel maturation. C) Vascular maturation, remodelling and regression induced by flow to give rise to a mature plexus.

As shown in figure 1.4, the process of tip/stalk cell selection has been studied extensively to understand how blood vessels develop and if these pathways could be used to treat diseases. The mechanisms by which new blood vessels are formed is very well controlled. Following the receipt of VEGF-A and its interaction with the receptor VEGFR2, VEGF signalling will start establishing the "tip" cell phenotype. The expression of Delta-like ligand 4 on the surface of the cell signals to the "stalk" cells, establishing a higher Notch signalling in the neighbouring cell. This "lateral inhibition" phenomenon (Fig. 1.4) and its well-balanced machinery is fundamental for the extension of the vascular network and the maintenance of homeostasis.
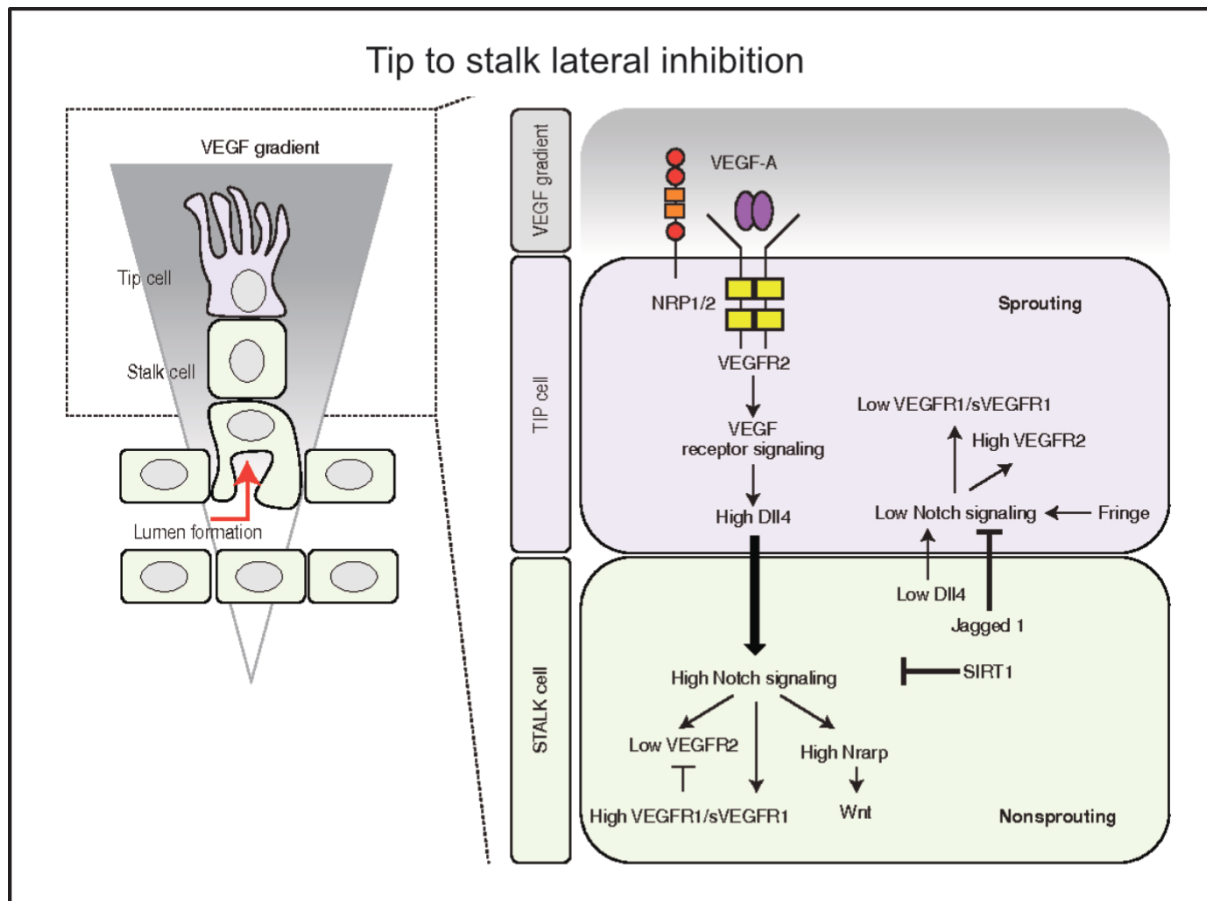
Figure 1.4: Tip/stalk cell specification during sprouting angiogenesis (Blanco and Gerhardt, 2013). The tip and stalk cell phenotype during angiogenesis is mainly driven by VEGF and Notch signalling. The first step of this specification is the creation of a VEGF gradient, interacting with VEGFR2 at the surface of ECs. The internalisation of the signal is enhanced by Neuropilins 1 and 2 (Nrp1/2) to induce VEGF signalling and upregulate the expression of Delta-like ligand 4 (DLL4) in the tip cell. The interaction of DLL4 with Notch1 receptor on the stalk cell induces high Notch signalling. In turn, Notch signalling is responsible for the reduction of VEGFR2 expression, the increased expression of Jagged1, VEGFR1 and Notch signalling targets such as Nrarp. The low DLL4 expression and high Jagged1 expression in the stalk cell induces the maintenance of low Notch signalling in the tip cell, via the interaction with the glycosyltransferase Fringe, and the high expression of VEGFR2. Other molecules such as the histone deacetylase Sirtuin 1 (SIRT1) modulate the lateral inhibition amplitude by direct inhibition of Notch signalling in the stalk cells.

New sprouts will then fuse by anastomosis (Fig. 1.3B) and create a novel lumen by the formation of vacuoles or by cytoskeleton and membrane rearrangement (Potente et al., 2011). The last step of blood vessel formation is called "arteriogenesis" and consists in the recruitment of mural cells (Carmeliet, 2000), originating from different progenitors depending on the organ (Chen et al., 2016; G. Wang et al., 2015; Yamazaki and Mukouyama, 2018). These mural cells prevent vessel regression, control blood flow and secrete growth factors as well as extracellular matrix (ECM), their recruitment is necessary for the formation of the vascular hierarchy, growth, stabilization and maturation (Jain, 2003). Platelet-derived Growth Factor (PDGF), and its receptor β (PDGFR-β), is the molecule, along with VEGF, that is mainly responsible for the

recruitment of the pericytes (Benjamin et al., 1998) while smooth muscle cell recruitment is driven by the onset of hemodynamic forces (Padget et al., 2019).

As shown in figure 1.5, several pathways are involved in the development, maturation and maintenance of EC identity and phenotype. For example, the close interaction of ECs with perivascular cells is mandatory for the establishment of organ-specific function. In the brain, Wnt signalling induces the maturation of ECs to form a tight blood-brain barrier whereas in the endocrine glands VEGF-A is responsible for the formation of fenestrated endothelia. Through direct cell to cell contact or the release of growth factors, perivascular cells play a central role in EC maturation. This interaction is governed by VEGF signalling (Eilken et al., 2017; Evensen et al., 2009), TGF-β signalling (Jarad et al., 2017) and recent studies have also highlighted the role of Notch receptors in the recruitment of pericytes and vessel stabilisation(Liu et al., 2010; Tefft et al., 2022).
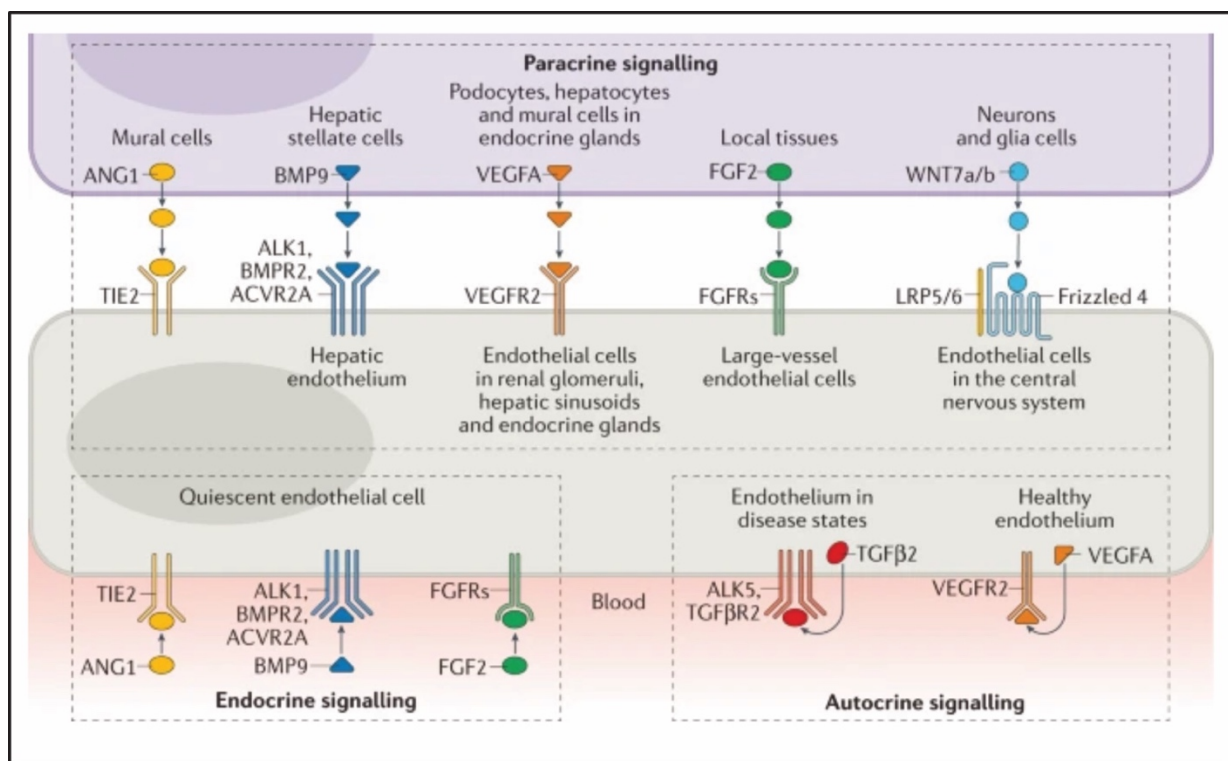
Figure 1.5: Molecular signalling involved in endothelial cell maturation and quiescence (Ricard et al., 2021). Endothelial cells receive paracrine, endocrine and autocrine signalling that are essential for their quiescence. Paracrine signalling is essential for the tissue-specific maturation of ECs as described by BMP signalling in the liver, VEGF signalling in the formation of fenestrated endothelia or Wnt signalling in the central nervous system. Endocrine signalling such as the Tie2/ANG1 crosstalk, the secretion of FGF2 by organs or the secretion of BMP9 from the liver are essential for the quiescence of ECs. On the other side, autocrine signalling, especially transforming growth factor-β (TGFβ) signalling has been linked to endothelial cell dysfunction. ANG1, angiopoietin 1; ACVR2A, activin A receptor type 2A; ALK, activin receptor-like kinase; BMP9, bone morphogenetic protein 9; BMPR2, bone morphogenetic protein receptor type 2; FGF, fibroblast growth factor; FGFR, fibroblast growth factor receptor; LRP, lipoprotein receptor-related protein; TGFβR, transforming growth factor-β receptor; TIE2, angiopoietin 1 receptor; VEGFR, vascular endothelial growth factor receptor.

c. Haemodynamic forces in vascular biology

As described earlier, the onset of the flow in the embryo correlates with the modelling of the vasculature in response to chemical and biomechanical stimuli and leads to the formation of new blood vessels via sprouting angiogenesis mainly. Blood pressure and forces in blood vessels are mandatory for the proper function of blood vessels and to maintain homeostasis. Flow within newly formed capillary networks is a primary factor regulating their mature architecture. EC can sense differential flow in different branches and modify their phenotype to either stabilise (regular flow) or prune (low or oscillating flow) them (Fig. 1.3C).

The endothelium, as first sensor of blood pressure and hemodynamics forces, is also dependent on physiological regulation of these physical cues. In physiological conditions, the quiescent state of the endothelial barrier is maintained by normal levels of shear stress (Lin et al., 2000). In angiogenic conditions, studies have shown the predictability of the location of the sprout due to a positive drop in blood pressure in parts of the endothelium (Ghaffari et al., 2015). At the cellular level, shear stress experienced by ECs has also been linked to the production of NO (nitric oxide), important component regulating blood flow, cell adhesion or thrombosis (Ghimire et al., 2017; Tousoulis et al., 2012) as illustrated in figure 1.6. The exposure to disturbed flow is known to induce expression of NF-kB, increasing the production of adhesion molecules, chemokines and inflammatory response (Fig. 1.6)(Chiu and Chien, 2011; Nakajima and Mochizuki, 2017; Wettschureck et al., 2019).

EC flow perfusion and shear stress sensing has also been linked to the TGF-β family through bone morphogenetic proteins (BMPs). BMP9 and BMP10 have been identified as effector of activin receptor-like kinase 1 (ALK1) on endothelial cells and play a central role in EC quiescence and angiogenesis (David et al., 2008, 2007). Binding of circulating factor BMP9 and BMP10 to Alk1 and its co-effector Endoglin under flow conditions induce pSMAD1/5/8 activation to maintain EC quiescence (Ayuso-Íñigo et al., 2021; Baeyens et al., 2016; Ricard et al., 2021).
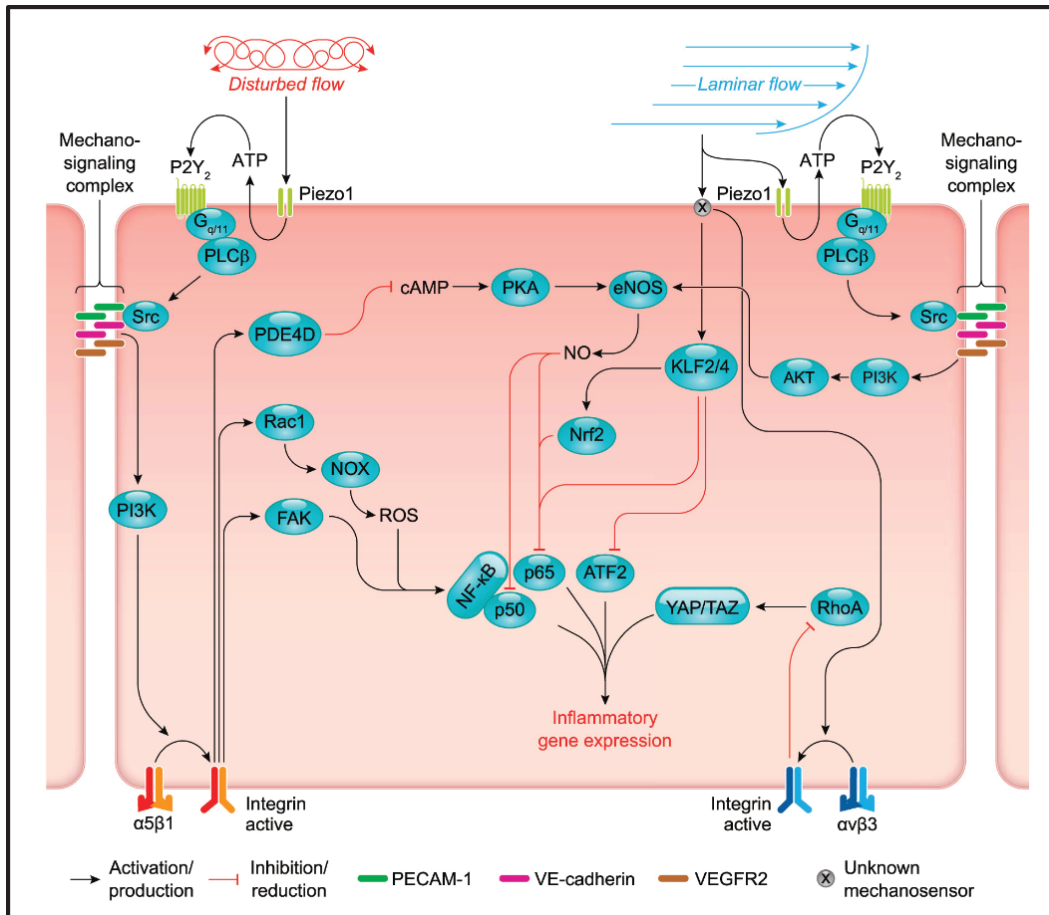
Figure 1.6: Flow sensing in endothelial cell (Wettschureck et al., 2019). Disturbed flow, detected by Piezo1, induces the activation of integrin α5 via G protein alpha subunits Galphaq and Galpha11(Gq/G11) mediated signalling and PECAM/VE-Cadherin complex, leading to an NF-kB activation through Focal adhesion kinase (FAK) activation. Activation of integrin α5 also induces expression of small GTPase Rac1 that activates NADPH oxidase (NOX) to produce reactive oxygen species (ROS) and further activate NF-kB. In parallel integrin α5 activation has been shown to interact with phosphodiesterase 4D (PDE4D) leading to reduced levels of cyclic Adenosine monophosphate (cAMP) and Protein kinase A (PKA) triggering the reduction of activity of the central anti-inflammatory protein endothelial Nitric oxide synthase (eNOS), responsible for NO production. In normal laminar flow conditions, the mechanosensing complex induces the expression of eNOS through a Phosphoinositide 3-kinase (PI3K)/ Protein kinase B (AKT) pathway instead of activating integrins. The production of nitric oxide ((NO) then inhibits NF-kB activity and the inflammatory response. The laminar shear stress also inhibits Yes-associated protein (YAP)/ transcriptional coactivator with PDZ-binding motif) TAZ activity through a signalling cascade involving integrin β3 and RhoA. Krüppel-like factors (KLFs) such as KLF2 and 4 also play a pivotal role in flow sensing and their expression is induced by laminar shear stress, leading to an inhibition of activating transcription factor 2 (ATF2).

In the body, variation of blood vessel diameter is accompanied by very different shear stress, resulting from the frictional force of the blood flow. It is estimated that big veins experience low wall shear stress (<1 dyne/cm^2) where small venules are subject to a higher shear stress estimated between 20 and 40 dyne/cm^2. On the arterial side, the higher blood pressure results in shear stress estimated between 60 and 80 dyne/cm^2 in small arterioles where it is the highest, and between 5 to 20 dyne/cm^2 in big arteries (Ballermann et al., 1998; Cunningham and Gotlieb, 2005). This range of shear stress is highly affected by the curvature of blood vessels,

with studies showing up to 600 dyne/cm^2 in carotid bifurcations (Zarins et al., 1983). Physiological levels of shear stress are also responsible for the expression of VCAM-1 and ICAM-1, whose expression is upregulated in lower shear stress zones (usually <5 dyne/cm^2)(Cunningham and Gotlieb, 2005), leading to increased cell adhesiveness and a higher chance of atherosclerotic plaque formation (Cybulsky and Gimbrone, 1991; Walpola et al., 1995). The development of atherosclerosis is notably linked with impaired shear stress and blood flow, leading to ECs dysfunction and the release of growth factors, transmigration of leucocytes and coagulation problems. Several other diseases such as hypertension, thrombosis or vascular diseases have been linked to hemodynamic dysregulation (Ando and Yamamoto, 2022).

In parallel to maintaining vascular function as demonstrated in the bone (Ramasamy et al., 2016), blood flow has been shown to play a central role in blood vessel identity and EC specification. Several studies have also linked blood flow dynamics with arteriovenous specification (le Noble et al., 2004). For example, shear stress is involved in EC phenotype through the control of cell cycle needed for an EC to acquire arterial phenotype (Fang et al., 2017; W. Luo et al., 2021). The molecular mechanism behind the acquisition of EC phenotype mainly involves Notch signalling as described by the role of NOTCH1 receptor as a mechanosensor (Mack et al., 2017).

3- <u>**Blood vessel heterogeneity and organ specificity**</u>

Blood vessels exhibit remarkable intra and inter-tissue heterogeneity throughout the body (Potente and Mäkinen, 2017). Even though the mechanism of tissue-specification is not yet completely understood, it has been shown that specific endothelial cells are essential for organ development (Kusumbe et al., 2014; Lammert et al., 2001). As described above, blood vessels are capable of rapid changes in morphology and can colonize parts of the body that are subjects to hypoxia or require size growth, during development or during reparative processes (Gomez-Salinero and Rafii, 2018). This results in the formation of blood vessels with specialised functions and heterogeneous composition. Understanding endothelial and blood vessel plasticity and heterogeneity is paramount to reproduce these mechanisms *in vitro* and to generate biomimetic and human relevant models of functional blood vessels *in vitro*.

a. Endothelial cell heterogeneity

Blood vessels have been studied for years but it is only recently that studies on organ-specific endothelium shed the light on the importance of organotypic endothelium and their role in organ development and regeneration (Rafii et al., 2016). From a relatively homogenous population of progenitors, ECs, through the experience of different hemodynamic forces and micro-environment, acquire different phenotypes depending on their spatial localisation.

ECs differ in phenotype and functions throughout the body. For, example, the blood-brain barrier is formed of a continuous layer of endothelial cells with tight junctions allowing only small molecules to penetrate the brain. On the contrary, the liver sinusoidal endothelial cells form a discontinuous endothelium and create a permeable barrier. Apart from clear differences in morphology and molecular identity as well as origins, organ-specific endothelium have been shown to be essential for a lot of different mechanisms such as osteogenesis (Kusumbe et al., 2014), blood-brain barrier formation (Obermeier et al., 2013) or liver regeneration (Ding et al., 2010). The origin of this heterogeneity at the organ-level and intra-organ is still being investigated but several studies have shed light on genetic and epigenetic programming, trans-differentiation of progenitors and influence of the environment on EC phenotypes (Fig. 1.7).
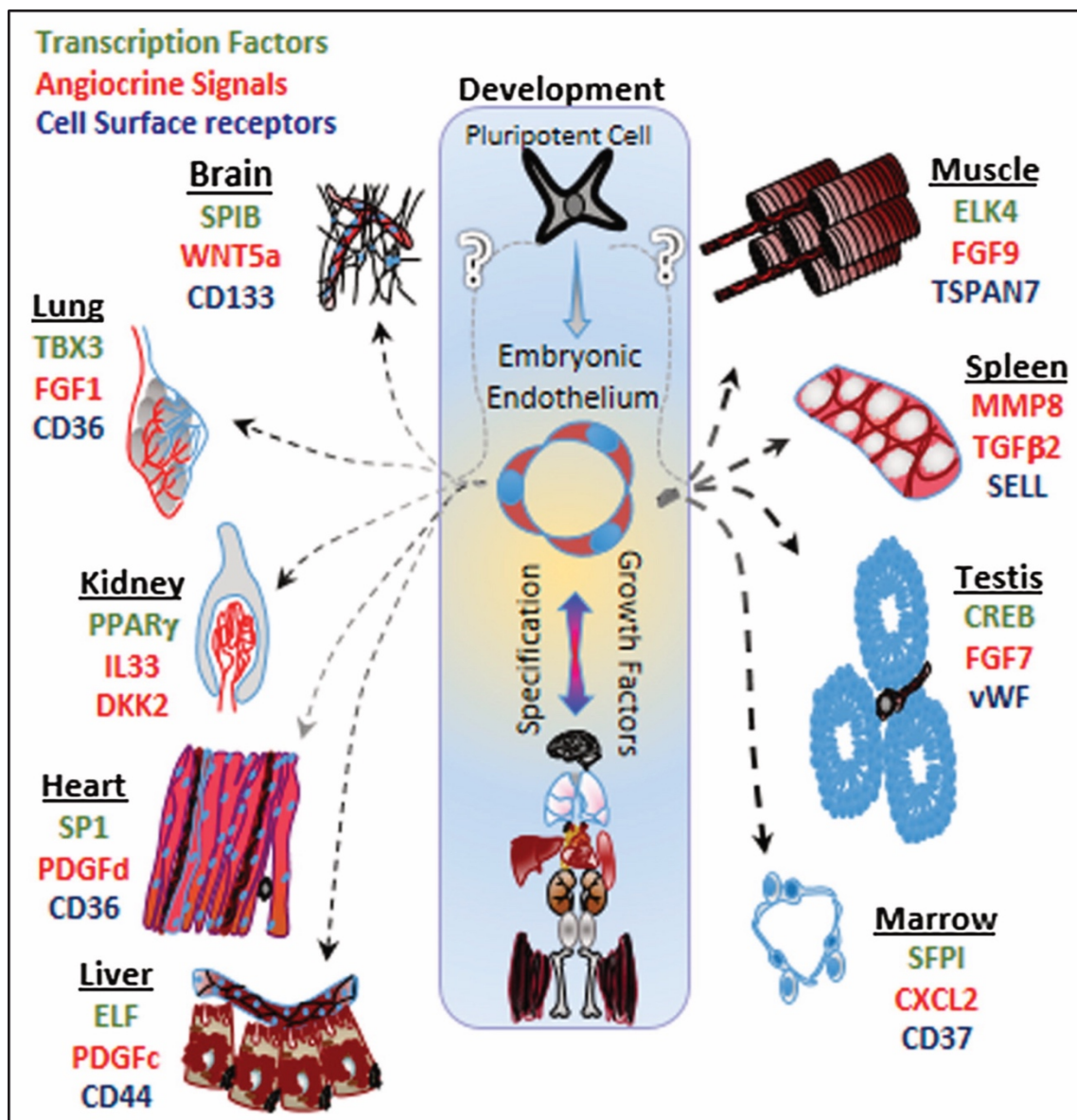
Figure 1.7: Overview of organ-specific endothelial heterogeneity.(Nolan et al., 2013). Organ-specific endothelial cells acquire their phenotype during development through specification in the different organs. Specific growth factors, environments and cell-to-cell interactions are responsible for the specification of these ECs and lead to the expression of organ-specific transcription factors (green), angiocrine signals (red) and cell surface receptors (blue). SPIB: Spi-B transcription factor; WNT5a: Wnt family member 5A; CD133: Cluster of differentiation 133 (Prominin 1); TBX3: T-Box transcription factor 3; FGF1: fibroblast growth Factor 1; CD36: Cluster of differentiation 36 (Glycoprotein 4); PPAR-γ: Peroxisome proliferator-activated receptor gamma; IL33: Interleukin 33; DKK2: Dickkopf WNT Signalling Pathway Inhibitor 2; SP1: Transcription factor Sp1; PDGFd: Platelet Derived Growth Factor D; ELF: E74 Like ETS Transcription Factor 1; PDGFc: Platelet Derived Growth Factor C; CD44: Cluster of differentiation 44 (Homing cell adhesion molecule); ELK4: ETS Transcription Factor ELK4; FGF9: Fibroblast Growth factor 9; TSPAN: Tetraspanin-7; MMP8: metalloproteinase-8; TGFβ2: Transforming growth factor-beta 2; SELL: Selectin L; CREB: cAMP response element-binding protein; FGF7: Fibroblast growth factor 7; vWF: Von Willebrand factor; SFPI: split-finger protein 1; CXCL2: Chemokine (C-X-C motif) ligand 2; CD37: Cluster of differentiation 37: Leucocyte antigen.

i. Genetic and epigenetic control of heterogeneity

The recent development of modern molecular techniques and advanced mammalian models have helped elucidating several molecular mechanisms involved in EC phenotypic diversity

(Aird, 2007a, 2007b; Herbert and Stainier, 2011; Minami and Aird, 2005; Rocha and Adams, 2009).

Several genes are expressed constitutively in every EC in the body and defined as endothelial-specific lineage markers. Examples of these genes include members of ETS, Sox and GATA transcription factor families (De Val and Black, 2009). Some junctional proteins such as VE-Cadherin, although shared with blood progenitors, have also been defined as endothelial lineage markers (Lampugnani et al., 1995).

Apart from arteriovenous specification (discussed later), ECs acquire organ-specific gene expression profiles during the formation of organs via the crosstalk with specific environments (Augustin and Koh, 2017). These genes have mainly been identified via global gene expression studies (Chi et al., 2003; Kalucka et al., 2020) and participate in EC phenotype and organ-specific functions.

In the central nervous system, neuroepithelial cells express Wnt ligands Wnt7a and Wnt7b, promoting vascular invasion and EC differentiation to create the blood-brain barrier (Stenman et al., 2008). The resulting unique molecular signature of the brain vasculature and the blood-brain barrier has been investigated and revealed brain-specific endothelial cell markers such as Mfsd2, involved in fatty acid transport (Ben-Zvi et al., 2014), Gpr124, involved in Wnt signalling (Zhou and Nathans, 2014) or GLUT1, necessary for the high glucose intake of the brain.

Another organ displaying remarkable EC diversity and specialisation is the liver. Hepatic vasculature is composed of an arterial system with a nutritive role and a venous side coming from the intestine with nutrient filled blood, both linked by a sinusoidal vasculature allowing filtration. Liver sinusoidal ECs have important scavenging (Sørensen et al., 2012) and immunological functions (Knolle and Wohlleber, 2016). They acquire liver-specific functions through the expression of GATA4 (Géraud et al., 2017) and are essential for liver zonation and hepatocyte proliferation through the expression of Wnt ligands (Rocha et al., 2015; B. Wang et al., 2015).

Genetic and epigenetic regulation of EC phenotype are also central to the development of the lymphatic system. Lymphatic EC (LECs) appear early in the embryonic development via the differentiation of a subpopulation of venous ECs expressing Prox1 (Wigle, 2002, p. 1; Wigle and Oliver, 1999, p. 1). The lymphatic vasculature further develops to form lymph sacs with LECs expressing lymphatic-specific markers such as LYVE-1, Podoplanin or VEGFR-3 (Karkkainen et al., 2004; Yang and Oliver, 2014). Interestingly, LECs show a very plastic phenotype, as shown by their differentiation into blood vessels if experiencing blood flow (C.-

Y. Chen et al., 2012; Das et al., 2022), highlighting the necessary molecular feedback loop involved in maintaining LEC phenotype (Srinivasan et al., 2014).

As illustrated by this example of LEC plasticity, ECs require a constant signalling from their environment to maintain their organ-specific phenotype.

ii. Influence of the tissue microenvironment

Blood vessels in the body experience a range of microenvironments, from very stiff environment in the bone to very soft environment in the brain. As described above, EC phenotype acquisition involves the combination of genetic and epigenetic programming and the right biomechanical cues. Signalling from neighbouring cells, biochemical and biophysical cues as well as the ECM composition are fundamental for organ-specific EC function.

One of the key factors contributing to the microenvironment is the level of oxygen. As the first functional organ in the body, the vasculature is able to sense oxygen or lack of oxygen, known as hypoxia. This ability is essential for the development of organs and the patterning of the vascular tree is intimately linked with the levels of oxygen in the body. Maintaining oxygen homeostasis is crucial for the organ function and blood vessels possess several known molecular pathways involved in sensing hypoxia. The hypoxia inducible factors (HIFs) are the central effector of the vascular signalling and are regulated by oxygen sensors known as prolyl hydroxylase domain proteins (PHDs) as shown in figure 1.8. The degradation of HIFs in normoxia is inhibited in hypoxic conditions, followed by their nuclear translocation and the transcription of hypoxia-induced genes involved in processes such as angiogenesis, ECM remodelling or metabolic activity.

Studies exploring the role of microenvironment on EC specialisation began with the evidence that vWF (von Willebrand Factor) expression was induced by the cardiac microenvironment after transplantation of auricular blood vessels into the heart microenvironment (Aird et al., 1997). Since then, multiple studies have shown the crosstalk between the vasculature and other associated cells in the formation and maturation of heterogeneous organ-specific EC.

As described above, the VEGF family has an important role in EC biology, from sprouting angiogenesis to differentiation (Ferrara, 2002; Gerhardt et al., 2003). At the organ level, VEGF-A also plays an important role in vascularisation and in regeneration as well as organ-specific acquisition of fenestrae in the liver or pancreas for example (Brissova et al., 2006; Carpenter et al., 2005).
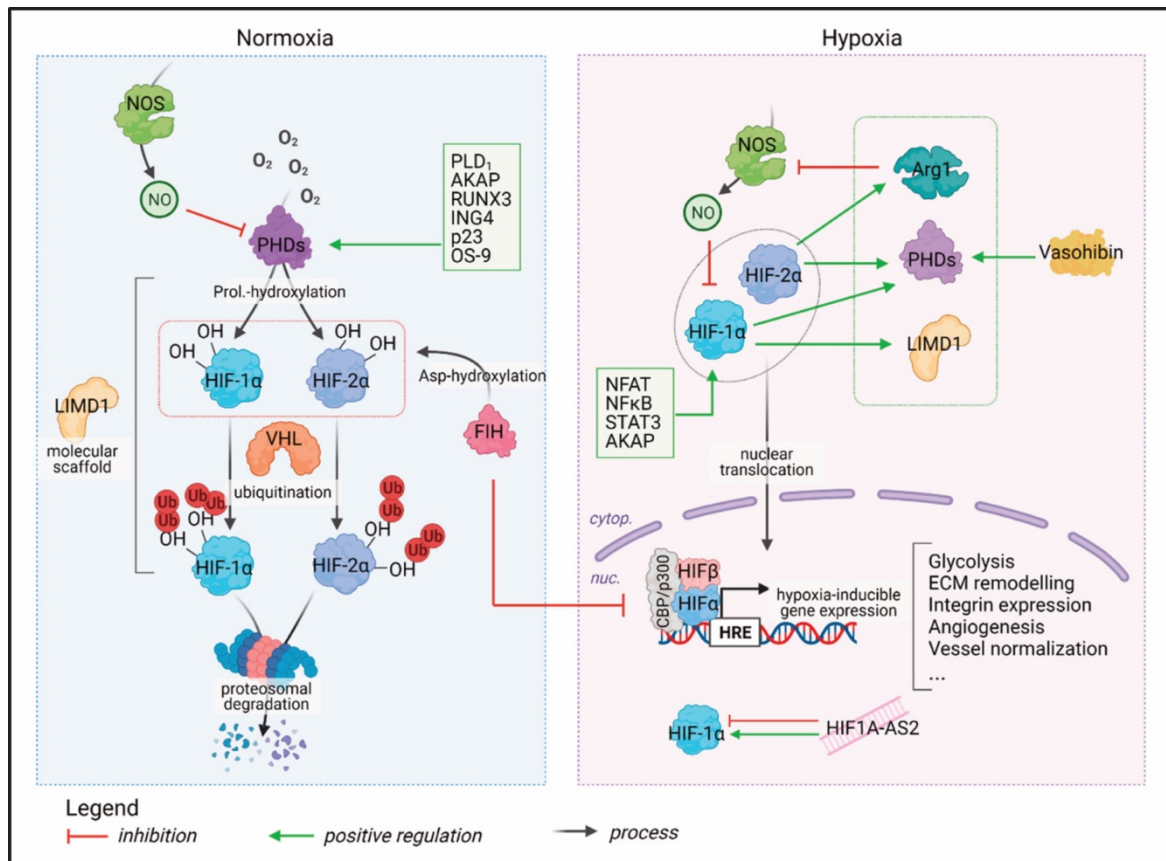
Figure 1.8: Molecular pathways involved in hypoxia sensing in endothelial cells. In normoxic conditions, PHDs hydroxylate HIF-1α or 2α, leading to their degradation by the Von-Hippel-Lindau (VHL) protein. Several other proteins such as LIM domain containing 1 (LIMD1), involved in the complex assembly with VHL, and regulators of PHD activity (green box) contribute to HIFs degradation. Following hypoxia sensing, HIF-1During hypoxia-associated events, including inflammation or tumor growth, HIF-1α is activated by several proteins (green box) and increases the transcription of PHDs, LIMD1 and Nitric Oxide Synthase (NOS) which will inhibit HIF-1 activity. HIF-2α can also induce Arginase 1 expression, inhibiting NOS, reducing NO production and reducing HIF-1α inhibition. HIF1α-AS2 (Antisense RNA 2) plays a role in HIF1 induction in the first few hours of hypoxia before inhibiting its activity. The protein Factor inhibiting HIF1 (FIH) helps HIF hydroxylation in normoxia while inhibiting the transcription of hypoxia-inducible gene expression in hypoxic conditions. PLD1: Phospholipidase D1; AKAP: A-Kinase anchor proteins; RUNX3: RUNX family transcription factor 3; ING4: Inhibitor of growth 4; NFAT: Nuclear factor of activated T cells; NF-kB: Nuclear factor kappa-light-chain-enhancer of activated B cells; STAT3: Signal transducer and activator of transcription 3.

ECs from endocrine glands are also susceptible to different molecules and growth factors due to their spatial localisation. The identification of EG-VEGF (Endocrine Gland VEGF)(LeCouter et al., 2001), inducing proliferation, migration and fenestration in these organs, shed the light on organ-specific angiocrine signalling. It demonstrated a close crosstalk between ECs and their surrounding cells, with endocrine glands selectively promoting capillary growth with this specific molecule. The implication of VEGF activity is also key for the absence of vascularisation in avascular organs, as described in the cornea (Ambati et al., 2006). Other mechanisms involving the microenvironment have been described to direct organ-specific EC phenotype. As described above, Wnt signalling from the neuroepithelium is

necessary for ECs to acquire blood-brain barrier phenotypes (Stenman et al., 2008). Close cell-cell interactions are also responsible for bone vasculature phenotype via NOTCH signalling (Ramasamy et al., 2014).

Finally, the vasculature can also be influenced by its microenvironment in pathological conditions such as cancer. It is well documented that tumour-associated vasculature possess a specific morphology, lose their function and are characterised by the presence of large chaotic vessels experiencing leakage with a total loss of arteriovenous organisation (Nyberg, 2008; Potente et al., 2011). This phenotype has been associated with the presence of different cell types in the tumor microenvironment such as myeloid cells (Mazzieri et al., 2011) or cancer-associated fibroblasts (Joshi et al., 2021). The tumor vasculature can also be influenced by the tumor ECM composition, as reported by the role of MMPs (Metallopeptidases) in releasing pro-angiogenic molecules such as tumstatin, a fragment coming from collagen cleavage (Hamano et al., 2003). On the other side, studies have shown the role of p53 tumor suppressor in the synthesis of antiangiogenic factors also coming from collagen fragments by upregulating collagen hydroxylase (Teodoro et al., 2006). Furthermore, some tumors such as glioblastoma have the ability to create their own vasculature through the differentiation of cancer "stem-like" cells into ECs (Wang et al., 2010). This unique microenvironment created by the close interaction of cancer cells, blood vessel and the ECM is being investigated and has been the target for several anti-angiogenic and vascular normalisation strategies, with the aim to increase efficacy of traditional therapies (Ebos and Kerbel, 2011; Eelen et al., 2020; Jain, 2005)

EC specification by the microenvironment also includes the formation of hemogenic endothelium, giving rise to haematopoietic progenitors through endothelial-to-haematopoietic transition (Gritz and Hirschi, 2016). This process is controlled by neighbouring Notch signalling and secretion of molecules such as retinoic acid (Chanda et al., 2013; Gama-Norton et al., 2015; Kumano et al., 2003; Kathrina L. Marcelo et al., 2013). Other examples of endothelial plasticity include endothelial-to-mesenchymal cell transition (EndMT) during heart development or in pathological conditions such as fibrosis, artherosclerosis or cancer (Dejana et al., 2017; Piera-Velazquez et al., 2011) in case of disruption of proper stimuli. Recent findings have also highlighted the possibility of an "endothelial stem cell" or adult endothelial progenitors (EPCs), able to form colonies *in vitro* and repopulate damaged vasculature in animal models (Wakabayashi et al., 2018).

b. Mural cells heterogeneity

Due to their important role in blood vessel functions, ECs have been extensively studied however, the mural cell component of blood vessel has received growing interests in recent years.

Along the vascular tree, mural cells present different origins, morphologies, phenotypes and functions. While ECs originate from mesodermal progenitors, pericytes and vSMCs have origins as diverse as the neural crest for the brain (Korn et al., 2002), the mesothelium for the gut (Wilm et al., 2005) and liver (Asahina et al., 2011) or even endothelial cell (Chen et al., 2016) and myeloid progenitors (Yamazaki et al., 2017).

i. Pericytes

Pericytes compose one of the mural cell populations, their main role being the stabilisation and development of small blood vessels and the maintenance of homeostasis and vascular function in many organs (Armulik et al., 2011; Teichert et al., 2017). Many studies on the role of pericytes attributed different functions to these cells from vessel stabilisation (Lindahl et al., 1997), blood flow regulation (Hall et al., 2014) or even tissue repair (Crisan et al., 2008; Göritz et al., 2011). Pericytes also display a phenotypic diversity throughout the body depending on their localisation. Several types of pericytes have been reported such as NG2+/ α-SMA- capillary pericytes, NG2-/ α-SMA+ venular pericytes or NG2+/ α-SMA+ arteriolar pericytes. Although their principle role is not to regulate circulation as smooth muscle cells, it has been reported that some possess contractile properties and have been linked with the regulation of microcirculation by expressing smooth muscle α-actin (α-SMA) (Alarcon-Martinez et al., 2018; Fernández-Klett et al., 2010; Hall et al., 2014).

Over the years, several studies have questioned the ability of pericytes to give rise to different lineages and function as mesenchymal stem cells or stromal cell progenitors. Pericytes have been described as precursors of mesenchymal stem cells (Crisan et al., 2008), adipose progenitors (Tang et al., 2008), myogenic progenitors (Dellavalle et al., 2007) or fibrotic fibroblasts (Göritz et al., 2011).

The blurry distinction between pericytes and the potential differentiation of these into MSCs or other cell lineage is mainly due to the shared markers (i.e PDGFR-B) between so-called pericytes and other perivascular cells as reviewed previously (Armulik et al., 2011). This hypothesis of pericyte multipotency has since been challenged by a study on lineage tracing of pericytes and smooth muscle cells using another marker, Tbx18, to show that, although

pericytes are multipotent *in vitro* they do not contribute to any other lineages *in vivo*. (Guimarães-Camboa et al., 2017). Recent single cell RNA-sequencing data also report distinct populations or pericytes, vSMCs and fibroblasts across different organs (Muhl et al., 2020), with specific transcriptional profiles of PCs and SMCs throughout the arteriovenous axis (Vanlandewijck et al., 2018). Different functions of pericytes have also been highlighted in the brain, from blood flow and blood-brain barrier integrity to a role in neurodegenerative diseases (Armulik et al., 2010; Hall et al., 2014; Vanlandewijck et al., 2018; Yang et al., 2022).

ii. Smooth muscle cells

Smooth muscle cells (SMC) are located in the perivascular area and represent the main biomechanical support in the vessel wall. Their roles include the regulation of vascular contractility and tone, which in turn maintains blood pressure. Furthermore, SMCs secrete ECM and regulate vessel maturation (G. Wang et al., 2015).

During embryonic development, SMCs arise from different tissues, and will cover distinct blood vessels depending on their spatial localisation. SMCs covering the descending aorta mostly originate from mesodermal lineages such as lateral plate or paraxial mesoderm (Wasteson et al., 2008). SMCs found in the kidney are differentiated from mesenchymal cells migrating from the metanephric mesenchyme (Xu et al., 2014). The mesothelium, the epithelial tissue protecting internal organs and also of mesodermal origin, has been found to produce SMCs in the lungs and in the gut (Que et al., 2008; Wilm et al., 2005). Studies have also reported the derivation of SMCs from tissues not derived from mesodermal lineages such as the neural crest to form the branchial arches arteries (Xie et al., 2013)

SMCs have been divided into two distinct groups depending on their function and phenotype. The first is comprised of quiescent cells, responsible for the contractile phenotype and expressing SMC-specific proteins such as smooth muscle α-actin (SMαA), smooth muscle myosin heavy chain (SMMHC) and calponin. These cells can undergo a "phenotypic switch" and dedifferentiate to a "synthetic" subset, with a more proliferating and ECM-producing state. These cells are responsible for blood vessel maturation as described earlier and the formation of scar tissue after injury (Yoshida et al., 2008). In pathological conditions such as atherosclerosis, the synthetic phenotype is responsible for the uncontrolled proliferation of cells and genesis of the atherosclerotic plaque (Milutinović et al., 2019; Ross and Glomset, 1973)

4- **Arteriovenous specification**

The process of arteriovenous specification is essential for the vascular tree formation and results in two distinct populations of endothelial cells. First, veins and arteries differ by their morphology (Fig. 1.9). The difference in morphology is a consequence of the hemodynamic (Potente et al., 2011), resulting in a thicker layer of mural cells surrounding arteries and creating more elastic vessels to accommodate and regulate blood flow. In addition to the vessel morphology, endothelial cells forming the inner layer are also different in shape. Venous arterial cells are short and wide cells, not aligned with the blood flow, they contain valves and have a high proliferation rate. Arterial endothelial cells are long and narrow cells aligned in direction of the flow and are slowly proliferating.
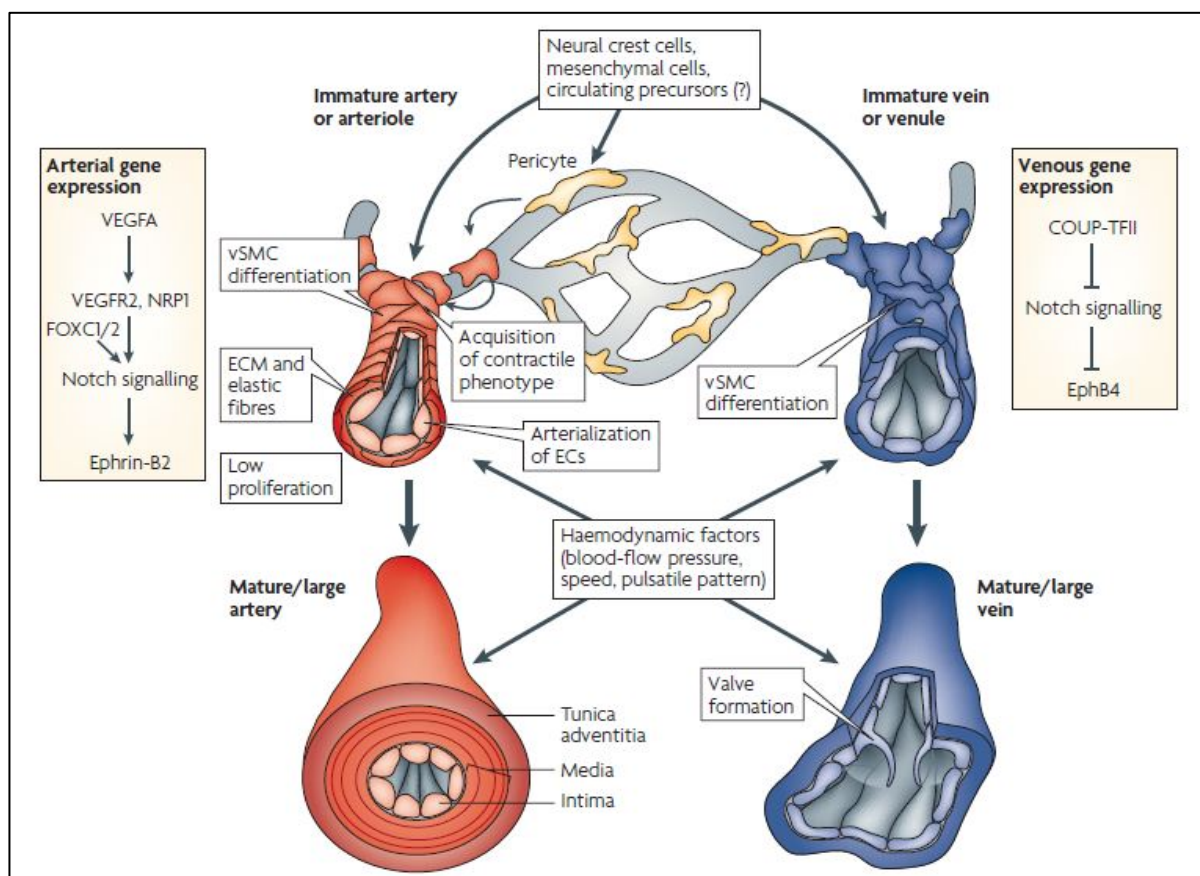
Figure 1.9: Schematic of arteriovenous specification and mural cell recruitment (Adams and Alitalo, 2007). The closed vascular circulation is comprised of arterial and venous cells forming arteries and veins of different sizes, matured and stabilized by the recruitment of mural cells. Veins are covered by fewer mural cells than arteries due to the differences in hemodynamic factors. Venous endothelial cells (vECs) are short and wide cells, form valves, are not aligned in the direction of the flow and possess a specific gene expression profile. NR2F2 (nuclear receptor subfamily 2, group F, member 2 also known as COUPTF2) is responsible for Notch signalling suppression, allowing expression of the venous marker EphB4. Arteries are surrounded by many layers of mural cells and smooth muscle cells responsible for blood flow regulation and the contractile phenotype. Arterial endothelial cells (aECs) are long and narrow cells aligned in the direction of the flow, proliferate less than vECs and possess their own phenotypic signature. Most of the signalling inducing arterial phenotype involves VEGF-A which will bind to VEGFR2 and NRP1 promoting, in partnership with the forkhead box transcription factors FOXC1 and FOXC2, Notch signalling via the expression of Notch ligand Delta-like-4 (DLL4). The high Notch signalling in aECs is mandatory for the expression of arterial specific genes such as Ephrin-B2 (Fish and Wythe, 2015).

All these morphological and structural characteristics were thought to be consequences of the unique environment faced by the 2 types of vessels and endothelial progenitors were presumably specified with the creation of circulation. Studies have now shown that specification of arterial and venous EC occur before any flow onset and it is genetically encoded during the development (Jain, 2003).

Numerous studies on animal models were able to discriminate molecular markers in order to characterize arteriovenous specification and link them to known pathway (Fig. 1.10)(Bussmann et al., 2011; Wang et al., 1998; Yamashita, 2007).
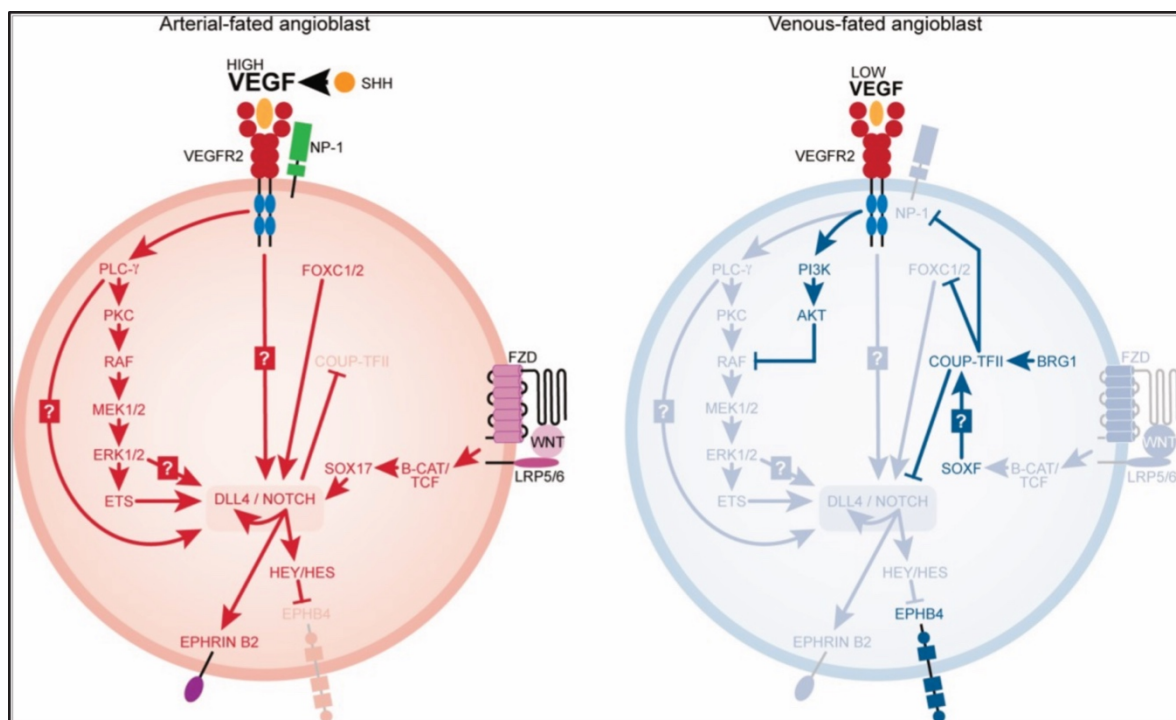
Figure 1.10: Schematic of the different molecular pathways involved in arteriovenous specification of angioblasts (Fish and Wythe, 2015). Sonic Hedgehog (SHH) acts upstream to induce VEGF expression which binds to VEGFR2. In aECS progenitors, VEGFR interacts with the co-receptor NRP1 to induce the Phospholipase C (PLC) activity and triggers the MAPK(MEK)/ERK (mitogen-activated protein kinases/extracellular signal-regulated kinases) cascade. The ERK signalling requires the activation of ETS (E26 Transformation specific) transcription factors, such as ETV2 (ETS variant 2) and ERG (ETS-related gene), to induce Notch signalling. In parallel, VEGF induces DLL4 expression in a positive feedback loop to induce Notch receptors (Notch 1 and Notch4) expression. Notch intracellular domain (NICD) represses venous phenotype by repressing chicken ovalbumin upstream promoter transcription factor II (COUP-TFII/n2rf2) in aECS and inducing the expression of HEY/HES transcription factor that repress the expression of the venous marker EphB4. Finally, Wnt/B-catenin canonical pathway has also been linked to arterial phenotype maintenance by inducing the transcriptions factors for the Sox (SRY-box) family and FoxC1/2 (Forkhead Box protein C1/2), reinforcing the DLL4/Notch signalling. In vECS, the transcriptional coregulator Brahma-related gene-1 (BRG1) induces COUPTFII expression. COUPTFII is responsible for the repression of Notch signalling and Nrp1 expression, resulting in MAPK/ERK repression and EphB4 expression.

The acquisition of arterial or venous fate is a result of a molecular cascade involving different known pathways summarized in Table 1.1.

Molecule/Pathway	Functions	References
Sonic Hedgehog	-Morphogen -Induces VEGF secretion in the embryo	(Pola et al., 2001)
VEGF signalling	Binding to VEGFR2 (KDR) triggers arteriovenous specification by activating Notch signalling.	(Ehebauer et al., 2006; Mukouyama et al., 2005; Swift and Weinstein, 2009)
Notch pathway	-Arterial phenotype specification	(Ehebauer et al., 2006; Fernández-Chacón et al., 2021; You et al., 2005; Zhong et al., 2001)
Neuropilin 1 and 2	-VEGF co-receptor -Facilitates VEGF binding - Nrp1 essential for arterial phenotype	(Herzog et al., 2001; Staton et al., 2007; Yamazaki and Mukouyama, 2018)
Phospholipase C gamma	-Activated by VEGF signalling -Arterial specification -Activates MAPK/ERK cascade	(Hong et al., 2006; Lawson et al., 2003)
MAPK/ERK	-Downstream of VEGF -ERK activation mandatory for arterial fate	(Fish and Wythe, 2015; Hong et al., 2006; Pardanaud et al., 2016)
PI3K (Phosphoinositide 3-kinases)	-Downstream of VEGF -Activated in venous specification	(Fish and Wythe, 2015; Hong et al., 2006)
ETS factors	- ETV2 master regulator transiently expressed in progenitors -ERG maintains endothelial phenotype	(De Val et al., 2008; De Val and Black, 2009; Ginsberg et al., 2012)
FOXC1/2	- Synergistic activity with ETS -Induces DLL4/Notch signalling	(De Val et al., 2008; De Val and Black, 2009)
Wnt/B-catenin pathway	- Induces Notch signalling in arterial specification	(Corada et al., 2010)
SoxF family	-Sox17 induces Notch1 in arterial phenotype -Sox7 and Sox18 induce venous phenotype and COUPTFII	(Chiang et al., 2017; Swift et al., 2014)
COUPTFII	-Main venous marker - Acts upstream of VEGF/Notch to repress arterial phenotype	(You et al., 2005)
Ephrin/Eph receptor pathway	-Cell surface markers differentially expressed in veins and arteries -ephrin B2 as arterial marker -EphB4 as venous marker	(Adams et al., 1999; Fish and Wythe, 2015; Pasquale, 2005; Wang et al., 1998)
Hey/Hes transcription factors	-Notch-regulated -Regulate ephrin/Eph expression	(Fish and Wythe, 2015; Wiese et al., 2010)

Table 1.1: Molecules and pathways involved in arteriovenous specification.

It seems clear that Notch signalling is integrated in several pathways and plays a central role in arteriovenous specification. Understanding the precise series of event leading to arteriovenous specification is key to reproduce this complexity *in vitro*.

Apart from the molecular and morphological identity, veins and arteries are also facing a different environment responsible for differences in metabolism, biochemical or proliferation pattern of the endothelial cells.

The most obvious difference faced by arterial and venous endothelial cells is the changes in hemodynamic forces and mechanical forces. Shear stress is linked to maturation of endothelial progenitors and arterial specification, by inducing Notch-related signalling (Obi et al., 2009). Recently, the effects of shear stress on endothelial proliferation status and arteriovenous specification have been highlighted by studies on cell cycle (Fang et al., 2017). It is established that shear stress is responsible for Notch activation and maintaining a high Notch signalling in arteries, but it also plays a role in cell cycle arrest via cell cycle inhibitors, enabling the specification of EPCs into aECs (W. Luo et al., 2021). Recent studies on endothelial metabolism have highlighted new potential pathways that could be implicated in arteriovenous specification (Eelen et al., 2015). For example, fatty acid oxidation flux are more important in aECs than vECs and glycolysis disruption has been linked to defects in blood vessel formation and specification as well as angiogenesis (Eelen et al., 2015).

In conclusion, endothelial cells are a heterogeneous cell population that continuously adapt to their environment to maintain body homeostasis. The mechanism of arteriovenous specification is a complex process involving genetic programming, biochemical as well as mechanical forces. Even if the genetic programming seems important in the process of arteriovenous specification, it is not enough to commit endothelial cells, as shown by chimeras studies where arterial and venous EC could repopulate both veins and arteries and remain plastic until late in the development of the embryo (Moyon et al., 2001).

5- <u>**Stem cells in vascular biology**</u>

Vascular cells culture has been used for decades to study EC and mural cells biology, but cultures of primary cells *in vitro* have well-known limitations. Heterogeneity of blood vessels can be assessed *in vitro* by culturing organ-specific EC, pericytes or smooth muscle cells but they lose their phenotype rapidly upon *in vitro* passaging. One of the solutions is to study these aspects directly *in vivo* but these are expensive, can be hard to investigate and implicate ethical issues.

Stem cell technology and the discovery of induced pluripotent stem cells have opened the way toward the differentiation and use of stem-cell derived vascular cell to create *in vitro* models of blood vessel (Takahashi and Yamanaka, 2006). The ability to use embryology knowledge and apply it into stem cell differentiation will provide new insights into the processes of vasculogenesis and angiogenesis in the earliest phases of development and this knowledge is key to the creation of organ-specific vascular cells and to study their role in organ development and disease progression.

Furthermore, knowledge regarding vascular cells differentiation and functions is a key to develop better tissue engineering strategies. With blood vessels mainly composed of ECs, pericytes and smooth muscle cells and the heterogeneity of these blood vessels coming from all these different cell sources (although mainly from ECs), we will review the different approaches to derive stem cells into vascular cells and the current ability to obtain organ-specific vascular cells.

a. Differentiation protocols
i. Stem cell-derived endothelial cells

Endothelial cells play the main role of maintaining homeostasis by filtering blood and allowing passage of solutes throughout the body and insures immune surveillance via a close interaction with immune cells. EC diversity across and within organs is directly linked to their functions and essential for proper organ function as described above (Nguyen et al., 2021). For tissue engineering purposes, having appropriate EC population seems to be essential. But until now, most EC used in tissue engineering approaches have been primary cells (HUVEC as gold standard) that poorly recapitulates tissue specific aspects. Stem cell technology allows the study of blood vessel development and could allow the differentiation of organ-specific ECs tailored to the organ of interest (Augustin and Koh, 2017; Marcu et al., 2018; Rafii et al., 2016).

The first use of PSCs differentiation into endothelial cells have been described 2 decades ago (Levenberg et al., 2002; Yamashita et al., 2000) with the intent of creating *in vitro* vascular

models using embryonic stem cells. Several differentiation protocols, using hESC and hiPSC have since been created to derive PSCs into ECs, with different uses, as described in table 1.2.

EC Stem cell model	Differentiation	Use	Reference
hESC-derived ECs	2D differentiation	Flk1-positive cells from embryonic stem cells, characterisation and contribution to vasculature *in vivo*	(Yamashita et al., 2000)
hESC-derived ECs	EB formation	hESC-derived EC from embryoid bodies characterised *in vitro* and implanted into mice.	(Levenberg et al., 2002)
hESC and hiPSC-derived ECs	OP9 differentiation	Characterisation and tube formation assay.	(Taura et al., 2009)(Choi et al., 2009)
hiPSC-derived EC	2D differentiation	CADASIL patient-specific iPSC-derived ECs to study the disease in co-culture with iPSC-derived MCs	(Kelleher et al., 2019)
hiPSC-derived ECs	EB in suspension	Phenotyping, inflammatory response, leucocyte adhesion, cytokine production and leucocyte transmigration	(Adams et al., 2013)
hESC and hiPSc-dervied arterial and venous EC	2D differentiation	Venous and arterial specific gene expression and function through xeno-free differentiation.	(Zhang et al., 2017)
hESC and hiPSC-derived 3D organoids containing ECs and PCs	Cell aggregates to create vascular organoids	Transplantation in mice to study diabetic vasculopathy. Deciphering effects of diabetes on vascular function.	(Wimmer et al., 2019)
hESC-derived EC	Brain organoids	Transplantation of brain organoids with embedded hESC-derived EC overexpressing ETV2	(Cakir et al., 2019)
hiPSC-derived brain microvascular EC	2D differentiation	Used in perfused microvessels to study shear, permeability and inflammatory response	(Linville et al., 2019)
hESC and hiPSC-derived ECs	2D differentiation	Used in the treatment of hind-limb ischemia embedded in extracellular matrix gel.	(Lee et al., 2017)
hESC and hiPSC-derived ECs	2D differentiation	Characterisation, gene expression, metabolomic profile and functional properties.	(Patsch et al., 2015)
hPSC-derived ECs	2D differentiation	Isolation, characterisation and functional evaluation of PSC-EC.	(Orlova et al., 2014)
hESC and hiPSC ECs	EB differentiation followed by 2D expansion	Co-implantation of hPSC-derived EC and iPSC to treat murine ischemic limb	(Dar et al., 2012)
hESC-derived ECs	2D differentiation	hESC-derived EC specification towards liver specific EC with transcription factor overexpression	(De Smedt et al., 2021)
hESC and hiPSC ECs	2D differentiation	iPSc-ECFC resembling cord blood ECs, used to repair ischemic mouse retina and limb.	(Prasain et al., 2014)

hiPSC-derived ECs	2D differentiation	iPSC-EC model of patient with pulmonary hypertension	(Gu et al., 2017)
hESC and hiPSC ECs	EB differentiation	Liver-specific PSC-derived EC characterised and used in intrahepatic transplantation.	(Gage et al., 2020)
hESC and hiPSC ECs	2D differentiation	hPSC-derived BBB-specific ECs phenotyping and barrier properties study.	(Lippmann et al., 2012)
hESC and hiPSC ECs	2D differentiation	Chemically defined differentiation of vEC and aEC and characterisation	(Rosa et al., 2019)
hiPSc-EC	Embryoid body formation	aEC specialisation through flow conditioning	(Sivarapatna et al., 2015)
hESC and hiPSC ECs	Cell aggregate	ECs in heart-forming organoids	(Drakhlis et al., 2021)
hESC and hiPSC ECs	2D differentiation	Cardiac EC and cardiomyocytes co-differentiation	(Giacomelli et al., 2017)
hESC and hiPSC ECs	Intestinal organoids	Intestinal EC co-differentiation in intestinal organoids and transcriptional characterisation	(Holloway et al., 2020)
hESC and hiPSC ECs	Kidney organoids	Kidney EC co-differentiation in kidney organoids.	(Low et al., 2019)
hiPSC-EC	Embryoid body formation	Choroidal EC differentiation and characterisation	(Mulfaul et al., 2020)
hiPSC-EC	2D differentiation	iPSC-EC used in a retinal pigment epithelium-choriocapillaris complex	(Manian et al., 2021)
hESC and hiPSC ECs	2D differentiation	iPSC-derived EC from cardiogenic and hemogenic mesoderm.	(Palpant et al., 2017)

Table 1.2: Existing differentiation protocols to create endothelial cells from PSCs and their use.

The advent of iPSC technology (Takahashi and Yamanaka, 2006) allowed the generation of patient-specific ECs (Gu et al., 2017), and the ability to create models of genetic diseases *in vitro.* Diverse range of techniques have been used and described to differentiate ECs, either in 2D or 3D, using knowledge from embryology and cocktails or growth factors and cytokines to derive PSC into mesodermal progenitors and then further differentiate into ECs. Markers and functional characterisation of PSC-derived ECs are described in following paragraph/chapters. Angiogenesis models represent important tools to study vascular function, cancer vascularisation or vascular development (Bentley et al., 2014; Malinda, 2009; Nowak-Sliwinska et al., 2018; Potente et al., 2011) but usually employ primary ECs. Such assays can be repurposed using stem cell-derived vascular cells to decipher molecular pathways involved in physiological and pathological angiogenesis (Gu et al., 2017; Kelleher et al., 2019; Taura et al., 2009; Wimmer et al., 2019). hiPSC-ECs can also be a useful model to study EC behaviour and cell-cell interaction in 2D, for example inflammatory response, leucocyte adhesion, vascular permeability or immune cell transmigration (Adams et al., 2013; Linville et al., 2019; Zhang et al., 2017) or serve as a model for pharmacological studies to create appropriate disease models or study anti-angiogenic drugs.

Furthermore, hiPSC-EC are being investigated as a solution to create vascular grafts, tissue-engineered blood vessels and alternative in transplantation for ischemic diseases, with proof-of-concept in mice studies (Lee et al., 2017). The translational use of these cells have increased the interest to develop differentiation protocols in absence of animal-derived factors (Zhang et al., 2017).

One of the limitations of stem cell differentiation is the heterogeneity in cells created as well as their degree of maturation (Paik et al., 2018). To improve maturation of PSC-derived ECs, different approaches have been attempted. Functional improvement has for example been described following glycocalyx formation as a result of mitochondrial maturation (Tiemeier et al., 2019). Overexpression of transcription factors involved in EC differentiation such as ETV2 have been used to create more homogeneous EC population and with higher yield (Cakir et al., 2019; De Smedt et al., 2021). This technique also allows the organ-specific maturation of ECs, which is of most importance for tissue-engineering purposes, with overexpression of tissue-specific transcription factors or EC integration in organoids (Cakir et al., 2019; De Smedt et al., 2021; Nguyen et al., 2021). The need for appropriate *in vitro* disease models and to decipher molecular mechanisms involved in organ-specification has been addressed with the creation of protocols to attempt generating diverse organ-specific EC populations. Arteriovenous specification (Arora et al., 2019) has been achieved with different VEGF concentrations (Rosa et al., 2019), NOTCH pathway activation (Zhang et al., 2017) or through the flow conditioning (Sivarapatna et al., 2015). Lately, exciting models of organ-specific iPSC-EC have also been described using co-differentiation of endogenous EC populations in models of retinal pigment epithelium-choriocapillaris complex (Manian et al., 2021), kidney organoids (Low et al., 2019) or intestinal organoids (Holloway et al., 2020).

The creation of organ-specific EC is of great value to study angiocrine signalling and the role of capillaries in organ development, but more complex models will be needed to create vascularised tissues that withstand flow and recreate *in vivo*-like environment, including perivascular populations.

ii. Stem cell-derived pericytes

Pericytes play an important role in the vessel stabilization and development, especially of small calibre blood vessels (Armulik et al., 2011; Teichert et al., 2017). Depending on their spatial localization, they have diverse origins as described earlier, from mesodermal to neural crest progenitors (Asahina et al., 2011; Korn et al., 2002; Yamazaki et al., 2017; Yamazaki and

Mukouyama, 2018). Functions of pericytes also differ depending on the organ, with implication in blood flow regulation in the brain (Hall et al., 2014) to tissue repair in multiple organs (Crisan et al., 2008; Göritz et al., 2011).

As described earlier, pericytes form a very heterogeneous population and can also give rise to different lineages such as mesenchymal stem cells (Crisan et al., 2008), adipose progenitors (Tang et al., 2008), myogenic progenitors (Dellavalle et al., 2007) or fibrotic fibroblasts (Göritz et al., 2011). Their shared markers with other stromal cells (i.e PDGFR-B)(Armulik et al., 2011) has made their study difficult but new insights into their development with PSCs can help decipher their unique role. As for ECs, this heterogeneity can be reproduced with the integration of developmental processes in protocols to differentiate PSCs to PCs (Table 1.3).

PC Stem cell model	Differentiation	Use	References
hESC and hiPSC Pericytes	2D differentiation	iPSC-PC from mesoderm and neural crest intermediates from healthy and AD patients. Gene expression and barrier properties	(Faal et al., 2019)
hiPSc and hESC-derived perivascular cells	2D differentiation	hiPSc/hESC- derived pericytes in comparison to hiPSC-SMCs (morphology, gene expression and phenotypes)	(Wanjare et al., 2014)
hESC and hiPSC-derived 3D organoids containing ECs and PCs	Cell aggregates to create vascular organoids	Basement membrane ECM secretion and EC-PC interaction in healthy and diabetic models.	(Wimmer et al., 2019)
hESC and hiPSC Pericytes	Semisolid colony forming followed by 2D differentiation	iPSCs were derived into capillary and arteriolar type PCs and functionally characterised.	(Kumar et al., 2017)
hPSC-derived ECs	2D differentiation	Isolation, characterisation and functional evaluation of PSC-EC.	(Orlova et al., 2014)
hESC and hiPSC-PCs	EB differentiation followed by 2D expansion	Co-implantation of hPSC-derived EC and iPSC to treat murine ischemic limb	(Dar et al., 2012)
hiPSC-derived PCs	2D differentiation	Rapid differentiation of iPSC-PC along with iPSC-EC, characterised by flow cytometry, immunofluorescence and functional assays.	(Aisenbrey et al., 2021)
hiPSC-derived PCs	2D differentiation	hiPSC-PC and EC in 2D and 3D to create a BBB model and assess permeability	(Jamieson et al., 2019)
hESC and hiPSC Pericytes	2D differentiation	Creation of a BBB model with iPSC-derived EC, PC and astrocytes. In-depth characterisation amyloid accumulation study and the role of pericytes in cerebral amyloid angiopathy progression.	(Blanchard et al., 2020)
hESC and hiPSC Pericytes	2D differentiation	Neural crest stem cell-derived PCs to create a BBB model.	(Stebbins et al., 2019)

Table 1.3: Existing differentiation protocols to create pericytes from PSCs and their use.

Due to their close relation with ECs, protocols differentiating ECs can also be used to get a population of mesodermal progenitors that can be sorted and then expanded into pericytes

(Aisenbrey et al., 2021; Dar et al., 2012; Orlova et al., 2014) or co-differentiated in 3D microenvironments (Blanchard et al., 2020; Wimmer et al., 2019). Pericytes can also be differentiated on their own, via mesodermal or neural crest progenitors as described previously (Faal et al., 2019; Jamieson et al., 2019; Kumar et al., 2017; Stebbins et al., 2019; Wanjare et al., 2014). Markers and functional characterisation of PSC-derived PCs are described in following chapters/paragraphs.

Similarly to EC differentiation protocols, PCs can be differentiated and specialised to acquire organ specificity and phenotype variety as found *in vivo*. Kumar et al. described a protocol to differentiate PSC into PCs from a mesodermal precursors into capillary and arteriolar types (Kumar et al., 2017). By modulating PDGF, EGF, TGFβ and VEGF signalling, PCs were matured into Desmin/SMA low NG2+/CD274+ PCs, described as capillary PCs and exhibiting a pro-inflamatory phenotype, or Desmin/SMA high NG2+/DLK1+ PCs, described as arteriolar PCs with a more contractile phenotype.

PCs can also be matured towards organ-specific phenotypes, with growing interest from the field in brain-specific PCs due to their central role in CNS function (Armulik et al., 2010; Hall et al., 2014; Jeske et al., 2020). Neural-crest derived PCs have been described in the context of Alzheimer's disease with the differentiation of pericytes from APOE3/4 mutations allowing the modelling of amyloid accumulation *in vitro* (Blanchard et al., 2020; Faal et al., 2019). The creation of adequate blood-brain barrier models is also of great interest due to the BBB role in CNS function and drug permeability. Pericytes play a central role in the formation and function of the BBB and are essential for the tight junctions responsible for selective permeability in the CNS vasculature (Armulik et al., 2010; Hall et al., 2014). Creating appropriate models to study such processes led to an increased interest in brain-specific pericytes to integrate into artificial models of healthy BBB (Jamieson et al., 2019; Stebbins et al., 2019) or decipher mechanisms responsible for pathological conditions such as Alzheimer's disease (Blanchard et al., 2020).

Recent interest into mural cell biology and their function in organ-specific functions is increasing our knowledge on how specific cell types interact in health and disease, with RNA-sequencing allowing population discrimination at the single cell level (Vanlandewijck et al., 2018). Nonetheless, work remains to study the differences between perivascular cells (Wanjare et al., 2014) and understand their specific role in development to recreate appropriate *in vitro* models including ECs, PCs and SMCs.

iii. Stem cell-derived smooth muscle cells

Smooth muscle cells represent the major perivascular cell population in big blood vessels and arteries. Their roles include ECM deposition, vessel stabilisation and blood flow regulation. Their heterogeneous origin has also been described earlier and gives rise to a very diverse blood vessel coverage (G. Wang et al., 2015). SMCs are composed of cells with different functions, with contractile SMCs, responsible for vessel contraction, and synthetic SMCs responsible for cell repopulation and ECM deposition. To reproduce adequate models of SMCs *in vitro*, several differentiation protocols of PSCs into SMCs have been developed (Table 1.4).

PSC-derived SMCs have mostly been differentiated through 2D culture, to obtain a relatively pure and scalable population of cells. As for PCs, SMCs have been derived in parallel to ECs through a mesodermal intermediate (Patsch et al., 2015). SMC maturation was induced by adding of PDGF-BB, serum or TGFB-1 in the culture medium (Cheung et al., 2012; Wanjare et al., 2014).

To reproduce the embryonic heterogeneity observed *in vivo*, several studies have shown the possibility to differentiate SMCs from different mesodermal lineage or the neurectoderm (Cheung et al., 2012; Kelleher et al., 2019). This allowed the opportunity to create better disease models such as a CADASIL (Cerebral Autosomal Dominant Arteriopathy with Sub-cortical Infarcts and Leukoencephalopathy) with iPSC possessing a NOTCH3 mutation and leading to several vascular malfunctions (Kelleher et al., 2019). iPSC-derived SMCs have also been able to recapitulate premature senescence in a model of progeria (Liu et al., 2011) or recapitulate the pathology seen in Marfan aortas such as defects in ECM production, contraction or increased apoptosis (Granata et al., 2017).

With the importance of SMCs in the creation of blood vessel for tissue engineering purposes, protocols using only chemically defined conditions have also been developed and yielded sufficient amounts of iPSC-SMCs (Cheung et al., 2012). Although some reports have claimed the possibility to create tissue engineered vascular grafts using hiPSC-derived vascular cells (J. Luo et al., 2020), most of the protocols still yield an immature population of SMCs and investigations are needed to increase the yield and function of stem cell-derived vascular cells.

SMC Stem cell model	Differentiation	Use	References
hESC-derived ECs and mural cells	2D differentiation	Flk1-positive cells from embryonic stem cells, characterisation and contribution to vasculature *in vivo*	(Yamashita et al., 2000)
hiPSC- MCs	2D differentiation	CADASIL patient-specific iPSC. Co-culture with ECs to study EC-MC interaction as well as growth factor secretion.	(Kelleher et al., 2019)
hiPSc and hESC-derived SMCs	2D differentiation	hiPSc/hESC- derived synthetic and contractile vascular smooth muscle cells with assessed functionality.	(Wanjare et al., 2013)
hiPSc and hESC-derived perivascular cells	2D differentiation	hiPSc/hESC- derived synthetic and contractile vascular smooth muscle cells in comparison to hiPSC-PCs (morphology, gene expression and phenotypes)	(Wanjare et al., 2014)
hESC and hiPSC-derived SMCs	2D differentiation	Characterisation, gene expression, metabolomic profile and functional properties.	(Patsch et al., 2015)
hiPSC-derived vSMCs	2D differentiation	Hypertension cohort patient-derived iPSC differentiated into vSMCs characterised and studied for contractile function.	(Biel et al., 2015)
hESC and hiPSC-derived SMCs	2D differentiation	Stem-cell derived SMC from different embryological lineages were differentiated. Their functionality, response to cytokines activity against *ex vivo* SMCs were investigated.	(Cheung et al., 2012)
hiPSC-derived SMCs	2D differentiation	SMCs were derived from iPSC obtained from patients with Marfan syndrome. iPSC-SMC were able to recapitulate the pathology and were extensively characterised.	(Granata et al., 2017)
hESC and hiPSC-derived SMCs	2D differentiation	SMCs were derived from iPSC obtained from patients with Hutchinson–Gilford progeria syndrome (HGPS)	(Liu et al., 2011)
hESC and hiPSC Pericytes	Semisolid colony forming followed by 2D differentiation	iPSCs were derived into mature SMCs and functionally characterised.	(Kumar et al., 2017)
hiPSC-derived vSMCs	2D differentiation	Large scale generation of iPSC-vSMCs to create tissue-engineered vascular grafts	(J. Luo et al., 2020)
hiPSC-derived vSMCs	2D differentiation	Xenogenic-free hiPSC-derived vSMCs characterised for gene expression and cellular functions.	(J. Luo et al., 2021)
hiPSC-derived vSMCs	EB differentiation followed by 2D culture	Fully characterised hiPSC-vSMCs used to create TEVBs	(Gui et al., 2016)

Table 1.4: Existing differentiation protocols to create SMCs from PSCs and their use.

Overall, several studies have shown the ability to reproduce stages of embryonic development to differentiate stem cells in vitro and create vascular and perivascular cells. However, as seen by the number of different protocols published, reproducing these results in different labs and

recreating mature population of stem cell derived vascular cells has proven challenging. Although there is no doubt on the ability to produce relatively mature populations of ECs and perivascular cells, most of the effort is now focused on the creation of organ-specific cells that will be able to recreate a functional microenvironment and support organ growth. The main challenge remains recreating the appropriate environment to induce the differentiation of ECs and vascular cells towards and organ-specific phenotype. Since recreating *in vitro* the exact conditions of differentiation in vivo is almost impossible (length, cell interaction, medium composition…), studies have tried to bypass some of these aspects to push their stem cell derived progenitors towards maturity. The most common strategy to obtain a tissue-specific signature in vascular cells has been the overexpression of certain transcription factors involved in development as shown in the creation of stem cell derived liver-specific endothelial cells (De Smedt et al., 2021; Gómez-Salinero et al., 2022). Other studies have shown the ability of vascular cells to mature towards an organ-specific phenotype by co-culturing these cells to recreate an adequate 3D micro-environment (Blanchard et al., 2020; Giacomelli et al., 2017; Kumar et al., 2021; Low et al., 2019). However, even with the expression of tissue-specific markers by ECs or perivascular cells, these cells often lack functional maturation and cannot yet replace primary cells. Obtaining fully mature organ-specific vascular cells derived from stem cells is a key challenge for the next years considering the importance of these cells in organ development and function. To achieve this, several strategies will have to be combined such as the optimisation of cell culture conditions, 3D microenvironments, biomechanical properties and functional maturation.

b. Phenotyping of vascular cells

Phenotyping primary, stem and differentiated cells is key to evaluate cell functions and changes in response to perturbations. In the field of vascular biology, standard low-throughput techniques including gene and protein expression analyses (qRT_PCR, western-blot) have provided many insights into the biology of vascular cells.

Typical assays rely on 2D cultures and the first readout to appreciate the efficiency of the EC differentiation is cell morphology, with the specific cobblestone-like structure of endothelial cells (Haudenschild, 1984; Jaffe et al., 1973). Recognising PCs or SMCs only with their morphology in culture is not as straightforward as for ECs due to their shared morphology with other stromal cells such as fibroblasts with a big cell forming protrusions (Kumar et al., 2017; Orlova et al., 2014). Morphology can also be assessed at higher resolution and specifically with

SEM pictures of EC-specific junctions, revealing continuous or discontinuous endothelia (Aird, 2007a; Bazzoni and Dejana, 2004; Marcu et al., 2018).

To assess differentiation and measure the efficiency of the differentiation, gene expression techniques such as RT-qPCR or bulk RNA-seq are also useful (Chavkin and Hirschi, 2020; Chi et al., 2003; Cleuren et al., 2019; Goveia et al., 2020; Kalucka et al., 2020, 2020; Lukowski et al., 2019; Paik et al., 2018; Pasut et al., 2021).

Investigating system-level functions at different scales (cells, tissue organs or organisms) requires capturing information regarding system status in response to a variety of perturbations. To enable these analyses, high-throughout (HT) technologies such as SC-RNA-sequencing and HT imaging and image analysis have been developed.

High throughput stem-cell based drug screenings can be used to develop new drugs efficiently and at a reduced cost. 2D and 3D assays to assess specific aspects of vascular biology described above can be used as basis for image-based or OMICS screenings and these systems can be exposed to libraries of potential drug candidates. Lab automation technologies are facilitating the transition between low and high-throughput and currently allowing very high experimental throughput. In parallel analytical technologies must be developed to analyse very large datasets.

OMICS and next generation sequencing technologies have provided unprecedented insight into the transcriptional and epigenetic landscape underpinning cell functions and have highlighted phenotypic heterogeneity in cell populations previously thought to be homogeneous (Kalucka et al., 2020). OMICS has also provided key information regarding regulatory networks operating during EC differentiation (Kanki et al., 2017). However, gene expression studies have limited power to capture high level and dynamic functions such as angiogenesis and they are still relatively expensive.

Image-based screenings are emerging as a powerful technology to evaluate connection between cell phenotype and functions both of which can be defined by morphological or gene/protein expression criteria (Caicedo et al., 2017). Image-based screenings are ideally suited to study cell-cell relations and functions at defined timepoints or in time course experiments and the ability to assess multiple proteins and genes expression is constantly increasing. Several studies including large cohorts of patient-derived iPSCs have been studied through high content imaging to decipher variations in cell behaviour such as optimal ECM components for the differentiation of stem cells or iPSC line genetic variations leading to phenotypic variation between donors (Ong et al., 2018; Vigilante et al., 2019).

c. Markers and functional assays used in vascular cell differentiation

Directed differentiation of iPSC into vascular cells involves targeting key pathways involved in embryological development by recombinant growth factors/cytokines or small molecules treatment. The efficiency of differentiation is evaluated by cell phenotyping upon differentiation protocols of varying lengths (6 days to 1-2 months in culture). A typical first line of phenotype screening along differentiation protocols is low throughput gene expression analysis (e.g. by qRT-PCR) where certain genes are used as markers of SC, hemangioblasts precusrsors, EC, PC or SMC. The most common are listed in table 1.5.

Lineage	Marker	Function	Reference
EC markers	ETV2	-endothelial cell differentiation master regulator	(Lee et al., 2008; Park et al., 2005; Tsang et al., 2017)
	KDR (VEGFR2)	-receptor for VEGF	(Terman et al., 1992)
	CD31 (PECAM1)	-cell-cell adhesion protein found at the intercellular junction. -involved in leucocyte transmigration	(Albelda et al., 1990; Lertkiatmongkol et al., 2016)
	VE-Cadherin	-main intercellular junction protein -involved in angiogenesis and endothelial function	(Lampugnani et al., 2018, 1992)
	ERG	-late endothelial-specific transcription factor	(De Val and Black, 2009; Nikolova-Krstevski et al., 2009)
	vWF	-glycoprotein involved in hemostasis and blood vessel formation	(Aird et al., 1997; Randi et al., 2018)
	COUPTF-II	-transcription factor involved in venous phenotype identity	(Aranguren et al., 2013; You et al., 2005)
	NRP1-2	-membrane co-receptors for VEGF	(Fish and Wythe, 2015; Herzog et al., 2001; Mukouyama et al., 2005)

Brain-specific EC	Mfsd2a	-membrane lipid transport protein	(Ben-Zvi et al., 2014)
	Slc7a	-amino acid transporter	(Tărlungeanu et al., 2016)
Liver-specific EC	VEGFR3	-VEGF receptor	(Ding et al., 2010)
	Factor VIII	-blood clotting protein	(Ding et al., 2010)
	GATA4	-transcription factor essential for liver development	(Géraud et al., 2017)
Bone-specific EC	Endomucin	-mucin at the surface of ECs, expressed differently in subtypes of bone blood vessels	(Kusumbe et al., 2014)
Bone marrow-specific EC	Sca-1	-cell surface marker involved in haematopoiesis	(Itkin et al., 2016)
Lung-specific EC	CD166 (ALCAM)	-leucocyte cell adhesion molecule	(Gebb and Stevens, 2004; Goveia et al., 2020; Masedunskas et al., 2006)
Pericyte markers	NG2	-proteoglycan involved in proliferation and function	(Ozerdem et al., 2001; Schlingemann et al., 1996)s
	PDGFR-β	-cell surface tyrosine kinase receptor, involved in developmental processes	(Armulik et al., 2011, 2010; Hellstrom et al., 1999; Song et al., 2005)
	Desmin	-intermediate filament involved in cytoskeleton stability	(Hellstrom et al., 1999; Song et al., 2005)
	α-SMA	-actin protein essential for the contractile phenotype	(Alarcon-Martinez et al., 2018; Nehls and Drenckhahn, 1991)
	CD13	-transmembrane aminopeptidase	(Kunz et al., 2008)

	CD146	-cell adhesion molecule expressed by different vascular cells	(J. Chen et al., 2017; Crisan et al., 2008)
Smooth muscle cells markers	α-SMA	-actin protein essential for the contractile phenotype -higher expression than in PCs	(Gabbiani et al., 1981; Hellstrom et al., 1999; Smyth et al., 2018)
	Desmin	-intermediate filament involved in cytoskeleton stability -higher expression than in PCs	(Bolmont et al., 1990; Hellstrom et al., 1999; Smyth et al., 2018)
	SM22α	-Actin-binding protein involved in cytoskeletal organisation and vascular remodelling	(Duband et al., 1993; Feil et al., 2004)
	CNN1	-actin filament associated protein involved in contraction	(Duband et al., 1993)
	SM-MHC	-main contractile protein	(Miano et al., 1994)

Table 1.5: Markers used to characterise ECs, organ-specific ECs, PCs and SMCs.

The success of stem cell differentiation is often measured by assessing the expression of one or few of these markers, whether it is at the mRNA level or at the protein level. One of the main hurdles of directed stem cell differentiation is also the low yield of cells expressing the marker of interest after differentiation, resulting in a heterogeneous population of cells. In the example of EC differentiation, protocols often include a step of purification via the selection of cells expressing cell-surface markers such as CD31 or VE-Cadherin, via bead activated or fluorescence activated cell sorting (Zhang et al., 2017).

Although important to assess the efficiency of differentiation, gene expression or protein expression profiles might not reveal the full extent of maturation of cells. Several functional assays have been developed to evaluate the degree of maturation of stem cell-derived vascular cells. Common assays to assess EC maturation include the evaluation of key functions of the endothelium such as leucocyte adhesion (Filippi, 2019; Kalogeris et al., 1999; Rosa et al., 2019), nitric oxide production (Tousoulis et al., 2012), low density lipoprotein (LDL) uptake, response to shear stress, oxygen consumption or permeability (Adil and Somanath, 2020;

Zhang et al., 2017). Stem cell-derived EC should also be able to remodel to form function 3D structures and form perfusable vessels via vasculogenesis and angiogenic sprouting. These assays can be performed with only ECs in exogenous matrices (fibrin/collagen gel, bead assays, lumen formation assays) or in co-culture with other cells (PCs, SMCs, fibroblasts) to evaluate perivascular cell recruitment and vessel maturation (Giacomelli et al., 2017; Kumar et al., 2017; Nowak-Sliwinska et al., 2018). Assays assessing the phenotype of perivascular cells are fewer, with studies mainly focusing on cell-to-cell interactions and recruitment to the vessel (Kumar et al., 2017; Orlova et al., 2014; Stratman et al., 2009) or contractility phenotypes (Kumar et al., 2017). Ultimately, the maturation of stem cell-derived vascular cells is assessed by transplantation in animal models and observation of their integration in the host circulation (Malinda, 2009; Orlova et al., 2014; Samuel et al., 2013; Zhang et al., 2017).

Finding the right balance of biochemical and biophysical cues to generate mature stem cell-derived cells will be crucial for the creation of adequate disease models and tissue engineering purposes.

6- **Vascular tissue engineering**

The prevalence of cardiovascular and ischemic diseases leads to an urgent need of grafts and vessel replacement techniques as current models of artificial vascular grafts struggle to increase life expectancy. Furthermore, lack of proper vascularization is a common limitation of tissue engineering techniques and functional vascularisation is still missing in most models (Song et al., 2018).

The derivation of endothelial stem cells and the creation of blood vessels from stem cells aims at creating an alternative to coronary bypasses and could be a source of autologous grafts in the future as well as an alternative to primary cells to study blood vessel development and maturation. The stem cell technology is promising and holds great hopes for future clinical applications, but the lack of robust and reproducible differentiation still represents a barrier to recreate biomimetic iPSC model of tissue specific vasculature. Furthermore, current differentiation protocols still give rise to relatively immature cells and cannot yet replace donor cells.

a. Vascular tissue engineering and vascular grafts

As discussed above, differentiation protocols are important to create genetically programmed cells, but the maturation process of blood vessels *in vitro* will require to recreate the mechanical forces in place during organ development and homeostasis. Future vascular tissue engineering will also have to create custom non-immunogenic vascular grafts with a long life-span and low thrombogenicity. Several studies have shown the creation of synthetic tissue engineered vascular grafts, using different techniques such as layer by layer assembly, different scaffold methods and decellularized scaffolds (Chan et al., 2017), to create big vessels. Despite some success in the fabrication of grafts with primary cells or even with stem cells (Sundaram et al., 2013), some major challenges remain.

As mentioned above, all the protocols to differentiate stem cells used in these studies are serum-based, raising concerns about the immunogenicity. Furthermore, cells created poorly recapitulate arteriovenous specification or organ-specific maturation and fail to integrate the cell-cell contact with perivascular cells crucial for blood vessel maturation. Finally, the biomechanical properties of vascular grafts need to be optimized by implementing the right number of mural cells and endothelial cells in combination with extracellular matrix components as attempted by others (Gui et al., 2014). Failing to reproduce the appropriate environment could lead to the creation of grafts that can't withstand biomechanical cues *in vivo*.

The vasculature is composed of a hierarchical network of blood vessels and it seems obvious that engineering arteries and veins as well as big vessels (>1cm) represent a different challenge compared to engineering microvasculature (<1mm) (Song et al., 2018), not only in term of cell and layer composition, but also in the differences that those vessels experience in the body. For clinical applications as well as tissue engineering purposes (disease modelling, organ-on-a-chip) and more fundamental studies into blood development and regeneration, it is important to create models composed of both mature micro and macro-vasculature.

b. 3D models of blood vessels

Among all the different factors involved in blood vessel maturation, fluid shear stress appears to be essential (Fang et al., 2017; Obi et al., 2009). Not only blood flow is essential for EC to acquire and maintain their phenotype (Mack et al., 2017), but it is also central in the maturation of vasculature to modify the vascular tree and respond to stimuli. Applying the right mechanical forces *in vitro* requires to be able to control and regulate the volume and pressure of flow

entering the circulation. In order to recreate the three-dimensional microvasculature environment, several groups have used tissue engineering techniques and microfluidics (Fig. 1.11)(M. B. Chen et al., 2017; Haase and Kamm, 2017; Hachey et al., 2021; Hasan et al., 2014; Song et al., 2018; Wang et al., 2016). Vascular tissue engineering techniques include top-down methods aiming at creating an artificial environment mimicking the blood vessel, usually by moulding cylinders of different sizes, with or without ECM components, and allow endothelial cells to coat those channels (Fig. 1.11A-C). Bottom-up techniques include cell embedding in custom hydrogels, with or without co-culture to induce ECM production, as well as bioprinting methods. These methods aim at leaving the cells shape their own vasculature system (Fig. 1.11D-I).

While some studies use top-down techniques to create tubular-like structures that resemble blood vessels and are immediately perfusable, they are not able to recreate autonomous anastomosis between endothelial cells and a proper microvasculature, neither arteriovenous specification (M. B. Chen et al., 2017; Zheng et al., 2012). Regarding bottom-up studies (Wang et al., 2016), while sprouting and anastomosis are achievable and lumen formation allows a proper flow circulation, the microvasculature assembly requires a long time, is random and results in an heterogenous population of cells. An optimized method could be developed by combining these two techniques.

Furthermore, the vascular maturation process is key to achieve biomimetic vessels *in vitro*. This implies that models need to integrate mural cells and allow arteriogenesis as well as support a flow similar to the blood flow *in vivo*. Studies have demonstrated the possibility to add primary pericytes in the same environment as endothelial cells (M. B. Chen et al., 2017; Zheng et al., 2012), resulting in pericytes surrounding the vessels and enhancing the permeability properties of the endothelium. Nevertheless, studies using functional and mature stem cell-derived vECs, aECs and pericytes in microfluidic devices have not been yet reported.
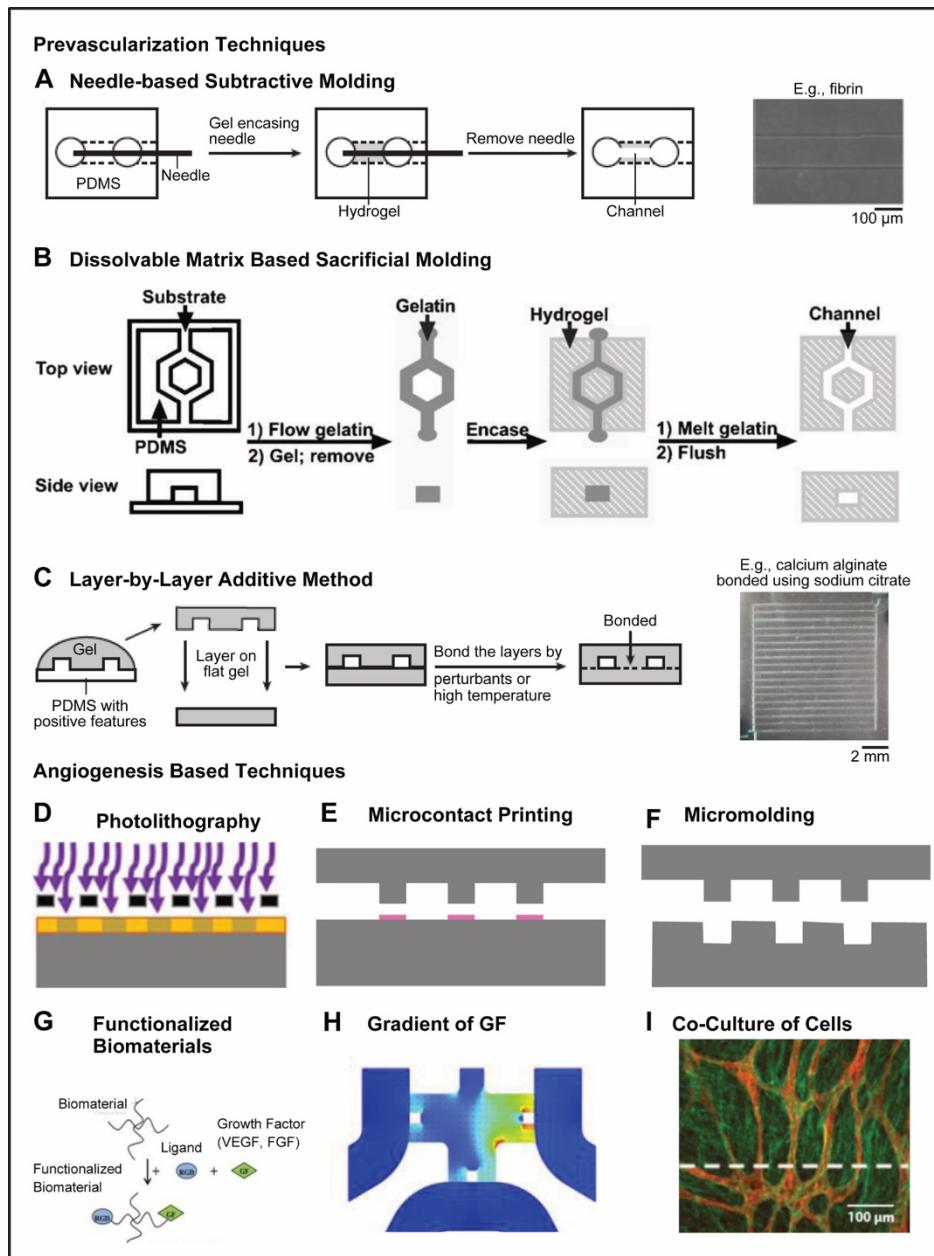
Figure 1.11: Summary of microvasculature tissue engineering techniques (Hasan et al., 2014). Prevascularization techniques are top-down techniques consisting in creating a mould, with prefabricated vessels in which cells are seeded, by subtractive (A, B) or additive methods (C). Vasculogenesis or angiogenesis-based techniques are bottom-up techniques consisting in creating scaffolds or hydrogels that will enable the cells to create their own microvascular network. Among those techniques are printing techniques as well as bioprinting (D, E, F), functionalization of biomaterials (G), microfluidic devices to create gradient of growth factors (H) or co-culture of cells (I).

Finally, although studies have shown the positive effect of shear stress and flow on arterial specification and maturation (Fang et al., 2017; Obi et al., 2009), little is known about the synergetic effect of shear stress and genetic programming on arterial specification and maturation.

7- **Microfluidic systems**

Microfluidic devices are miniaturised chips containing microchannels and chambers used to study fluid dynamics in a constrained environment. They are linked to the macro-environment by different holes and tubing that are often necessary to control the fluid pressure, temperature or composition. Microfluidic systems represent an exciting field in regenerative medicine as they can be coupled with tissue engineering techniques and biomaterial fabrication to achieve a more complete blood vessel model including the right cell types and biomechanical cues (Hasan et al., 2014). Indeed, microfluidic devices allow the introduction of a custom flow, can be easily adapted, scaled up or down and allow to control growth factor concentration and cell behaviours as well as biomechanical forces. Ideally a microfluidic chip for blood vessel formation and maturation will require both capillaries to create microvasculature as well as venules and arteries to create a biomimetic vascular hierarchy. To date, protocols to create vasculature *in vitro* are incomplete due to their inability to create a biomimetic and continuously perfusable vasculature for a very long term.

a. **Development of microfluidic devices and current techniques used in vascular tissue engineering**

Development of appropriate platforms for the creation of vascularised tissues is key to achieve long term culture and perfusion. The creation of vascularised tissues has been at the centre of interest for decades in the field of tissue engineering. Techniques to introduce a vascular components in tissue engineered constructs have been used for more than two decades ago (Borenstein et al., 2002).

Early attempts to integrate blood vessel structure into tissues constructs either for tissue engineering purposes or *in vitro* modelling consisted in the introduction of biodegradable sheets of polycaprolactone (PCL) or poly(lactic-co-glycolic) acid (PLGA) into 3D constructs but revealed complicated to perfuse (Du et al., 2008; King et al., 2004).

The development of hydrogel engineering and the ability to create 3D microenvironments in ECM allowed the creation of sacrificial moulding (Fig. 1.11B) as a model of vascular network (Golden and Tien, 2007). These techniques, called pre-vascularisation techniques were first used to create channels that can be coated with ECs and perfused (Fig. 1.11A-C), but these models lack vascular hierarchy and remodelling.

i. Photolithography and soft lithography

The development of photolithography and soft lithography has accelerated the creation of complex models incorporating a vascular component.

Photolithography is used to create features of desired size and shape on a variety of substrates (mainly Silicon wafers). Photolithography consists in the exposure of a photosensitive polymer to a light with a designated wavelength through a mask. After washing of the polymer, the polymerised pattern emerges leaving an image of the mask (Fig. 1.12a-c). This technique has been developed for the microfabrication of computer chips for example. It has been used for the creation of blood vessel models *in vitro* but has several limitations such as its cost and the limited sizes of features (Cokelet et al., 1993).

Soft lithography techniques have been created to resolve these issues and create cheap and high quality microfluidic devices (Shin et al., 2012; Whitesides et al., 2001; Xia and Whitesides, 1998). It consists in the use of an elastomeric material (most likely PDMS, polydimethylsiloxane) moulded onto a wafer with the desired pattern and then peeled to obtain a microfluidic device (Fig. 1.12d-f). This method allowed the creation of several identical chips for a low cost and down to the nanometre scale (Whitesides et al., 2001).

PDMS is the most commonly used elastomer to create LOC devices due to its elastic behaviour and its ability to create small microchannels. Furthermore, its transparency, ease of use, controllable stiffness, gas permeability and relatively low cost make it a perfect candidate for the fabrication of microfluidic devices. However, PDMS also has the disadvantage of absorbing small hydrophobic molecules and cannot be used for some applications. To solve this issue, several other alternatives to PDMS have been used for the creation of micro physiological systems (Campbell et al., 2021). For example, other types of elastomers have been used such as polystyrene, with relatively the same properties as PDMS with a lower absorption but at higher cost (Davenport Huyer et al., 2019). Recent advances in 3D printing have allowed the use of thermoplastics for the creation of LOC devices at relatively low cost but with low flexibility and transparency. Studies have also shown the possibility to assemble micro physiological systems with glass or other silicone monomers but these materials appear difficult to fabricate, non-flexible or non-permeable to gas (Harink et al., 2014; Hirama et al., 2019). Alternatively, hydrogels have been used alone without structures to host cells but lack mechanical integrity (Grigoryan et al., 2019).

The use of the Lab-on-chip devices at greater scale accelerated the development of hydrogel-based vasculogenesis and angiogenesis platforms. First created in photocrosslinkable gelatin methacrylate hydrogels (Y.-C. Chen et al., 2012), vascular networks with a functional lumen can now be associated with a microfluidic system (Chen et al., 2013; M. B. Chen et al., 2017; Hsu et al., 2013; Kim et al., 2013; Song and Munn, 2011). These platforms use ECs (with or without perivascular cells) embedded in hydrogels (mostly fibrin or collagen) and let them mature for few days to create tubular structures that can then be perfused by a pressure drop (via the use of syringe pumps mainly).
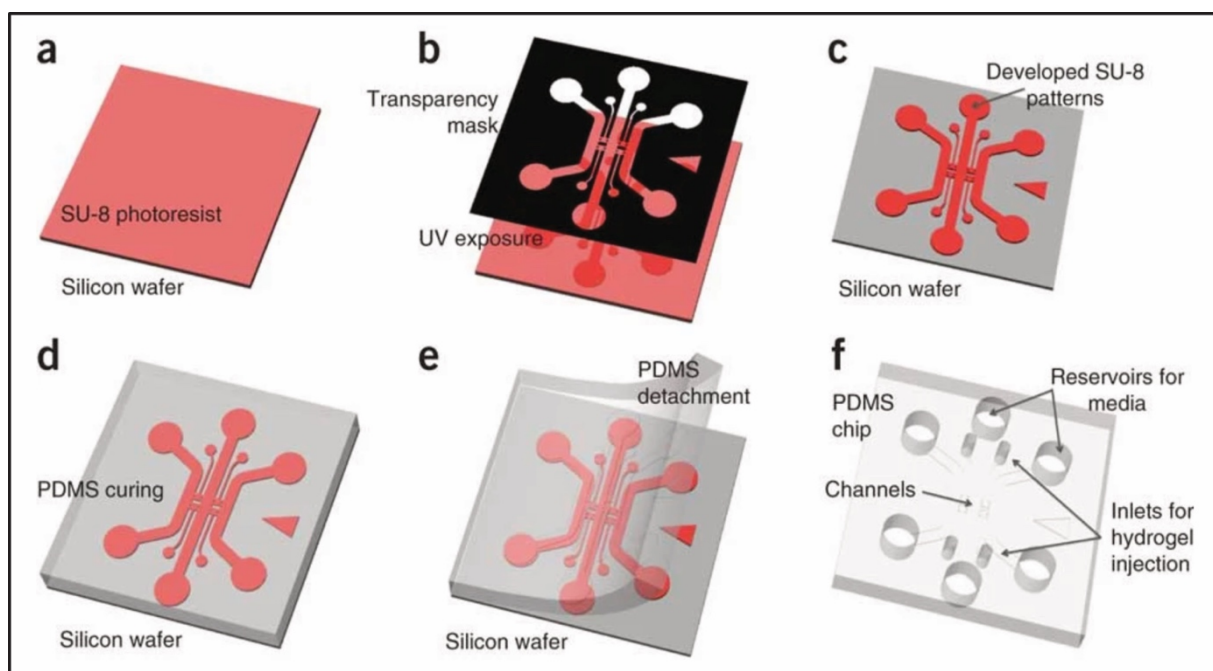
Figure 1.12: (a–f) Schematics of the photolithography (a–c) and soft lithography (d–f) procedures.(Shin et al., 2012) (a) SU-8 is spin-coated and prebaked on a bare wafer. (b) With a transparency photomask (black), UV light is exposed on the SU-8. (c) Exposed SU-8 is then baked after exposure and developed to define channel patterns. (d) PDMS mixed solution is poured on the wafer and cured. (e) Cured PDMS is then peeled from the wafer. (f) The device is trimmed, punched and autoclaved ready for assembly.

Since then, the creation of engineered microvascular networks has been extended to create several platforms to study tumor cell extravasation (M. B. Chen et al., 2017), permeability (Offeddu et al., 2019), vasculogenesis (Whisler et al., 2014), angiogenic responses (Kim et al., 2016) or organ-specific responses such as in the blood-brain barrier (Campisi et al., 2018). This technique still has some limitations such as the relative cost of the wafer created by photolithography, its low scalability and its poor flexibility (a wafer is needed each time the design needs to be adapted).

b. 3D printing and 3D-printed microfluidics
i. 3D printing techniques

First techniques used in 3D printing for additive manufacturing were used for industrial purposes. The rapid development of benchtop 3D printers and the creation of inexpensive printing materials (e.g., photo-polymerising resins and thermoplastic filaments) has made this kind of technology affordable for consumers and it is nowadays widely used by both industries and amateurs. The term 3D-printing encompasses several techniques (Fig. 1.13) but commonly described the conversion of a computer assisted design (CAD) into a 3D physical object.

The most common kind of 3D printers are using fused deposition modelling (FDM), where the object is printed layer by layer by deposition of a melted polymer (Fig. 1.13). FDM printers are relatively low cost and can be used to print big pieces of thermoplastic rapidly (up to 100mm/sec of extrusion, $\sim$ 5min for a 1cm^3 cube depending on the speed and infill settings). Other types of 3D printing include selective laser sintering to create metal/plastic objects via powdered metal/plastic sintering or adhesion layer by layer via laminated object manufacturing. Metal objects can also be cut and glued together layer by layer via laminated object manufacturing. More advanced techniques of 3D printing have also been created such as inkjet printing, using photocurable ink embedded in a support material.

Finally, to create objects with higher resolution than FDM printers, stereolithography printers have been created and optimised in the last decade to become very affordable for consumers. Stereolithography printers use a layer-by-layer approach using a photochemical process by which a laser beam crosslinks monomers and polymers in a resin bath. This technique using resin has been developed to create complex 3D printed models and refined from DLP (Digital Light Processing) printers using a light projector to more precise resin printers using SLA and laser beams, increasing the final resolution of the print. The different 3D printing techniques have distinct resolutions, with their use limited to specific purposes. Only the inkjet and stereolithography techniques can go down to 20μm, while the other techniques cannot go lower than 100μm resolution.

The recent advances in 3D printing manufacturing (Fig. 1.13) has allowed the possibility to lower down resolutions of prints at reasonable dimensions to produce microfluidic devices, especially with the introduction of digital light processing stereo-lithography (DLP-SLA) printers (Amin et al., 2016; Comina et al., 2014; Sanchez Noriega et al., 2021).
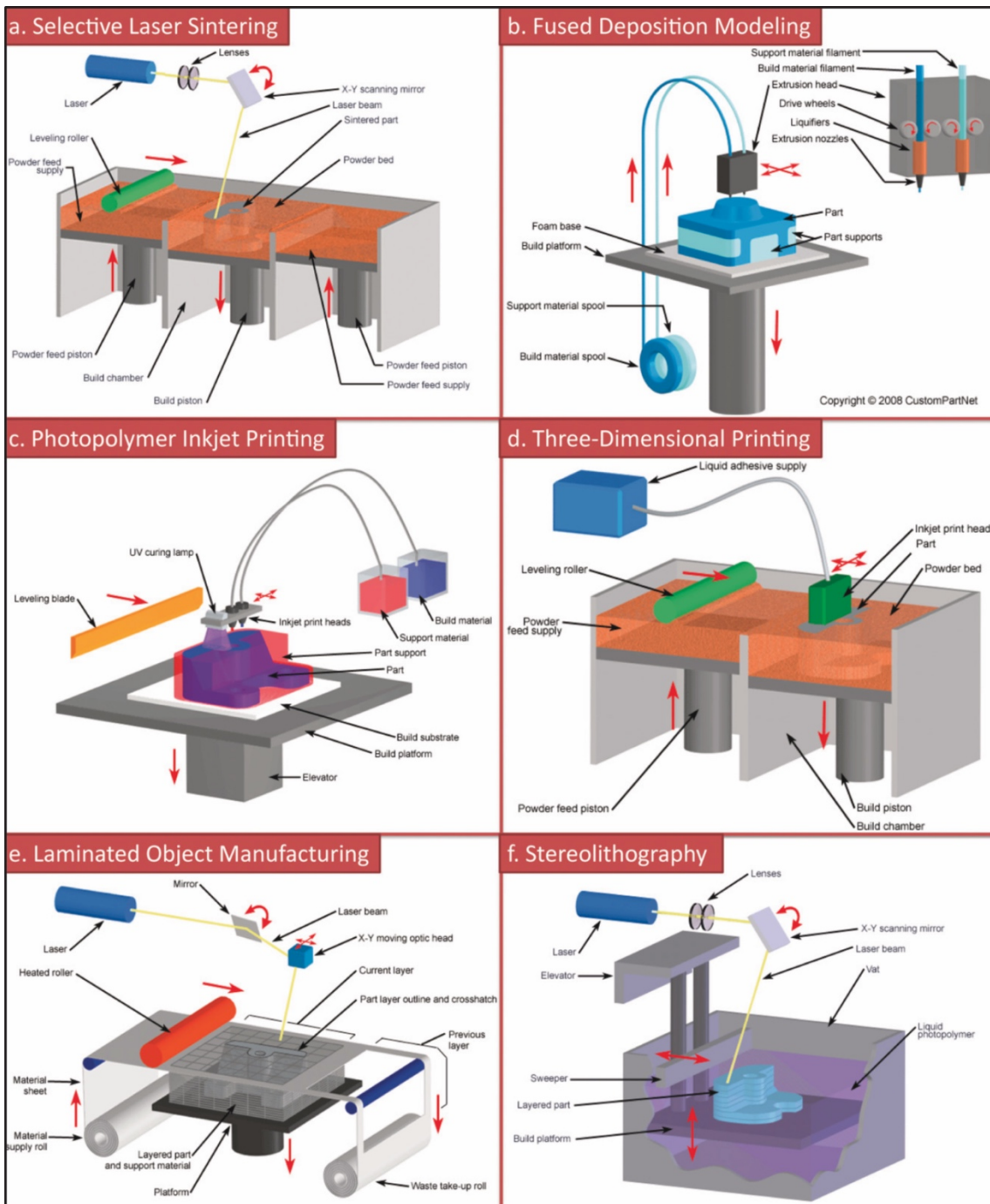
Figure 1.13: Different 3D printing techniques. (Au et al., 2016) A) Selective laser sintering using a powder bed. B) Fused deposition modelling using melted polymers. C) Photopolymer inkjet printing using a support and a photopolymerised build material. D) Three-Dimension printing, using the same process as selective sintering but with an adhesive to replace the sintering step. E) Laminated Object manufacturing, using laser cutting and layer assembling of materials. F) Stereolithography, using a light source to selectively polymerise layer by layer a curable material.

ii. 3D-printed microfluidics

Benchtop DLP-SLA 3D printers can be bought for few hundred pounds while conventional SU-8 photolithography (SU-8 PL, Fig 1.12) requires working in a clean room environment and uses expensive equipment (illuminators with mask alignment facilities, spin coater, silicon wafers for SU-8 photoresist) and extensive training. 3D printers can be used on the bench and prints can be processed with standard lab consumables, resulting in 3D printed templates costing usually less than £1 per unit against £100 minimum per wafer using SU-8 resin. Another advantage of the 3D-printed microfluidic templates is the ability to create thicker objects (several cm in height including features of varying heights) while SU-8 wafers must be very thin due to the spin coating and UV light penetration in the resin.

Despite these advantages, one current limitation of 3DP in comparison to SU-8 PL is the features resolution (min ~30 µm for commercial DLP 3DP and below 1µm for SU-8 PL). 3D printed microfluidic devices can also have features that vary between prints with individual printers giving different results depending on the resolution, speed of print or composition of the resin. Furthermore, due to the use of light processing, printers can lose in resolution with time due to a progressive loss in calibration or loss in transparency in the tank containing resin. These defects can induce differences in the layer thickness due to the diffusion of the laser and can lead to low material strength when very small features are printed.

Nonetheless, several studies have used 3D printing to create Lab-on-chip devices. 3D-printed LOC devices can be used directly to culture cells after washing and post-processing. For example, LOC devices printed via SLA have been used to engineering neurovascular organoids (Salmon et al., 2022). However, the composition of the UV-curable resins, often made with (meth)acrylate, can be toxic for cells or have poor cell adhesion properties. To avoid this issue, protocols to create LOC devices in biocompatible PDMS after casting on 3D printed templates, as commonly performed in traditional soft lithography methods (Comina et al., 2014) have been developed. The creation of a template by 3D printing allows a higher flexibility and lower cost than the conventional photolithography method and also allows embedding of tubing to create safer connection with microfluidic systems (Comina et al., 2014). These templates have for example been used to create LOC devices to study leucocyte adhesion (Hernández Vera et al., 2019).

3D printing has also been studied in the creation of vascular tissues in the form of sacrificial ink printing or bioprinting (Song et al., 2018). Sacrificial ink printing consists in the creation of acellular constructs with dissolvable ink that will later be filled with ECs (Miller et al., 2012).

More sophisticated protocols have developed methods to print ECs and vascular cells embedded in hydrogels and printed to form vascular tissues (Bertassoni et al., 2014; Kolesky et al., 2016, 2014). Although promising, this technology still suffers from the low resolution in the print due to the deposition of hydrogels and the difficulty to couple it with perfusion systems.

c. Perfusion of Lab-on-chip devices

The creation of models of blood vessels *in vitro* requires introducing physiological flow and flow dynamics must be tailored to the application, depending on the type of blood vessel created. Physiological intraluminal flow is not only essential for organ functions and nutrient exchanges, it also plays an important role in vascular cell phenotypes and disease progression (C.-Y. Chen et al., 2012; Fang et al., 2017; Lin et al., 2000; Ramasamy et al., 2016; Walpola et al., 1995). Blood vessels experience different forces *in vivo* such as shear stress, circumferential stress and transmural pressure, reproducing these mechanical forces is key to mature vascular models *in vitro* (Haase and Kamm, 2017).

Microfluidic devices have been coupled with different types of perfusion system (Fig. 1.14), from passive gravity-driven wells to active syringe pumps and computer-assisted peristaltic pumps (Byun et al., 2014; Shemesh et al., 2015).

Passive systems often make use of gravity-driven pressure and different reservoirs of cell culture medium with different heights (Fig. 1.14A-D)(Marimuthu and Kim, 2013). These systems are broadly used and have been successful in creating perfusable blood vessel network due to the creation of a pressure drop in between the reservoirs (Campisi et al., 2018; Chen et al., 2013; M. B. Chen et al., 2017). The main advantage of passive systems is their accessibility, with the need to only add reservoirs in the design of the LOC, but they require continuous medium change and do not produce a continuous and stable flow.

Active systems are more complex with defined conditions allowing the user to control flow over time and get a more stable perfusion. Most used active perfusion systems are syringe pumps (Fig. 1.14E-F), that are syringe installed on top of a reservoir and pushed mechanically by a piston. Syringe pumps are relatively inexpensive but cannot produce a closed circulation as experienced in the body. Peristaltic pumps (Fig. 1.14G-I) are also common and work by moving the liquid in compressible hoses by applying pressure through a circular movement. Other active systems include the use of osmosis-driven flow or centrifugal pumping (Fig. 1.14J-K), less commonly used.

Overall, passive pumping systems are easy to setup and relatively inexpensive but not appropriate for long term culture, with un unstable flow rate or extensive intervention needed. Active systems are more appropriate for the introduction of continuous and controlled flow *in vitro* and in microfluidic systems. Nevertheless, active pumping systems such as peristaltic pumps also have limitations such as a larger dead volume and the difficulty to adapt them for multiple LOC devices at a time.
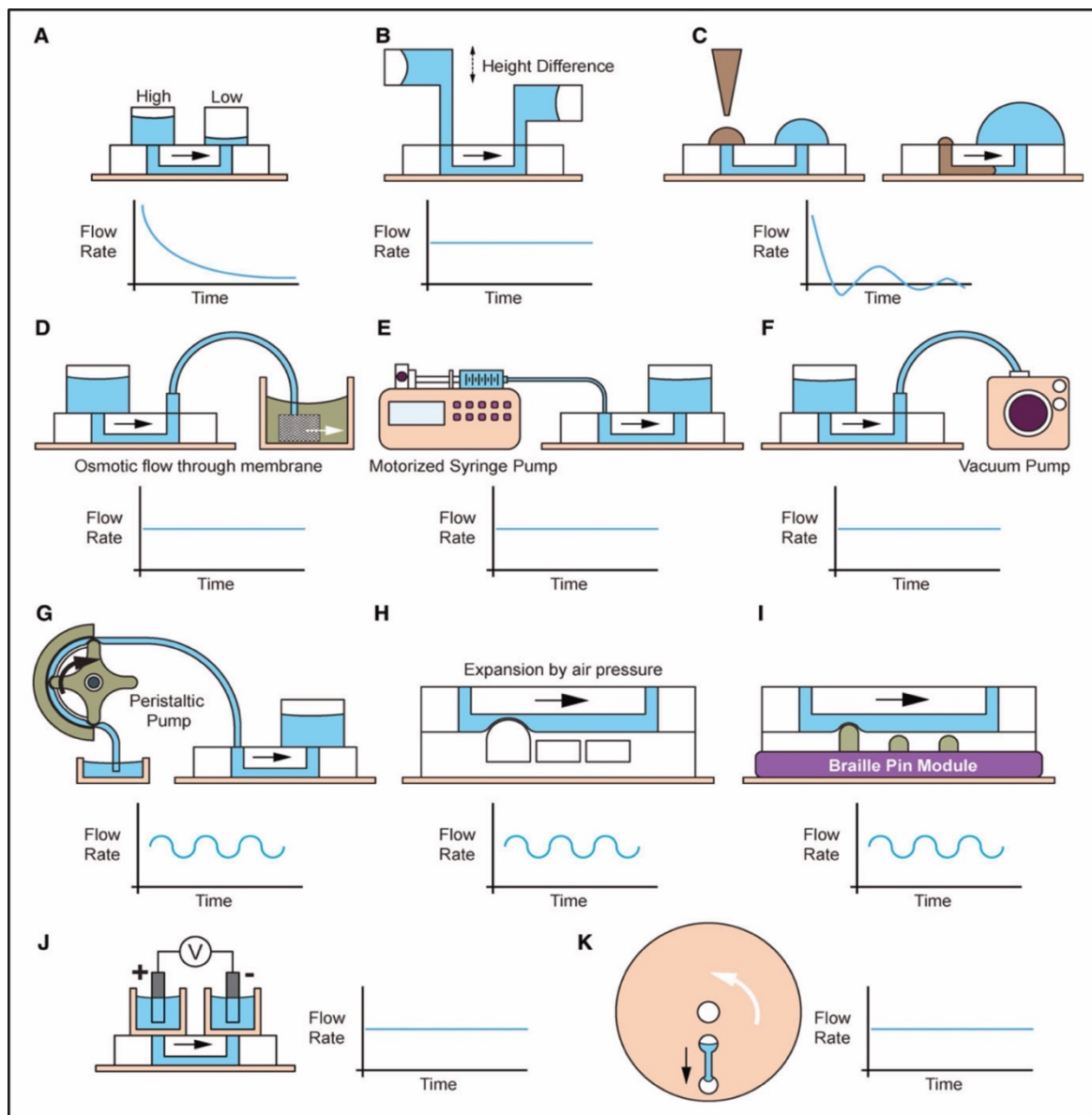
Figure 1.14: Types of pumps used in microfluidic systems and patterns of flow created. (Byun et al., 2014)(A-D) Passive systems with gravity-driven pumps with vertical (A) or horizontal (B) reservoirs, surface tension drops (C) or osmotic flow (D). (E-K) Active systems, with syringe pumps working with positive (E) or negative pressure (F), peristaltic pumps (G) by pneumatic (H) or braille pins pressure (I) or electrokinetic pump (J) and centrifugal pump of lab-on-a-disc (K).

8- __Conclusions from the literature__

The cardiovascular system plays a central role in organ development and function and understanding mechanisms of vascular development and maturation is essential to develop more effective therapies for life threatening diseases. Understanding these mechanisms will also enable creating biomimetic *in vitro* systems for tissue engineering purposes and developmental studies.

Mechanisms involved in blood vessel development and heterogeneity have received a lot of attention lately due to their role in organ-specific blood vessel phenotypes. This degree of difference is due to genetic and epigenetic programming as well as the influence of the microenvironment on blood vessel phenotypes but knowledge on the functional consequences of this heterogeneity is still missing. The lack of functional characterisation of ECs and the importance of heterogeneity at the population and monolayer level could be central to understand the failure of vasculature-targeting pharmaceutical treatments.

The current knowledge on iPSC differentiation into endothelial cells and mural cells allows the creation of distinct populations of vECS and aECs but protocols are heterogeneous in terms of yield and efficiency and lack functional characterisation. Further studies are needed to understand the cascade of events need to create mature blood vessels from stem cells. Furthermore, lacking information on the role of vascular cell and perivascular interactions in the development of blood vessels could be recapitulated with appropriate stem cell models.

Finally, the development of tissue engineering methods such as microfluidics and Lab-on-chip devices allowed the study of mechanical forces on endothelial cells and blood vessel formation. But current models of microvasculature *in vitro* lack a proper blood vessel hierarchy, arteriovenous specification, control of spatial and temporal network formation as well as maturation. In addition, little is known about the conditions necessary for perfusion-dependent and independent blood vessel maturation. To date, *in vitro* models still lack the ability to create continuously perfused blood vessels and poorly recapitulate organ-specific environments.

Due to the difficulty to study the blood vessel formation and maturation *in vivo* in real time, it appears mandatory to create a model *in vitro* mimicking these processes and being able to monitor it step by step will allow the study of molecular pathways and optimal conditions for vascular development.

9- **Aims and objectives**

This project aims to develop perfusable, mature and tissue specific capillary networks *in vitro*. Specific aims include:

Aim 1: Investigating EC heterogeneity *in vitro* to understand the molecular mechanisms involved in arteriovenous and organ-specific vascular maturation.

Aim 2: Generate stem cell-derived vascular cells including aECs, vECs, PCs, and SMCs.

Aim 3: Determine perfusion-independent conditions to induce assembly and maturation of tissue-specific vascular networks and study the effect of cell co-culture and 3D matrices on blood vessel formation.

Aim 4: Design, employ and validate a Lab-on-chip device to investigate perfusion-dependent mechanisms of vascular formation and maturation, with control over spatial and temporal network formation.

Aim 5: Create a continuously perfusable Lab-on-chip platform to grow functional capillary networks *in vitro*.

The lack of a proper blood vessel model *in vitro* limits the progress of tissue engineering and resolving the problem inherent to the field represent high hopes for clinical applications. The following study aims at combining stem cell technology and tissue engineering methods to recreate a blood vessel *in vitro* model as complete and accurate as possible. Studying the synergistic effects of genetic programming and biomechanical forces could give new insights into blood vessel development and maturation.

Chapter 2: Investigating the molecular mechanisms involved in endothelial cell monolayers' heterogeneity.

1- **Introduction**

Blood vessels form an interconnected network responsible for supplying blood and nutrients and enabling gas exchange with almost all cell in the human body. Endothelial cells (EC) line the inner layer of blood and lymphatic vessels and they are the interface between blood and all vascularised organs (Carmeliet, 2003). EC are key regulators of metabolism via selective permeability, immune cell trafficking and inflammation by allowing leucocyte extravasation, development, tissue repair, and regeneration through angiocrine signalling (Potente et al., 2011).

EC across human tissue display a remarkable degree of phenotypic heterogeneity (Aird, 2007a, 2007b). For example, arterial, venous, and lymphatic EC (aEC, vEC, LEC respectively) are generated by distinct developmental pathways and have different shapes and functions reflected in differential activation of molecular signalling pathways (e.g., NOTCH signalling pathway, NSP). In homeostasis, each tissue has different proportions of aEC, vEC and LEC which co-develop with the tissue acquiring specialised functions sustained by specific molecular programs. Furthermore, during developmental and reparative angiogenesis, EC can acquire "angiogenic" phenotypes whereby specialised EC lead the formation of new sprout (Tip cell) and trailing EC either compete for the Tip role or contribute to the elongation of the growing stalk (Stalk cells).

 These differences can be associated with different populations of blood vessels, from venous, arterial or capillary EC, but also in the same tissue, organ or even at the single blood vessel level (Augustin and Koh, 2017; Lee et al., 2022). This phenotypic heterogeneity of ECs has been extensively studied for its implication in organ development (Kusumbe et al., 2014; Lammert et al., 2001) and in relation with the onset of diseases (Potente and Mäkinen, 2017). The study of EC heterogeneity has been accelerated by the introduction of OMICS technologies such as single cells RNA-sequencing (Chavkin and Hirschi, 2020; Goveia et al., 2020; Kalucka et al., 2018). These studies shed light on the extensive phenotypic differences in EC populations from single organs. However, transcriptomic data, lack, spatial information, protein expression for key pathways, and cell to cell interaction details.

It is known that EC phenotypes are tightly regulated, by their environment, the cells surrounding blood vessels and the biomechanical forces they experience (Carmeliet, 2003;

Potente et al., 2011; Ramasamy et al., 2016) and these variables are hardly picked up by transcriptomic data. The integrity of EC monolayers is crucial for the maintenance of organ function and homeostasis by ensuring the permeability of solutes crucial for organ function (Abu Taha et al., 2014; Obermeier et al., 2013). This encompasses the ability of the monolayer to regenerate and to integrate a variety of signals from both the apical and the luminal side of the endothelium to perform important tasks at the system level (McCarron et al., 2017). To do so, ECs are interconnected by a system of inter-endothelial junctions that is dynamically regulated to integrate signals at a fast pace (minutes)(Cao et al., 2017; Seebach et al., 2020). This endothelial-specific junction complex has been extensively studied and involves junctional proteins such as Cadherin 5 (CDH5, Vascular Endothelium (VE)-Cadherin)(Abu Taha et al., 2014; Bentley et al., 2014; Lampugnani et al., 2018), CD31 (PECAM, platelet endothelial cell adhesion molecule) (Lertkiatmongkol et al., 2016; Newman et al., 1990), specific claudins such as Claudin 5 in the blood brain barrier (Jia et al., 2014) or occludins (Furuse et al., 1993). Previous attempts at understanding the crosstalk between ECs involving VE-Cadherin have been focused on angiogenic sprouting. VE-Cadherin has been extensively characterised as one of the most important junctional protein in EC junctions and is involved in cell rearrangement in sprout selection through a tight control of Notch signalling (Bentley et al., 2014; Cao et al., 2017; Lampugnani et al., 2018). However, the dynamics and regulation of intercellular junctions in the maintenance of ECs monolayers in conditions that do not involve sprouting angiogenesis are poorly understood.

Apart from the regulation of junctional proteins, NSP is involved in several EC functions such as EC phenotypic identity and heterogeneity. NSP involves a set of ligands and receptors responsible for cell-cell crosstalk (Ehebauer et al., 2006). To get information on how EC monolayers acquire their phenotype (organ-specific functions, morphology, junctional status, interaction with immune cells) and integrate signals, models have been created either *in vitro* or *in silico* (Abu Taha et al., 2014; Lee et al., 2022). Such *in silico* models can predict the behaviour of cells in healthy or pathological conditions but cannot integrate every pathway known to affect EC monolayer dynamics. To date, *in vivo* models able to discriminate the complexity of EC dynamics, intercellular junction and Notch signalling at the single cell level are still missing. Several studies on EC heterogeneity have used *in vitro* modelling to study junction rearrangement, Notch signalling or single cell level monolayer dynamics (Abu Taha et al., 2014; Kim and Cooper, 2018) but tools to study these processes in parallel are not yet available due to the difficulty to get viable Notch reporter and the complexity of the pathway.

In this chapter, we focused on creating an experimental model of EC monolayer that can be used to study spatial and phenotypical heterogeneity at the population and at the single cell level. We first investigated available resources of EC transcriptomics to explore, and then validate with our own organ-specific EC culture, heterogeneity at the population level. We wanted to understand how different population of ECs from separate organs can have different angiogenic potential, response to stimuli or integrate signals. To find an unbiased way to measure these variables, we created a tool to study endothelial cell heterogeneity using high content image analysis, that we called endothelial cell profiling tool (ECPT) and used cultured organ-specific ECs to mimic *in vivo* endothelium monolayers. This tool allowed us to analyse more than 300,000 cells from different vascular beds and characterise cell cycle, morphology and junctional status, Notch signalling and spatial information in EC monolayers. We report striking differences between venous, arterial and microvascular ECs at the population level and uncover surprising Notch activation diversity at the single cell level. We present an open-source pipeline that can be adapted for analysis of several cell types and coupled with a semi-automated image analysis allowing unique integration of big data sets. The degree of heterogeneity found *in vitro* via ECPT is then investigated *ex vivo* via the staining and analysis of EC monolayers of mice aortas, validating the functional relevance of heterogeneity across different EC types.

Altogether, we develop a method to decipher EC heterogeneity via the integration of data on spatial (cell-cell interaction) and phenotypical (cell cycle, morphology, junctional status and Notch signalling) EC heterogeneity and uncover key mechanisms involved in phenotypic diversity.

2- **Materials and Methods**

Cell culture

HUVECs, HSaVECs, HCAECs, HAoECs, HPMECs, HDMECs and HCMECs (all PromoCell) were plated on 10 μg/ml fibronectin (from human plasma, Promocell)-coated flasks, grown in EGMV2 medium (Promocell), detached with Accutase (Thermo Fisher Scientific, Waltham, MA), and used by passage 5. We analysed two distinct donors for each cell type, which were chosen excluding diseases affecting the vasculature (e.g., diabetes). Donor's age was between 50 and 63 years. For experiments, 4×10^{4} ECs per well were seeded in fibronectin-coated 96-well plates (μClear, Greiner) and cultured for 48 or 96 h under basal (EGMV2, Promocell) or activated (EGMV2+50 ng/ml VEGFA, Peprotech, London, UK) conditions in triplicate paralleling conditions described previously (Andriopoulou et al., 1999). The EC formed confluent monolayers at microscopic inspection [phase contrast, 10×–20× original magnification (OM; as indicated on objective)] at the time of immunostaining and image acquisition.

Immunostaining

Cells were fixed with 2% paraformaldehyde in phosphate-buffered saline (PBS) for 10 min at room temperature. Cells were blocked 1h with PBS supplemented with 1% fetal bovine serum (FBS) and permeabilised with 0.1% Triton X-100. Cells were then incubated for 1h at room temperature with primary antibodies against CDH5 (VE-cadherin; Novusbio NB600- 1409, 1μg/ml final), NOTCH1 (Abcam, ab194122, Alexa Fluor 647- conjugated, 1 μg/ml final) and Hes1 (Abcam, ab119776, 1 μg/ml final). Plates were washed and incubated 1h with 1 μg/ml secondary Alexa Fluor 488-conjugated and Alexa Fluor 555-conjugated antibody (Thermo Fisher Scientific), Hoechst 33342 (1 μg/ml, Sigma) and Phalloidin-Atto 647N (Sigma). All antibodies used in immunostaining were previously validated for specificity by western blot analysis (Fig. S4 in the manuscript) (Supplementary table 1).

Image acquisition

We obtained images with an Operetta CLS system (PerkinElmer, Waltham, MA) equipped with a 40× water immersion lens (NA 1.1). In each well, three areas were acquired. Each area is composed of nine microscopic fields at 40× OM. We standardised acquisition parameters (light- emitting diode power, exposure time) throughout different experiments and used

HUVECs as a standard for calibration in all experiments. We analysed an image database containing 28,000 images (7000 fields in four fluorescence channels) extracted from nine independent experiments conducted on EC lines from two different donors each. Two intraexperiment replicates were conducted for each experiment.

Endothelial cell profiling tool

We used a combination of machine learning-aided image segmentation (ImageJ) (Schindelin et al., 2012) and an image-based cell profiling tool (CellProfiler)(Carpenter et al., 2006) to extract the phenotype of single EC in monolayers. Our workflow enables the measurement of EC morphology (area, perimeter, shape descriptors and cell neighbours), NOTCH1, HES1, CDH5 and DNA intensities, and the characterisation of inter-endothelial junctions (IEJs). In the present study, we chose to analyse only selected features with recognised functions in EC biology. Image texture features were measured and only used during the training of ML algorithms (Caicedo et al., 2017; Jones et al., 2008), which in turn were used to classify junction morphology and LM cells. ECPT scripts and methods including FIJI/ImageJ macros for image importing and pre-processing are detailed at https://github.com/exr98/HCA-uncovers-metastable-phenotypes-in-hEC- monolayers.

We imported and standardised the results into R studio excluding artefacts and mis-segmented cell objects (extreme values in cell area or signal intensity, NAs in measurements). We then calculated continuous and categorical (cell cycle) parameters. Following guidelines suggested by Caicedo *et al.* (2017), we pre-processed the database to exclude mis-segmented cells and to normalise the measurements prior to dimensionality reduction or single factor analysis. We reformatted and tidied the database and calculated summary statistics using packages from the Tidyverse packages collection (https://www.tidyverse.org; Dplyr, Tidyr, Tibble, Forcats, Purr and Ggplot2).

We conducted PCA analysis on ECPT parameters (Cell morphology, intensity, neighbourhood and junctional status, Table 1 in the manuscript) using the prcomp function (R Stats package) generating 12 PCA components. All plots in figures are generated using the Ggplot2 R package.

We created a Shiny application (https://CRAN.R-project.org/ package=shiny) for interactive selection and visualisation of data of interest. All files containing the code required to

reproduce all the plots in the paper and to run the Shiny application using our dataset are available on https://github.com/exr98/HCA-uncovers-metastable-phenotypes-in-hEC-monolayers.

Western blotting

Cells were scraped in the presence of RIPA buffer (Sigma-Aldrich) containing protease (Millipore, UK) and phosphatase inhibitors (Sigma-Aldrich, UK), left on ice for 15 min, and centrifuged at 13,000 g for 5 min in a refrigerated microfuge. Supernatants were assessed for total protein using the BCA protein quantitation kit (Thermo Fisher Scientific). 15 μg of protein were separated on NuPAGE 4–12% Bis-Tris gels (Invitrogen) before being transferred to nitrocellulose membranes (GE Healthcare, Amersham, UK). After probing with primary and secondary antibodies, membranes were developed using ClarityTM Western ECL Substrate (Bio-Rad, UK) and read using a ChemiDoc system (Bio-Rad). Antibodies for NOTCH1 (1:500; Abcam, ab194122), HES1 (1:1000; Abcam, ab119776), VE-cadherin (1:500; Novus bio NB600- 1409) and β-tubulin (1:1000; Cell Signaling Technology) were used. Goat anti-mouse-IgG and anti-rabbit-IgG horseradish peroxidase (HRP)- conjugated antibodies were from Dako (Agilent).

RNA extraction and qRT-PCR

Total RNA was extracted and purified using the Monarch total RNA miniprep kit according to the manufacturer's instructions. The resulting RNA was quantified using Nanodrop (ISOGEN Life Science). For quantitative real-time PCR (qRT-PCR), 1 μg of RNA was used for reverse transcription using the iScript cDNA synthesis kit (Bio-Rad). The gene expression analysis was carried out using the SsoAdvanced^{TM} Universal SYBR Green Supermix (Bio-Rad) and analysed by means of a Stratagene Mx3000P (Agilent Technologies) in real time, primers used are listed in supplementary table 2.

En face preparation and whole mount staining of mouse aorta

For en face preparation of aortas, 2–8-month-old mice were anaesthetized with intraperitoneal injections of xylazine (10 mg kg−1) and ketamine (80 mg kg−1) and perfusion fixed with 1% PFA–PBS. Aortas were fixed for 1 h in 4% PFA–PBS, washed with PBS and blocked with FBS (5% FBS + 0.01% Triton-X) for 1 h at room temperature. Immunostaining was performed

after permeabilization (0.1% Triton- X for 10minutes at RT) using primary antibodies diluted in blocking solution (VE-Cadherin, #14-1441-82, 5 g/ml final and HES1, #PA5-28802, 5 g/ml final, Thermo Fisher Scientific) for 48h at 4°C, followed by extensive washing using blocking solution at RT. Aortas were then incubated with Alexa Fluor 488-conjugated and Alexa Fluor 555-conjugated antibody (Thermo Fisher Scientific) and Hoechst 33342, for 24h at 4°C, washed and mounted on a coverslip with Mowiol (Sigma-Aldrich). The aortas were imaged, and z-stacks were obtained using a Leica Sp8 confocal microscope with a 40X air objective.

Statistical analysis

To compare multiple groups, we used one-way ANOVA followed by Tukey's HSD post-hoc test. We considered $P<0.05$ (*) statistically significant and $P<0.01$ (**), $P<0.001$ (***) and $P<0.0001$(****) highly significant.

To evaluate linear correlation between continuous variables we calculated Pearson's correlation coefficient I and considered $P<0.001$ as highly statistically significant.

Comparisons between intensity distributions were performed by two- sided Kolmogorov–Smirnov (KS) test as implemented in the 'stats' R package. We considered comparisons with $P<0.01$ to be statistically significant and reported corresponding distance index (D).

Statistical significance in global and local Moran's analyses is computed by random permutations as implemented in the adespatial R package we used 999 permutations in each test. We considered $P<0.05$ in Gmi or Lmi to be statistically significant (Dray, 2011).

Data availability

All raw and elaborated data are available at https://github.com/exr98/HCA-uncovers-metastable-phenotypes-in-hEC-monolayers. To facilitate data exploration and re- use we have developed a dedicated data browser using the Shiny app environment. Original images are available upon request to the authors.

3- **Gene expression levels in EC populations.**

a. **Existing transcriptomic data on EC reveals intra and inter-population heterogeneity**

ECs in different tissues have highly heterogeneous phenotypes to meet the specific needs of each microenvironment, leading to blood vessels with very permeable monolayers and discontinuous ECs in organs such as liver, or very tight junctions and low permeability in the blood brain barrier (Augustin and Koh, 2017). These different phenotypes are not only indispensable to keep organ homeostasis but also key to achieve proper organ development. Several levels of diversity in the vascular tree have been identified, such as the striking differences in arterial/venous specification but also the single cell dynamics in tip/stalk cell definition in sprouting angiogenesis (Jakobsson et al., 2010). At the systemic level, blood vessels from single organs have been studied (Lukowski et al., 2019; Vanlandewijck et al., 2018) but a comprehensive picture of the whole EC heterogeneity had been lacking.

Recently, the development of techniques to sequence RNA have allowed in-depth characterisation of cells from entire organs and adapted to vascular biology (Chavkin and Hirschi, 2020). Bulk RNA-seq data have first been generated to obtain information on organ-specific transcription profiles or angiocrine signalling specific to ECs (Nolan et al., 2013).

At an even better resolution, an effort to create an atlas of the different EC populations in mice has been created via single cell RNA-seq and the analysis of more than 30,000 single cells (Fig. 2.1)(Kalucka et al., 2020).
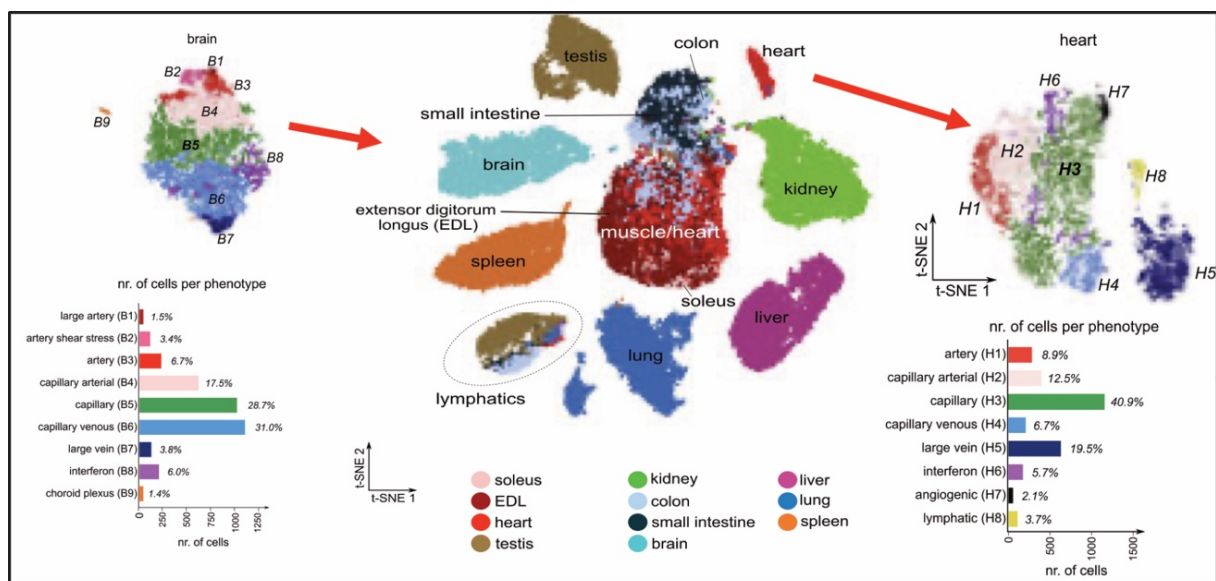
Figure 2.1: Gene expression analysis by scRNA-seq of organ-specific ECs from mice tissues (Kalucka et al., 2020). Endothelial cells from different organs from mice (soleus, kidney, liver, extensor digitorum longus, colon, lung, heart, small intestine, spleen, tesist and brain) have been studied and clustered depending on their gene expression. T-SNE plots show the extent of heterogeneity between different populations of ECs between the

First, the 11 organs studied showed several populations of distinct EC from arterial, venous or different capillary beds. These ECs clustered in individual groups corresponding to the single organs, with enriched gene expression in transmembrane transport in ECs from organs like the brain or testis or in immunoregulation in lung or liver ECs.

Furthermore, gene expression analysis intra-organ revealed striking heterogeneity in EC populations from single organs such as the heart or lungs as documented in their online resource (https://www.vibcancer.be/software-tools/ec-atlas, Figure 2.2).
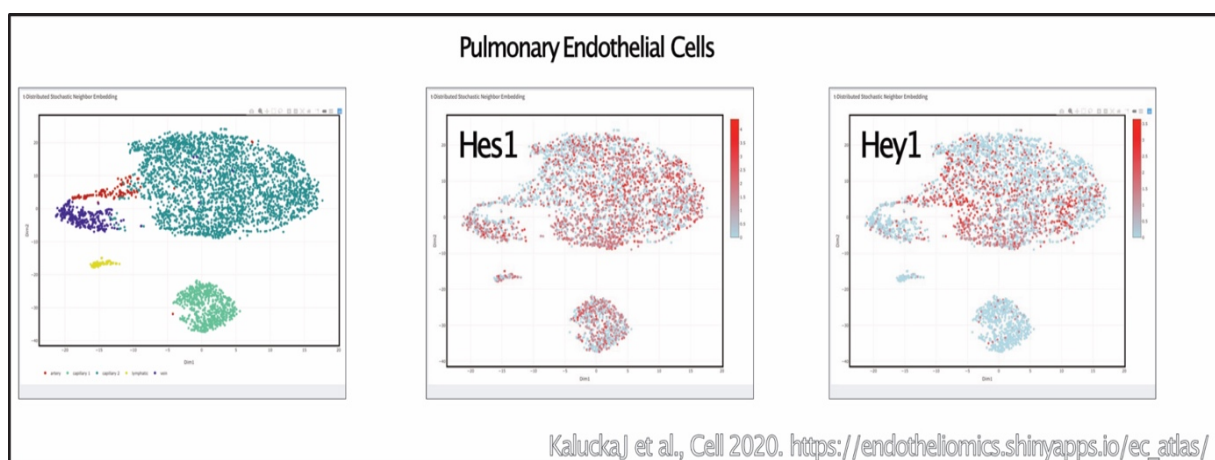
Figure 2.2: Gene expression analysis by scRNA-seq of pulmonary ECs from mice tissues (Kalucka et al., 2020). t-SNE plots obtained on the online tool https://endotheliomics.shinyapps.io/ec_atlas/ comparing the different populations of ECs obtained from the single cell RNA-sequencing of pulmonary ECs. T-SNE plot on the left shows the different populations (yellow: lymphatics, blue: venous, red: artery, light green; capillary 1, dark green: capillary 2) of ECs within the pulmonary ECs. Expression of Hes1 (middle t-SNE plot) and Hey1 (right t-SNE plot) show the heterogeneity of Notch-related gene expression in the same population of pulmonary endothelial cell.

A closer look at the intra-organ heterogeneity in the lung confirms the inherent differences in the arterio/venous specification but also highlights some unexpected single-cell heterogeneity between the different groups. Gene expression for NSP is important for the EC identity and is expected to be higher in arterial population than venous population (Fernández-Chacón et al., 2021; Fish and Wythe, 2015). The clustering of ECs from the lung reveals that, not only single cells from the same population (venous, arterial, capillary or lymphatic ECs) have differential expression of up to 4 times the basal expression, but also that arterial ECs have a substantially lower HES1 expression than venous EC. These single cell transcriptome analysis of ECs reveals an intriguing level of heterogeneity inter and intra-population.

b. Gene expression analysis of cultured organ-specific ECs

Cultured ECs have been used for decades to study specific processes such as angiogenic sprouting or to study EC-specific permeability and junctions (Adil and Somanath, 2020; Lampugnani et al., 1995). The gold standard in vascular biology is Human Umbilical Vein Endothelial Cell (HUVEC) due to their relative abundancy and phenotype *in vitro*. Nevertheless, HUVEC cannot fully recapitulate organ-specific functions of ECs and differ extensively from other mature veins, capillary or arterial EC due to their foetal venous origin. The study of organotypic functions and the onset of monolayer heterogeneity requires more specific EC models.

Here, we obtained different organ-specific EC population from several distinct vascular beds, ranging from big vessel such as the aorta (HAoEC), the coronary artery (HCAEC) and veins such as the umbilical vein (HUVEC) and saphenous vein (HSaVEC) to microvascular cardiac (HCMEC), pulmonary (HPMEC) and dermal (HDMEC) ECs. These were chosen from patient without specific diseases to avoid particular phenotypes. The cultured EC had similar morphologies, the typical spindle-shaped ECs, but we could also observe a degree of heterogeneity in between the lines as illustrated by their morphology while cultured on fibronectin (SFig. 2.1).

To confirm the gene expression results described above, we performed gene expression analysis with RT-qPCR on the different lines cultured in standard conditions (Fig. 2.3).

First, to validate the phenotype of these different organ-specific EC, we evaluated their expression for 2 EC-specific genes, VE-Cadherin (CD144, CDH5) and KDR (VEGFR2). All the ECs studied expressed robustly these genes with some observed heterogeneity at the population level. Although the expression of VE-Cadherin is similar in all the lines, the saphenous vein ECs (HSAVEC) expresses a higher level of VE-Cadherin than the rest. A further investigation into EC arteriovenous specification and Notch signalling with the expression of markers such as NOTCH1, JAG1, DLL4 and HEY2 revealed some unexpected heterogeneity. Surprisingly, as reported above, the models of arterial ECs did not get the highest expression of Notch signalling genes such as NOTCH1 receptor and Notch ligands DLL4 and JAGGED1 with all the EC lines studied having a similar expression of these markers. However, the analysis of HEY2, a transcription factor regulated by Notch signalling, revealed a reported high level of expression in arterial ECs compared to venous ECs.

Furthermore, this gene was also highly expressed in microvascular ECs in a similar way to the expression of Notch related genes observed previously in the RNA-sequencing data.
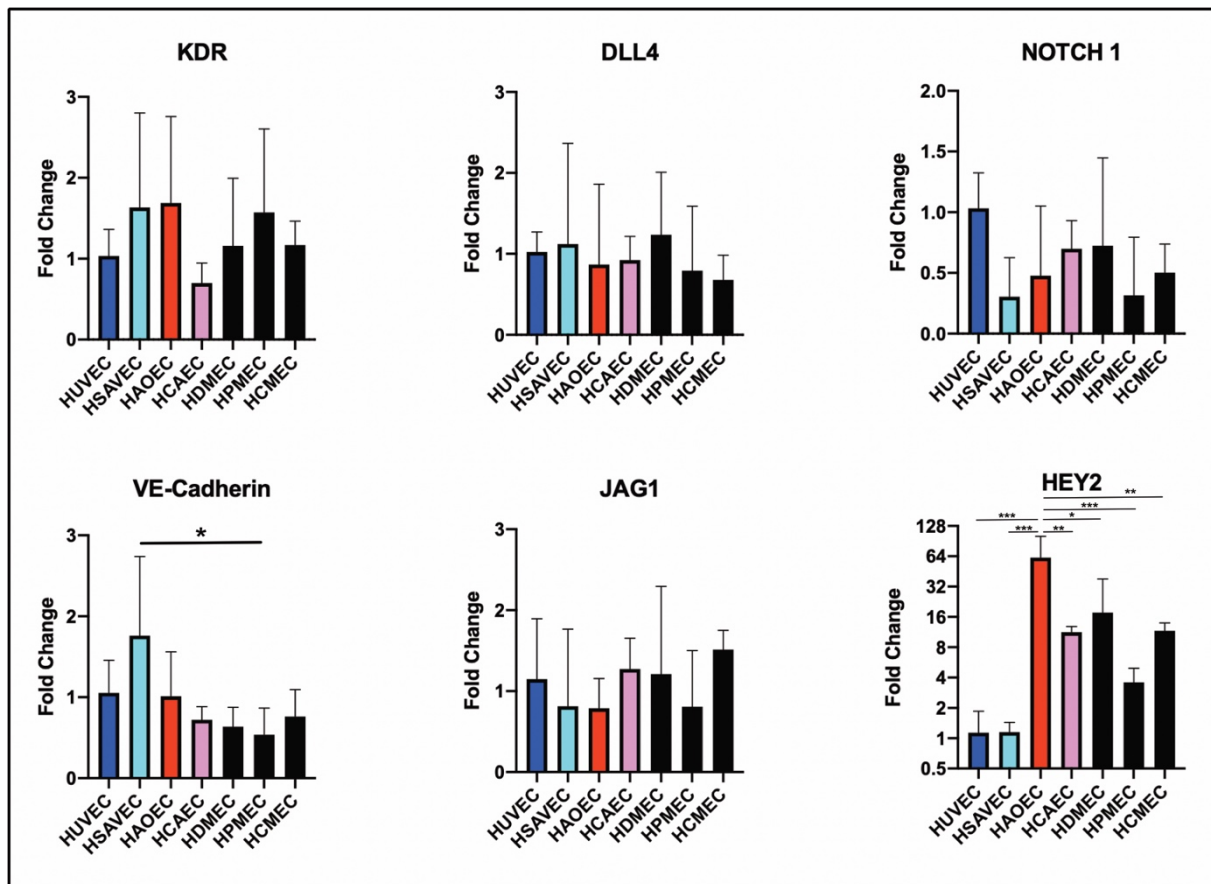
Figure 2.3: Bulk gene expression analysis reveals differential gene expression of cultures ECs from different tissues. Analysis of expression of selected genes in HUVEC, HSAVEC, HAoEC, HCAEC, HDMEC, HPMEC and HCMEC for pan-endothelial markers (VE-Cadherin and KDR) and arteriovenous specification markers/Notch signalling related genes (DLL4, NOTCH1, JAG1 and HEY2). Two donors for each cell type, measurements for donors are assembled. (n=4).

Overall, the analysis of gene expression of different organ-specific ECs revealed a degree of heterogeneity intra and inter-population consistent with previous reports. However, the sole analysis of transcriptomics data does not supply information on the relevance of this heterogeneity at the functional level and additional tools are needed to understand the origin and importance of EC heterogeneity.

4- **<u>Studying EC heterogeneity with high content imaging</u>**

The analysis of EC monolayer regulation requires to consider processes such as cell-to-cell interaction, collective migration and intercellular junction dynamics. Such finely tuned mechanisms can only be studied by the analysis of EC monolayers in the right environment. Unfortunately, accessing human samples of intact blood vessels remains very challenging technically and for obvious supplying issues. Several studies have looked at the EC monolayer using *ex vivo* mice blood vessels to investigate mechanisms such as endothelial junction stability for example (Hakanpaa et al., 2015). However, due to their small size, obtaining intact blood vessels from different tissues in mice is also challenging and most studies are performed on big vessels. With the aim of recreating a model of human EC monolayer as biomimetic as possible, we decided to use different organ-specific ECs from patients cultured in two dimension and coupled with high-content fluorescence imaging to decipher mechanisms involved in EC heterogeneity at the population and at the single cell level (Fig. 2.4).

Several studies have described the use of monolayer imaging techniques in the ability to capture EC-specific phenotypes such as junction remodelling or collective migration(Abu Taha et al., 2014; Millán et al., 2010). The use of live reporters such as GFP-tagged VE-Cadherin have been described to follow via live imaging the junctional status of single ECs in a monolayer. However, the creation of several lines of organ-specific ECs to follow processes in live imaging while having minimal effect on EC phenotype has proven technically challenging. Furthermore, several important pathways involved in EC monolayer dynamics such as Notch signalling cannot be followed live due to the lack of robust live reporters to date.
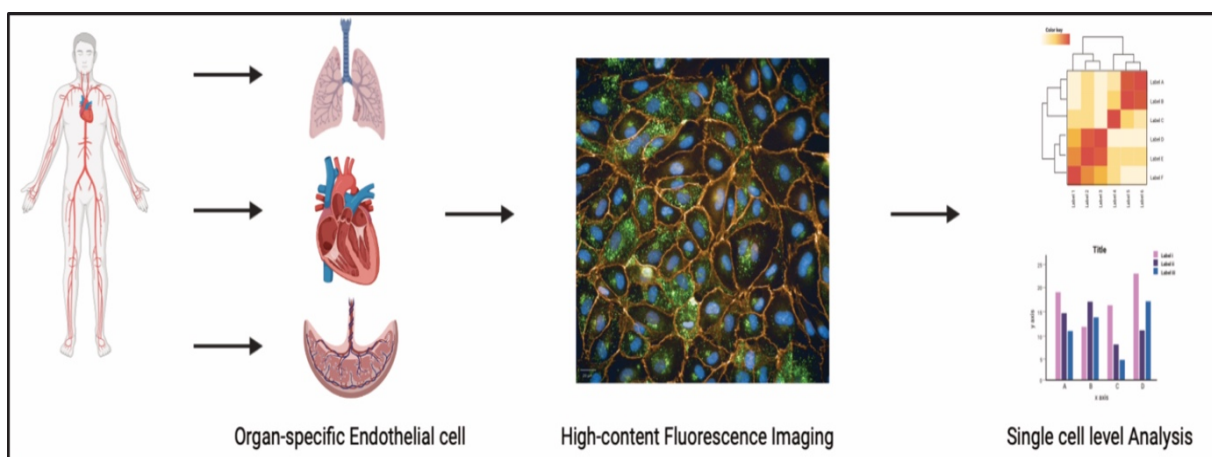
Figure 2.4: Schematics the method used to study EC heterogeneity with high content imaging and single cell level analysis. (Created with Biorender.com). Organ-specific endothelial cells from different donors were used to study endothelium-specific heterogeneity with high-content fluorescence imaging. Imaging allows the analysis of EC behaviour at the single cell level.

For these reasons and to build on previous work done in the lab (Wiseman et al., 2019), we decided to study EC heterogeneity in cultured ECs after fixation and immunostaining for proteins of interest such as VE-Cadherin proteins involved in the Notch pathway. As seen in figure 2.5, preliminary staining of HUVEC, HAoEC and HPMEC showed remarkable heterogeneity between populations of ECs in terms of junctions as showed by VE-Cadherin staining, Notch signalling, as showed by Notch intracellular domain (NICD) or in terms of morphology and cytoskeleton organisation (F-actin staining.) These results further demonstrate the ability of ECs in culture to keep their intrinsic heterogeneity and comforted us to pursue an in-depth analysis of EC diversity with high-content imaging.
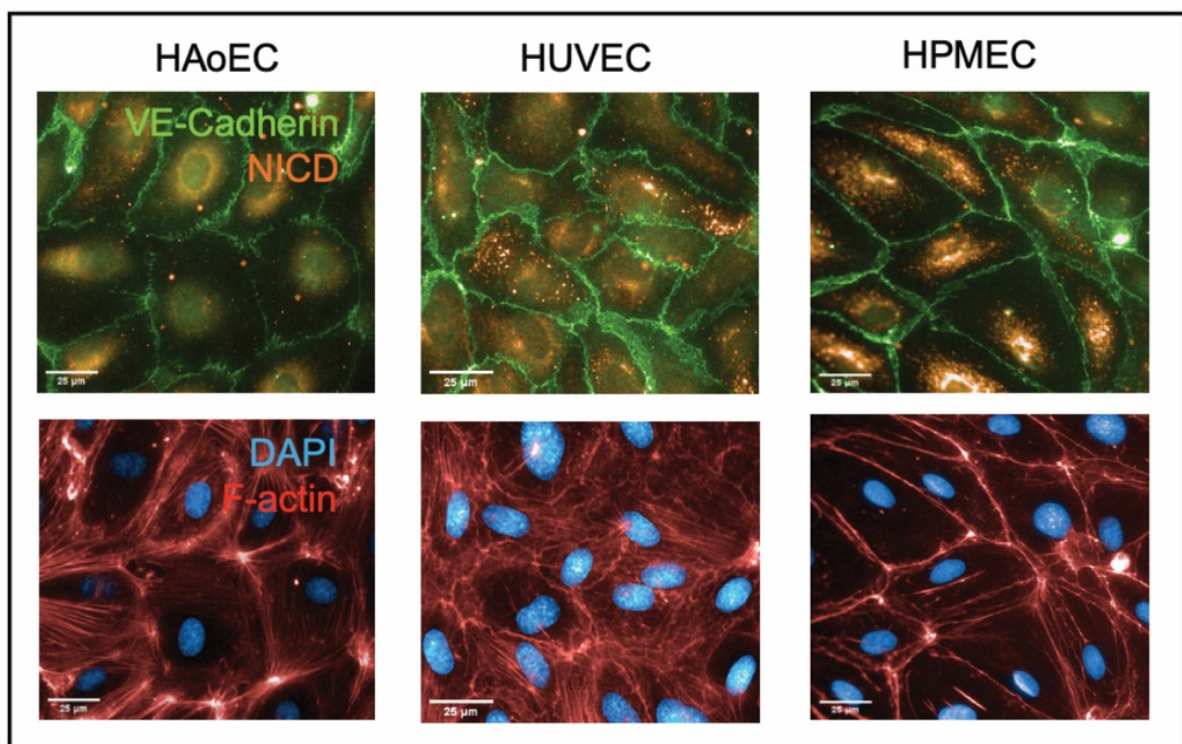
Figure 2.5: Overview of EC heterogeneity. Microphotographs comparing HUVECs, HAoEC and HPMEC untreated immunostained for VE-cadherin (green), NICD (orange), F-actin (red) and DAPI (blue); (scale bar: 25μm).

The Company of Biologists

RESEARCH ARTICLE

High-content image analysis to study phenotypic heterogeneity in endothelial cell monolayers

Francois Chesnais[1], Jonas Hue[1], Errin Roy[2], Marco Branco[1], Ruby Stokes[1], Aize Pellon[3], Juliette Le Caillec[1], Eyad Elbahtety[1], Matteo Battilocchi[2], Davide Danovi[2,4] and Lorenzo Veschini[1,*]

ABSTRACT

Endothelial cells (ECs) are heterogeneous across and within tissues, reflecting distinct, specialised functions. EC heterogeneity has been proposed to underpin EC plasticity independently from vessel microenvironments. However, heterogeneity driven by contact-dependent or short-range cell–cell crosstalk cannot be evaluated with single cell transcriptomic approaches, as spatial and contextual information is lost. Nonetheless, quantification of EC heterogeneity and understanding of its molecular drivers is key to developing novel therapeutics for cancer, cardiovascular diseases and for revascularisation in regenerative medicine. Here, we developed an EC profiling tool (ECPT) to examine individual cells within intact monolayers. We used ECPT to characterise different phenotypes in arterial, venous and microvascular EC populations. In line with other studies, we measured heterogeneity in terms of cell cycle, proliferation, and junction organisation. ECPT uncovered a previously under-appreciated single-cell heterogeneity in NOTCH activation. We correlated cell proliferation with different NOTCH activation states at the single-cell and population levels. The positional and relational information extracted with our novel approach is key to elucidating the molecular mechanisms underpinning EC heterogeneity.

KEY WORDS: Endothelial cells, High-content analysis, Machine learning, NOTCH, Heterogeneity

INTRODUCTION

Endothelial cells (ECs) form the inner layer of blood and lymphatic vessels, and play major roles in tissue development, angiogenesis, inflammation and immune cell trafficking (Potente et al., 2011). ECs are functionally plastic and rapidly adapt to changes in the environment to preserve homeostasis. Local EC dysregulation is a hallmark of diseases such as atherosclerosis, ischemia and cancer (Park-Windhol and D'Amore, 2016). ECs from different tissues and vascular beds (e.g. arteries, capillaries and veins) exhibit distinct metabolism, morphology and gene expression (Augustin and Koh,

[1]Academic centre of reconstructive science, Faculty of Dentistry Oral & Craniofacial Sciences, King's College London, Guy's Hospital, Great Maze Pond, London SE1 9RT, UK. [2]Centre for Stem Cells and Regenerative Medicine, King's College London, Guy's Hospital, Floor 28, Tower Wing, Great Maze Pond, London SE1 9RT, UK. [3]Centre for host-microbiome interactions, Faculty of Dentistry Oral & Craniofacial Sciences, King's College London, Guy's Hospital, Great Maze Pond, London SE1 9RT, UK. [4]bit.bio, Babraham Research Campus, The Dorothy Hodgkin Building, Cambridge CB22 3FH, UK.

*Author for correspondence (lorenzo.veschini@kcl.ac.uk)

F.C., 0000-0002-0247-7908; J.H., 0000-0001-5688-6160; M.B., 0000-0002-3545-0920; D.D., 0000-0003-4119-5337; L.V., 0000-0003-3820-7472

2017), and contribute in diverse ways to tissue development and regeneration (Itkin et al., 2016; Kusumbe et al., 2014). It is well established that ECs are phenotypically heterogenous not only among different tissues, reflecting specialised organ-specific functions (Rafii et al., 2016), but also within the same tissue. Maintenance of endothelial homeostasis depends on new ECs substituting senescent cells, and the role of endothelial progenitor cells with high repopulating potential has been highlighted in endothelia of large vessels (Yoder, 2018).

Inter-endothelial adherens junctions (IEJs) are dynamically regulated by VE cadherin (CDH5) shuffling between the cell membrane and intracellular compartments. This process presents variations across vascular beds (Augustin and Koh, 2017) and involves molecular mechanisms including VEGF receptors, cytoskeletal proteins and NOTCH family members. VE cadherin and NOTCH signalling are well studied in angiogenesis and development. Nonetheless, the role of these molecular mechanisms in EC monolayer maintenance is less clear and this knowledge is essential to understand vessel homeostasis in different organs in the human body. So far, a comprehensive analysis of EC cultures exploring and quantifying phenotypic variance has proven prohibitively difficult because of lack of adequate tools.

Single-cell phenotyping has identified and characterised intermediate cell states (MacLean et al., 2018; Siu et al., 2020), and demonstrated correspondence between phenotypes and function (Dueck et al., 2016). However, challenges in discriminating functional phenotypic variance from biological noise have emerged (Eling et al., 2019). Single-cell transcriptomic (sc-OMICS) data is becoming available (mostly in mouse) (Kalucka et al., 2020) and could, in principle, advance the characterisation of human ECs (Tikhonova et al., 2019) and provide an overview of molecular processes in distinct EC populations. Nonetheless, sc-OMICS data lacks spatial information, which is essential to map variable phenotypes to function and is also required to understand higher-level functions depending on cell–cell connectivity. Of note, the EC cell cycle and their rapid adaptative phenomena, such as rapid increase of endothelial permeability upon VEGF stimulation are regulated by built-in sensing mechanisms that depend on cell–cell interaction (Acar et al., 2008). Importantly, EC monolayers maintain their integrity over years while exerting a variety of system-level functions, which are emerging properties of cells in contact (McCarron et al., 2017). It has been proposed that endothelial adaptability and diversity of functions within an EC population depends on cell heterogeneity (McCarron et al., 2019).

To examine individual cell heterogeneity and extract spatial information from EC monolayers, we developed an endothelial cell profiling tool (ECPT) based on high-content image analysis (HCA). ECPT captures a wealth of cellular, subcellular and contextual information enabling extensive characterisation of the cell cycle and IEJs. This unbiased approach allows quantification of EC

Journal of Cell Science

1

heterogeneity measuring feature variance (Eling et al., 2019). Taking advantage of machine learning based methods, we performed automated and accurate classification of IEJs using junctional CDH5 immunostaining, and evaluation of NOTCH activation at the single cell level. In total, we analysed data from >20,000 images across nine independent experiments detailing selected measurements from >300,000 cells including individual junction objects. Overall, we present (1) a novel tool for single EC profiling at a previously inaccessible scale, (2) the validity of this analysis to quantify previous observations and (3) new key relationships across features that are distinct between different EC types.

RESULTS
Challenging quantification of endothelial cell heterogeneity by high-content imaging

Although heterogeneity of ECs has been proposed, few transcriptomic studies have successfully quantified the phenotypic variance of ECs within the same vascular bed (Chavkin and Hirschi, 2020). We previously reported the value of specific vascular endothelial (VE) cadherin (CDH5) and NOTCH quantification to benchmark ECs in intact monolayers (Wiseman et al., 2019) and now extend our observations to include relational information between individual cells. These cannot currently be retrieved with single cell transcriptomic analysis. We cultured primary human umbilical vein ECs (HUVECs), human aortic ECs (HAoECs) and human pulmonary microvascular ECs (HPMECs) for 48 or 96 h in the absence or presence of VEGF. We aimed for sufficient cells to reach confluency upon adhesion and spreading (∼24 h), and we cultured for a further 24 or 72 h to enable formation of stable IEJs. ECs demonstrate a uniform cobblestone morphology under low magnification, confirming monolayer stabilisation.

Immunostaining and live imaging of EC monolayers has highlighted differences in cell morphology and junction patterns in response to stimuli or under distinct cell culture conditions (Abu Taha et al., 2014; Lampugnani et al., 1992; Seebach et al., 2016; Vestweber et al., 2009). We focussed on analysing proliferation, junctions, and NOTCH activation. We stained for CDH5, NOTCH1 (or the actin cytoskeleton), HES1 (a NOTCH target gene) and nuclei. In line with previous literature, qualitative inspection at high magnification revealed remarkable morphological differences between the cell types in culture (Fig. 1).

EC junctions have been linked to specific function and phenotypes (Abu Taha et al., 2014; Lampugnani et al., 1995). Linear and stabilised junctions are present in the mature quiescent phenotype; jagged and discontinuous junctions results from proliferation, migration or the immature/mesenchymal phenotype; reticular patterns, observed in more stabilised junctions, can be also observed as transient structures (Kim and Cooper, 2018) and are associated with immune cell transmigration (Fernández-Martín et al., 2012).

In our study, HUVECs, HAoECs and HPMECs showed different junction patterns and cell morphology in standard *in vitro* culture conditions. Inspection of NOTCH1 and HES1 staining intensity and localisation at the single-cell level appeared to be highly heterogeneous both intra-population and inter-population (Fig. 1). Measuring and scoring individual EC phenotypes to demonstrate, quantify and explain EC heterogeneity at single cell resolution is a prohibitively tedious and biased approach if not automated. Therefore, we set out to create a dedicated platform that can seamlessly and comprehensively quantify variance of phenotypic parameters in cultured EC monolayers.
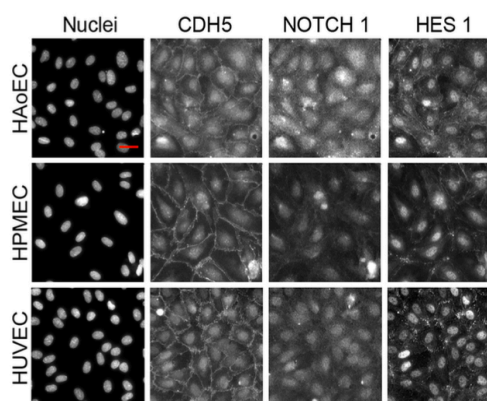
Fig. 1. Overview of EC heterogeneity. Microphotographs comparing HUVECs, HAoECs and HPMECs stained for DNA (Hoechst 33342, nuclei), VE-cadherin (CDH5), NOTCH1 and HES. Images representative of nine experiments. Scale bar: 50 µm.

Creation of a semi-automated image analysis pipeline for EC phenotyping

We developed a method to profile EC phenotypes at the single-cell level based on extracted high-content analysis (HCA) features: Endothelial Cell Profiling Tool (ECPT, Fig. 2 and Appendix 1 at https://github.com/exr98/HCA-uncovers-metastable-phenotypes-in-hEC-monolayers). We used open-source software to generate an image analysis workflow able to take input from fixed or live images, with the aim of characterizing EC heterogeneity at the single-cell level (Fig. 2). Features and benchmark comparisons between ECPT and available tools is presented in Table 1. Fig. 2A demonstrates the unique capability of ECPT to precisely segment cells according to junctional CDH5 staining. Accurately segmenting cells is key to all downstream analyses and to evaluate cell junctions. However, CDH5 staining is very heterogeneous across different cell populations including those of different origins (e.g. HAoECs, HPMECs and HUVECs) and treatment (e.g. untreated versus VEGF-treated ECs). In terms of image analysis, this renders standard thresholding techniques insufficient to appropriately contrast large collections of images for segmentation. To overcome this problem, we developed a workflow in Fiji/ImageJ leveraging the Weka segmentation, a powerful machine learning (ML) tool. Fig. 2Ai shows the original CDH5 image, Fig. 2Aii shows the corresponding output images following application of a Weka model based on an annotated dataset of 70 CDH5 images chosen randomly across our database of >20,000 images. Fig. 2Aiii shows an overlay of individual junction objects. Individual junctions between two cells are precisely identified via ECPT and junction features are measured. Different junction classes were obtained by applying ML-aided object classification (Cell Profiler Analyst, CPA using Fast Gentle Boosting) based on a the measurements of a junction and colour code in Fig. 2Aiii. Nuclei segmentation and downstream measurements were performed using standard Cell Profiler (CP) modules and thresholding methods (Otsu, Fig. 2Bi) to evaluate nuclear morphology, cell cycle (Fig. 2Bii) and NOTCH signalling (Fig. 2C).

Overall, extending our previous proof-of-principle study (Wiseman et al., 2019), we chose features describing cell proliferation, morphology, spatial organisation, NOTCH activation and ML-aided classification of junctions. We then applied the ECPT

2
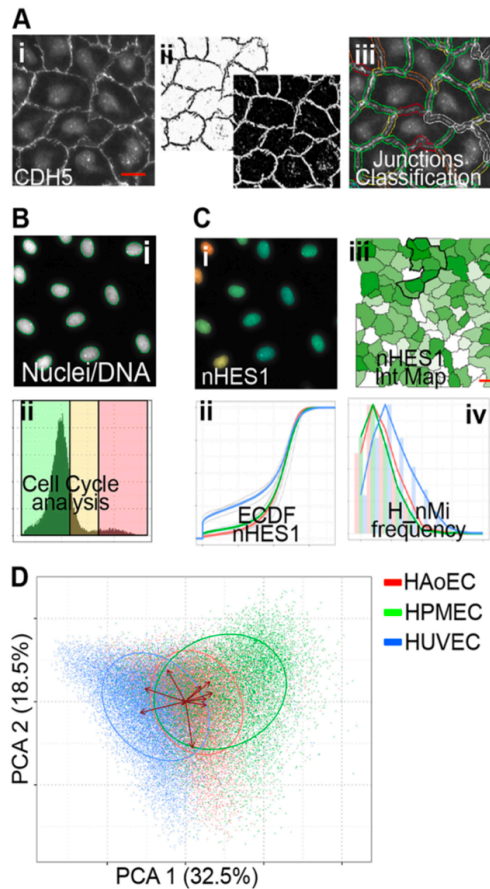
Fig. 2. Image segmentation and ECPT features. (A) Acquisition of high resolution (40× OM) images on each channel. The CDH5 channel (i) is used to segment the cells and outline the cell junctions using Weka segmentator Fiji (ii), allowing individual junction and cells segmentation (iii). (B) Nuclei are stained with Hoechst 33342 (i) and the intensity is used to segment nuclei and measure DNA intensity to perform cell cycle analysis (ii). (C) Measurements of HES1 nuclear signal intensity (i). Empirical cumulative distribution functions (ECDF) across all images by cell type (ii). Example nHES1 intensity map (iii) and frequency of cells with negative nLMi relative to HES1. (D) Single cells PCA analysis on untreated EC cultured for 96 h. Arrows indicate loading of different variables. Colours in C and D represent EC type. Scale bars: 50 μm.

workflow to a dataset composed of >20,000 images from nine independent experiments obtaining a bulk of >300,000 single cells across different cell types (i.e. HAoECs, HPMECs and HUVECs) and experimental conditions (i.e. initial cell density, time in culture and VEGF treatment).

We first asked whether HAoECs, HPMECs and HUVECs could be distinguished solely using the chosen features. We set to capture variance within our multivariate datasets, to identify discrete populations among heterogeneous cells and to understand, which parameters had greater weight in defining cell phenotype. Principal components analysis (PCA) based dimensionality reduction cumulatively captured 51.1% of the variance (Fig. 2D). HAoECs,

HPMECs and HUVECs did not form distinct clusters and the cell populations were partially overlapping. Nevertheless, cell populations segregated according to the first two PCA components. This indicates that our parameters of choice capture key differences in the three EC populations. To understand the origin of this heterogeneity we dissected individual sets of features dependent on the same biological mechanism. We developed a dedicated user-friendly, open-source interface using the shiny package within Rstudio (https://shiny.rstudio.com) inspired by guidelines described previously (Lord et al., 2020). This shiny application allows subsetting through interactive and iterative selection of single cells or groups of cells for further comparison and analysis within R studio (Appendix 1 at https://github.com/exr98/HCA-uncovers-metastable-phenotypes-in-hEC-monolayers). We welcome readers to further explore our dataset available at https://github.com/exr98/HCA-uncovers-metastable-phenotypes-in-hEC-monolayers). To understand certain phenotypic differences in detail, we quantified variance of a few selected traits: proliferation, junction stability and NOTCH activation.

Single-cell analysis of cell cycle

The integrated Hoechst 33342 nuclei signal intensity, commonly used as a proxy for DNA content in flow cytometry, was analysed based on previously published protocol (Roukos et al., 2015) to evaluate cell proliferation. The different stages of cell cycle (G1, S and G2/M) are thus defined via thresholding, with distinct peaks for G1 and G2/M (Fig. 3A). Late mitotic (LM) cells were detected by ML-aided object classification using features of Hoechst (DNA) and CDH5 stainings, including texture features (Fig. 3A). This automated method allowed us to overcome specific limitations of previous approaches (Jones et al., 2009; Roukos et al., 2015).

Cell density is a well-established determinant of EC proliferation (Andriopoulou et al., 1999; Bazzoni and Dejana, 2004); therefore, we first set out to establish whether cell densities were homogeneous across cell types and different experiments.

By subculturing HUVECs, HAoECs and HPMECs under the same standardised conditions, we noticed that these EC types present different intrinsic proliferation rates. We thus quantified proliferating cells and compared subconfluent and confluent cells, which were also cultured for 48 h or 96 h upon seeding, as a longer time in culture has been shown to further stabilise the EC monolayer (Bazzoni and Dejana, 2004).

Proliferation was higher in subconfluent HAoECs and in HUVECs at baseline (average 16.9% and 13.8% of dividing cells per field) and lower in HPMECs (average 7.8%). VEGF induced a small detectable increase in proliferation in all subconfluent ECs (18.9%, 9.6% and 16.2% in HAoECs, HPMECs and HUVECs, respectively). In subconfluent cultures, an average of 3.5% to 6.7% of cells were LM, demonstrating cells were effectively dividing at the time of the experiment.

In confluent cultures, the proliferation was lower in all ECs except HPMECs, which maintained values as in subconfluent conditions. In confluent cultures, the percentage of cells in cell cycle ranged from 9.8% to 12.7% in all ECs with little differences between control and VEGF-treated conditions. Longer culture conditions also had little effect on proliferation rates. In all confluent cultures examined, the average percentage of LM cells dropped to values between 1.2% and 2%. Overall, our results are consistent with previous observations and demonstrate that EC proliferation is affected by cell density. Furthermore, confluent cultures under our conditions have low proliferation rates, consistent with that observed *in vivo* (∼4.8% of

Table 1. ECPT features and comparison with other available software

Feature	Feature type	Software	ECPT_V1	ECPT_V2	Description	Benchmark
PE Harmony/ Columbus importer	Pre-processing	FIJI/ImageJ	YES	Improved	Imports images from PE Harmony and Columbus platform allowing custom labelling. Autodetects n of columns, rows, images, and channels. Allows performing image pre-processing (e.g. scaling, illumination correction). Improved speed in V2.	In native image analysis environments, several of the following features are not available or limited. Processing could be done via python scripting to improve performance.
WEKA elaboration	Pre-processing	FIJI/ImageJ	YES	NC	Applies trained WEKA models to batch of images. Allow to select channel to be elaborated, model and to label class names for easier post-processing.	Arguably one of the best open-source pixel level segmentator using a familiar GUI (to ImageJ users).
WEKA models for CDH5 segmentation	Pre-processing	FIJI/ImageJ	YES	Improved	A WEKA model for junctions' segmentation trained on our full dataset. Efficiently segments junctions in all our images passing quality check but a new model might be required on different datasets.	Junction Mapper. Individual images need to be thresholded individually.
Automatic image quality check	Pre-processing	Cell Profiler (CP)	NO	YES	In V2 we introduced an image quality check prior to object segmentation to avoid the need to manually select good quality images sets.	Same implementation as in Caicedo et al. (2017).
Cell/nuclei/ junctions segmentation	Objects (OBJ) detection	Cell Profiler	YES	Improved	CP modules to identify object of interest using standard CP modules. Segmentation is aided by intensity maps obtained through WEKA pre-processing. Improved junctions' identification in V2 due to improved WEKA model and restructuring of CP elaboration. V2 identifies junctions as individual objects.	Standard OBJ segmentation similar efficiency in all platforms tested.
Junctions classification	OBJs class	CP analyst	YES	Improved	Classification of junctions according to measurements of junction objects. Improved in speed, accuracy, and quality of data by detection of whole junctional objects.	Not easily available in other software tested. CPA is user friendly, and parameters can be selected in a flexible way. Requires some experience with CPA for optimal results.
Cell classification	OBJs class	CP analyst	YES	Not changed	Classification of cells according to presence or absence of stress fibres.	Not easily available in other software tested. CPA is user friendly, and parameters can be selected in a flexible way. Requires some experience with CPA for optimal results.
Extraction of spatial relationships information	OBJs detection	Cell Profiler	NO	YES	In V2 modules for establishment of neighbour relationship between individual junctions and cell object were introduced. This allows describing interaction between cells in terms of weighted interaction matrices essential for Spatial Autocorrelation Analysis (SAA).	Not available in any other tool to the best of author's knowledge
Detection of individual NOTCH puncta	OBJs detection	Cell Profiler	YES	NO	In V1 the measurement of individual NICD puncta was retained to mirror analyses in Wiseman et al., 2019. After restructuring of experimental and analysis setup we chose to remove this feature in favour of more robust nuclear intensity.	As for CDH5 based segmentation, WEKA allows achieving excellent results for pixel level segmentation.
Cell Maps export	Cross platform IO	CP/FIJI/R	NO	YES	In V2 we introduced the possibility to share segmented objects across platforms which is key to exploit the potential of adespatial R package, i.e. to perform SAA across ~3000 images.	Not available in any other tool to the best of author's knowledge.
R elaboration	Data analysis	R Studio	YES	Improved	Scripts for all data processing performed in the work are provided as example allowing to reproduce all the data presented. Improvements in V2 include more consistent layout and scripts for SAA and relative visualisation.	Data input and output, and elaboration in the R environment is more flexible than other platforms tested. E.g. SAA is impossible to implement in out-of-the-box tools tested by authors so far.

89
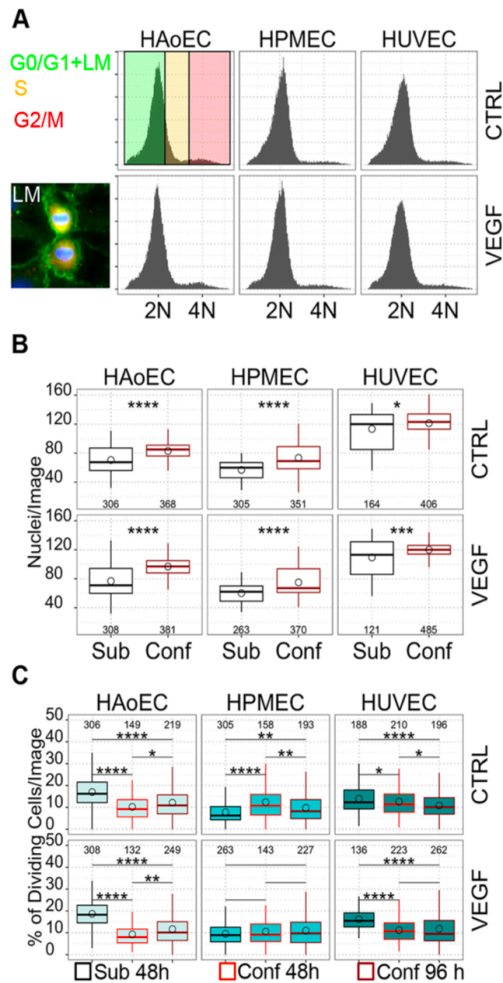
Fig. 3. Cell cycle analysis. (A) Histogram plots of DNA intensities by cell type (HUVECs, HAoECs and HPMECds) and treatments [control (CTRL) and VEGF]. Cells are classified in cell cycle phases depending on the signal intensity. Inset displays LM cells engaged in mitosis which were detected and quantified using CPA. (B) Number of nuclei per image (cell density) in sub-confluent (black) or confluent (red) experiments for the three different EC types (HUVECs, HAoECs and HPMECs) and treatments (CTRL and VEGF). (C) Percentage of dividing cells (S, G2/M, LM) per image in HAoEC, HPMEC and HUVEC with or without treatment with 50 ng/ml VEGF in subconfluent or confluent conditions. The box represents the 25–75th percentiles, and the median (line) and mean (circle) is indicated. The whiskers extend to the maximum or minimum values within a 1.5× interquartile range (IQR) distance from the box hinge. Outliers not represented. n of observations for each statistical comparison indicated as annotations in individual plots. *P<0.05, **P<0.01, ***P<0.001, ****P<0.0001 (one-way ANOVA followed by Tukey's post-hoc HSD test).

cells in S, G2 or M phases as measured by scRNA-seq of mouse aortic endothelium; Lukowski et al., 2019).

Together these data validate the use of ECPT to characterise EC cell cycle under different experimental conditions. These are key quality controls when analysing cell phenotype and dynamic structures, such as inter-EC junctions.

Analysis of morphology and cytoskeleton arrangement

Cell morphology statistics were obtained directly from cell objects segmentation. Fig. 4A shows cell area comparisons across EC types and cell cycle stage in either subconfluent (red, green and blue traces) or confluent (dashed grey traces) conditions. Overall, the three cell types had different average area and, as expected in subconfluent cultures, cell area increased with phases of cell cycle (between G0/G1 and G2/M phases) (Ginzberg et al., 2018). In confluent cultures, cell area did not change across phases of cell cycle and confluent cells had lower proliferation rates. VEGF treatment did not induce significant differences in cell area in these conditions.

Analysis of the width-to-length ratio (WLR) in confluent cultures (Fig. 4B) shows a clear reduction in WLR in VEGF-treated cells, demonstrating cell elongation and confirming effectiveness of VEGF treatment. No difference was noted in WLR across different EC types or cell densities. By qualitative inspection of phalloidin-stained cells, we noticed that different ECs had qualitatively different distribution of actin cytoskeleton (see Abu Taha et al., 2014; Millán et al., 2010). In our subconfluent conditions, HAoECs, HPMECs and HUVECs demonstrated different frequencies of cells with stress fibres (Fig. 4C). Data analysis showed that HAoECs and HUVECs had the highest proportion of cells with stress fibres, whereas HPMEC had the lowest frequency. VEGF treatment induced a significant increase of cells with stress fibres for HAoECs but a decrease in HUVECs, whereas HPMECs maintained a low level - like baseline.

Overall, the EC types analysed were remarkably different in terms of cell area and arrangement of cytoskeleton. As expected, cell area increased with progression of cell cycle in subconfluent cultures, but this effect was less prominent in confluent conditions where cells had lower, yet appreciable, proliferation rates. As expected, VEGF treatment clearly induced elongation in all cell types and induced cytoskeleton rearrangement in HAoECs and HUVECs.

Analysis of junction heterogeneity

The description of EC junction dynamics and morphology has been of great interest due to the link with vascular permeability and angiogenesis. In general, non-proliferating ECs are also those with continuous ('stabilised') IEJs, while migrating or proliferating EC demonstrate jagged or discontinuous junctions, which are rapidly remodelling (Fernández-Martín et al., 2012; Millán et al., 2010). Average population measurements have been used by us (Veschini et al., 2011, 2007; Wiseman et al., 2019) and others to assess stability of EC monolayers, which in turn correlate with functions such as trans-endothelial permeability to large proteins (Ferrero et al., 2004). Assessing IEJs at the single-cell level enables subtle nuances in inter-endothelial cells connectivity within the same monolayer to be highlighted. Nonetheless, measuring and classifying junctional signal by image analysis is technically challenging, and no currently available software can evaluate multiple images in a standardised way.

To overcome this obstacle, we automated analysis of CDH5 pattern and junction morphology using the ML capabilities of CPA and integrated this into ECPT. Previous studies on EC junction (Brezovjakova et al., 2019; Seebach et al., 2015; Wiseman et al., 2019) did not analyse the proportion of different junction pattern; our method classifies objects from whole junctions using an expert-trained ML algorithm (CPA with Fast Gentle Boosting, Appendix 1 at https://github.com/exr98/HCA-uncovers-metastable-phenotypes-in-hEC-monolayers). In line with the literature in the
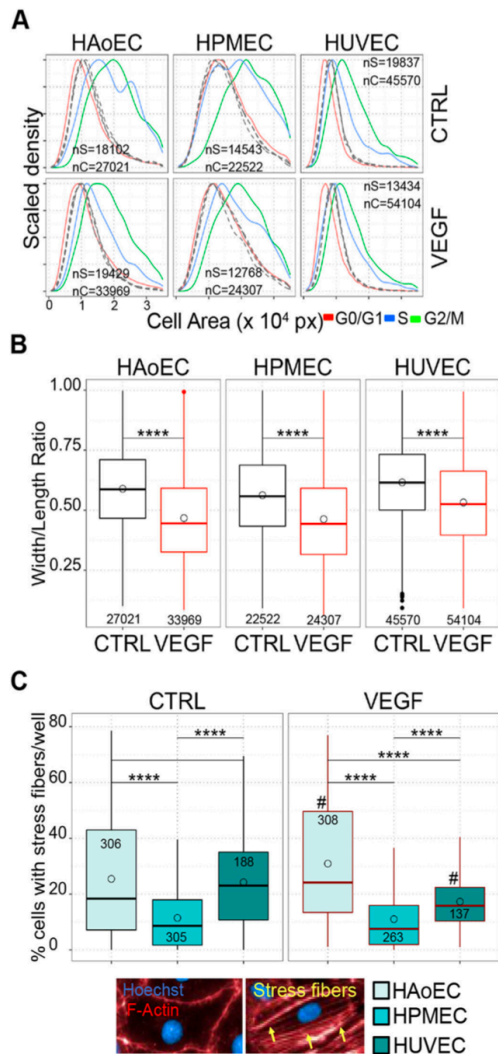
Fig. 4. Analysis of cell morphology and cytoskeleton. (A) Scaled density plots showing distribution of cell areas across cell types (HAoECs, HPMECs and HUVECs) and treatment [control (CTRL) and VEGF] in sub-confluent (coloured traces, colour code as shown in legend) or confluent (dashed grey traces) conditions. (B) Width-to-length ratio (WLR) of cell areas across cell types (HAoECs, HPMECs and HUVECs) and treatment (CTRL and VEGF). (C) Analysis of stress fibres across cell types (HAoECs, HPMECs and HUVECs) and treatment (CTRL and VEGF). The box represents the 25–75th percentiles, and the median (line) and mean (circle) is indicated. The whiskers extend to the maximum or minimum values within a 1.5× interquartile range (IQR) distance from the box hinge. Outliers not represented. n of observations for each representation or statistical comparison indicated as annotations in individual plots. ****P<0.0001 (one-way ANOVA followed by Tukey's post-hoc HSD test).

field (Seebach et al., 2016), we classified junctions in a scale from 0 to 5 (Fig. 5A). J0, J1 and J2 are discontinuous, highly jagged and jagged junctions, respectively. J3 and J4 are linear, with J4 having a

continuous CDH5 signal distributed over a larger area than J3. J5 junctions are visually reminiscent of the reticular junctions previously described (Millán et al., 2010) but could also appear as transient structures (Kim and Cooper, 2018; Seebach et al., 2020). J0 junctions might result from mis-segmented cells; therefore in downstream analyses we considered cells with less than 20% J0 junction type.

Fig. 5B shows the average percentage of junctions of each type across the three EC lines examined. HAoECs had a prevalence of the J1, J2 and J3 types with scarce J4. HPMECs were characterised by a high proportion of J4 junctions, whereas HUVECs had a high proportion of the J2 type. Overall, HPMECs and HUVECs had opposing phenotypes, whereas HAoECs were more heterogeneous. Time in culture upon seeding has been shown to affect junction response to perturbation (Andriopoulou et al., 1999), therefore we set to evaluate this effect under our experimental conditions. Fig. 5C shows the average percentage of junctions of each type per cell per field comparing cells cultured for either 48 h or 96 h. The effect of longer culture in all cells was an increase in J4 and J5 types, with a corresponding decrease in J3. Furthermore, a decrease in the highly jagged J1 type with a proportional increase in the less jagged J2 type was also noted. Overall, we conclude that longer time in culture significantly and positively affects junction quality in line with previous reports (Andriopoulou et al., 1999; Bazzoni and Dejana, 2004). Finally, we set to evaluate the effect of VEGF treatment in our system. As shown in Fig. 5D, the main effect of VEGF treatment on confluent cells cultured for 96 h upon seeding was a sharp increase in J3 with a corresponding decrease in all the other junction types.

Altogether, these data demonstrate that the EC lines are very heterogeneous in respect to IEJs, and that many cells have a composition of different junctions, which might also reflect differential connectivity with different neighbours. This junctional heterogeneity has been previously described and can now be detected and quantified by our ECPT. This suggests that IEJ architecture can be regulated locally as all cells were cultured under identical experimental conditions and all individual ECs within monolayers exposed to the same environment. Overall, we showed that image analysis and supervised ML can be used to characterise EC junctions and highlight differences at the population level. Our workflow was able to efficiently distinguish changes in junction morphology after different time in culture or VEGF treatment and the junctional status of single cells can be used to study intra-population heterogeneity.

Analysis of NOTCH activation

NOTCH signalling is a key modulator of EC development and function, but assessment of signal heterogeneity in EC monolayers and its potential role in regulating these functions is currently lacking.

To assess heterogeneity in NOTCH signalling in our experiments we measured the intensities of intra-nuclear NOTCH1 (nN1) and intra-nuclear HES1 (nHES1) by ECPT. Fig. 6A illustrates the density distribution of the two signal intensities for all cells in our dataset at baseline, demonstrating bulk differences between EC types. Analysis of mean signal intensity by microscopy field did not highlight striking differences across EC types and treatment. However, inspection of density distributions highlighted differences, and suggests that these might originate in different repartitions of cells across signal intensities. To investigate this aspect, we binned signal intensities as illustrated by the banding in Fig. 6A and calculated summary statistics by microscopic field for these bins. The results of these analyses for nN1 and nHES1 are shown in Fig. 6B,C. Analysis of nN1 highlighted differences in

6
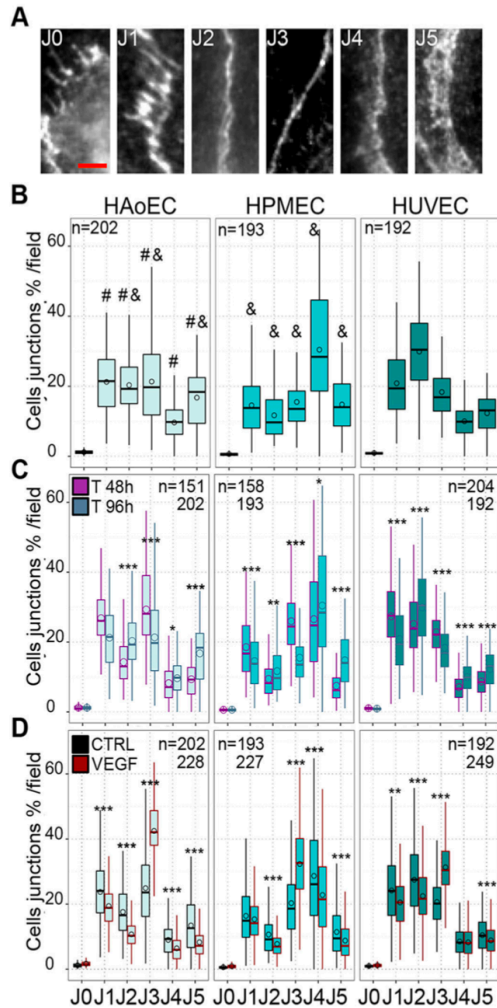
Fig. 5. Image-based EC junction analysis. (A) Examples of junctional structures imaged in EC monolayers. The junctions are classified as J0 (not a junction or highly discontinuous), J1 (highly jagged and discontinuous), J2 (jagged), J3 (linear), J4 (linear reinforced signal) and J5 (linear/reticular). (B) Percentage of cells in the different categories for across cell types under control (CTRL) conditions and cultured for 96 h. (C) Repartition of the cells in the different classes after 48 h or 96 h in culture. (D) Percentage of cells in the different classes in basal conditions or after VEGF treatment.. The box represents the 25–75th percentiles, and the median (line) and mean (circle) is indicated. The whiskers extend to the maximum or minimum values within a 1.5× interquartile range (IQR) distance from the box hinge. Outliers not represented. n of observations for each statistical comparison indicated as annotations in individual plots. *$P<0.05$, **$P<0.01$, ***$P<0.001$, &$P<0.001$ against HPMECs, #$P<0.001$ against HUVECs (one-way ANOVA followed by Tukey's post-hoc HSD test).

proportion of cells with either intermediate (2^8) or high (2^{10}) signal. At baseline, HAoECs had the lowest percentage of cells in the intermediate intensity category and the highest percentage of cells in

the high category. The opposite was true for HUVECs, whereas HPMECs displayed a similar percentage in the two categories and were intermediate between the other EC types. VEGF treatment set the moderate cells at intermediate levels for all cell types, while it increased the percentage of high cells in HUVECs.

Fig. 6C shows the analysis for nHES1 where cells were binned according to a $\log_{10}$ scale (bins referred to as low, intermediate, high and very high hereafter). HAoECs and HPMECs had both a lower average percentage of cells in the low intensity category and a greater percentage of cells in the high intensity category (13.7% and 56.9% in HAoECs, and 13.5% and 51% in HPMECs, respectively) in comparison to HUVECs (22.3% and 46.1%). VEGF treatment induced a marked decrease in the average percentage of low intensity cells and a corresponding increase in high intensity cells in HAoECs (6.8% and 61.5%) and had the opposite effect in HUVECs (30.8% and 44.7%).

We then evaluated the effect of differential time in culture by comparing nHES1 distribution in cells cultured for 48 h or 96 h. Fig. S1A displays density distributions of nHES1 intensity, which demonstrated marked changes in HAoECs and HUVECs and less difference in HPMECs. Fig. S1B shows that the overall effect of longer culture was a marked reduction of cells in the low intensity bin and a corresponding increase in the high bin in HAoECs and HUVECs, whereas HPMECs were mostly unaffected.

Altogether, these results are in line with baseline gene expression levels of HES1 in the three EC types (Fig. S2) and with previous gene expression studies (Chi et al., 2003) where arterial ECs demonstrated higher levels of NOTCH signalling than venous ECs.

We also demonstrated previously unappreciated high levels of NOTCH signalling in HPMECs, which were higher than HUVECs, as also confirmed by gene expression analysis (Fig. S2).

Importantly, our analysis highlights that: (1) NOTCH signalling is not homogeneous in ECs within monolayers, (2) all monolayers examined have similar ranges of nN1 and nHES1 signal intensities, and (3) bulk differences (e.g. qRT-PCR, Fig. S2) result from different proportions of low, intermediate or high signalling cells.

To estimate functional consequences of these observations, we evaluated correlation between downstream NOTCH signalling and the cell cycle. We found that the single-cell levels of nHES1 were increased in cells engaged in cell cycle (∼2-fold increase between G0/G1 and S and a further ∼2-fold increase between S and G2/M) and decreased in dividing cells (∼2-fold among LM and G0/G1) (Fig. 6D). These observations were invariant across cell types, treatment and time in culture. It might be expected that cycling ECs would have low NOTCH signalling as it has been previously shown that NOTCH signalling causes cell cycle arrest and inhibition of proliferation (Fang et al., 2017; Luo et al., 2021). In fact, all cell types in all phases of cell cycle had a significant proportion of cells with low nHES1 (Fig. 6D, shown as outlier dots in boxplots) and mitotic LM cells had an average or low level of nHES1.

We conclude from all data on nHES1 that, as expected and reported before (Fang et al., 2017), confluent ECs have relatively high basal levels of NOTCH signalling. However, we also observed that, within the same population, some cells have low levels of nHES1. To interpret previous reports and our current data, we hypothesize that sustained NOTCH signalling in confluent EC monolayers acts as a molecular break to limit cell cycle progression. Further, we postulate that this exists as an escape mechanism by which cells can have low local levels of nHES1 allowing cell cycle finalisation despite sustained signalling at population level. Many previous studies have highlighted the role of NOTCH in mediating tissue patterning by mechanisms of lateral inhibition and in certain

92
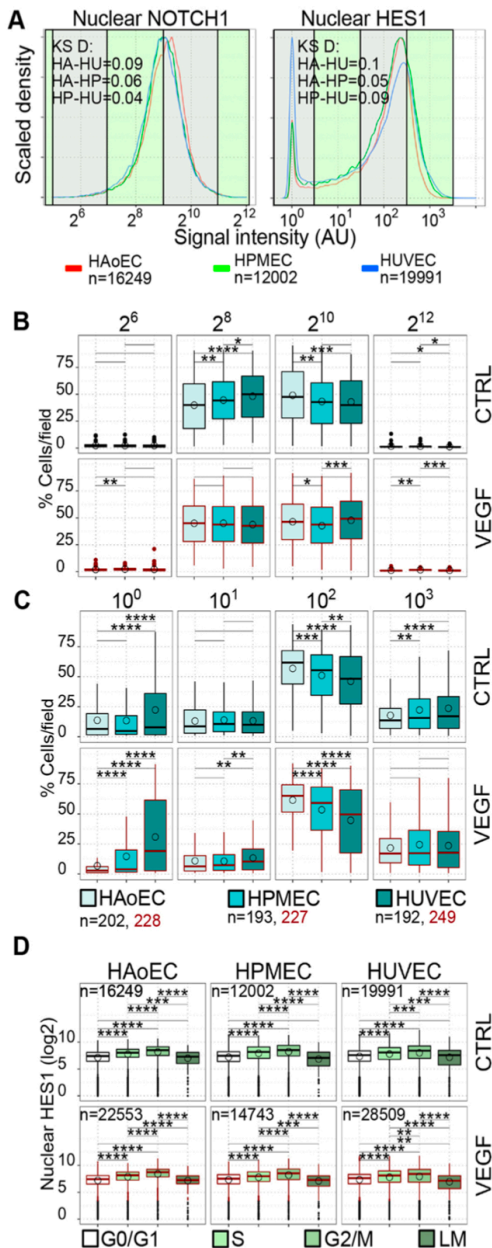
Fig. 6. Analysis of NOTCH activation. (A) Scaled density distributions of nN1 and nHES1 for HAoECs, HPMECs and HUVECs (coloured traces corresponding to legend). Distances between distributions are shown as annotations in plots [Kolmogorov–Smirnov (KS) D, $P<0.001$ for all reported D]. Green/transparent banding on plots indicates boundaries of selected intensity bins. AU, arbitrary units; HA, HAoECs; HP, HPMECs; HU, HUVECs. (B) Percentage of cells per image (microscopy field) pertaining to different intensity bins (nN1) and EC types. (C) Percentage of cells per image (microscopy field) pertaining to different intensity bins (nHES1) and EC types. (D) Intensity of nuclear HES signal (single cells) across phases of cell cycle, cell types (HAoEC, HPMEC, HUVEC) and treatment (CTRL, VEGF). The box represents the 25–75th percentiles, and the median (line) and mean (circle) is indicated. The whiskers extend to the maximum or minimum values within a 1.5× interquartile range (IQR) distance from the box hinge. Points outside this range are indicated as outlier dots. n of observations for each statistical comparison indicated as annotations under or in individual plots. *$P<0.05$, **$P<0.01$, ***$P<0.001$, ****$P<0.0001$ (one-way ANOVA followed by Tukey's post-hoc HSD test).

neighbourhoods and across entire monolayers. We first ran the population level analysis (global Moran's, as detailed in Fig. S3 and Materials and Methods) across all images in our dataset using either nN1 or nHES1 signals as inputs and length of junction object as the weighting parameter since estimated strength of neighbours' interaction depends on extent of cell–cell contact.

Fig. 7A shows that, on average, 25.7–40.4% of microscopic fields across cell types and VEGF treatment had a statistically significant positive Moran's index (pGMi). Furthermore, 1.9–4.7% of microscopic fields had a statistically significant negative Moran's Index (nGMi), whereas 57.1–71.7% had randomly distributed cell intensities for nHES1. HUVECs had the highest percentage of microscopic fields with a pGMI.

Thus, the first key finding upon global Moran's analysis is that most microscopic fields analysed (irrespective of cell type and treatment) had randomly distributed cell intensities, highlighting the presence of intermediate cell states at the local population level. However, a sizeable fraction of the populations analysed shown evidence of clustered or sparse cell distributions, suggesting that lateral inhibition and lateral induction are effectively active in the system. The average positive and negative global Moran's indexes for all images analysed was ∼0.4 and ∼−0.3. These are intermediate values (extremes are 1 and −1 as illustrated in Fig. S3), which suggest that clustering or sparse distributions were detected in cell neighbourhoods smaller than the microscopic field analysed. Overall, global Moran's analysis confirms that the observed bulk population distributions of nHES1 (Fig. 6A) are reflective of local arrangement after considering spatial relationships, and suggests that clustering or sparseness can emerge in the wider population. To confirm and extend these observations, we performed local Moran's analysis, which considers the immediate cell neighbourhood.

Fig. 7B illustrates one example of such analysis for both NOTCH (upper panels) and HES1 (lower panels). The intensity maps associated with nN1 and nHES1 highlight local heterogeneity in signalling and the P-value maps indicate which cells in the map have statistically significant local Moran's index (LMi, either positive or negative).

Comparisons of intensity and P-value maps highlight clusters of cells with either similar or dissimilar signal values, which were predicted by global Moran's analysis and confirms that these clusters are smaller than the microscopic field (5–20 cells). 84% of all images had at least one cell with a statistically significant negative LMI (nHES1) and 50% of all images had at least one cell with a statistically significant positive LMI (nHES1). The frequency

context lateral induction. We therefore set out to estimate the involvement of these processes using our ECPT.

Spatial autocorrelation analysis of NOTCH signalling

To evaluate the role of lateral inhibition and lateral induction mechanisms, we used spatial autocorrelation analysis (Moran's analysis) to assess the distribution of nN1 and nHES1 signals in cell
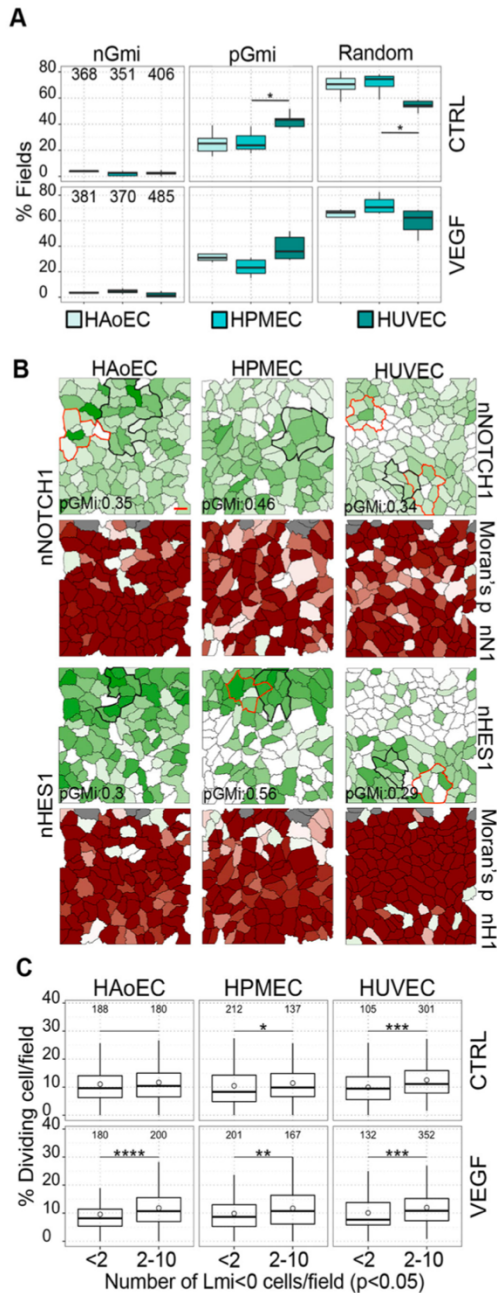
Fig. 7. Spatial autocorrelation analysis. (A) Box plots representing percent of fields with either significant ($P<0.05$) positive or negative global Moran's index (pGMi, nGMi) or random cell distributions ($P>0.05$ in both pGMI and nGMI) by cell type and treatment. (B) Representative maps of cells with significant pMGi and relative Local Moran's analysis. Green coloured maps refer to intensity of either nuclear NOTCH1 (log_{10}) or HES1 (log_2) signal (white=low intensity, dark green high intensity). Red coloured maps refer to P-value of local Moran's index LMi (white $P<0.05$, dark red $P=1$). Outlines in intensity maps indicated neighbourhood of selected cells with significant LMi associated with either positive (black) or negative (red) LMi. (C) Boxplot (by EC type) representing percentages of dividing cells per images grouped in bins with low <2 or higher (2–10) numbers of cells with negative and significant LMi per field. The box represents the 25–75th percentiles, and the median (line) and mean (circle) is indicated. The whiskers extend to the maximum or minimum values within a 1.5× interquartile range (IQR) distance from the box hinge. Outliers not represented. n of observations for each statistical comparison indicated as annotations under or in individual plots. *$P<0.05$, **$P<0.01$, ***$P<0.001$, ****$P<0.0001$ (one-way ANOVA followed by Tukey's post-hoc HSD test).

These observations confirm those of the global analysis and show that the distribution of nHES1 within EC monolayers is largely random and independent of cell type or exposure to VEGF treatment. However, monolayers are interspersed with neighbourhoods of cells that are engaged in lateral induction or inhibition processes as exemplified in Fig. 7B.

If cell proliferation is correlated with these phenomena as hypothesized above, we expect that cells able to progress through the cell cycle would be laterally inhibited to express lower levels of HES1 and escape cell cycle arrest. If that were the case, we would also expect to find more cells progressing through the cell cycle in areas where lateral inhibition is prevalent. To test this hypothesis within the limits of our experimental setup, we compared microscopy fields with below – or above – average number of nLMi cells. Fig. 7C shows the results of this analysis, confirming that microscopy fields with above average numbers of nLMI cells also had higher numbers of cells in cell cycle (Fig. 7C). As expected, no difference was found when considering abundance of pLMi cells.

Overall, we conclude that local lateral inhibition mechanisms can inhibit HES1 expression in a few cells within an EC population and thus increase the probability of individual cells progressing through the cell cycle.

Finally, as we had observed that longer times in culture quantitatively affected the distribution of nHES1 intensities (Fig. S1A,B), we sought to evaluate qualitative effects in Lmi. Fig. S1C shows comparisons between counts of images containing 0 to 8 cells with negative Lmi (nLMi) and demonstrates that longer time in culture reduced the proportion of images with higher number of nLMi cells (without change in pLMi cell counts). Overall, longer time in culture reduced the number of cells engaged in lateral inhibition without subverting the overall distributions of cells with scattered presence of either small homogeneous cell clusters or laterally inhibited cells.

DISCUSSION

ECs exert an outstanding variety of specialised functions (Augustin and Koh, 2017; Rafii et al., 2016), which are reflected in EC phenotypical heterogeneity. EC diversity arises during development and is preserved through homeostasis. The activation of differential genetic programmes interplays with microenvironmental factors (Adams and Alitalo, 2007; Chi et al., 2003). Interestingly heterogeneity within the same vascular bed, where microenvironmental factors are likely only undergoing minor fluctuations, has been observed *in vivo* (McCarron et al., 2019) and

of nLMi were 1.6±1.2, 1.4±1.3 and 2.8±1.8 nLMI cells/per field (mean±s.d.) in HAoECs and HPMECs and HUVECs. Average frequencies of pLMi were 0.6±0.8, 0.6±1 and 1±1.4 cells/field for HAoECs, HPMECs and HUVECs, and VEGF treatment did not induce substantial changes in nLMi or pLMi frequencies.

deemed crucial to understand variable functions within the same EC type.

These mechanisms require similar cells to preserve discrete, diverse and adaptable phenotypes, and the time scale at which these changes happen can be smaller than that of gene expression (Chapman et al., 2016; Stepanova et al., 2021). Thus, to justify rapid phenotype switches it is necessary to involve inherently dynamic processes, such as junctional plasticity. Direct evaluation of dynamic changes in cell connectivity still poses considerable technical hurdles, and despite great advances in live-microscopy, comprehensive cell phenotyping of single cells at the population level still relies heavily on end-point experiments. Although observation of fixed cells cannot provide information on the exact dynamics of the system, extensive profiling of single cells can inform about cell dynamic behaviours and help to develop hypotheses, which can then be evaluated experimentally or with computational methods (Altschuler and Wu, 2010).

To gain a better understanding of EC heterogeneity, connectivity and emerging dynamic behaviours (McCarron et al., 2019, 2017), we developed ECPT and characterised three EC lines under standard conditions or supra-physiological levels of VEGF (like those observed in cancer). In line with previous studies (Chi et al., 2003), our data demonstrate that human aortic, umbilical vein and pulmonary microvascular ECs present distinct phenotypes (Figs 1–7), which are maintained at steady state and are independent of microenvironmental stimuli. HAoECs, HPMECs and HUVECs displayed different intrinsic proliferative potential and demonstrated a diffuse ability to proliferate, in contrast to the idea that ECs undergo terminal differentiation and lose proliferative capacity (Yoder, 2018). Our image-based analysis of cell cycle based on DNA intensity highlighted interesting differences between the different EC lines in subconfluent conditions, with HUVECs and HAoECs proliferating faster than HPMECs, and an overall small increase in the dividing cell number after VEGF treatment. In confluent conditions, all cell types settled to a lower proliferation rate, which was similar for all EC types.

It is well established that cytoskeleton arrangement correlates with differential EC phenotypes in different contexts. ECs exposed to flow display stress fibres aligned with direction of flow and migrating ECs display similar stress fibres along the direction of migration. Analysis of the EC cytoskeleton (Fig. 4) demonstrated distinctive profiles in line with proliferation statuses in HAoECs, HPMECs and HUVECs, with microvascular HPMECs having the lowest numbers of stress fibres. At the same time, all cells demonstrated intra-population heterogeneity with intermixing of cells with or without stress fibres in individual monolayers (Fig. 4). This suggests a high degree of cellular rearrangement as indicated by time-lapse microscopy experiments showing that live ECs in monolayers constantly rearrange their shape and connections (Kim and Cooper, 2018).

Differential EC functions lead to variance in IEJs, which in turn regulate traffic of molecules and solutes in and out of capillaries and inhibit coagulation by preventing exposure of the underlying subintimal layer in arteries and veins. Analysis of IEJ in three different EC populations highlighted a high degree of junctional heterogeneity. In line with the data discussed above and existing literature, we show that HAoECs (arterial) had more linear junctions than HUVECs (venous), which instead tended to form highly dynamic jagged junctions. Importantly, HPMECs had the most linear/stabilised junctions, whereas HAoECs had more heterogeneous jagged/linear junctions and stress fibres (Fig. 4). This is reminiscent of the unique role the pulmonary and arterial

vessels play in regulating solute exchange or adapting to high flow, respectively. This is in line with recent sc-RNA sequencing data demonstrating that >40% of murine HAoEC express mesenchymal genes (Lukowski et al., 2019) and are therefore expected to display morphological and junctional heterogeneity accompanied by stress fibres.

In agreement with results reported before (Bazzoni and Dejana, 2004), longer culture times and VEGF treatment in our experiments induced characteristic changes in cell morphology and promoted more continuous junction types across all EC types.

Distinctive features among different EC populations seem to be hard coded within cell gene expression programme, as cells from individual donors had vastly overlapping phenotypes and the features were maintained in all lines upon several passages in culture.

If the decision to enter the cell cycle or to maintain stable junctions were dependent on clear-cut differential gene expression, we would expect to find a limited collection of homogeneous phenotypes. However, we find a continuous range of EC phenotypes within the same EC monolayer. To interpret EC intra-population heterogeneity, we focussed on NOTCH signalling for its well-established role as a coordinator of the opposing functions of EC proliferation (Fang et al., 2017; Luo et al., 2021) and junctional complex stabilisation (Bentley et al., 2014).

Furthermore, the NOTCH pathway is one of the main drivers of endothelial cell heterogeneity and is linked to vascular maturation, arteriovenous specification and angiogenic sprouting (Fish and Wythe, 2015; Hellström et al., 2007; Potente et al., 2011; Torres-Vázquez et al., 2003). Although NOTCH signalling dynamics have been studied in HUVECs and retina, it is still unclear how it affects EC heterogeneity in different organs. Nuclear NOTCH1 (N1-ICD; where ICD is intracellular domain, generically NICD) acts as a transcription co-factor to induce the expression of target genes, such as the HES/HEY family of transcription factors, and is therefore active in the nucleus. In line with previous results on HEY1 and HEY2 expression in HUVECs (Aranguren et al., 2013), we hypothesised that ECs within monolayers would have a homogeneous level of NOTCH signalling that was either low or absent in venous ECs and high in arterial ECs. One study has reported appreciable baseline NICD levels in HPMECs by western blotting (Zong et al., 2018) but not in comparison with other EC lines. Recent single-cell RNA sequencing data of human lungs has highlighted heterogeneity among arterial, venous, and microvascular ECs, which displayed intermediate phenotypes (Kalucka et al., 2020). Interestingly, activation of NOTCH downstream target genes also seems heterogeneous across and within EC populations (Travaglini et al., 2020). Fluctuations in NOTCH signalling have been hypothesised in EC monolayers and demonstrated in EC during sprouting angiogenesis where NOTCH acts as a bistable switch (Ubezio et al., 2016). It has been demonstrated that leading tip cells induce NOTCH signalling in trailing stalk cells via Dll4–NOTCH1 leading to lateral inhibition of the tip cell phenotype (Ubezio et al., 2016), whereas ECs within a stabilised monolayer cannot acquire a tip cell phenotype and all ECs receive, in principle, similar NOTCH stimulation from neighbours.

By measuring NOTCH1 and HES1 levels in individual ECs, we found that different ECs within their monolayer had different levels of NOTCH activation, which was also reflected in different bulk gene expression measures of NOTCH target genes (HES1). However, the clearest differences across cell types and treatments were found in relative proportions of cells with differential signal within the same EC population, suggesting that individual cells can

10

acquire differential phenotypes, which can be modulated by VEGF treatment (Fig. 6). This degree of heterogeneity in NOTCH signalling in neighbouring cells also strongly suggests that the NOTCH phenotype is regulated dynamically in EC monolayers, with lateral inhibition and lateral induction being two potential candidate mechanisms. To investigate this hypothesis, we performed spatial autocorrelation analysis (Fig. 7), which demonstrated a high degree of heterogeneity of NOTCH and HES1 in ECs within the same monolayer. If either lateral inhibition or lateral induction were the prevailing mechanism in regulating the NOTCH phenotype in ECs, we would expect sparse or uniform spatial distribution of NOTCH and HES1 activation. However, we found a high degree of randomness in the spatial distribution of these signals. Alternatively, the two mechanisms might act in concert to produce qualitatively different cell distributions, which seems plausible as all EC types analysed expressed both Dll4 and Jagged1 ligands (Fig. S2), which have been shown to be involved in lateral inhibition and lateral induction, respectively (Pedrosa et al., 2015). When we performed local spatial autocorrelation analysis, we confirmed that both mechanisms seem to occur together and our results are in line with previous mathematical models (Boareto et al., 2016) showing that concurrent lateral inhibition and induction can generate intermediate cell states. Our current data demonstrate that intermediate phenotypes in both nN1 and nHES1 are common in all ECs analysed, irrespective of treatment, and that lateral induction or lateral inhibition patterns emerge locally. This complex spatial distribution does not seem compatible with stabilised phenotypes and rather suggests a scenario where cell phenotype is dynamically regulated and can change over time to exert differential functions while maintaining a stable balance across the wider population.

Novel spatialised mathematical models of NOTCH signalling could be used in future work to assess whether NOTCH is sufficient to generate the heterogeneity we found in our experiments or whether further layers of regulation need to be accounted for.

To evaluate the functional consequences of our findings, we asked whether spatial patterning accompanied by differential signalling could affect other parameters in our dataset. We did not find any correlation between the extent or spatial distribution of nN1 and nHES and junction status, possibly because junctions are remodelled at a very fast pace in cultured ECs (Kim and Cooper, 2018) and thus our experimental context using fixed cells might fail to resolve processes at this timescale. When we considered cell proliferation, we found that HES1 was, on average, higher in cells progressing through the cell cycle but several cells had low levels irrespective of their cell cycle status. When we compared the abundance of laterally inhibited cells with dividing cells at the population level, we consistently found that populations containing more of these cells were also proliferating at a slightly higher pace. Overall, our data suggest that the decision to initiate and progress through cell cycle in continuous monolayers with high basal levels of NOTCH signalling is regulated by the extent (and possibly duration) of lateral inhibition in the local cell neighbourhood. Moreover, we show that the formation of patches of cells with similar NOTCH signalling is a common finding in EC monolayers *in vitro*. It will be interesting to investigate whether this is reflected *in vivo* and the functional consequences of this phenomenon considering previous work has identified patches of cells with differential Ca^{2+} signalling and density of endothelial M3 muscarinic acetylcholine receptors (AchRM3s) *in vivo* (McCarron et al., 2019, 2017). However, *in vivo* investigations will still pose significant technical challenges to high throughput analyses such as those presented here.

It will be also interesting in future work to evaluate whether the patterns observed in our experiments are stable or remodelled over time, and the timescales of these changes. The ECPT presented in this work is a step forward in comparison to available platforms (see Table 1) and represents a bridge between experimental and computational setups, where experimental ECPT data can be used to guide development of spatialised mathematical models, which in turn can be used to guide further experimentations. The experimental setup introduced in the present work does not extend to resolving highly dynamic processes; however, ECPT paves the way towards quantifying more advanced experiments, such as measurements of gene transcription by fluorescence *in situ* hybridization (FISH) or live imaging using fluorescent reporters.

Overall, the ECPT allows for the evaluation of cell-intrinsic mechanisms of monolayer maintenance and plasticity, excluding variability caused by microenvironmental factors, in line with previous observations on blood vessel heterogeneity *in vivo* originating from EC rather than perivascular cells (Chavkin and Hirschi, 2020). It will be important to elucidate in future studies how the crosstalk with perivascular cells and microenvironment can affect emerging endothelial behaviours.

We envisage that coupling our ECPT workflow with live imaging setups, computational modelling and single cells transcriptomic analysis will open the way to a much deeper understanding of emerging dynamic endothelial behaviours and thus help to develop novel more effective therapies for regenerative medicine, prevention of cardiovascular diseases and the treatment of cancer.

MATERIALS AND METHODS
Cell culture
HAoECs, HPMECs and HUVECs (all PromoCell) were plated on 10 µg/ml fibronectin (from human plasma, Promocell)-coated flasks, grown in EGMV2 medium (Promocell) in the absence of antibiotics, detached with accutase (Thermo Fisher Scientific, Waltham, MA), and used by passage 5. We analysed two distinct donors for each cell type, which were chosen excluding diseases affecting the vasculature (e.g. diabetes). Donor's age (HAoECs, HPMECs) was between 50 and 63 years. For experiments, 4×10^4 ECs per well were seeded in fibronectin-coated 96-well plates (µClear, Greiner) and cultured for 48 or 96 h under basal (EGMV2, Promocell) or activated (EGMV2+50 ng/ml VEGFA, Peprotech, London, UK) conditions in triplicate paralleling conditions described previously (Andriopoulou et al., 1999). The EC formed confluent monolayers at microscopic inspection [phase contrast, 10×–20× original magnification (OM; as indicated on objective)] at the time of immunostaining and image acquisition.

Immunostaining
Cells were fixed with 2% paraformaldehyde in phosphate-buffered saline (PBS) for 10 min at room temperature. Cells were blocked 1 h with PBS supplemented with 1% fetal bovine serum (FBS) and permeabilised with 0.1% Triton X-100. Cells were then incubated for 1 h at room temperature with primary antibodies against CDH5 (VE-cadherin; Novusbio NB600-1409, 1 µg/ml final), NOTCH1 (Abcam, ab194122, Alexa Fluor 647-conjugated, 1 µg/ml final) and Hes1 (Abcam, ab119776, 1 µg/ml final). Plates were washed and incubated 1 h with 1 µg/ml secondary Alexa Fluor 488-conjugated and Alexa Fluor 555-conjugated antibody (Thermo Fisher Scientific), Hoechst 33342 (1 µg/ml, Sigma) and Phalloidin-Atto 647N (Sigma). All antibodies used in immunostaining were previously validated for specificity by western blot analysis (Fig. S4).

Image acquisition
We obtained images from slides with an Operetta CLS system (PerkinElmer, Waltham, MA) equipped with a 40× water immersion lens (NA 1.1). In each well, three areas were acquired. Each area is composed of nine microscopic fields at 40× OM (Fig. S1). We standardised acquisition parameters (light-emitting diode power, exposure time) throughout different experiments

and used HUVECs as a standard for calibration in all experiments. We analysed an image database containing 28,000 images (7000 fields in four fluorescence channels) extracted from nine independent experiments conducted on EC lines from two different donors each. Two intraexperiment replicates were conducted for each experiment.

Endothelial cell profiling tool

We used a combination of machine learning-aided image segmentation (ImageJ) (Schindelin et al., 2012) and an image-based cell profiling tool (CellProfiler) (Carpenter et al., 2006) to extract the phenotype of single EC in monolayers. Our workflow enables the measurement of EC morphology (area, perimeter, shape descriptors and cell neighbours), NOTCH1, HES1, CDH5 and DNA intensities, and the characterisation of inter-endothelial junctions (IEJs). In the present study, we chose to analyse only selected features with recognised functions in EC biology. Image texture features were measured and only used during the training of ML algorithms (Caicedo et al., 2017; Jones et al., 2008), which in turn were used to classify junction morphology and LM cells. ECPT scripts and methods including FIJI/ImageJ macros for image importing and pre-processing are detailed in Appendix 1 at https://github.com/exr98/HCA-uncovers-metastable-phenotypes-in-hEC-monolayers.

We imported and cleaned the results into R studio excluding artefacts and mis-segmented cell objects (extreme values in cell area or signal intensity, NAs in measurements). We then calculated continuous and categorical (cell cycle) parameters. Following guidelines suggested by Caicedo et al. (2017), we pre-processed the database to exclude mis-segmented cells and to normalise the measurements prior to dimensionality reduction or single factor analysis. We reformatted and tidied the database and calculated summary statistics using packages from the Tidyverse packages collection (https://www.tidyverse.org; Dplyr, Tidyr, Tibble, Forcats, Purr and Ggplot2).

We conducted PCA analysis on ECPT parameters (Cell morphology, intensity, neighbourhood and junctional status, Table S1) using the prcomp function (R Stats package) generating 12 PCA components. All plots in figures are generated using the Ggplot2 R package.

We created a Shiny application (https://CRAN.R-project.org/package=shiny) for interactive selection and visualisation of data of interest. All files containing the code required to reproduce all the plots in the paper and to run the Shiny application using our dataset are available on https://github.com/exr98/HCA-uncovers-metastable-phenotypes-in-hEC-monolayers.

Western blotting

Cells were scraped in the presence of RIPA buffer (Sigma-Aldrich) containing protease (Millipore, UK) and phosphatase inhibitors (Sigma-Aldrich, UK), left on ice for 15 min, and centrifuged at 13,000 g for 5 min in a refrigerated microfuge. Supernatants were assessed for total protein using the BCA protein quantitation kit (Thermo Fisher Scientific). 15 µg of protein were separated on NuPAGE 4–12% Bis-Tris gels (Invitrogen) before being transferred to nitrocellulose membranes (GE Healthcare, Amersham, UK). After probing with primary and secondary antibodies, membranes were developed using Clarity™ Western ECL Substrate (Bio-Rad, UK) and read using a ChemiDoc system (Bio-Rad). Antibodies for NOTCH1 (1:500; Abcam, ab194122), HES1 (1:1000; Abcam, ab119776), VE-cadherin (1:500; Novus bio NB600-1409) and β-tubulin (1:1000; Cell Signaling Technology) were used. Goat anti-mouse-IgG and anti-rabbit-IgG horseradish peroxidase (HRP)-conjugated antibodies were from Dako (Agilent).

RNA extraction and qRT-PCR

Total RNA was extracted and purified using the Monarch total RNA miniprep kit according to the manufacturer's instructions. The resulting RNA was quantified using Nanodrop (ISOGEN Life Science). For quantitative real-time PCR (qRT-PCR), 1 µg of RNA was used for reverse transcription using the iScript cDNA synthesis kit (Bio-Rad). The gene expression analysis was carried out using the SsoAdvanced™ Universal SYBR Green Supermix (Bio-Rad) and analysed by means of a Stratagene Mx3000P (Agilent Technologies) in real time, primers used are listed in Table S2.

Statistical analysis

To compare multiple groups, we used one-way ANOVA followed by Tukey's HSD post-hoc test. We considered $P<0.05$ (*) statistically significant and $P<0.01$ (**), $P<0.001$ (***) and $P<0.0001$ (****) highly significant.

To evaluate linear correlation between continuous variables we calculated Pearson's correlation coefficient I and considered $P<0.001$ as highly statistically significant.

Comparisons between intensity distributions were performed by two-sided Kolmogorov–Smirnov (KS) test as implemented in the 'stats' R package. We considered comparisons with $P<0.01$ to be statistically significant and reported corresponding distance index (D).

Statistical significance in global and local Moran's analyses is computed by random permutations as implemented in the adespatial R package we used 999 permutations in each test. We considered $P<0.05$ in Gmi or Lmi to be statistically significant (Dray, 2011).

Data availability

All raw and elaborated data are available at https://github.com/exr98/HCA-uncovers-metastable-phenotypes-in-hEC-monolayers. To facilitate data exploration and re-use we have developed a dedicated data browser using the Shiny app environment. Original images are available upon request to the authors.

References

Abu Taha, A., Taha, M., Seebach, J. and Schnittler, H.-J. (2014). ARP2/3-mediated junction-associated lamellipodia control VE-cadherin-based cell junction dynamics and maintain monolayer integrity. *Mol. Biol. Cell* **25**, 245-256. doi:10.1091/mbc.e13-07-0404

Acar, M., Mettetal, J. T. and van Oudenaarden, A. (2008). Stochastic switching as a survival strategy in fluctuating environments. *Nat. Genet* **40**, 471-475. doi:10.1038/ng.110

Adams, R. H. and Alitalo, K. (2007). Molecular regulation of angiogenesis and lymphangiogenesis. *Nat. Rev. Mol. Cell Biol.* **8**, 464-478. doi:10.1038/nrm2183

Altschuler, S. J. and Wu, L. F. (2010). Cellular heterogeneity: do differences make a difference? *Cell* **141**, 559-563. doi:10.1016/j.cell.2010.04.033

Andriopoulou, P., Navarro, P., Zanetti, A., Lampugnani, M. G., Dejana, E. (1999). Histamine induces tyrosine phosphorylation of endothelial cell-to-cell adherens junctions. *Arterioscler. Thromb. Vasc. Biol* **19**, 2286-2297. doi:10.1161/01.ATV.19.10.2286

Aranguren, X. L., Beerens, M., Coppiello, G., Wiese, C., Vandersmissen, I., Lo Nigro, A., Verfaillie, C. M., Gessler, M. and Luttun, A. (2013). COUP-TFII orchestrates venous and lymphatic endothelial identity by homo- or hetero-dimerisation with PROX1. *J. Cell Sci.* **126**, 1164-1175. doi:10.1242/jcs.116293

Augustin, H. G. and Koh, G. Y. (2017). Organotypic vasculature: From descriptive heterogeneity to functional pathophysiology. *Science* **357**, eaal2379. doi:10.1126/science.aal2379

Bazzoni, G. and Dejana, E. (2004). Endothelial cell-to-cell junctions: molecular organization and role in vascular homeostasis. *Physiol. Rev.* **84**, 869-901. doi:10.1152/physrev.00035.2003

Bentley, K., Franco, C. A., Philippides, A., Blanco, R., Dierkes, M., Gebala, V., Stanchi, F., Jones, M., Aspalter, I. M., Cagna, G. et al. (2014). The role of differential VE-cadherin dynamics in cell rearrangement during angiogenesis. *Nat. Cell Biol* **16**, 309-321. doi:10.1038/ncb2926

Boareto, M., Jolly, M. K., Goldman, A., Pietilä, M., Mani, S. A., Sengupta, S., Ben-Jacob, E., Levine, H. and Onuchic, J. N. (2016). Notch-Jagged signalling can give rise to clusters of cells exhibiting a hybrid epithelial/mesenchymal phenotype. *J. R. Soc. Interface* **13**, 20151106. doi:10.1098/rsif.2015.1106

Brezovjakova, H., Tomlinson, C., Mohd Naim, N., Swiatlowska, P., Erasmus, J. C., Huveneers, S., ~~Gautillera, Frankina, Good, Braga V. M. et al.~~ (2019). Junction Mapper is a no~~[https://doi.org/10.1016/j.coph.2019.03.008]~~ contact phenotypes. *eLife* **8**, e45413. doi:10.7554/eLife.45413

Caicedo, J. C., Cooper, S., Heigwer, F., Warchal, S., Qiu, P., Molnar, C., Vasilevich, A. S., Barry, J. D., Bansal, H. S., Kraus, O. et al. (2017). Data-analysis strategies for image-based cell profiling. *Nat. Methods* **14**, 849-863. doi:10.1038/nmeth.4397

Carpenter, A. E., Jones, T. R., Lamprecht, M. R., Clarke, C., Kang, I. H., Friman, O., Guertin, D. A., Chang, J. H., Lindquist, R. A., Moffat, J. et al. (2006). CellProfiler: image analysis software for identifying and quantifying cell phenotypes. *Genome Biol.* **7**, R100. doi:10.1186/gb-2006-7-10-r100

Chapman, G., Major, J. A., Iyer, K., James, A. C., Pursglove, S. E., Moreau, J. L. M. and Dunwoodie, S. L. (2016). Notch1 endocytosis is induced by ligand and is required for signal transduction. *Biochim. Biophys. Acta* **1863**, 166-177. doi:10.1016/j.bbamcr.2015.10.021

Chavkin, N. W. and Hirschi, K. K. (2020). Single cell analysis in vascular biology. *Front. Cardiovasc. Med.* **7**, 42. doi:10.3389/fcvm.2020.00042

Chi, J.-T., Chang, H. Y., Haraldsen, G., Jahnsen, F. L., Troyanskaya, O. G., Chang, D. S., Wang, Z., Rockson, S. G., van de Rijn, M., Botstein, D. et al. (2003). Endothelial cell diversity revealed by global expression profiling. *Proc. Natl. Acad. Sci. U. S. A* **100**, 10623-10628. doi:10.1073/pnas.1434429100

Dray, S. (2011). A New Perspective about Moran's Coefficient: Spatial Autocorrelation as a Linear Regression Problem. Moran系数的新视角:空间自相关视为线性回归问题: Spatial Autocorrelation as a Linear Regression Problem. *Geogr. Anal* **43**, 127-141. doi:10.1111/j.1538-4632.2011.00811.x

Dueck, H., Eberwine, J. and Kim, J. (2016). Variation is function: Are single cell differences functionally important?: Testing the hypothesis that single cell variation is required for aggregate function. *BioEssays News Rev. Mol. Cell. Dev. Biol.* **38**, 172-180. doi:10.1002/bies.201500124

Eling, N., Morgan, M. D. and Marioni, J. C. (2019). Challenges in measuring and understanding biological noise. *Nat. Rev. Genet* **20**, 536-548. doi:10.1038/s41576-019-0130-6

Fang, J. S., Coon, B. G., Gillis, N., Chen, Z., Qiu, J., Chittenden, T. W., Burt, J. M., Schwartz, M. A. and Hirschi, K. K. (2017). Shear-induced Notch-Cx37-p27 axis arrests endothelial cell cycle to enable arterial specification. *Nat. Commun.* **8**, 2149. doi:10.1038/s41467-017-01742-7

Fernández-Martín, L., Marcos-Ramiro, B., Bigarella, C. L., Graupera, M., Cain, R. J., Reglero-Real, N., Jiménez, A., Cernuda-Morollón, P., Correas, I., Cox, S. et al. (2012). Crosstalk between reticular adherens junctions and platelet endothelial cell adhesion molecule-1 regulates endothelial barrier function. *Arterioscler. Thromb. Vasc. Biol* **32**, e90-102. doi:10.1161/ATVBAHA.112.252080

Ferrero, E., Scabini, S., Magni, E., Foglieni, C., Belloni, D., Colombo, B., Curnis, F., Villa, A., Ferrero, M. E. and Corti, A. (2004). Chromogranin A protects vessels against tumor necrosis factor α–induced vascular leakage. *FASEB J.* **18**, 554-556. doi:10.1096/fj.03-0922fje

Fish, J. E. and Wythe, J. D. (2015). The molecular regulation of arteriovenous specification and maintenance. *Dev. Dyn. Off. Publ. Am. Assoc. Anat* **244**, 391-409.

Ginzberg, M. B., Chang, N., D'Souza, H., Patel, N., Kafri, R. and Kirschner, M. W. (2018). Cell size sensing in animal cells coordinates anabolic growth rates and cell cycle progression to maintain cell size uniformity. *eLife* **7**, e26957. doi:10.7554/eLife.26957

Hellström, M., Phng, L.-K., Hofmann, J. J., Wallgard, E., Coultas, L., Lindblom, P., Alva, J., Nilsson, A.-K., Karlsson, L., Gaiano, N. et al. (2007). Dll4 signalling through Notch1 regulates formation of tip cells during angiogenesis. *Nature* **445**, 776-780. doi:10.1038/nature05571

Itkin, T., Gur-Cohen, S., Spencer, J. A., Schajnovitz, A., Ramasamy, S. K., Kusumbe, A. P., Ledergor, G., Jung, Y., Milo, I., Poulos, M. G. et al. (2016). Distinct bone marrow blood vessels differentially regulate haematopoiesis. *Nature* **532**, 323-328. doi:10.1038/nature17624

Jones, T. R., Carpenter, A. E., Lamprecht, M. R., Moffat, J., Silver, S. J., Grenier, J. K., Castoreno, A. B., Eggert, U. S., Root, D. E., Golland, P. et al. (2009). Scoring diverse cellular morphologies in image-based screens with

iterative feedback and machine learning. *Proc. Natl. Acad. Sci. USA* **106**, 1826-1831. doi:10.1073/pnas.0808843106

Jones, T. R., Kang, I. H., Wheeler, D. B., Lindquist, R. A., Papallo, A., Sabatini, D. M., Golland, P. and Carpenter, A. E. (2008). CellProfiler Analyst: data exploration and analysis software for complex image-based screens. *BMC Bioinformatics* **9**, 482. doi:10.1186/1471-2105-9-482

Kalucka, J., de Rooij, L. P. M. H., Goveia, J., Rohlenova, K., Dumas, S. J., Meta, E., Conchinha, N. V., Taverna, F., Teuwen, L.-A., Veys, K. et al. (2020). Single-cell transcriptome atlas of murine endothelial cells. *Cell* **180**, 764-779.e20. doi:10.1016/j.cell.2020.01.015

Kim, J. and Cooper, J. A. (2018). Septins regulate junctional integrity of endothelial monolayers. *Mol. Biol. Cell* **29**, 1693-1703. doi:10.1091/mbc.E18-02-0136

Kusumbe, A. P., Ramasamy, S. K. and Adams, R. H. (2014). Coupling of angiogenesis and osteogenesis by a specific vessel subtype in bone. *Nature* **507**, 323-328. doi:10.1038/nature13145

~~Lampugnani,~~ M. G., Resnati, M., Raiteri, M., Pigott, R., Pisacane, A., Houen, G., ~~…,~~ P. and Dejana, E. (1992). A novel endothelial-specific membrane protein is a marker of cell-cell contacts. *J. Cell Biol.* **118**, 1511-1522.

Lampugnani, M. G., Corada, M., Caveda, L., Breviario, F., Ayalon, O., Geiger, B. and Dejana, E. (1995). The molecular organization of endothelial cell to cell junctions: differential association of plakoglobin, beta-catenin, and alpha-catenin with vascular endothelial cadherin (VE-cadherin). *J. Cell Biol.* **129**, 203-217. doi:10.1083/jcb.129.1.203

Lord, S. J., Velle, K. B., Mullins, R. D. and Fritz-Laylin, L. K. (2020). SuperPlots: Communicating reproducibility and variability in cell biology. *J. Cell Biol.* **219**, e202001064. doi:10.1083/jcb.202001064

Lukowski, S. W., Patel, J., Andersen, S. B., Sim, S.-L., Wong, H. Y., Tay, J., Winkler, I., Powell, J. E. and Khosrotehrani, K. (2019). Single-cell transcriptional profiling of aortic endothelium identifies a hierarchy from endovascular progenitors to differentiated cells. *Cell Rep* **27**, 2748-2758. e3. doi:10.1016/j.celrep.2019.04.102

Luo, W., Garcia-Gonzalez, I., Fernández-Chacón, M., Casquero-Garcia, V., Sanchez-Muñoz, M. S., Mühleder, S., Garcia-Ortega, L., Andrade, J., Potente, M. and Benedito, R. (2021). Arterialization requires the timely suppression of cell growth. *Nature* **589**, 437-441. doi:10.1038/s41586-020-3018-x

MacLean, A. L., Hong, T. and Nie, Q. (2018). Exploring intermediate cell states through the lens of single cells. *Curr. Opin. Syst. Biol.* **9**, 32-41. doi:10.1016/j.coisb.2018.02.009

McCarron, J. G., Lee, M. D. and Wilson, C. (2017). The endothelium solves problems that endothelial cells do not know exist. *Trends Pharmacol. Sci.* **38**, 322-338. doi:10.1016/j.tips.2017.01.008

McCarron, J. G., Wilson, C., Heathcote, H. R., Zhang, X., Buckley, C. and Lee, M. D. (2019). Heterogeneity and emergent behaviour in the vascular endothelium. *Curr. Opin. Pharmacol* **45**, 23-32. doi:10.1016/j.coph.2019.03.008

Millán, J., Cain, R. J., Reglero-Real, N., Bigarella, C., Marcos-Ramiro, B., Fernández-Martín, L., Correas, I. and Ridley, A. J. (2010). Adherens junctions connect stress fibres between adjacent endothelial cells. *BMC Biol.* **8**, 11. doi:10.1186/1741-7007-8-11

Park-Windhol, C. and D'Amore, P. A. (2016). Disorders of vascular permeability. *Annu. Rev. Pathol* **11**, 251-281. doi:10.1146/annurev-pathol-012615-044506

Pedrosa, A. R., Trindade, A., Fernandes, A. C., Carvalho, C., Gigante, J., Tavares, A. T., Diéguez-Hurtado, R., Yagita, H., Adams, R. H. and Duarte, A. (2015). Endothelial Jagged1 antagonizes Dll4 regulation of endothelial branching and promotes vascular maturation downstream of Dll4/Notch1. *Arterioscler. Thromb. Vasc. Biol.* **35**, 1134–1146. doi:10.1161/ATVBAHA.114.304741

Potente, M., Gerhardt, H. and Carmeliet, P. (2011). Basic and therapeutic aspects of angiogenesis. *Cell* **146**, 873-887. doi:10.1016/j.cell.2011.08.039

Rafii, S., Butler, J. M. and Ding, B.-S. (2016). Angiocrine functions of organ-specific endothelial cells. *Nature* **529**, 316-325. doi:10.1038/nature17040

Roukos, V., Pegoraro, G., Voss, T. C. and Misteli, T. (2015). Cell cycle staging of individual cells by fluorescence microscopy. *Nat. Protoc* **10**, 334-348. doi:10.1038/nprot.2015.016

Schindelin, J., Arganda-Carreras, I., Frise, E., Kaynig, V., Longair, M., Pietzsch, T., Preibisch, S., Rueden, C., Saalfeld, S., Schmid, B. et al. (2012). Fiji: an open-source platform for biological-image analysis. *Nat. Methods* **9**, 676-682. doi:10.1038/nmeth.2019

Seebach, J., Cao, J. and Schnittler, H. J. (2016). Quantitative dynamics of VE-cadherin at endothelial cell junctions at a glance: basic requirements and current concepts. *Discov. Craiova Rom.* **4**, e63. doi:10.15190/d.2016.10

Seebach, J., Klusmeier, N. and Schnittler, H. (2020). Autoregulatory "multitasking" at endothelial cell junctions by junction-associated intermittent lamellipodia controls barrier properties. *Front. Physiol.* **11**, 586921. doi:10.3389/fphys.2020.586921

Seebach, J., Taha, A. A., Lenk, J., Lindemann, N., Jiang, X., Brinkmann, K., Bogdan, S. and Schnittler, H.-J. (2015). The CellBorderTracker, a novel tool to quantitatively analyze spatiotemporal endothelial junction dynamics at the subcellular level. *Histochem. Cell Biol.* **144**, 517-532. doi:10.1007/s00418-015-1357-8

Siu, D. M. D., Lee, K. C. M., Lo, M. C. K., Stassen, S. V., Wang, M., Zhang, I. Z. Q., So, H. K. H., Chan, G. C. F., Cheah, K. S. E., Wong, K. K. Y. et al. (2020). Deep-learning-assisted biophysical imaging cytometry at massive throughput delineates cell population heterogeneity. *Lab. Chip* **20**, 3696-3708. doi:10.1039/D0LC00542H

Stepanova, D., Byrne, H. M., Maini, P. K. and Alarcón, T. (2021). A multiscale model of complex endothelial cell dynamics in early angiogenesis. *PLoS Comput. Biol.* **17**, e1008055. doi:10.1371/journal.pcbi.1008055

Tikhonova, A. N., Dolgalev, I., Hu, H., Sivaraj, K. K., Hoxha, E., Cuesta-Domínguez, Á., Pinho, S., Akhmetzyanova, I., Gao, J., Witkowski, M. et al. (2019). The bone marrow microenvironment at single-cell resolution. *Nature* **569**, 222-228. doi:10.1038/s41586-019-1104-8

Torres-Vázquez, J., Kamei, M. and Weinstein, B. M. (2003). Molecular distinction between arteries and veins. *Cell Tissue Res.* **314**, 43-59. doi:10.1007/s00441-003-0771-8

Travaglini, K. J., Nabhan, A. N., Penland, L., Sinha, R., Gillich, A., Sit, R. V., Chang, S., Conley, S. D., Mori, Y., Seita, J. et al. (2020). A molecular cell atlas of the human lung from single-cell RNA sequencing. *Nature* **587**, 619-625. doi:10.1038/s41586-020-2922-4

Ubezio, B., Blanco, R. A., Geudens, I., Stanchi, F., Mathivet, T., Jones, M. L., Ragab, A., Bentley, K. and Gerhardt, H. (2016). Synchronization of endothelial Dll4-Notch dynamics switch blood vessels from branching to expansion. *eLife* **5**, e12167. doi:10.7554/eLife.12167

Veschini, L., Belloni, D., Foglieni, C., Cangi, M. G., Ferrarini, M., Caligaris-Cappio, F. and Ferrero, E. (2007). Hypoxia-inducible transcription factor–1 alpha determines sensitivity of endothelial cells to the proteosome inhibitor bortezomib. *Blood* **109**, 2565-2570. doi:10.1182/blood-2006-06-032664

Veschini, L., Crippa, L., Dondossola, E., Doglioni, C., Corti, A. and Ferrero, E. (2011). The vasostatin–1 fragment of chromogranin A preserves a quiescent phenotype in hypoxia–driven endothelial cells and regulates tumor neovascularization. *FASEB J.* **25**, 3906-3914. doi:10.1096/fj.11-182410

Vestweber, D., Winderlich, M., Cagna, G. and Nottebaum, A. F. (2009). Cell adhesion dynamics at endothelial junctions: VE-cadherin as a major player. *Trends Cell Biol.* **19**, 8-15. doi:10.1016/j.tcb.2008.10.001

Wiseman, E., Zamuner, A., Tang, Z., Rogers, J., Munir, S., Di Silvio, L., Danovi, D. and Veschini, L. (2019). Integrated multiparametric high-content profiling of endothelial cells. *SLAS Discov. Adv. Life Sci. R D* **24**, 264-273.

Yoder, M. C. (2018). Endothelial stem and progenitor cells (stem cells): (2017 Grover Conference Series). *Pulm. Circ* **8**, 204589321774395. doi:10.1177/2045893217743950

Zong, D., Li, J., Cai, S., He, S., Liu, Q., Jiang, J., Chen, S., Long, Y., Chen, Y., Chen, P. et al. (2018). Notch1 regulates endothelial apoptosis via the ERK pathway in chronic obstructive pulmonary disease. *Am. J. Physiol. Cell Physiol* **315**, C330-C340. doi:10.1152/ajpcell.00182.2017
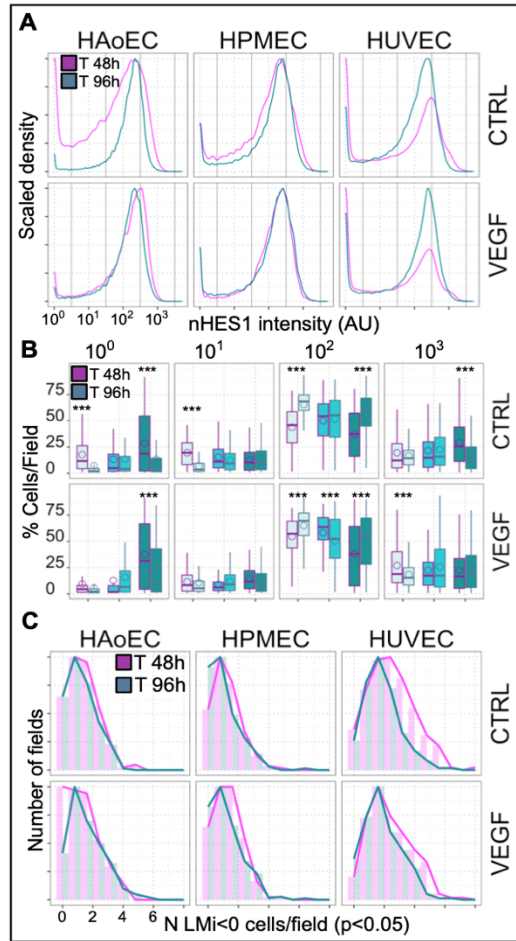
Fig. S1. Effect of long culture conditions on NOTCH activation.

A) Scaled density distributions of nN1 and nHES1 for HAoEC, HPMEC and HUVEC (coloured traces corresponding to 48h or 96h culture). **B)** Percent of cells per image (microscopic field) pertaining to different intensity bins (nN1) and EC types. **D)** Counts of fields according to numbers of nLMi cells/field, cell types (HAoEC, HPMEC, HUVEC) and treatment (CTRL, VEGF). * p<0.05, ** p<0.01, *** p<0.001, **** p<0.0001
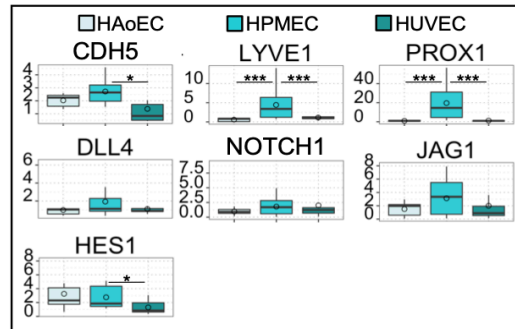
Fig. S2. Gene expression analysis: Analysis of expression of selected genes in HUVEC, HPMEC and HUVEC. Two donors for each cell type, measurements for donors are assembled. CDH5 (pan-endothelial marker), LYVE1 and PROX1 (lymphatic EC markers), DLL4, NOTCH1, JAG1 (NOTCH signalling), HES1 (NOTCH target gene). n=6 for all cell types for all genes except LYVE1 and PROX1 (n=8). * $p<0.05$, ** $p<0.01$, *** $p<0.001$, **** $p<0.0001$
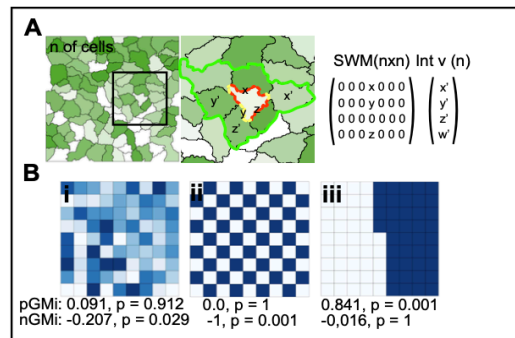
Fig. S3. Vignette of Moran's analysis. A) Cell maps for each individual field are extracted by ECPT. Cell neighbours and length of neighbour-neighbour junctions (x,y,z) are recorded into a spatially weighted matrix (SWM) of dimensions nxn (n is the number of cells in the respective field). Test parameter values (x', y', z', w', e.g., nH1 or nHES1 intensities) are recorded into a vector of length n. For each cell local Moran's values are computed by evaluating variance in signal with neighbours weighted by extent of interaction. **B)** Prototypic examples of global Moran's analysis in regular cells distributions. Random distribution of intensities yields pGMi and nGMi close to 0 (i). Sparse distributions yield pGMi close to 0 and nGMi approaching 1 (ii). Clustered distributions yield pGMi approaching 1 and nGmi close to 0 (iii).
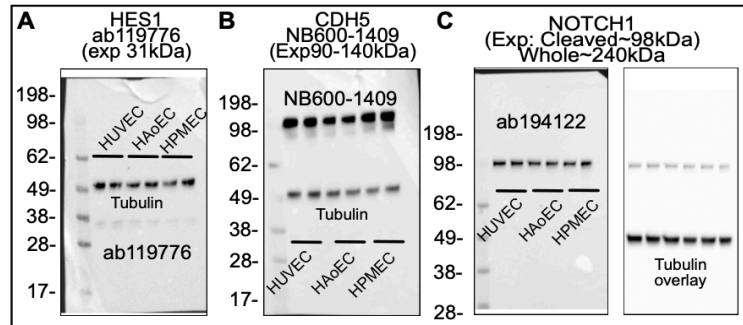
Fig. S4. Validation of antibodies specificity. A) Western Blot (WB) using ab119776 antibody against HES1 overlayed with tubulin, B) WB using NB600-1409 antibody against CDH5 overlayed with tubulin. C) WB using ab194122 against NOTCH1 intracellular domain. WB resolves a band 98kDa as expected from cleaved NOTCH1, whole NOTCH1 protein is not resolved by WB under our experimental conditions. All WB are performed using lysates from HUVEC, HAoEC and HPMEC as indicated.

Table S1. Primer sequences used in qRT-PCR.

Primer	Forward sequence	Reverse sequence
RPL19	CAGAAGATACCGTGAATCTAAG	TGTTTTTGAACACATTCCCC
CDH5	CGCAATAGACAAGGACATAAC	TATCGTGATTATCCGTGAGG
LYVE1	AGGCTCTTTGCGTGCAGAA	GGTTCGCCTTTTTGCTCACAA
PROX1	AAAGGACGGTAGGGACAGCAT	CCTTGGGGATTCATGGCACTAA
DLL4	GTCTCCACGCCGGTATTGG	CAGGTGAAATTGAAGGGCAGT
NOTCH1	GAGGCGTGGCAGACTATGC	CTTGTACTCCGTCAGCGTGA
JAG1	GTCCATGCAGAACGTGAACG	GCGGGACTGATACTCCTTGA
HES1	TCAACACGACACCGGATAAAC	GCCGCGAGCTATCTTTCTTCA

6- **Validation of the ECPT pipeline for *in vivo* analysis of EC monolayers**

a. **Mouse aorta as a model of EC monolayer**

To validate the findings in human cultured EC, we performed en face stainings of murine aortas as described previously (Hakanpaa et al., 2015). These monolayers had the advantage to keep the close contact between ECs and surrounding mural cells, allowing to study the role of perivascular cells in EC monolayer heterogeneity. To characterise the EC phenotypes in *ex vivo* aortas, we stained for the same junctional protein VE-Cadherin and HES1 as a downstream NOTCH-regulated gene. Figure 2.6A shows a representative image of murine aortic endothelium obtained as Z projection of a confocal stack (20μm with images taken at 1μm steps).
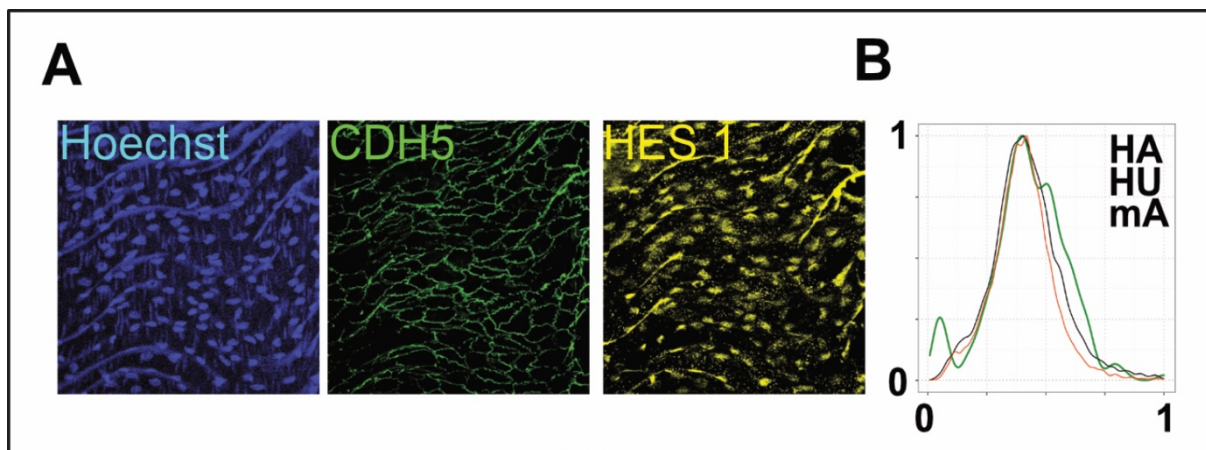
Figure 2.6: Implementation of ECPT to mice aorta endothelia in comparison to human cultured EC confirms relevant Notch heterogeneity. A) Confocal images of murine aortic endothelium immunostained for CDH5 (green) and HES1 (yellow). DNA was counter stained with Hoechst (blue). Each image corresponds to a maximal projection of a 20μm confocal stack. B) Density distribution plot of normalised HES1 intensities corresponding to mEC in aortic endothelium (green trace), HUVEC (red trace) and HAoEC (black trace).

As observed with the VE-Cadherin immunostaining, ECs in the murine endothelium show a diverse range of morphologies with some elongated cells against the flow as reported before as well as some bigger cells with a higher width to length ratio. The cells also exhibited linear junctions in parallel to the flow and some reinforced/reticulated junctions, although at a lesser rate than ECs cultured *in vitro*.

The analysis of HES1 immunostaining (yellow) demonstrates how each cell has different intensity of signal. Figure 2.6B (green trace) shows quantification of HES1 intensity across 3 images taken from 3 independent samples confirming heterogeneous distribution of HES1 intensities across aortic monolayers. Black and red overlay traces in figure 2.6B correspond to

measures of HAoEC and HUVEC monolayers demonstrating that *in vitro* data qualitatively resemble *in vivo* scenario.

Overall, these results demonstrate that Notch signalling in murine aortic endothelia is heterogeneous. This also demonstrates that the mechanisms underpinning the observed heterogeneity are preserved *in vitro* despite an absence of signalling from mural cells.

b. Implementation of ECPT for time dependant NOTCH inhibition to unravel NOTCH dynamics in EC monolayers.

To broaden the applications of the ECPT pipeline and get new insights on Notch dynamics, we implemented the Notch signalling analysis in cultured monolayers to time-dependant Notch signalling inhibition. Several studies have focused on the effect of Notch activation or inhibition on EC phenotypes but the timing of Notch signal transduction in the context of EC monolayers is still poorly understood. We exposed our cultured EC to the gamma secretase inhibitor DAPT, responsible for the inhibition of Notch signal transduction by limiting NICD cleavage. We measured nuclear NOTCH1 and HES1 in EC monolayers exposed to DAPT for different times to time Notch signalling inhibition using our ECPT (Chesnais et al., 2022a). Figure 2.7A shows a representative map of normalised HES1 intensities in HUVEC and HAoEC in control conditions or upon treatment with DAPT. As shown by the array of different intensities in the monolayer, the treatment with DAPT, even at high concentration (5µM), surprisingly did not have the expected effect of inhibiting HES1 signalling globally, with still some cells presenting high levels of HES1 expression.

The in-depth analysis of single cell expression of nuclear NOTCH1 and HES1 (Fig. 2.7B) revealed that the NSP inhibition in this setup was achieved by DAPT in all conditions but was relatively smoothened over time. We also observed that the inhibition of both NOTCH1 and HES1 was different in both HUVEC and HAoEC, with half inhibition achieved after 1h in HUVEC monolayers and in 4h in HAoEC. These results are in line with reported higher basal NSP in aortic ECs as reported by us and others (Chesnais et al., 2022a; Z. Luo et al., 2020). The exposure to DAPT for 24h further inhibited Notch signalling in HAoEC while this effect was not seen in HUVEC. Results in HUVEC closely mirror previous results using different experimental systems suggesting that the underlying Notch dynamics investigated in previous works is conserved in EC (Boareto et al., 2015; Monk, 2003; Nandagopal et al., 2019; Yoshioka-Kobayashi et al., 2020).

Overall, we show that, by implementing high-content image analysis to big sets of data, we can study molecular processes involved in EC monolayer dynamics and heterogeneity without the need to study these processes live and describe unexpected EC heterogeneity at the single cell level.
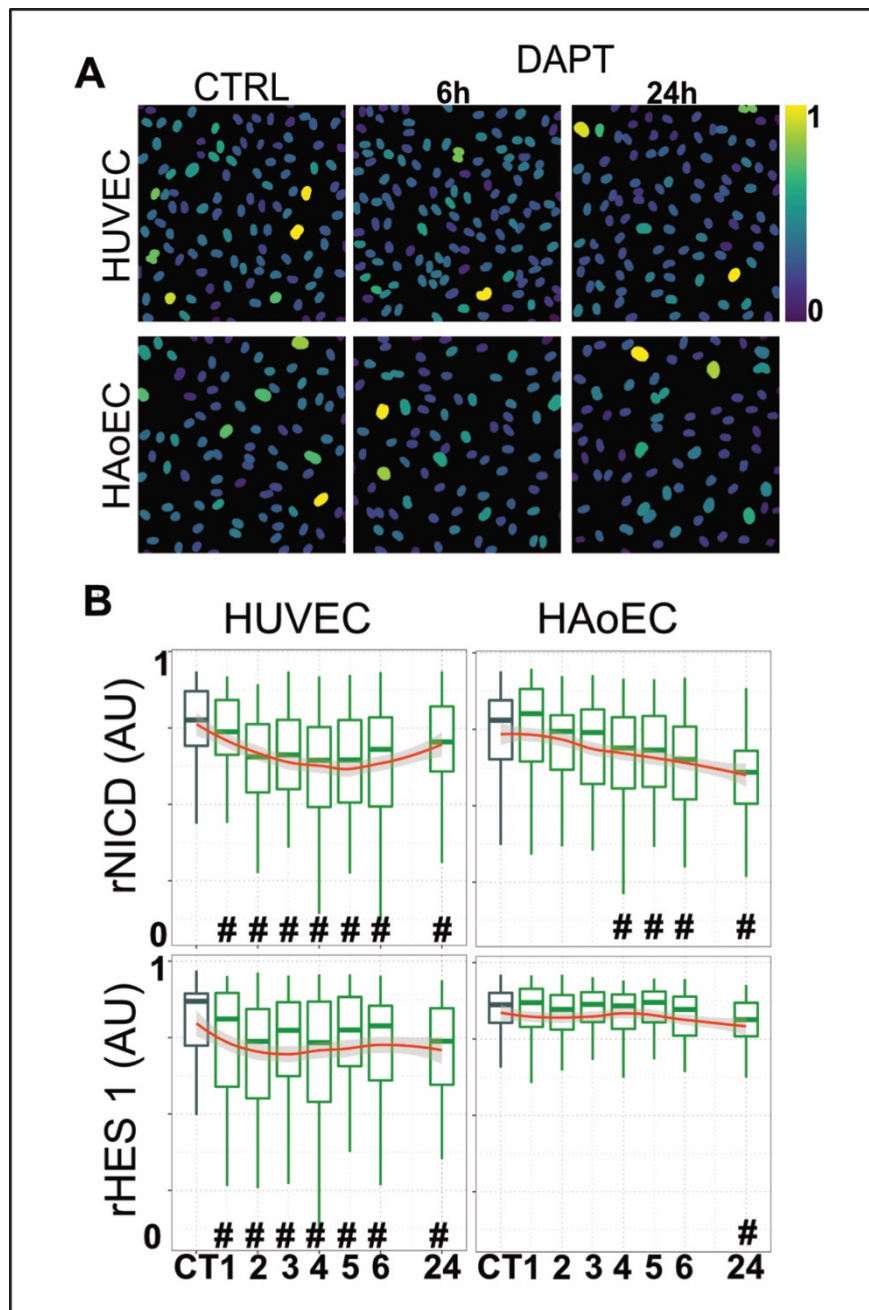
Figure 2.7: Time dependant inhibition of Notch signalling in EC monolayers. A) Representative HES1 maps obtained by ECPT analysis of HUVEC and HAoEC at baseline or treated with DAPT (5µM) for 6 or 24 hours. Colour scale represents normalised HES1 intensities. B) Box plots of individual KS distance measures from reference ECDF (untreated cells in grey) for HUVEC and HAoEC, either untreated or treated with DAPT for several hours. #p<0.01 against control.

7- **<u>Discussion</u>**

The vascular system possesses a remarkable diversity throughout the body in terms of morphology and function (Augustin and Koh, 2017). Blood vessel heterogeneity is mirrored by different EC phenotypes, result of specific genetic programming and also influenced by organ-specific microenvironment (Aird, 2007a, 2007b; Rafii et al., 2016). EC heterogeneity is crucial to proper organ development and regeneration, maintain organ homeostasis and perform organ specific function. Understanding how this heterogeneity arises during development and how the endothelium constantly regulates and responds to signal is important to decipher the role of blood vessels in health and disease.

To measure heterogeneity in EC, we analysed publicly available transcriptomic data from organ-specific EC. The relatively high number of cells analysed from tissues makes these repository useful tools to appreciate heterogeneity in EC populations. The recently published single-cell transcriptome of murine EC (Kalucka et al., 2020) validated previous results on highly heterogeneous gene expression from ECs from different organs. Surprisingly, we also realised the presence of highly heterogenous ECs in the same populations of cells from the same organ, on top of their respective differences in the arterio/venous tree. Intra-population heterogeneity in EC monolayers have already been reported and the ability of the endothelium to integrate several signals at a time has been linked to this phenomenon (Lee et al., 2022; McCarron et al., 2017). However, functional studies on the consequences of this single cell level diversity are still missing. Furthermore, transcriptomic data on murine cells cannot fully consider human-specific mechanisms of endothelial specialisation and studying EC behaviour and cultured human cells is still valuable to understand these mechanisms.

With the idea to study EC heterogeneity *in vitro*, we confirmed the results obtained by others (Chi et al., 2003) with the analysis of gene expression diversity in different organ-specific human EC cultured *in vitro*. The analysis of EC-specific (VE-Cadherin, KDR) and arteriovenous specification genes (DLL4, NOTCH1, HEY2, JAG1) in EC from arteries, veins or microvascular beds confirmed the results obtained by RNA sequencing. At the population level, these organ-specific ECs showed a high degree of heterogeneity, and this maintained heterogeneity validated the possibility to use human primary EC cultures, even isolated from their microvascular neighbours, and the intrinsic gene expression differences originating from wired genetic programming in ECs. Interestingly, we also observed that in cultured ECs as well

as in available transcriptomics data, ECs from arterial vessels had low expression levels of genes involved in arteriovenous specification such as HES1, HEY1 or Notch related genes. This phenomenon was also accompanied by a striking heterogeneity at the single cell level in expression of these genes in population of ECs from the same vessels, with certain genes being expressed up to 4 times more. This remarkable diversity in gene expression of ECs could be the origin of the monolayer heterogeneity. However, the scale at which these genes are regulated (hours) cannot explain dynamic processes involved in endothelial function such as junctional remodelling that is regulated at much faster pace (minutes). To evaluate such processes, better tools need to be developed to understand the dynamics and temporal regulation of EC monolayers at the single cell level.

To this end, we developed ECPT, endothelial cell profiling tool, using high-content image analysis and used it to characterise different organ-specific lines with the objective to study EC heterogeneity and behaviour in monolayers. We chose a model of venous EC (HUVEC), of arterial EC (HAoEC) and of microvascular EC (HPMEC) and cultured them in standard conditions or treated with VEGF to assess the differential behaviours in proliferation and morphology, junctional status and Notch signalling. To appreciate potential differences in proliferation of different EC we performed cell cycle analysis via measurement of fluorescently labelled DNA. By analysing individual nuclei intensity, we observed differential proliferation, with HPMEC proliferating slower than HUVEC and HAoEC and an overall small proportion of ECs proliferating when the monolayers were confluent. Interestingly, the treatment with VEGFA, although elongating the cells as expected, only had a minor effect on EC proliferation when confluent. We also described the versatility of the ECPT with the addition of cytoskeleton arrangement analysis. The characterisation of F-actin stress fibres in single cells also highlighted organ-specific cytoskeleton rearrangement with HAoECs possessing the most stress fibres out of the 3 cell lines. The in-depth characterisation of EC monolayer behaviour and cell cycle revealed an intrinsic heterogeneity between ECs from different organs to rapidly proliferate, migrate and rearrange in a monolayer in response to stimuli. Such heterogeneity kept in culture could give insights on the different behaviour observed *in vivo* such as resistance to anti-angiogenic treatments (for example switching phenotype from sprouting angiogenesis to intussusceptive angiogenesis)(Ribatti et al., 2019; Ribatti and Djonov, 2012) or problems following a vascular graft such as poor re-endothelialisation or inflammation (de Vries et al., 2016; Shi et al., 2001).

As described previously, junctional remodelling is crucial for EC function, playing a role in trans-endothelial migration and angiogenic processes. The ability to properly study dynamic junctional rearrangement is key to understand these processes. By employing semi-supervised machine learning algorithms, we characterised the VE-Cadherin junctions of the 3 different lines at the single junction level. Analysis of the junction morphology revealed very heterogeneous types of inter-endothelial junctions in between populations but also within populations of ECs. HUVEC and HAoEC had more jagged and discontinuous junctions while HPMEC possessed more linear junctions. These results, in line with the cytoskeleton analysis, could be explained by the origin of these ECs with aortic EC more prone to flow and remodelling, leading to more dynamic junctions, and the HPMEC role to tightly regulate gas exchange in the lungs.

To understand which molecular mechanisms led to this intra and inter-population heterogeneity, we focussed our analysis on Notch signalling. The Notch pathway has been extensively studied in the context of vascular biology for its role in angiogenesis and cellular identity. We decided to analyse both direct Notch interaction with the immunostaining of NOTCH1 receptor and the downstream gene HES1. Previous studies (Aranguren et al., 2013) have described a relatively homogeneous level of NSP in EC monolayers, but our analysis of HES1 and NOTCH1 intensities in single cells revealed a high degree of heterogeneity, in line with the single cell transcriptomics data. Although the mean intensity analysis between the different EC population did not reveal striking differences, the single-cell analysis revealed cells within the same monolayer with either high or low Notch signalling. Furthermore, we found that, contrary to what was expected, HPMEC had a relatively high degree of Notch activation, still lower than arterial ECs but higher than venous EC. These results revealed that Notch signalling was dynamically regulated and that specific populations of capillary ECs exhibit a high basal NSP activation.

To further investigate how this heterogeneity at the single cell level occurs, we investigated known processes in Notch signalling such as lateral inhibition or induction. To do so, we performed spatial autocorrelation analysis at the single cell level. This allowed us to observe both high and low level of HES1 and NOTCH1 in monolayers, occurring at the same time in neighbouring ECs within the monolayer, indicating both lateral induction and inhibition. This high level of heterogeneity in a random manner in the monolayer, with small clusters of cells with the same level of NSP activation and cells in an intermediate state, confirms results

obtained computationally and experimentally (Boareto et al., 2016; Lee et al., 2022; McCarron et al., 2017). The single cell level analysis also allowed us to correlate the spatial patterning of Notch with cell cycle and junction statuses. Although we couldn't find any evidence of correlation between HES1 expression and the junction morphology, we found populations with higher proliferating capacity in correlation with laterally inhibited cells, suggesting a role of Notch signalling in the cell cycle regulation. The spatial analysis of Notch signalling in EC monolayers revealed interesting phenotypes and heterogeneity in the extent of lateral inhibition/induction, with cells in different stages. This correlates with recent work on EC monolayer confirming the hypothesis that the endothelium could possess specialised clusters of cells that integrate signals in a parallel way. These clusters of cells within the monolayer could rapidly respond to stimuli or injuries by quickly proliferating, migrating or perform sprouting angiogenesis. Further models, *in silico* or *in vivo* as recently described (Chesnais et al., 2022b; Lee et al., 2022), will be needed to confirm the role of these processes in the maintenance of EC function and phenotype.

Overall, the use of our ECPT pipeline allowed the unbiased analysis of a large dataset to uncover how heterogeneity affects EC behaviour. The combination of different open-source software to characterise our EC monolayers allows a relative freedom to adapt the pipeline for different applications. This is often challenging with already available image analysis pipeline that are fixed in design and do not allow customised application. The detailed protocol and available code and data used for the study also encourages the exploration of the dataset and the use of the pipeline to study other cellular behaviour with image analysis. The singular use of image analysis to study EC monolayers allowed us to provide a unique insight on the spatial interactions at the single cell level, which would be difficult to study with other approaches such as RNA sequencing. However, the study of monolayer distribution in fixed cells presented here cannot recapitulate the exact temporal regulation of EC monolayers and future studies will be needed to adapt the pipeline for live imaging. Furthermore, the use of immunostaining reduces the ability to study several pathways in parallel due to the relatively low number of channels.

To validate the observations made *in vitro* in human ECs, we also performed immunostainings in murine aortas. As observed in cultured ECs, the murine endothelium showed a certain level of heterogeneity. At the junctional level, qualitative observation of the VE-Cadherin junctions showed a degree of heterogeneity in terms of morphology, even with the close contact of

perivascular cells. This was also accompanied by HES1 level heterogeneity at the single cell level, similar to the one observed *in vitro*. These results are in line with observations in human EC monolayers on the intra-population heterogeneity of NSP but will require further investigation possibly in live imaging to understand the dynamics of this phenotype.

Finally, to grasp a better view on the dynamic phenotype occurring in EC monolayers, we chemically inhibited Notch signalling in our cultured human ECs and observe the effect on a time-dependent manner. The treatment with DAPT over a period of 24h revealed an expected reduction in Notch signalling in both HUVEC and HAoEC but at significantly different rates. The HUVEC were rapidly (~1h) affected by the treatment in terms of HES1 and NOTCH1 intensity while the effect on HAoEC required a longer period of treatment (~4h). This effect might be due to the differences in basal Notch expression and the higher NSP in aortic endothelia in basal conditions compared to venous ECs. Furthermore, even with a reduction in Notch signalling, we could still observe cells with high Notch activity in both lines and at any time point in the treatment. This suggest that the heterogeneity observed in every condition described above is important for the maintenance of EC phenotypes and could have implications on future therapeutic strategies.

Overall, the work described in this chapter highlights crucial cell-intrinsic regulations of the EC monolayer including an intra-population heterogeneity at the single cell level. These results are in line with previous observations on EC phenotypes including the integration of signals in the endothelium by small populations of ECs (Lee et al., 2022; McCarron et al., 2019, 2017; Simmons et al., 2005) and the origins of blood vessel heterogeneity attributed to ECs rather than perivascular cells (Chavkin and Hirschi, 2020). The role of Notch signalling diversity at the single cell level as well as its dynamics in the regulation of EC function is still to be clarified, and future live imaging experiments could uncover the molecular mechanisms behind this phenotype. Moreover, the nature of the data presented here with high content image analysis and single cell information will be of great interest for the elaboration of mathematical models to predict and simulate the behaviour of ECs in monolayers and help decipher the development of these heterogeneous phenotypes.The precise understanding of blood vessel and EC heterogeneity will be of great interest for the development of therapeutic strategies in pathologies like cancer or cardiovascular diseases. The coupling of single cell transcriptomics with techniques such as high content imaging to understand EC behaviour

will be crucial to understand the mechanisms involved in the onset and progression of these specific pathologies.

Chapter 3: Stem cell-derived models of vascular cells to recapitulate blood vessel heterogeneity.

1- Introduction

Blood vessels carry nutrients and oxygen and remove metabolic waste in all tissues in the human body and most cells in human tissues reside at a maximum distance of 100 microns from blood capillaries. Blood vessels are gatekeepers of immunity and are increasingly recognised for their role in supporting tissue growth during development. Alterations of vessel homeostasis is a hallmark of several pathologies including cardiovascular diseases and cancer (Potente et al., 2011). Unsurprisingly, pharmacological targeting of vascular cells is a very active research field (Ebos and Kerbel, 2011). Among the most common pharmacological interventions involving blood vessels are the anti-angiogenic therapies such as anti-VEGF molecules or strategies to normalise the intra-tumoral vasculature (Eelen et al., 2020; Jain, 2005; Ribatti et al., 2019).

Key components of blood vessels are endothelial cells (ECs) and perivascular cells including pericytes (PCs), smooth muscle cells (SMCs) and perivascular immune cells (e.g., macrophages and fibroblasts). EC have been demonstrated to be the most heterogeneous vascular cells by functional and OMICS studies (Chi et al., 2003; Kalucka et al., 2020). In fact, EC in different tissues as well as arteries, veins and capillaries within the same tissue display characteristic gene expression profiles as described earlier (Adams and Alitalo, 2007). EC heterogeneity is an evolutionarily conserved feature emerging early during embryonic development. In contrast, heterogeneity in gene expression of perivascular cells is less evident and seems associated with environmental cues and restricted tissue access (e.g., perivascular glia in the brain, multipotent potential as scar tissues or myogenic progenitors) rather than intrinsically different genetic programs (Armulik et al., 2011; Dellavalle et al., 2007; Göritz et al., 2011; Yamazaki and Mukouyama, 2018).

It is becoming apparent that understanding the molecular program underpinning vascular heterogeneity is key to developing pharmacological interventions targeted to specific tissues or diseases. Furthermore, reproducing this heterogeneity in model systems is key to developing innovative regenerative medicine strategies including drugs for treatment of ischemic tissues or non-healing wounds.

The discovery of embryonic pluripotent stem cells (PSCs) and the later invention of induced pluripotent stem cells (iPSCs)(Takahashi and Yamanaka, 2006) created a tool to study early

embryonic developmental stages. The optimisation of differentiation protocols to derive PSC into vascular cells allows the possibility to study early events of vasculogenesis and angiogenesis and gain knowledge on vascular development. This model can also be used as guide to understand how blood vessel and EC heterogeneity arise.

Furthermore, with the short number of donors and increasing need for supply, PSCs represent a potentially limitless source of cells to be used in future transplantation strategies and tissue engineering approaches. To date, vascularisation strategies for tissue engineered constructs have been unsuccessful and further knowledge into the mechanisms of tissue-specific vascularisation is needed. The creation of functional population of vascular cells from PSC will be essential for such applications to be successful.

The embryonic emergence of ECs is well documented (as mentioned in chapter 1) and several protocols to differentiate ECs from PSCs have been developed. Using defined conditions and growth factors, PSCs are differentiated first towards a mesodermal precursor that will later be specialised into the vascular lineage. Studies have shown the possibility to differentiate stem cells into ECs via embryoid bodies (Adams et al., 2013; Gage et al., 2020; Mulfaul et al., 2020), inside cell aggregates or organoids (Cakir et al., 2019; Drakhlis et al., 2021; Holloway et al., 2020; Low et al., 2019), or in directed differentiation in 2D (Orlova et al., 2014; Palpant et al., 2017; Prasain et al., 2014; Zhang et al., 2017). Furthermore, these cells can be specialised into organ-specific endothelium via co-culture with organoids for example (Cakir et al., 2019; Drakhlis et al., 2021; Holloway et al., 2020; Low et al., 2019) or pushed towards an arterial or venous fate via modulation of pathways involved in arteriovenous specification (Arora et al., 2019; Rosa et al., 2019; Zhang et al., 2017). Nevertheless, stem cell-derived ECs often arise as an heterogeneous population, with a yield of differentiation between 10 to 30% (Browne et al., 2021; Kusuma et al., 2013; Natividad-Diaz et al., 2019) necessitating a purification step by cell sorting. Although, expressing markers of interest, these ECs are rarely characterised functionally to investigate their angiogenic potential or capacity to withstand blood flow. Finally, most protocols still use xenogeneic products such as foetal bovine serum (FBS) or Matrigel^{TM}, making the translational use of these progenies difficult.

Mural cells such as pericytes, smooth muscle cells or fibroblasts play a crucial role in vessel stabilisation and maturation, blood flow control and regeneration processes. Their embryonic origin is less understood in comparison to that of ECs, with some mural cells coming from the mesodermal lineage (Armulik et al., 2011; Asahina et al., 2011; Yamazaki et al., 2017; Yamazaki and Mukouyama, 2018) and others from neural crest progenitors (Korn et al., 2002). This knowledge from *in vivo* studies has also been translated into protocols to differentiate

PSCs into PCs and SMCs from both progenitors (Aisenbrey et al., 2021; Faal et al., 2019; Kumar et al., 2017; Orlova et al., 2014). These have also been reported in the creation of organ-specific models *in vitro* such as brain-specific pericytes (Faal et al., 2019; Kelleher et al., 2019; Linville et al., 2019; Vatine et al., 2019). Nevertheless, studies on PSC-derived perivascular cells also lack functional characterisation such as the ability to cover blood vessel, regulate blood flow or secrete appropriate ECM components. Their differentiation also relies on specific markers that are shared with other lineages, and the use of FBS can give rise to heterogeneous populations of cells.

In the work described in this chapter, we focused on obtaining mature populations of vascular cells from stem cells. We used and adapted published protocols to differentiate ECs and perivascular cells from PSCs and characterised the different populations obtained. We used directed differentiation to obtain ECs from different iPSC lines and further mature them towards arterial and venous ECs in defined xenogeneic-free conditions. Optimised protocols to generate EC were developed by using a human embryonic SC line (H9) inducibly overexpressing the pioneer transcription factor ETV2 followed by extensive phenotyping. Furthermore, we adapted existing protocols to obtain perivascular cells through directed differentiation of iPSC lines. Altogether, we differentiate and characterise population of vascular cells from hESC or iPSCs for future use in developmental studies and tissue engineering purposes.

2- **Materials and methods**

Cell culture

HAoECs and HUVECs (PromoCell) and iPSc-ECFCs (Axol) were plated on 10 µg/ml fibronectin (from bovine plasma, Promocell)-coated flasks, grown in EGMV2 medium (Promocell). Human pericytes from placenta (Promocell) were grown in pericyte growth medium 2 (Promocell) and normal human dermal fibroblasts (NHDF, Promocell) were grown in fibroblasts growth medium 2 (Promocell). Cells were routinely detached with Accutase^{TM} (Thermo Fisher Scientific, Waltham, MA), and used by passage 6.

Human stem cell maintenance

The human induced pluripotent stem cell lines Kegd-2, Hoik-1 and iPSC-GFP (HipSci Consortium) and the embryonic stem cell line H9-ETV2 (Stem cell Institute, Leuven) were cultured in E8 Flex medium (Gibco) on vitronectin-coated plates (10µg/10cm^2, truncated vitronectin, Gibco). iPSC colonies were routinely passaged using Versene-EDTA (Gibco).

EC differentiation into vEC and aEC

Two days before the differentiation, cells were split at a 1:4 ratio using Accutase^{TM} and plated on vitronectin-coated plates. On the day of the differentiation, cells were differentiated to mesoderm as previously described (Zhang et al., 2017). The medium was switched to EDM (Endothelial Differentiation Medium; DMEM/F12 (Gibco) supplemented with 64 ng/mL L-ascorbic acid-2-phosphate magnesium (Thermo), 14 ng/mL Sodium selenium (Thermo), 543 µg/mL NaHCO$_3$ (Thermo) and 10.7 µg/mL Transferrin(Thermo)) supplemented with 20 µg/mL Insulin (Thermo), 100 ng/mL FGF2 (Peprotech), 2ng/mL TGFB1 (Peprotech), 25 ng/mL Activin A (Peprotech), 5ng/mL BMP4 (Peprotech) and 1 µM CHIR99021 (STEMCELL Technologies) for 2 days, changed daily.

At day 2 of differentiation, medium was changed to induce endothelial differentiation. Venous endothelial cell differentiation was induced by switching to EDM supplemented with 20 µg/mL Insulin, 100 ng/mL FGF2 and 50 ng/mL VEGFA (Peprotech) for 4 additional days with daily medium change. Arterial endothelial cell differentiation was induced by switching to EDM without Insulin, supplemented with 100 ng/mL FGF2, 50 ng/mL VEGFA, 10 µM SB431542 (STEMCELL Technologies), 5 µM Resveratrol (STEMCELL Technologies) and 10 µM L690 (STEMCELL Technologies).

At day 6 of differentiation, cells were dissociated with Accutase™ and purified using magnetic-activated cell sorting. Cells were labelled with CD31 MicroBeads (Miltenyi Biotec) and separated using LS columns (Miltenyi Biotec). Cells were plated on fibronectin-coated plates ($10\mu g/10cm^2$) and maintained in the same medium for vECs, and L690 was removed for aECs.

EC differentiation with the H9-ETV2 line

H9-ETV2 were differentiated as previously described (De Smedt et al., 2021). Stem cells were detached with Accutase™ (Thermo Fisher Scientific, Waltham, MA) and seeded at a ratio of 1:6 in E8 Flex medium (Gibco) supplemented with $10\mu M$ Y-27632 (Tocris, UK). Medium was changed the next day to EDM with $5\mu g/mL$ doxycycline (Thermo Fisher Scientific). On day 2, cells were grown in EDM supplemented with $5\mu g/mL$ doxycycline (Thermo Fisher Scientific) and 2% foetal bovine serum (Thermo Fisher Scientific). Cells were passaged with Accutase™ (Thermo Fisher Scientific, Waltham, MA) on day 4, 8 and 12 on fibronectin (Promocell)-coated plates.

Pericyte differentiation

Human iPSCs were differentiated into mesoderm as described for iPSC-EC differentiation. At day 2, cells were differentiated as previously described (Kumar et al., 2017). Cells were plated with fibronectin (3 mg/mL, Promocell) and human collagen I (10 mg/mL, Thermo Fisher Scientific) in EDM supplemented with 10 ng/mL FGF2 (Peprotech) and 50 ng/mL PDGF-BB (Peprotech). After 3 days, immature PCs (imPCs) cells were dissociated with Accutase™ (Thermo Fisher Scientific) and plated on the fibronectin/collagen-coated plates in Pericyte growth Medium 2 (Promocell) for 14 days. Immature PCs were then matured on fibronectin/collagen-coated plates in Pericyte growth medium 2 (Promocell) with added SB431542 (10 mM) and PDGF-BB (50 ng/mL) or SB431542 (10 mM), PDGF-BB (10 ng/mL), VEGF (10 ng/mL), and EGF2 (2 ng/mL) to generate capillary PCs (PC1) and arteriolar PCs (PC2), respectively. Cells were routinely passaged with Accutase™ (Thermo Fisher Scientific) and cultured on the fibronectin/collagen-coated plates when they reached confluency.

Fibroblast differentiation

Human iPSCs were differentiated into mesoderm as described for iPSC-EC differentiation. After mesodermal induction, cells were differentiated into fibroblasts as described earlier (Kim et al., 2018). At day 2, medium was replaced to EDM supplemented with 5% FBS (Thermo

Fisher Scientific) and 10mg/mL EGF (Peprotech). At day 4, cells were detached with Accutase™ (Thermo Fisher Scientific) and plated on Collagen I (10 ng/mL, Thermo Fisher Scientific)- coated plates in the same medium supplemented with 0.5nM BMP4. At day 7, the medium is changed to DMEM supplemented with 5% FBS. At day 14, cells are detached and plated on non-coated plates in DMEM + 10% FBS (Thermo Fisher Scientific) until day 21.

Magnetic activated cell sorting

For the CD31 sorting, cells were dissociated with Accutase™ and purified using magnetic-activated cell sorting. Cells were labeled with CD31 MicroBeads (Miltenyi Biotec) and separated using LS columns (Miltenyi Biotec). The NG2 sorting required immunostaining of cells with NG2 antibody (abcam, ab83178, 1 µg/mL) for one hour at 4°C and then incubation with Microbeads anti rabbit (Miltenyi Biotec) for 30min before separating with LS columns (Miltenyi Biotec).

Matrigel assay

Matrigel™ (Corning) was mixed with DMEM-F12 (Gibco) at 1:1 ratio and 100 µL was pipetted into a 96-well plate and left 1h in the incubator to induce solidification. Cells were harvested using Accutase™ and seeded on top of the Matrigel™ at a concentration of 10 000 cells/well.

Fibrin bead assay

The bead fibrin gel assay (or Cytodex assay) was performed following a protocol previously published (Nakatsu et al., 2007). The day before the assay, cells are detached and mixed with Cytodex beads (Amersham) at a ratio of 400 cells per bead and incubated overnight for coating. The next day, beads are washed and resuspended in a 2mg/mL fibrinogen solution. The bead/fibrinogen solution is mixed with a 0.625 unit/mL thrombin solution and incubated 15min at 37°C to form the clot before the medium is added on top.

RNA extraction and qRT-PCR (quantitative reverse-transcription Polymerase Chain Reaction):

Total RNA was extracted and purified using the Monarch total RNA miniprep kit according to the manufacturer's instructions. The resulting RNA was quantified using Nanodrop (ISOGEN Life Science). For real-time PCR, 1µg of RNA was used for reverse transcription using the iScript cDNA synthesis kit (Bio-rad). The gene expression analysis was carried out using the

SSoAdvanced^{TM} Universal SYBR Green Supermix (Bio-rad) and analyzed by means of a Stratagene Mx3000P (Agilent Technologies) in real time, primers are referenced in supplementary table 2 with RPL19 as the household gene.

Immunostaining

Cells were fixed with 2% paraformaldehyde in phosphate-buffered saline (PBS) for 10 min at room temperature. Cells were blocked 1 h with PBS supplemented with 1% fetal bovine serum (FBS) and permeabilised with 0.1% Triton X-100. Cells were then incubated for 1 h at room temperature with primary antibodies against CDH5 (VE-cadherin; Novusbio NB600- 1409, 1µg/ml final), NOTCH1 (Abcam, ab194122, Alexa Fluor 647- conjugated, 1 µg/ml final) and Hes1 (Abcam, ab119776, 1 µg/ml final). Plates were washed and incubated 1 h with 1 µg/ml secondary Alexa Fluor 488-conjugated and Alexa Fluor 555-conjugated antibody (Thermo Fisher Scientific), Hoechst 33342 (1 µg/ml, Sigma) and Phalloidin-Atto 647N (Sigma).

Statistical analysis

To compare multiple groups, we used one-way ANOVA followed by Tukey's HSD post-hoc test. We considered $P < 0.05$ (*) statistically significant and $P < 0.01$ (**), $P < 0.001$ (***) and $P < 0.0001$(****) highly significant.

3- <u>**Stem cell differentiation to endothelial cells**</u>

Several differentiation protocols have been developed to differentiate ECs from PSCs as described earlier, but with various yields and degrees of maturation. To produce a population of ECs as pure as possible, we decided to follow protocols employing directed differentiation in 2D to avoid 3D differentiation, yielding to a heterogeneous mix of cells. The classical differentiation protocol to obtain ECs is through a mesodermal progenitor expressing VEGFR2 (KDR), followed by an induction to angioblasts, expressing ETV2, via VEGF signalling and further maturation to VE-Cadherin/CD3-expressing cells. These cells can then be matured towards organ-specific or pushed towards an arterial or venous phenotype (Fig. 3.1)
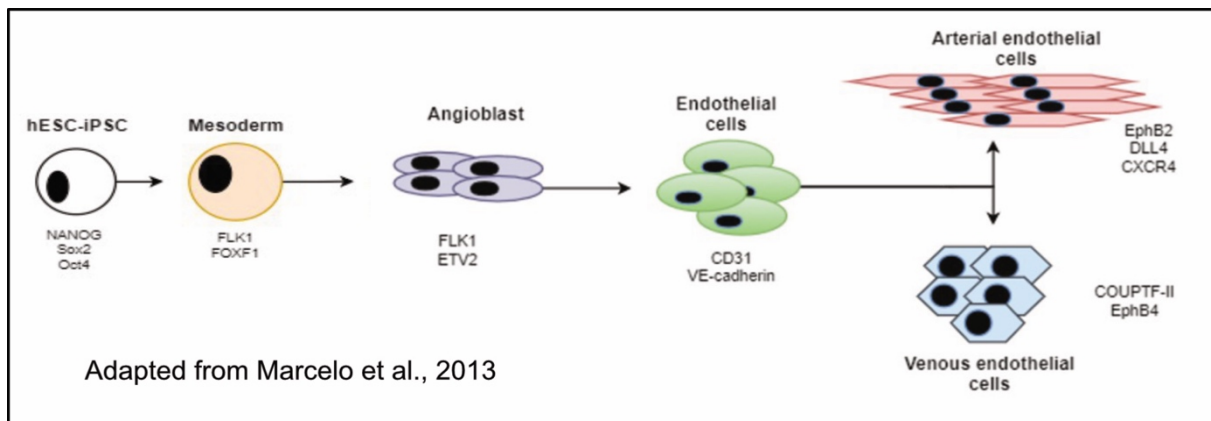
Figure 3.1: Schematic representation of the directed differentiation of ECs from PSCs, adapted from (Kathrina L. Marcelo et al., 2013). Pluripotent stem cells (induced or embryonic stem cells) are differentiated towards the mesoderm lineage and then specified to give rise to angioblasts, the endothelial cells precursors. Angioblasts are matured towards endothelial cells that can be further matured towards the arterial or the venous fate. NANOG: Homeobox protein NANOG; Sox2: SRY-box 2; Oct4: Octamer binding transcription factor 4; FLK1: kinase Insert domain receptor (KDR); ETV2: ETS Variant Transcription Factor 2; CD31: Cluster of differentiation 31 (PECAM: Platelet endothelial cell adhesion molecule); VE-Cadherin: Vascular endothelium cadherin; EphB2: Ephrin type-B receptor 2; DLL4: Delta-like Ligand 4; CXCR4: C-X-C chemokine receptor type 4; COUPTF-II: **c**hicken **o**valbumin **u**pstream **p**romoter transcription factor 2; EphB4: Ephrin type-B receptor 4

a. Protocol implementation for EC differentiation

To differentiate stem cells into ECs, healthy iPSC lines (Kegd-2, Hoik-1, iPSC-GFP, HipSci Consortium) were used and differentiated in chemically defined conditions as previously described (Zhang et al., 2017). This protocol allowed the rapid differentiation of arterial ECs (aECs) and venous ECs (vECs) without the use of Matrigel^{TM} or foetal bovine serum, animal product with a very high batch to batch variation resulting in heterogeneity between differentiations. Furthermore, this xenogeneic-free protocol can be used for future transplantation purposes. A timeline of the protocol illustrated with snapshots of cell morphology throughout the differentiation is presented in figure 3.2.
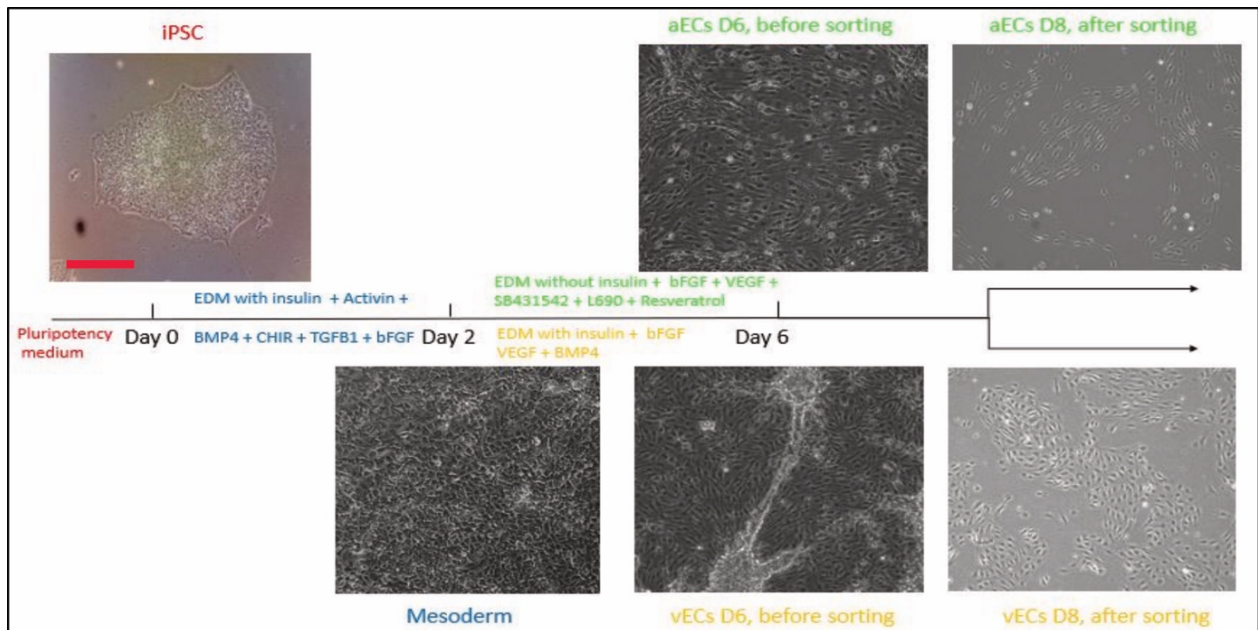
Figure 3.2: Schematic of the differentiation protocol used to differentiate aEC and vEC from PSCs as described previously (Zhang et al., 2017). Scale bar: 150µm. Induced pluripotent stem cells (iPSC) are maintained in pluropotency medium before the start of the differentiation at day 0 to start the mesoderm induction. Cells are differentiated towards the mesoderm lineage by switching to endothelial differentiation medium (EDM) with insulin, Activin-A, BMP4 (Bone Morphogenetiic Protein 4), CHIR (CHIR-99021: glycogen synthase kinase (GSK) 3 inhibitor) and bFGF (basic fibroblasts growth factor) for 2 days. At day 2, the mesoderm is differentiated towards the endothelial lineage by switching to EDM medium supplemented with insulin, bFGF, VEGF (Vascular endothelial growth factor) and BMP4 for to obtain venous endothelial cells (vEC) for 4 days befofr being sorted for CD31. To differentiate the mesoderm towards arterial endothelia cells, cells are kept in culture for 4 days in EDM without insulin supplemented with bFGF, VEGF, SB431542 (TGF-Smad inhibitor), L690 9 Inositol monophosphate inhibitor) and resveratrol for 4 days before being sorted for CD31.

Cells were first cultured in the presence of Activin A, bone morphogenetic protein 4 (BMP4) and CHIR99021, a Wnt/β-catenin activator, in order to give rise to KDR-positive mesoderm after 2 days of differentiation (Nostro et al., 2008). At day 2, cells were induced towards a venous or arterial fate. To induce vECs formation, cells were incubated in a medium containing insulin, basic fibroblast growth factor (bFGF) and VEGF, essential for ECs differentiation as well as BMP4 to repress arterial phenotype as previously demonstrated (Zhang et al., 2017). To induce aECs formation, cells were incubated in a medium without insulin containing bFGF and VEGF, supplemented with a transforming growth factor 1 (TGF-β1) pathway inhibitor (SB431542) an Inositol Monophosphate inhibitor (L690,330) and a Notch activator (Resveratrol). At day 6 of differentiation, the resulting population is mainly composed of endothelial progenitors but is still heterogeneous and some residual non-endothelial cells are still present (Fig. 3.2, aECs and vECs D6, before sorting). To purify the resulting population, cells are sorted with magnetic-activated cell sorting (MACS) and CD31-positive cells are replated and expanded (Fig. 3.2, aECs and vECs D8, after sorting).

First attempts at sorting ECs were unsuccessful, with very low yield of CD31-positive cells after MACS (<5%). The cells obtained after 6 days did not possess typical endothelial cell cobblestone morphology (Haudenschild, 1984) and big colonies of stem cells were still present as seen in figure 3.2 before sorting. We reasoned that if there was still rapidly growing PSCs or undifferentiated cells after the 6 days of differentiation, it was probably due to the inefficient differentiation of PSCs during the mesoderm induction phase. We hypothesized that lowering the seeding density of PSCs at the start of the differentiation and giving them more time to differentiate to mesodermal progenitors would result in lower number of undifferentiated PSCs before inducing endothelial fate. We attempted to lower the seeding density of PSCs from 1-1.5.10^6 cells per well of a 6well-plate (1-1.5.10^5/cm^2) in the original protocol (Zhang et al., 2017) to 2.5-5.10^5 cells per well of a 6well-plate (2.5-5.10^4/cm^2). This resulted in the necessity to extend the mesodermal induction from 2 days to 4 days to reach confluency. As seen in figure 3.3, lowering the seeding density increased the overall morphological homogeneity of cells obtained after 4 days and a seeding density of 2.5.10^5 cells almost abolished the proliferation of undifferentiated PSCs.
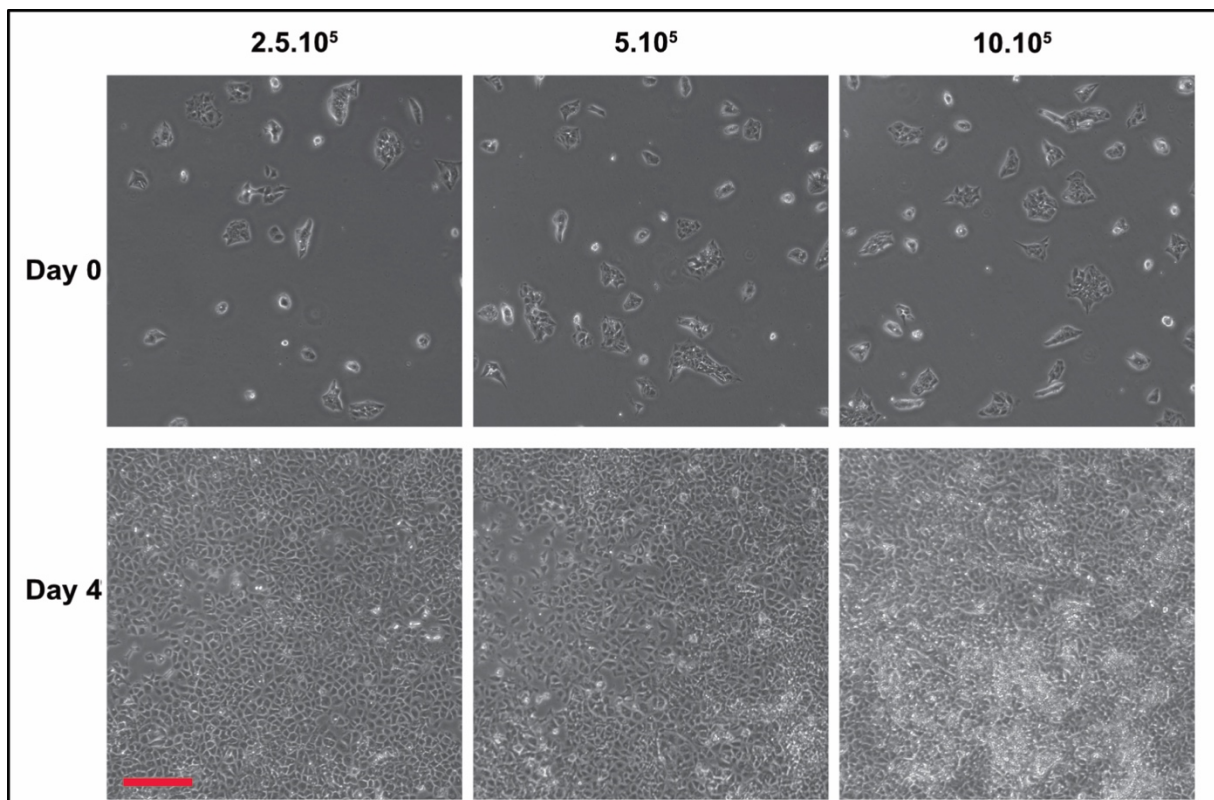
Figure 3.3: Influence of the seeding density on mesodermal progenitors' homogeneity. Cells were seeded at either 2.5, 5 or 10.10^5 cells per well and pictures were taken at day 0 of differentiation and after 4 days of mesoderm induction. Scale bar: 100μm.

After 4 days of EC induction and sorting, the vECs obtained have the typical endothelial morphology and grow in compact colonies with a morphology similar to HUVECs. The aECs obtained also grow in colonies but are more elongated and clearly differ from vECs. These cells can be expanded and passaged, at least up to 3 times (Fig. 3.4). As observed, both populations have differences in morphology, but we could also qualitatively attribute differences in proliferation, with aECs reaching confluency after split in twice the time it took for vEC to be confluent (data not shown). This correlates with previously reported effect of arterialisation on EC cell cycle (Fang et al., 2017; W. Luo et al., 2021).
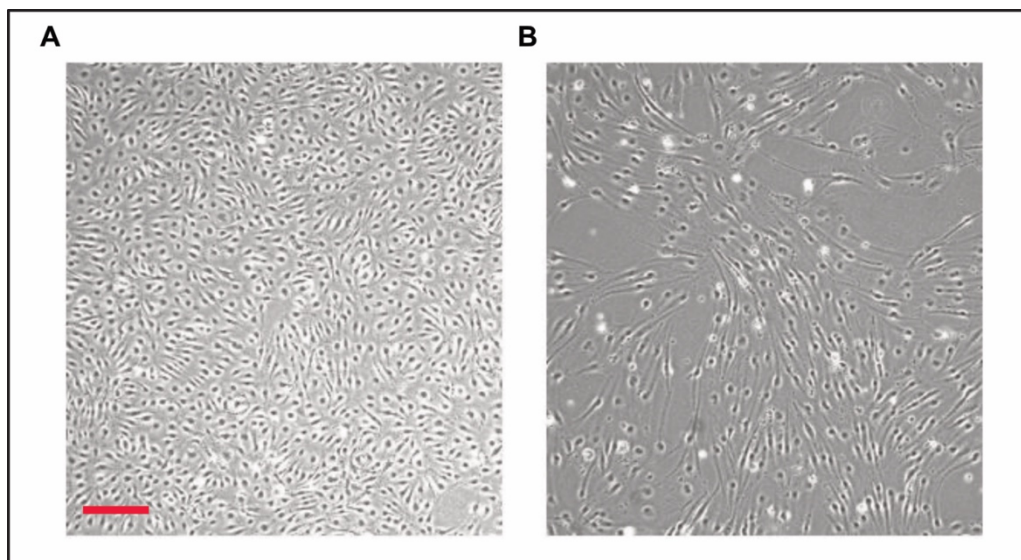
Figure 3.4: Photographs of vEC (A) and aEC (B) after 3 passages. Scale bar: 100μm. iPSCs were differentiated with the protocol described earlier (Zhang et al., 2017) towards venous (vEC) or arterial (aEC) endothelial cells and passaged when reached confluence. After 3 passages in their respective medium, cells still exhibit an endothelial morphology.

The improved protocol gave rise to a population of vECs and aECs with homogeneous morphology and in a short timeframe. However, phenotyping of these iPSC-derived ECs is needed to evaluate their degree of maturation.

b. Phenotyping of iPSC-ECs

Maturation of iPSC-EC is characterised by different assays, from gene expression evaluation of several EC-specific genes, protein expression or functional assays such as angiogenic assays or leucocyte adhesion (Butcher, 1991; Nowak-Sliwinska et al., 2018).

i. CD31-positive cells

Here, the first quantitative analysis of the efficiency of this differentiation is the yield of CD31-positive cells at the purification step. CD31 (PECAM1) is a cell surface marker shared by ECs and other cell types such as leukocytes and it is involved cell adhesion and transmigration (Muller et al., 1993). This EC lineage marker is only expressed in mature ECs and has been widely used to sort ECs from tissues or stem cell differentiation (Prasain et al., 2014; Travaglini et al., 2020; Zhang et al., 2017). We performed several differentiations on 3 different iPSc lines and evaluated the percentage of CD31-positive cells from the total number of cells sorted at day 8 of differentiation (4 days of mesoderm and 4 days of EC). As seen in figure 3.5, the percentage of cells obtained from the different lines was relatively homogeneous, around 10 to 15%. Although the mesoderm induction was optimised through lowering the seeding density, cells obtained after EC induction still appear to be heterogeneous. Even without use of serum or Matrigel^{TM}, the protocol still resulted in highly variable yields, from differentiation as low as 5% CD31-positive cells to few differentiations above 25% CD31-positive cells.
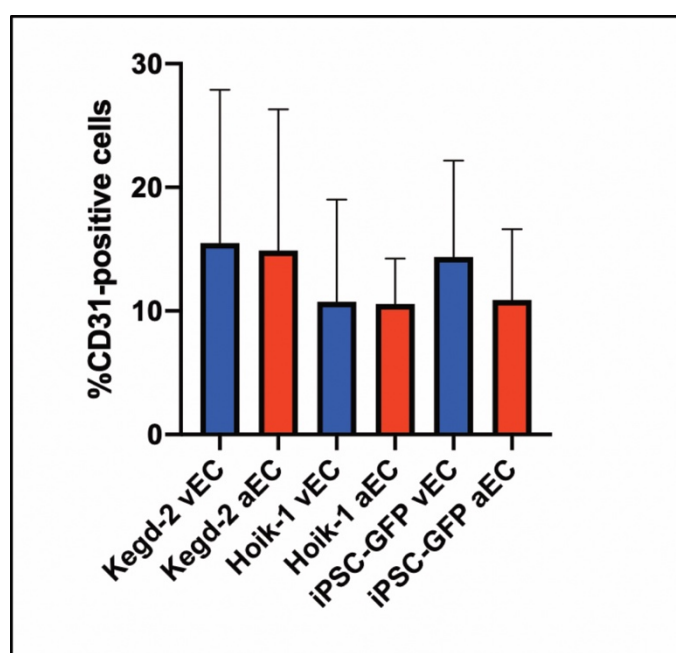
Figure 3.5: Percentage of CD31-positive cells obtained after sorting for three different iPSC lines (Kegd-2, Hoik-1 and iPSC-GFP) and differentiated into venous ECs (vEC) and arterial ECs (aEC). Cells were differentiated as previously described (Zhang et al., 2017) and sorted after 8 days of differentiation with magnetic activated cell sorting for CD31. aEC: arterial EC, vEC: venous EC.

ii. Gene expression profile reveals markers of maturation

To assess the degree of maturation of cells obtained with this protocol, we performed a gene expression analysis for EC-specific genes KDR and VE-Cadherin (Fig. 3.6). As observed, the expression of KDR and VE-Cadherin were very similar for the iPSC-ECs and HUVECs,

attesting the proper differentiation of iPSCs into mature ECs. Surprisingly, aECs has a very high expression of KDR (VEGFR2), which could be linked with a higher Notch and VEGF signalling. Thus, we decided to further characterise these cells to obtain information on their arteriovenous specification.
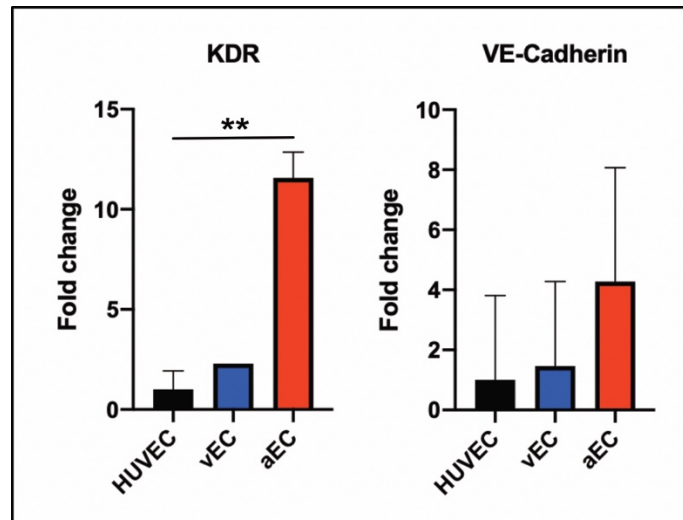
Figure 3.6: Gene expression profile of iPSC-EC reveals markers of maturation. Gene expression profile for HUVEC, vEC and aEC after CD31-sorting for KDR and VE-Cadherin. n=3. **p<0.01.

iii. Arteriovenous specification of iPSC-ECs

Blood vessel maturation encompasses the specialisation of ECs into different phenotypes depending on their localisation in the vascular tree. ECs possess a venous or arterial phenotypes in big blood vessels, also found in vascular capillary beds and a lymphatic phenotype in lymphatic vessels (Adams and Alitalo, 2007). The process of arteriovenous specification has been extensively studied and can be recapitulated *in vitro* for the differentiation of PSCs. Here, the culture of ECs in specific media containing VEGF, Notch signalling agonist, Activin/BMP/TGF-β inhibitor and an inositol monophosphatase inhibitor allowed the maturation of ECs towards an arterial fate.

To confirm the obtention of an arterial phenotype, we evaluated the gene expression profiles of our vECs and aECs for venous and arterial-specific genes (Fig. 3.7).
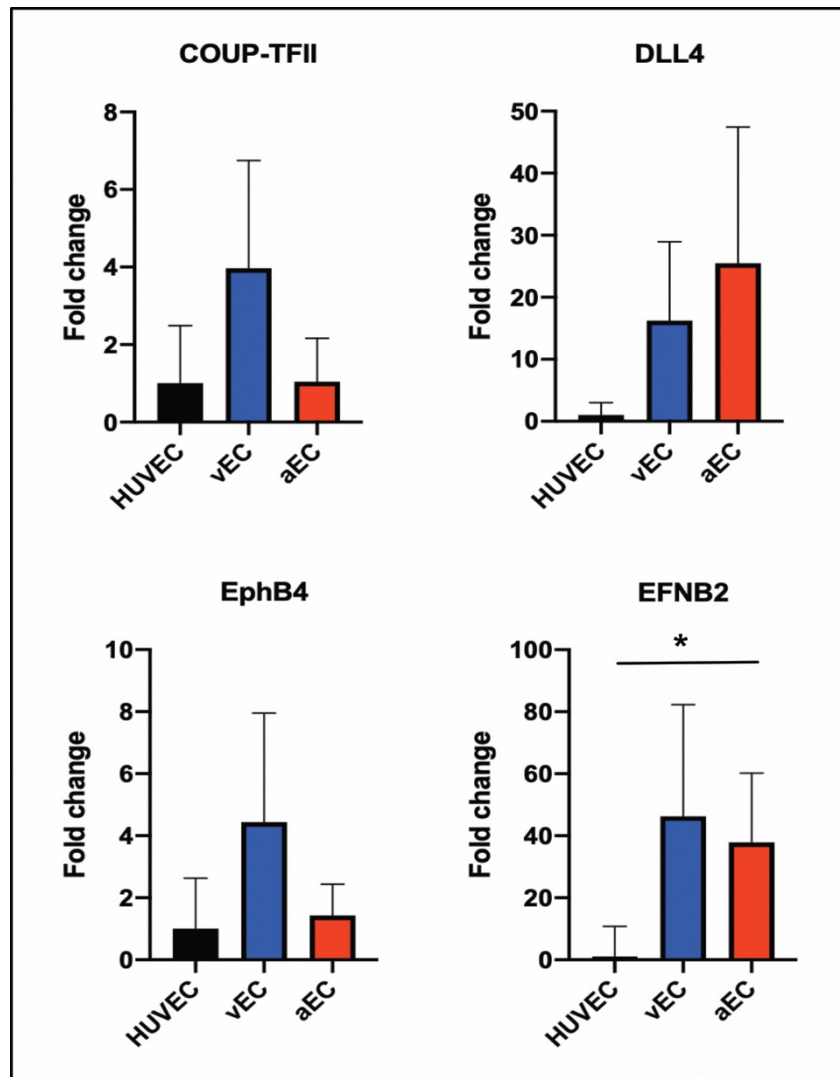
Figure 3.7: Gene expression profile of iPSC-EC reveals markers of arteriovenous specification. Gene expression profile for HUVEC, vEC and aEC after CD31-sorting for COUPTF-II, EphB4, DLL4 and EFNB2. n=3. *p<0.05.

To determine the venous specification, we evaluated the expression of the transcription factor COUP-TFII, responsible for venous phenotype by repressing Notch signalling (You et al., 2005), and the surface marker Ephrin type B receptor 4 (EphB4), involved in venous patterning (Wang et al., 1998). Although we could see a high expression of EphB4 and COUP-TFII in vECs, the differentiations gave heterogeneous expressions of venous-specific genes and both vECs and aECs had comparable expressions compared to HUVECs. The same highly heterogeneous expression was observed in between differentiations for arterial-specific genes DLL4, involved in Notch signalling, and Ephrin B2, ligand to EphB4 and expressed in arteries. iPSC-derived ECs appeared to have a higher overall Notch signalling than HUVECs, with a significant increase in expression of EFNB2 in aECs.

The analysis of gene expression was also confirmed by the immunostaining of iPSC-ECs for EC-specific markers such as ERG and VE-Cadherin and the arterial specific protein EFNB2 (Fig. 3.8).
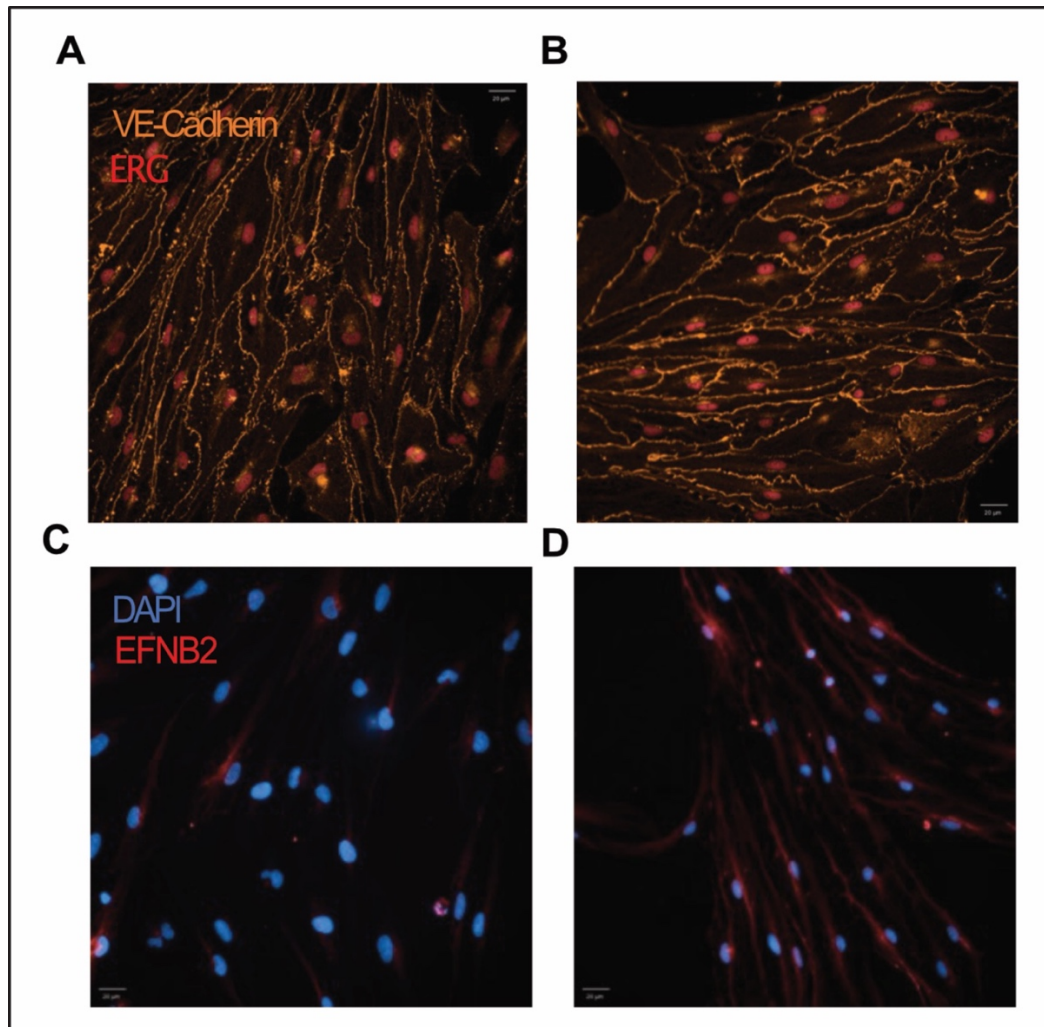
Figure 3.8: iPSC-EC express mature EC as well as arterial-specific markers. Cells obtained after the differentiation were immunostained for VE-Cadherin and ERG. Both vEC (A) and aEC (B) express mature markers. Arterial specification was assessed with the immunostaining for EFNB2, showing a lower expression in vEC (C) than in aEC (D). Scale bar: 25µm.

The expression of VE-Cadherin and ERG at the protein level confirms the mature phenotype of the iPSC-EC. VE-Cadherin is only expressed by fully differentiated ECs and ERG, unlike other transcription factor from the ETS family like ETV2 that is expressed transiently (Koyano-Nakagawa and Garry, 2017; Lee et al., 2008), is expressed only in mature vasculature and maintained throughout adulthood (Shah et al., 2016). This mature phenotype was also correlated with an increase in expression of arterial-specific EFNB2 in aEC compared to vEC as seen in figure 3.8C-D.

However, as seen in figure 3.8A-B, the VE-Cadherin staining highlighted big ECs forming a monolayer with holes and with a very thin junctional region, revealing discontinuous VE-Cadherin junctions with very little reticulation or double junction as observed in primary ECs (see chapter 2). Compared to the morphology observed in primary ECs, iPSC-ECs formed less compact colonies and we could observe over time the presence of big cells with protrusions in culture, resembling fibroblasts or mesenchymal cells morphology. Furthermore, we could observe a rapid decrease in cell proliferation after the first and second passages, with an even slower arterial EC population growth. Cells rarely reached confluency after the second passage, and this was associated with a lot of cell elongation and detachment as shown in figure 3.9.
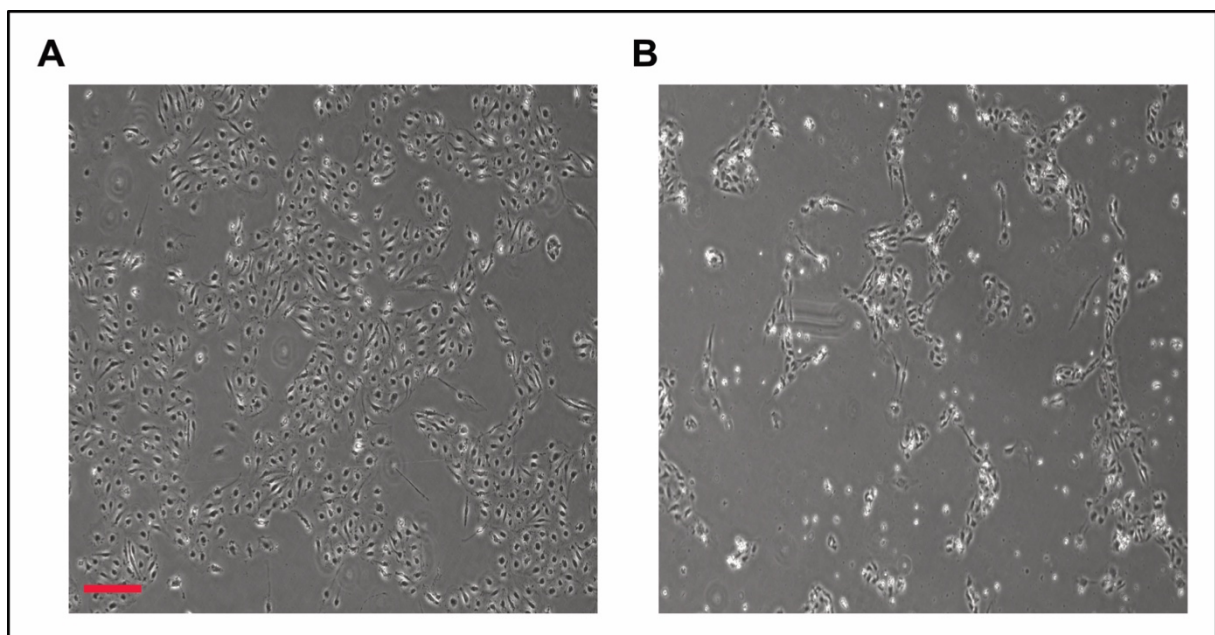
Figure 3.9: iPSC-EC detachment over time. vEC (A) and aEC (B) cultured as previously described (Zhang et al., 2017) could not be maintained in a proliferative state after 3 passages, as demonstrated by the cell elongation and detachment, especially important in the aEC population. Scale bar: 50μm

iv. Functional assays

As described earlier, the vasculature is formed early in development via vasculogenesis, the *de novo* formation of vessels from angioblasts, but stays dynamic in order to respond to organ growth or regeneration. Following an injury, blood vessels need to migrate and repopulate the injured region of interest to perform their physiologic functions. To do so, blood vessels, quiescent in healthy conditions, can respond to stimuli such as hypoxia or the release of angiogenic molecules via sprouting angiogenesis, as described earlier. Thus, evaluating the potential of iPSC derived ECs to form new blood vessels via vasculogenesis or sprout to form a mature vascular network is crucial to assess their functional relevance.

We decided to perform a typical vasculogenesis assay called "Matrigel assay" consisting in seeding ECs on a layer of Matrigel[TM] to assess their efficiency at creating a vascular network. Matrigel[TM] is composed of a mix of extracellular matrix and proteins secreted by mice sarcoma cells (Kleinman et al., 1986). The composition and stiffness of this hydrogel are adequate for the formation of blood vessel-like structures formed by ECs via migration and degradation of the 3D matrix (Kubota et al., 1988). As observed in figure 3.10, cells form these vessels in less than 24 hours.
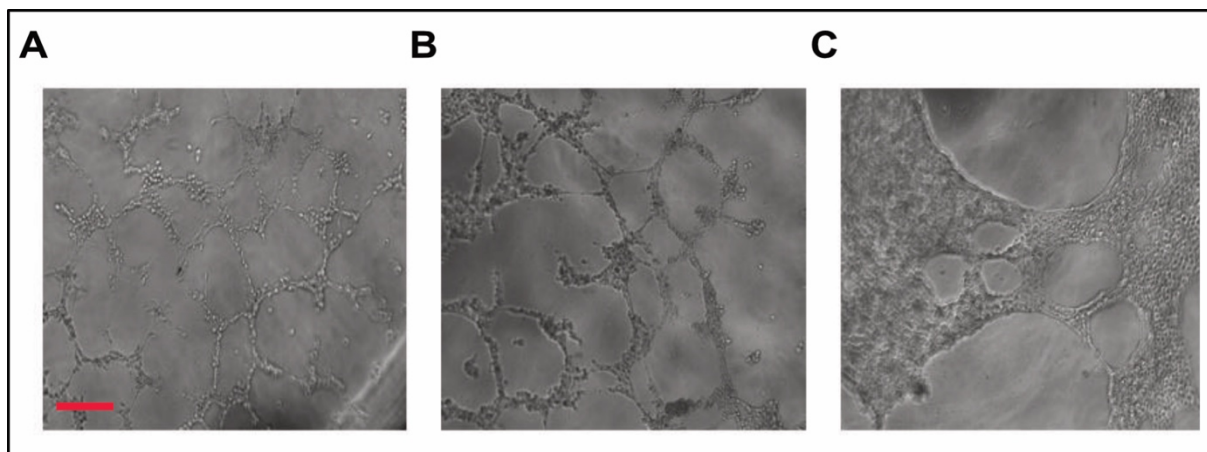
Figure 3.10: Matrigel assay to evaluate iPSC-EC vasculogenesis. HUVEC (A), vEC (B) and aEC (C) were seeded on Matrigel[TM] and cultured for 24h. Scale bar: 100μm.

To evaluate the functional maturation of our vEC and aEC, we compared them to the standard in the field, HUVECs. HUVECs formed thin vessel-like structures and organised all over the well in an interconnected network reminiscent of the vascular tree. As seen in figure 3.10B, vECs also formed these structures, although less spread-out than HUVECs. However, aECs failed to form any thinner networks on Matrigel[TM] and aggregated together to form bigger structures. After 24 hours, they had mostly degraded the Matrigel[TM] and formed only few connections as observed in figure 3.10C.

To further investigate their functional behaviour, we proceeded to investigate their ability to sprout in exogenous hydrogels. As described previously (Potente et al., 2011), ECs have the potential to degrade ECM via matrix metalloproteinases (MMPs) to invade the stroma and form new vessels. Among the different assays used to investigate sprouting angiogenesis (Nowak-Sliwinska et al., 2018), we decided to use the fibrin bead assay. Collagen coated beads are covered with ECs and embedded in a fibrin hydrogel to allow ECs sprouting from the beads (Nakatsu et al., 2007). To compare the ability of vECs and aECs to sprout, we also realised this assay with HUVECs, HAoECs and commercially available iPSC-ECFCs (Figure 3.11).
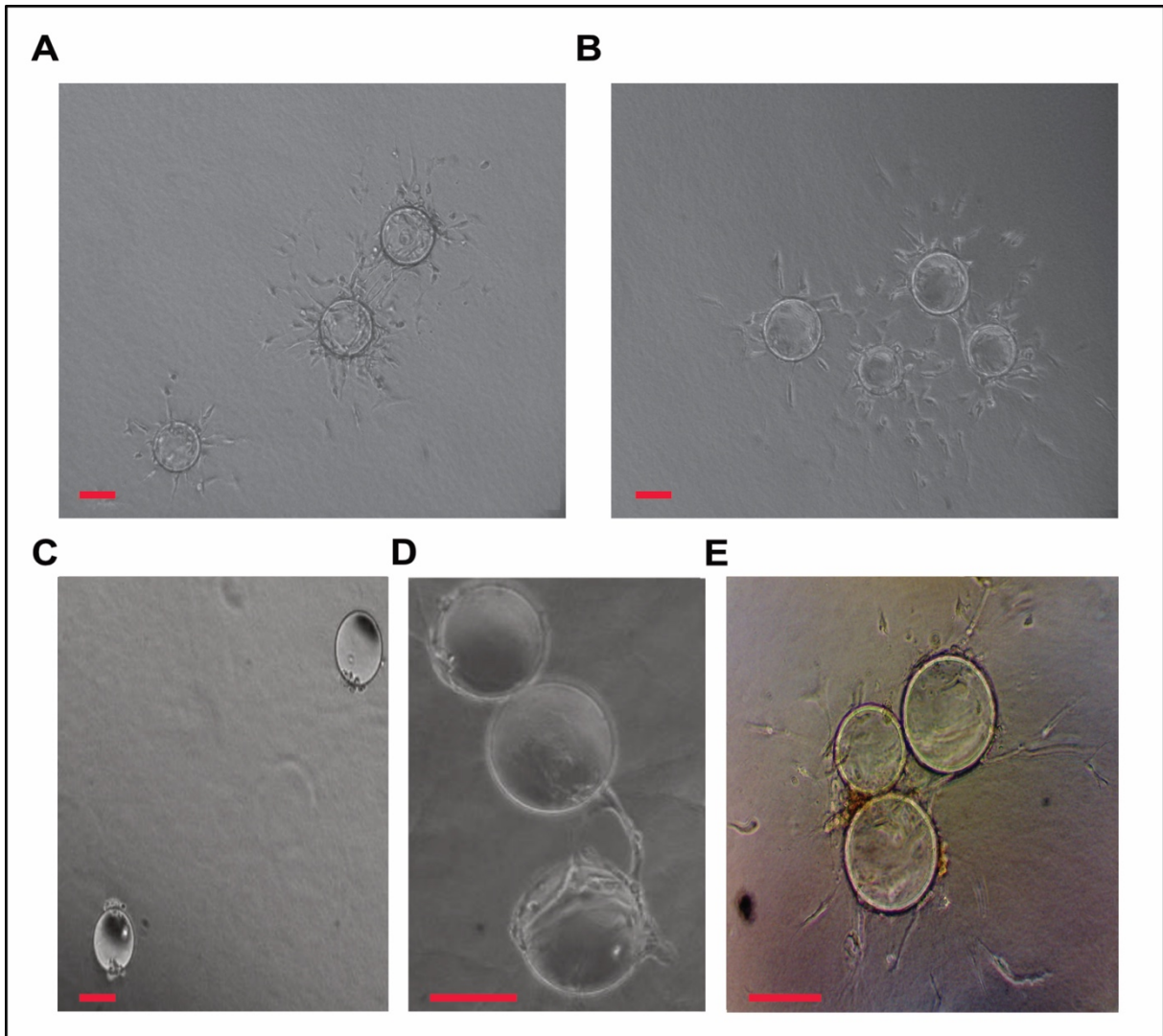
Figure 3.11: Bead fibrin gel assay to assess sprouting angiogenesis in different EC populations. HUVEC (A), HAoEC (B), vECs (C), aECs (D) and iPSC-ECFC (D) were seeded on beads, embedded in a fibrin gel and cultured for 48h under VEGF stimulation (50ng/mL). Scale bar: 50μm.

As seen in figure 3. 11A-B, ECs elongated and migrated from the beads into the hydrogel in a short timeframe, with some cells without contact with the bead after 48 hours. In HUVECs and HAoECs, almost ever ECs formed a sprout or migrated from the beads. However, vECs and aECs failed to form sprouts. Both populations of cells had a low adhesion to the collagen-coated beads and only few managed to form sprouts in the fibrin hydrogels. In comparison, iPSC-ECFCs, although less efficient than primary ECs, showed the potency to form angiogenic sprouts in fibrin hydrogels. Overall, ECs derived from PSCs showed a very low degree of functional maturation as illustrated by vasculogenesis and angiogenesis assays.

The use of developmental knowledge to differentiate stem cells into ECs has resulted in the differentiation of mature populations of specialised ECs, as described here and by others (Palpant et al., 2017; Rosa et al., 2019; Zhang et al., 2017). However, iPSC-derived ECs

obtained are still lacking the degree of maturation of primary ECs in terms of gene expression, protein expression or phenotype, as observed here.

c. ETV2 overexpression as a robust model to generate ECs from PSCs

Generating fully functional cells from PSCs has been a challenge since the implementation of PSC differentiation protocols. Stem cell-derived progenitors often lack a degree of maturation needed to be able to compare to primary cells taken from donors. This might be due to the accelerated protocols used compared to *in vivo* conditions or the lack of adequate 3D microenvironment and signalling. To overcome these issues, several studies have used genetic engineering to facilitate PSC differentiation. By overexpressing transcription factors responsible for cell differentiation or maturation, it is possible to obtain more mature populations of hepatocytes (Boon et al., 2020), myogenic progenitors (Rao et al., 2018) or oligodendrocytes (García-León et al., 2020) from stem cells.

i. Implementation of an ETV2-inducible stem cell line

Recent discoveries on cell differentiation and developmental programs have highlighted important transcription factors involved in EC differentiation (De Val and Black, 2009). The formation of ECs *in vivo* necessitates the temporal control of expression of different pathways as described earlier (Adams and Alitalo, 2007; Kathrina L. Marcelo et al., 2013). This cascade of event leading to EC differentiation is started by a "master regulator" of the endothelial lineage called Ets factor variant 2 (ETV2/ER71)(Kanki et al., 2017; Koyano-Nakagawa and Garry, 2017; Lee et al., 2008, p. 71). This transcription factor is essential and sufficient for the development of both the endothelial and haematopoietic lineages. By directing the fate of mesodermal progenitors (Rasmussen et al., 2011), ETV2 is responsible for the generation of VEGFR2 (KFDR)-positive mesodermal cells that will give rise to blood vessels.

To attempt generating a more mature population of ECs from PSCs, we received an inducible ETV2 overexpressing stem cell line from collaborators in the Verfaillie lab and used it as a previously described (De Smedt et al., 2021). The insertion of doxycycline inducible ETV2 overexpression cassette into an H9 line (Fig. 3.12A) allowed for the precise overexpression of ETV2 via the modulation of doxycycline concentration in the culture medium. The cassette, based on the Tet-on system as explained in figure 3.12C, allows the overexpression of ETV2 when doxycycline is added to the cell culture medium.
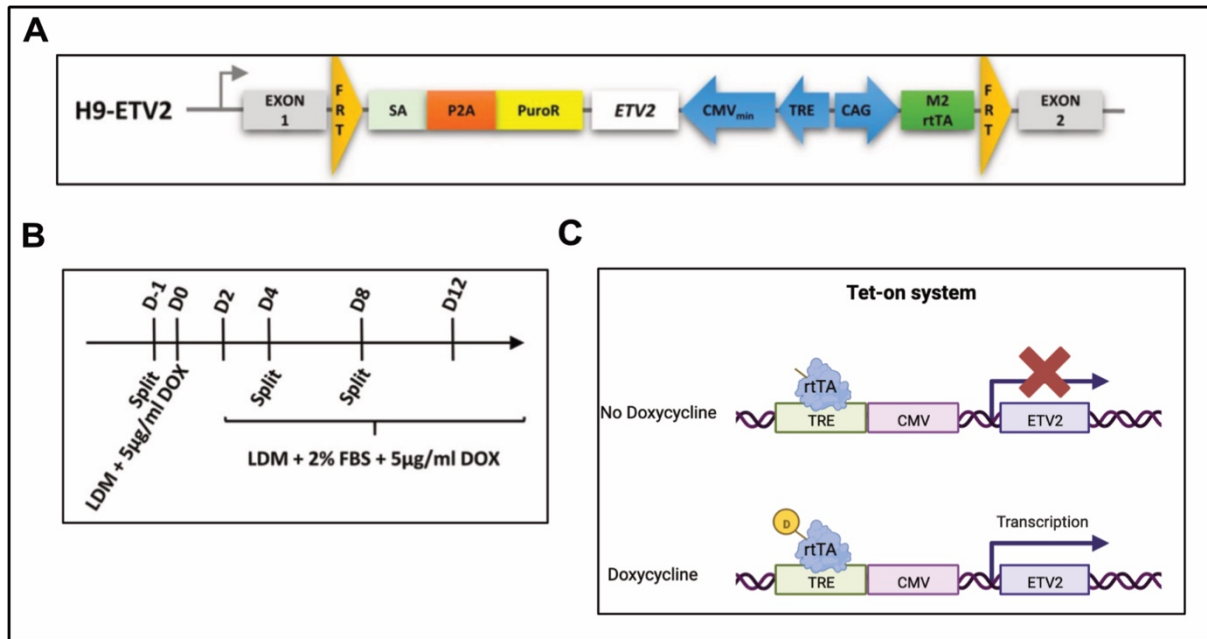
Figure 3.12: Implementation of an ETV2-overexpressing stem cell line.(De Smedt et al., 2021) A) Schematic of the cassette inserted into the H9-ETV2 line. B) Protocol timeline as previously described to differentiate H9-ETV2 PSCs into ECs. C) Schematics of the system Tet-on used in the study to overexpress ETV2 with the addition of doxycycline in the medium.

H9-ETV2 considerably accelerated the differentiation of PSCs into ECs. By following the protocol published with original publication (Fig. 3.12B)(De Smedt et al., 2021), we were able to get cells with an endothelial-specific morphology after 4 days in culture with doxycycline. The doxycycline was added from day 0 and kept in culture in following experiments unless described otherwise. These cells presented a very low amount of undifferentiated stem cells after 4 days and we could not observe any after a split to purify the population. The ETV2-overexpressing ECs could be passaged as described for several passages and kept proliferating. However, the protocol used for the differentiation of the H9-ETV2 contained Matrigel™ as a coating for the plates and used 2% FBS from day 2 onwards, adding some undefined variation into the differentiation.

ii. EC differentiation protocol and xeno-free differentiation

With the aim to use these cells for future tissue engineering strategies, we decided to implement a xenogeneic-free protocol of differentiation. First, we replaced the Matrigel™ by human recombinant vitronectin as a coating agent for the stem cells, which is more defined and does not contain any growth factors or undefined protein that can be found in Matrigel™. Then, we replaced the FBS with Knock-out serum replacement, a substitute to FBS with a controlled concentration of amino acids, vitamins and proteins as described previously (International Patent Application WO 98/30679)(Garcia-Gonzalo and Izpisúa Belmonte, 2008). After

selection of the stem cells keeping their phenotype on vitronectin, we performed a chemically defined protocol to obtain ECs from the H9-ETV2 line, as shown in figure 3.13.
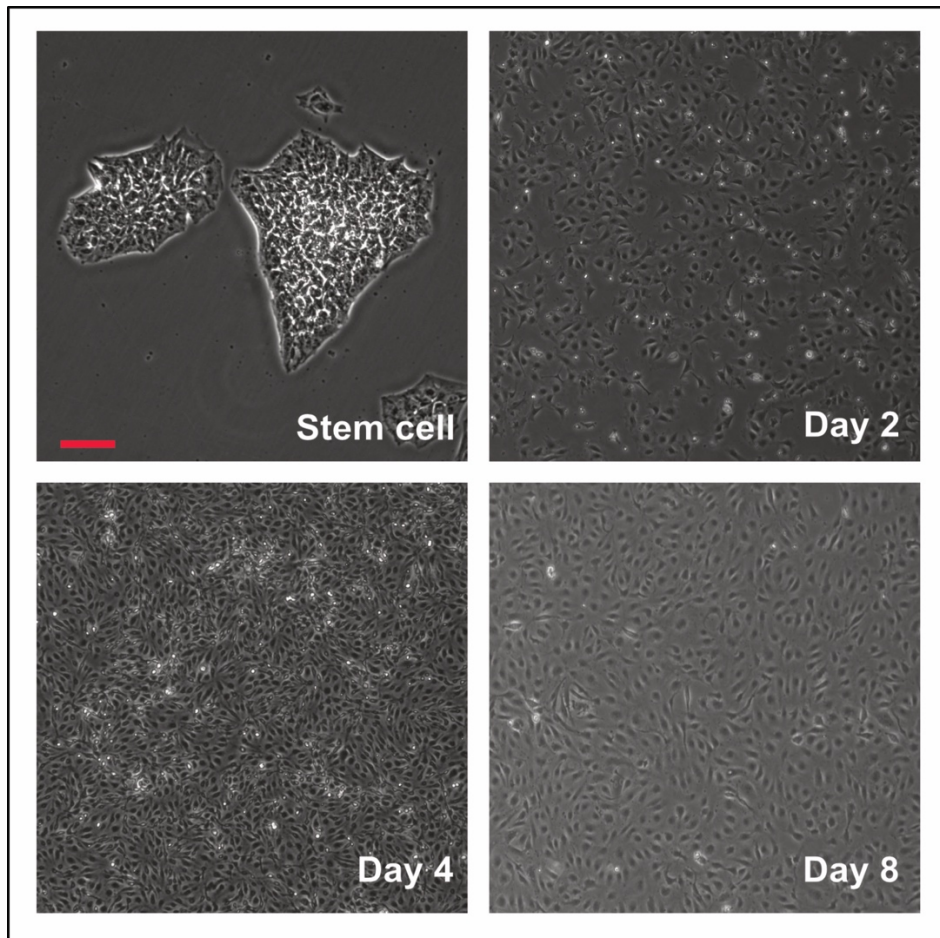
Figure 3.13: Chemically defined differentiation of the H9-ETV2 line into ECs. Cells were cultured on vitronectin instead of Matrigel^{TM} and the stem cell colonies were selected. Cells were then differentiated into ECs using the protocol as described, with the replacement of FBS with knockout serum. Scale bar: 50μm.

To confirm the mature phenotype of cells obtained with this method, we characterised the gene expression profile of the H9-ETV2 cells in comparison to HUVECs (Figure 3.14).
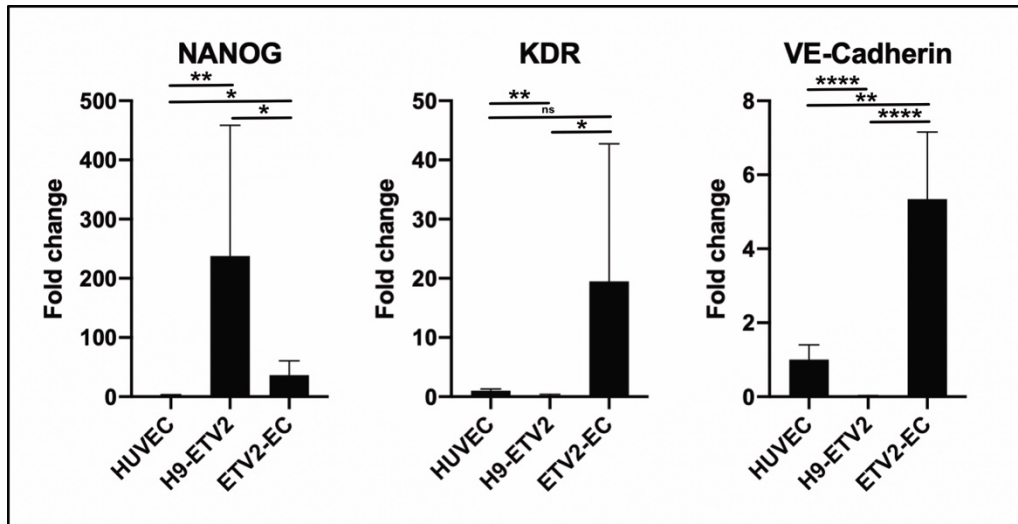
Figure 3.14: Gene expression profile of ETV2-EC reveals markers of EC maturation. Gene expression profile for HUVEC, H9-ETV2(stem cells) and ETV2-EC after splitting (day 4 to 8 of differentiation) for NANOG, KDR and VE-Cadherin. n=4. ns: non-significant p>0.05, *p<0.05, **p<0.01, ****p<0.0001.

Cells obtained after the first split (day 4 to 8 of differentiation) had a decreased NANOG expression compared to stem cells (H9-ETV2), but still retained a significantly higher expression compared to HUVECs, suggesting that some cells did not differentiate at that time. However, KDR and VE-Cadherin expression for the bulk population revealed a very high expression of these EC markers, confirming their differentiation towards EC progenitors. As seen for the iPSC differentiation described above, differentiations were still highly heterogeneous in terms of gene expression for the whole populations.

Although arteriovenous specification was not described in the original method, we wanted to know how the continuous expression of ETV2 affected the stem cell differentiation and further maturation. To do so, we compared the expression of arterial and venous-specific markers in ETV2-ECs with HUVECs and HAoECs (Figure 3.15).
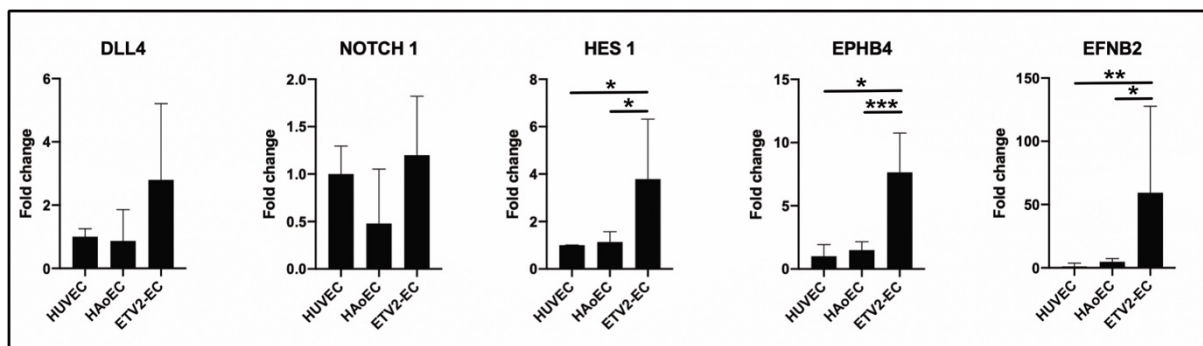
Figure 3.15: Gene expression analysis unveils high Notch signalling in ETV2-EC. Gene expression profile for HUVEC, HAoEC and ETV2-EC after splitting (day 4 to 8 of differentiation) for DLL4, Notch1, Hes1, EphB4 and EFNB2. n=4. *p<0.05, **p<0.01, ***p<0.001.

Overall, ETV2-ECs cultured in described conditions had a very high Notch signalling activation as observed by a similar expression of DLL4 and NOTCH1 than HAoECs and the higher expression of HES1, downstream target of Notch signalling. Interestingly, although at the population level Notch signalling was high, the expression of both EphB4 and EFNB2 were also significantly higher than primary cultured ECs, suggesting a mix of ETV2-ECs with different fate in the population. Both populations of stem cell-derived ECs obtained by directed differentiation or ETV2 overexpression appeared to have a high basal Notch activation. Although it has been shown to be essential for EC maturation and arteriovenous specification (Fernández-Chacón et al., 2021; Jakobsson et al., 2009; You et al., 2005), Notch signalling has also been linked to cell cycle arrests (Fang et al., 2017; W. Luo et al., 2021) and could lead to a premature decrease in cell proliferation.

iii. Influence of coating on EC proliferation rate

The cells obtained after a split had an endothelial morphology and kept proliferating. Nevertheless, we could also observe a decrease in proliferation and adhesion after 2 to 3 passages, as seen with the iPSC-EC previously differentiated.

To address this issue, we hypothesized that the extracellular matrix used in cell culture could influence cell phenotype including adhesion and proliferation rate. In the original paper describing the H9-ETV2 differentiation protocol (De Smedt et al., 2021), authors describe the ability of these cells to proliferate on Matrigel^{TM}-coated plates. Qualitative observations (raw cell counting, time to reach confluency) upon cell subculturing on vitronectin did not have any significant effect on the cell proliferation but it was slower with passages when cultured on fibronectin-coated plates as seen for primary ECs or other differentiation protocols. Fibronectin and collagen have been shown to play an important role in determining EC phenotype and differentiation from PSCs (Glaser et al., 2016; Wijelath et al., 2004). We hypothesized that the coating could have a significant effect on EC proliferation rate and proceeded to use this experimental setup with raw cell counts as readout to determine the optimal coating. To determine which coating was appropriate for the culture of differentiated ECs after the first split, we cultured the cells on Matrigel^{TM}, collagen, fibronectin or a mix of fibronectin and collagen (Fig. 3.16).

As observed in figure 3.16, the seeding of already differentiated ECs on Matrigel^{TM} resulted in very low attachment after stem cell maintenance had been transferred to vitronectin. Although,

some cells attached and recovered from the split, the growth on Matrigel™ was slow and clonal, with proliferation slowing rapidly.
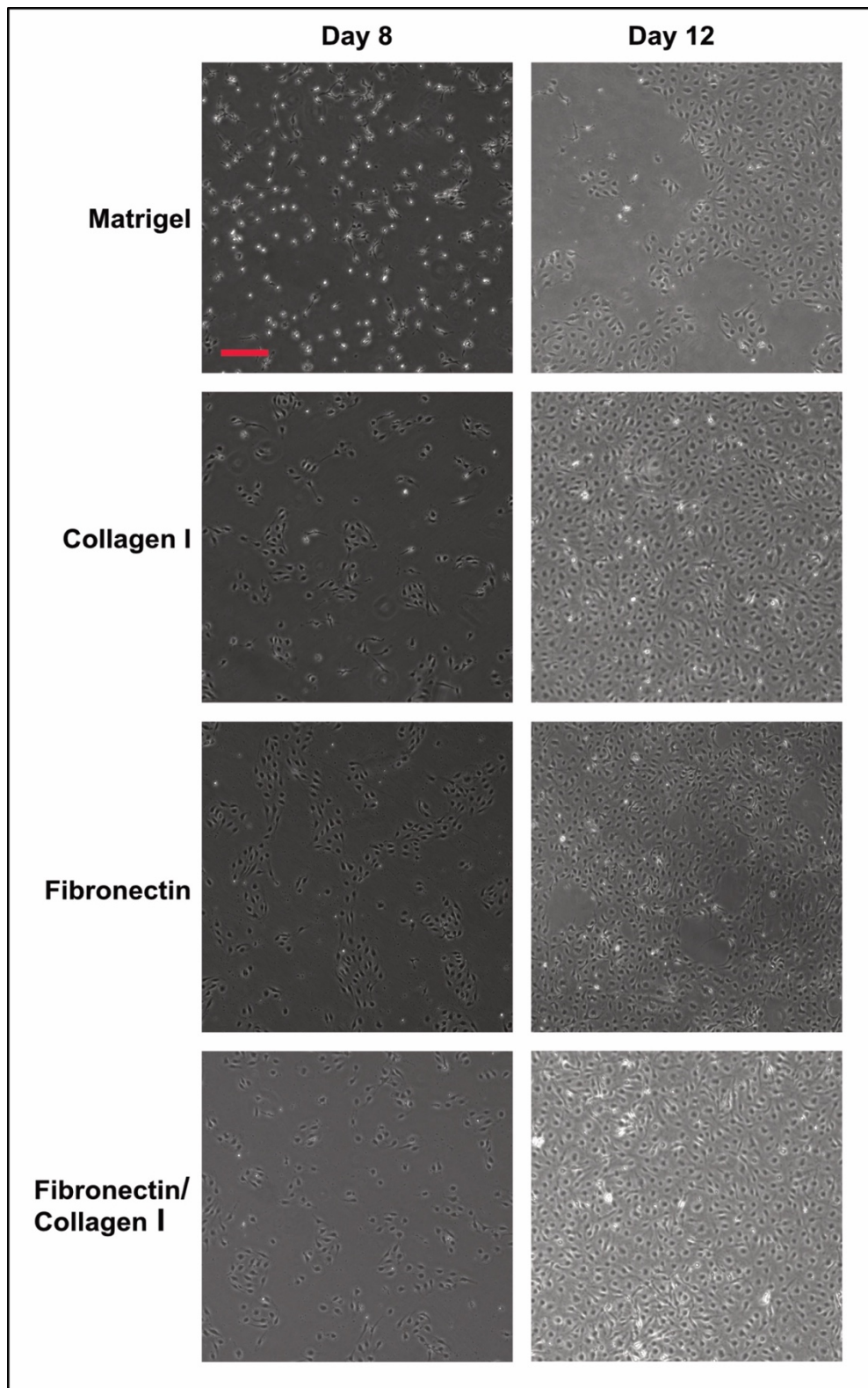
Figure 3.16: Influence of the coating on EC proliferation. H9-ETV2 were differentiated until day 8, splitted and seeded on different matrices. The morphology of the cells was assessed just after splitting at day 8 and after 4 days of culture on Matrigel™, collagen I, fibronectin or a mix of fibronectin and collagen. Scale bar: 50μm.

Vitronectin coating was not tested after the first split because it has less known effect on EC function and is less present in blood vessel microenvironment (Davis and Senger, 2005). The seeding on chemically defined matrices such as collagen I or fibronectin gave a better result than on Matrigel^{TM}. After 4 days of culture in standard conditions (DMEM+ 2% KO serum + doxycycline), cells were fully confluent in the collagen I and collagen I/Fibronectin mix conditions, with the EC seeded on fibronectin only coated plates at around 70-80% confluency as observed earlier. Due to the important role of fibronectin signalling on EC development and function (Davis and Senger, 2005; Wijelath et al., 2004), we decided to culture differentiated ECs on Collagen I/Fibronectin coated plates to improve EC proliferation.

iv. EC maturation, cell sorting and phenotyping

Endothelium maturation is driven by the integration of several pathways such as VEGF signalling, FGF signalling or Notch signalling among others (Adams and Alitalo, 2007; De Val and Black, 2009; Fish and Wythe, 2015; Herbert and Stainier, 2011). These signals are integrated from the microenvironment and come from neighbouring cells, extracellular matrix or biomechanical cues. In directed differentiation, the only signals that cells receive are the surface on which they adhere, their neighbouring cells and the medium that they receive.

To further mature the cells obtained with the H9-ETV2 line and create a more relevant cell culture medium, we completed the medium composition with growth factors known to be important in EC development and maturation. Among these important growth factors are basic fibroblast growth factor (bFGF, FGF-2) and vascular endothelial growth factor A (VEGF-A). bFGF is responsible for cell survival, proliferation and angiogenesis (Esser et al., 2015; Jih et al., 2001) and VEGF signalling is responsible for EC phenotype, cell fate and angiogenesis (Ferrara, 2002; Fish and Wythe, 2015; Gerhardt et al., 2003; Jakobsson et al., 2009; Potente et al., 2011). These growth factors are used in almost every EC differentiation protocol to maintain cell proliferation and phenotype (Palpant et al., 2017; Prasain et al., 2014; Zhang et al., 2017) and are the main growth factors used in primary EC culture media. Here, we supplemented our basal medium with bFGF and VEGF to see the effect on H9-ETV2 proliferation and morphology. As seen in figure 3.17, the addition of bFGF into the medium at day 2 of differentiation increased the proliferation of H9-ETV2 after the first split, with cells reaching confluency almost twice faster, at day 6 after 2 days after the first split instead of at day 8 after 4 days.
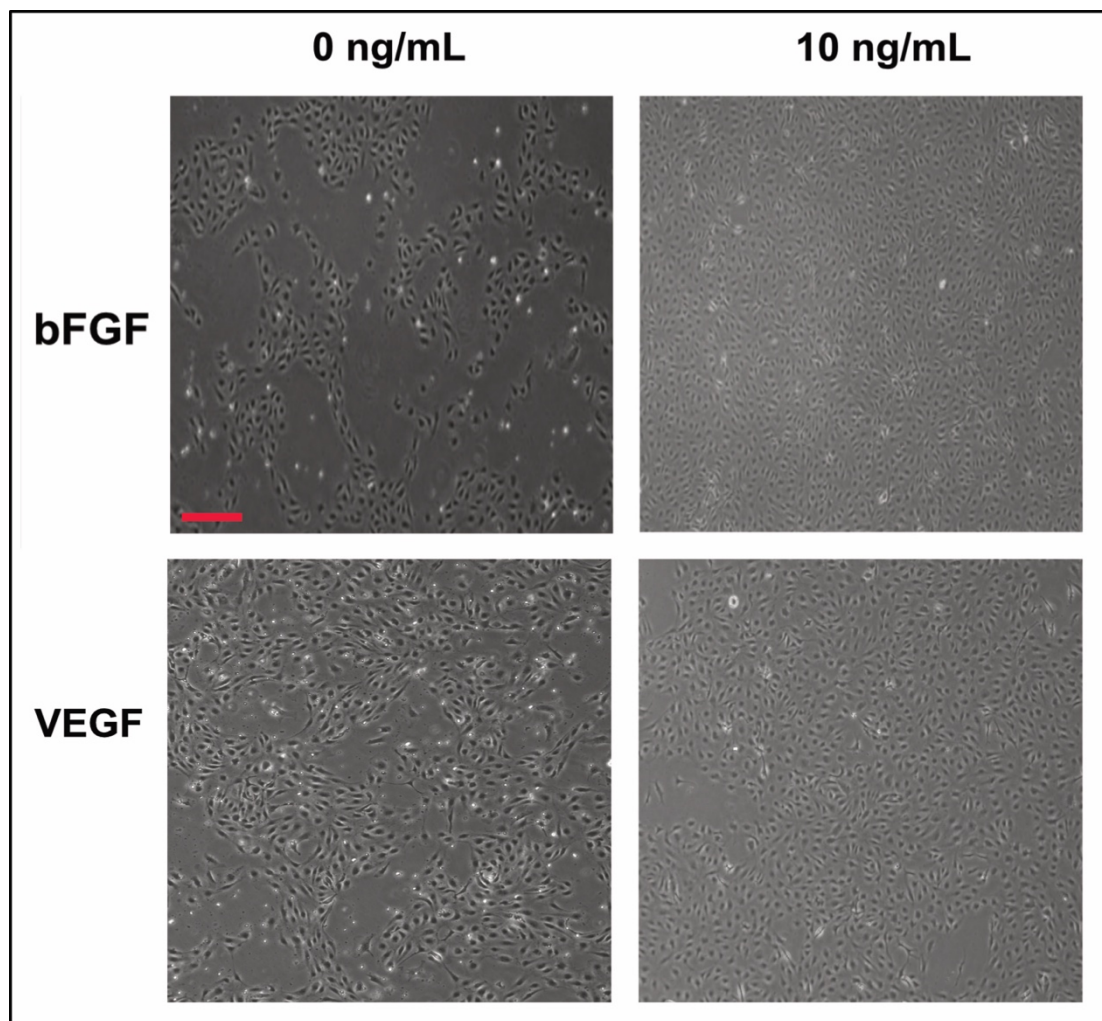
Figure 3.17: Influence of the medium composition on EC proliferation and phenotype. Photographs of the H9-ETV2 cells at day 6 of differentiation, 2 days after the first split. Cells were treated in normal conditions (DMEM + 2% serum + doxycycline) or with the addition of 10ng/mL bFGF or 10 ng/mL VGFA at day 2 of the differentiation. Scale bar: 50µm.

The addition of VEGF-A in the medium also influenced the cell morphology and proliferation, with cells appearing more elongated in culture as observed with primary ECs and described earlier. VEGF-A had a lesser impact on proliferation than bFGF but cells still reached confluency earlier than without VEGF-A in the medium. As expected, the addition of adequate growth factors in the differentiation medium improved the efficacy of the differentiation protocol and following experiments were conducted with the addition of bFGF and VEGF-A in the medium.

To compare the degree of maturation of our H9-ETV2 model with the protocol used earlier, we performed magnetic activated cell sorting of these cells for CD31. As observed in figure 3.18, cells obtained with the inducible line were far more homogeneous than the cells obtained with the protocol using iPSC and arteriovenous specification.
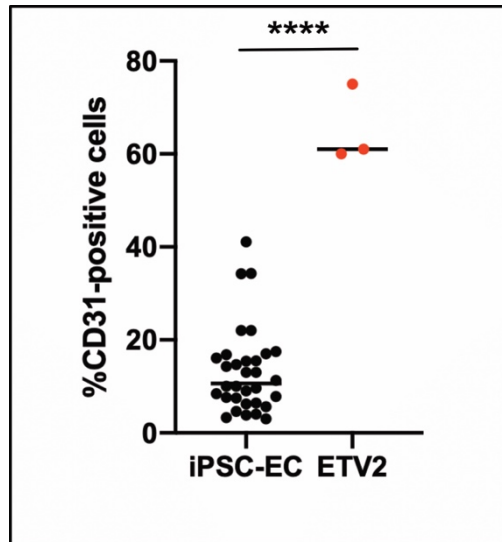
Figure 3.18: Influence of the ETV2 overexpression on PSC-EC differentiation. Cells were sorted via MACS for CD31 after 6 days of differentiation. iPSCs were differentiated using the directed differentiation protocol described earlier for 3 different iPSC lines (Zhang et al., 2017)(n=16). H9-ETV2 cells were differentiated using the optimised protocol and induced with the addition of doxycycline in the medium (n=3). ****p<0.0001.

The yield of CD31-positive cells obtained through the differentiation of the H9-ETV2 was on average 5 to 6 times higher than the yield obtained with the iPSC differentiation, with on average 65% of CD31-positive cells. This higher yield was mainly due to the homogeneity of the differentiation as observed in figure 3.13, 3.16 or 3.17, almost all the cells had an endothelial cell morphology, with no visible clusters of stem cells left before the first split at day 4. We conclude that broad and forced expression of ETV2 in our stem cell population led to this higher homogeneity in differentiation, as suggested by the higher cell death indicated by floating cells and a resulting monolayer of cells at day 4. Indeed, in the iPSC differentiation the wells were very full, with up to 2.10^6 cells per well of a 6 well plate and big 3D stem cell clumps at day 6 while the H9-ETV2 were in a monolayer and rarely more than 5.10^5 per well of a 6 well plate at day 4. This resulted in a lower number of cells getting sorted for CD31 but a way higher yield of CD31-positive cells in the H9-ETV2 population.

The overexpression of ETV2 allowed us to rapidly get a homogeneous population of CD31-positive cells that could be cultured in chemically defined conditions. Nevertheless, obtaining ECs from stem cells in such a short timeframe could result in an immature cell phenotype and these cells need to be compared to other EC models to evaluate their degree of maturation.

d. Phenotyping and comparison to primary EC lines

As described in chapter 2, high content imaging can be used to study EC heterogeneity and give insights on EC monolayer function (Chesnais et al., 2022a; Wiseman et al., 2019). We characterised different vascular beds for their inherent heterogeneity in cell cycle, junctional status and Notch signalling. Comparing the cells obtained from stem cell differentiation to primary EC obtained from patients can give us information on their maturation.

We therefore used the same markers to characterise H9-ETV2-EC generated using the optimised protocol described above in comparison to primary human EC (HUVEC or HAoEC) and iPSC-ECFC (Prasain et al., 2014). In order to compare them in the same conditions, we cultured H9-ETV2-EC on fibronectin-coated plates in very confluent conditions and in the same medium (EGMV2, Promocell) supplemented with doxycycline for the ETV2 line. Furthermore, we wanted to compare the phenotype of our cells to commercially available iPSC-EC (human iPSC-derived endothelial colony forming cells, Axol) and implemented our ECPT pipeline for these cells. As described earlier, we immunostained the cells for VE-Cadherin, HES1 and NOTCH1 and analysed their phenotype in confluent monolayers (fig. 3.19).

At the morphological level, cells had a typical endothelial morphology, except for the iPSC-ECFC that had a more elongated phenotype and no clear junctions. A closer look at the VE-Cadherin distribution confirmed that HUVEC. HAoEC and ETV2-ECs had a good interjunctional distribution of VE-Cadherin without holes in the monolayer while iPSC-ECFCs formed a discontinuous monolayer without a regular VE-Cadherin expression. Interestingly, a qualitative inspection HES1 and NOTCH1 intensity revealed high levels Notch signalling in both stem cell derived ECs.
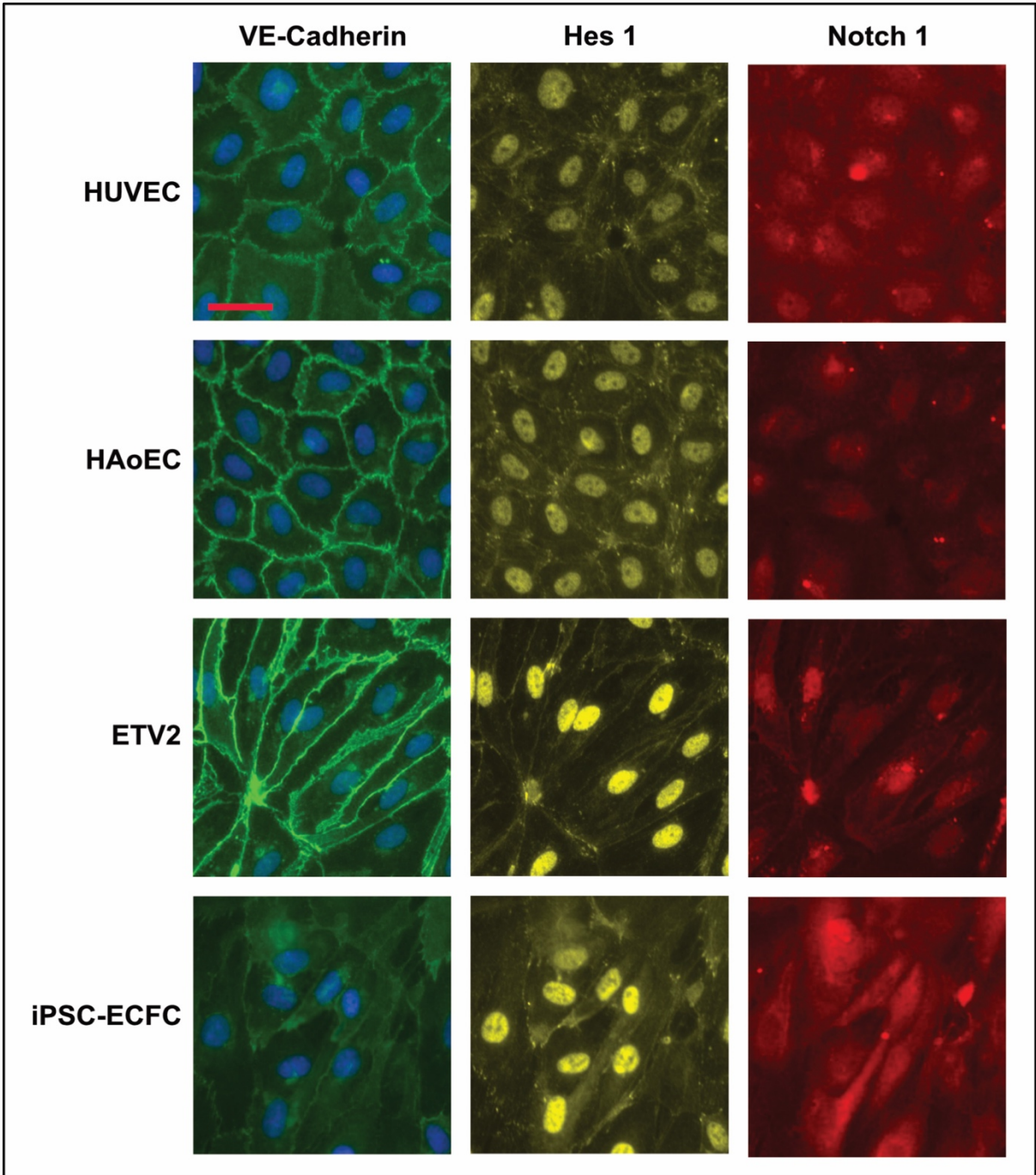
Figure 3.19: Phenotype heterogeneity in primary and PSC-derived ECs. HUVEC, HAoEC, ETV2 line and iPSC-ECFCs were cultured in standard conditions and grown to confluency before being immunostained for VE-Cadherin, Hes1 and Notch1. Scale bar: 25μm.

e. H9-ETV2 depend on doxycycline to keep their phenotype

As described earlier, ETV2 is an essential transcription factor for the development of ECs and is expressed in the mesoderm to give rise to KDR-expressing cells (Koyano-Nakagawa and Garry, 2017, p. 2; Lee et al., 2008, p. 71; Rasmussen et al., 2011). Its downstream targets include KDR, CD31, VE-Cadherin, Tie2 or Sox7 (Ferdous et al., 2009; Lee et al., 2008, p. 71). However, the expression of ETV2 is temporally restricted and is only expressed transiently in the embryo or in the differentiating PSCs at the mesodermal stage (Koyano-Nakagawa and Garry, 2017, p. 2; Lee et al., 2008, p. 71; Lindgren et al., 2015, p. 2).

In the original protocol for the ETV2 inducible line, the authors describe the continuous induction of ETV2 with doxycycline throughout the differentiation protocol and do not remove it at any point (De Smedt et al., 2021). To reproduce the temporal expression of ETV2 in the embryo, we decided to remove the doxycycline from the culture medium after the initial phase of induction. Doxycycline was removed after the first split while serum, bFGF and VEGF were kept in the medium to keep essential signalling for ECs. The morphology of cells obtained after 10 days of culture with or without doxycycline is shown in figure 3.20.
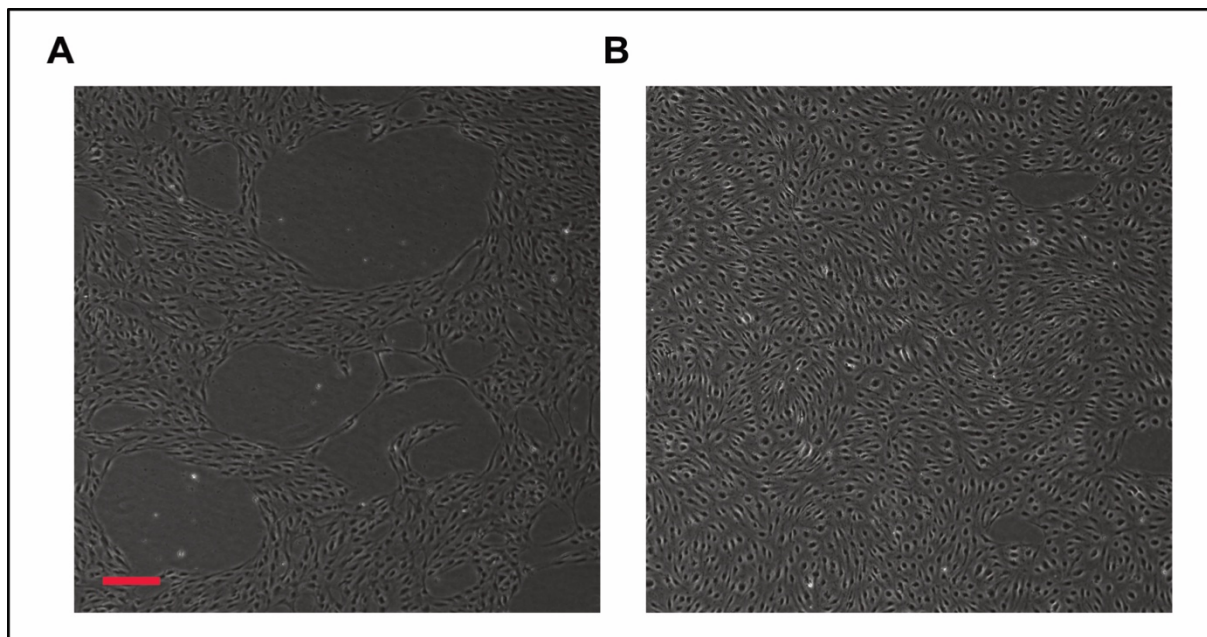
Figure 3.20: Influence of ETV2 overexpression on the H9-ETV2 phenotype. H9-ETV2 were differentiated in normal conditions until day 4 and the first split. Photographs were taken at day 10 of differentiation after removal of doxycycline at day 4 (A) or in standard conditions (B). Scale bar: 100μm.

The removal of doxycycline induced a reduction in proliferation, a higher cell detachment and the elongation of cells as observed in figure 3.20A. After 2 passages, ECs stopped proliferating and could not be expanded. Cells without doxycycline elongated and migrated in a way

reminiscent of sprouting angiogenesis, with cells leading a sprout and reaching out to other ECs.

Unfortunately, PSC-ECs alone cultured *in vitro* in 2D could not be kept in culture for times comparable to primary ECs. Even with the induction of EC-specific transcription factor ETV2, the cells obtained stopped proliferating after 4 passages. This phenomenon was observed for both stem cell differentiation protocol with EC being differentiated alone and in 2D, without the support of any perivascular cells or biomechanical cues as experienced *in vivo*.

4- <u>**Stem cell differentiation to perivascular cells**</u>

Perivascular cells play a major role in blood vessel function and development. Pericyte coverage is crucial for blood vessel maturation and has been linked to blood-brain barrier function, endothelium permeability or basement membrane formation (Armulik et al., 2011, 2010; Stratman et al., 2009). Smooth muscle cells are responsible for vasoconstriction, vessel elasticity and matrix production (G. Wang et al., 2015). Current models of blood vessels *in vitro* are often composed only of ECs and are representative of smaller calibre vessels. Incorporating perivascular cells into tissue engineered blood vessel models will be key to achieve development and maturation. Furthermore, achieving differentiation of perivascular cells from PSCs could allow the creation of tissue-specific blood vessels in a potentially unlimited number and allow the study of disease-specific models such as atherosclerotic arteries.

a. Pericyte differentiation

As described earlier, pericytes represent a very heterogeneous population of cells, with distinct origins and functions throughout the body (Yamazaki and Mukouyama, 2018). Pericyte disfunction is associated with numerous vascular diseases (Armulik et al., 2011; Yamazaki and Mukouyama, 2018) and neurodegenerative diseases such as autism (Tărlungeanu et al., 2016). To decipher the role of pericytes in vascular development and recreate healthy and pathological models in vitro, several protocols have been developed to differentiate pericytes from PSCs (Faal et al., 2019; Kumar et al., 2017; Orlova et al., 2014). With the same aim as for ECs, we decided to implement existing protocols to differentiate pericytes in 2D directed differentiation.

i. Implementation of pericyte directed differentiation protocols

Pericytes arise mainly from mesodermal progenitors, although some are derived from neural crest progenitors as described earlier (Faal et al., 2019). For this study, we decided to differentiate pericytes from the mesodermal lineage, due to the ease of implementation with our existing EC differentiation protocol. As they arise from common lineages, we first decided to use the cells from the iPSC-EC differentiation that were not positive for CD31 and that should be mesodermal progenitors, to differentiate into pericytes. Existing protocols to differentiate pericytes often use cell culture media supplemented with 10% FBS, bFGF and platelet-derived growth factor BB (PDGF-BB) with no protocols reported to differentiate pericytes in chemically defined conditions. Here, we seeded CD31-negative cells at day 6 of EC differentiation on collagen I coated plates and cultured them in commercially available pericyte medium (Pericyte growth medium, Promocell). As seen in figure 3.21, cells adhered well to the collagen, did not have any EC morphology and did not form colonies.
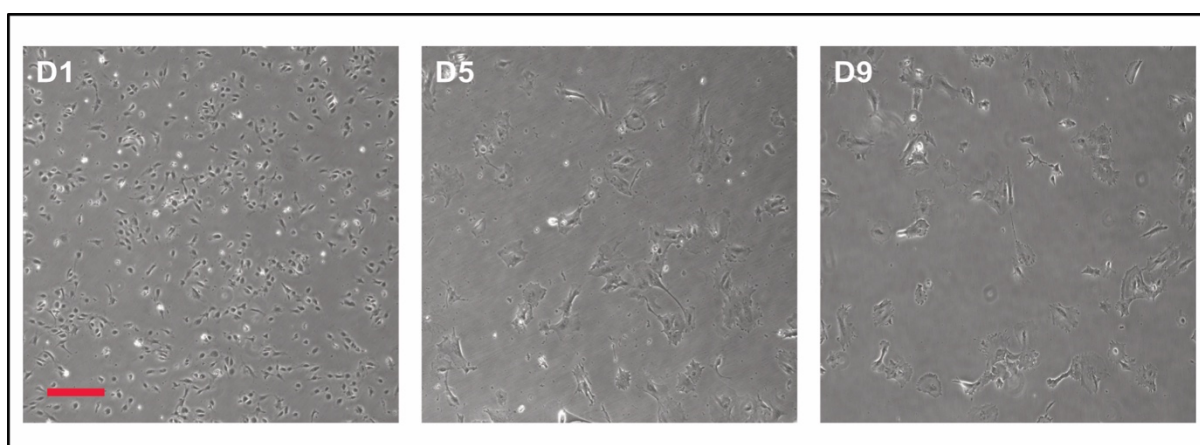
Figure 3.21: Pericyte differentiation from CD31-negative cells. Cells were differentiated towards vECs as described previously (Zhang et al., 2017) and sorted for CD31. CD31-negative cells were seeded at day 0 and cultured in pericyte medium. Photographs of the cell morphology were taken at day 1, 5 and 9 after seeding. Scale bar: 100μm.

However, the cells obtained and cultured in pericyte medium immediately stopped proliferating and did not reach confluency at any stage. The cells that did not detach adopted a large morphology, reminiscent of pericytes in culture but the yield obtained with this method was too low to characterise them further.

To obtain a more homogeneous and proliferating population of pericyte, we decided to implement existing protocols to directly differentiate pericytes from PSCs. Several protocols have been used to derive pericytes, but few have shown maturation of the cells. Using OP9 co-cultures (stromal cells lacking M-CSF and promoting the differentiation of stem cells down the

hematopoietic lineage (Nakano et al., 1994; Vodyanik et al., 2005)) and semisolid cultures, Kumar et al. described the potential of hPSCs to give rise to pericytes with either a "capillary" and "arteriolar" types namely PC1 and PC2 (Fig. 3.22). Capillary pericytes have been described NG2-positive aSMA-negative with a chemoattractant and anti-inflammatory phenotype (Stark et al., 2013) while arteriolar pericytes are NG2-positive and aSMA-positive cells with a more contractile phenotype (Armulik et al., 2011; Crisan et al., 2008; Kumar et al., 2017). To reduce the complexity of the protocol, we implemented our mesoderm differentiation protocol and removed the OP9 co-culture or the creation of colonies in semisolid medium.
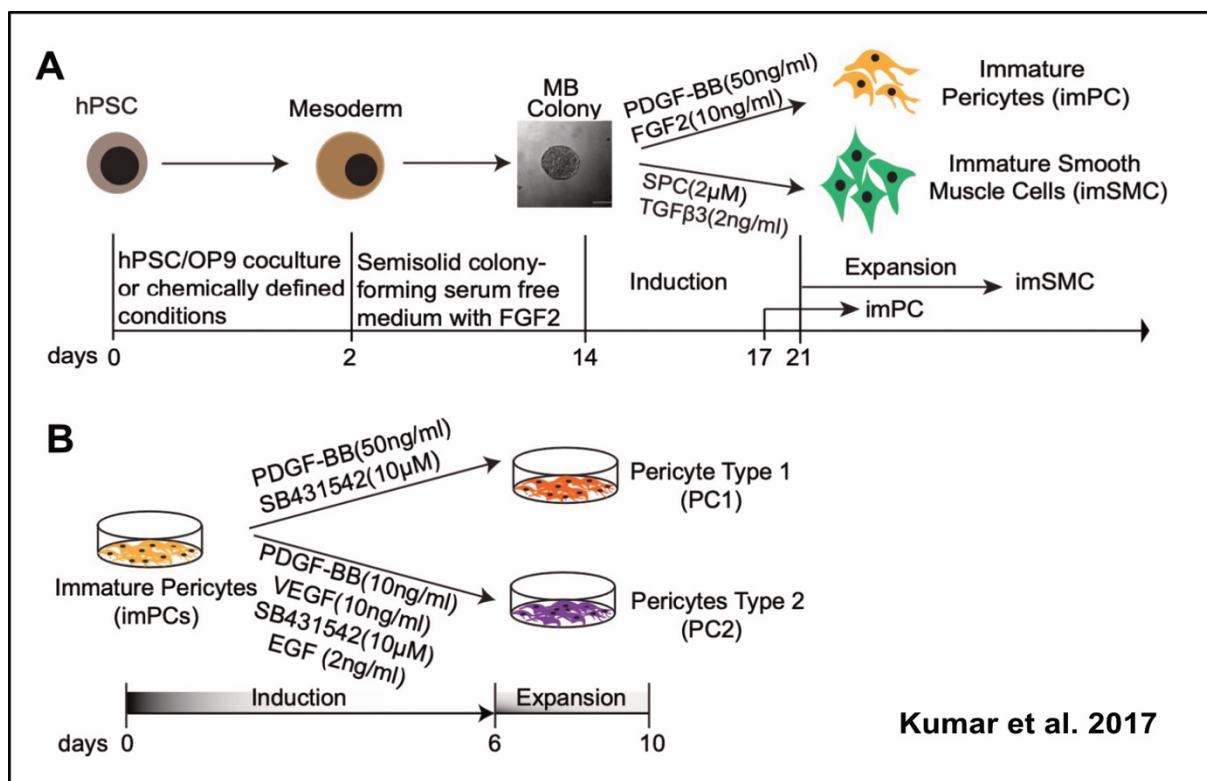
Figure 3.22: Pericytes differentiation protocol as previously described (Kumar et al., 2017). A) Schematic of the protocol used to differentiate hPSC into immature PCs and SMCs. hPSC (human pluripotent stem cells) are differentiated towards the mesoderm to form mesenchymoangioblasts (MB) colonies. Cells are then induced towards immature pericytes with PDGF-BB (Platelet growth factor BB) and FGF2 (Fibroblast growth factor 2) or towards immature smooth muscle cells with SPC (sphingosylphosphorylcholine) and TGFB3 (Transforming growth factor β 3). B) Schematic of the protocol used to mature PCs into PC1 and PC2. Immature PCs are specialised towards Pericyte type 1 by adding PDGF-BB and SB431542 (TGF-Smad inhibitor) to the medium for 6 days. PCs are specialised towards Pericyte type 2 by adding PDGF-BB, VEGF (Vascular endothelial growth factor), SB431542 and EGF (Epidermal growth factor) to the medium for 6 days.

After mesodermal induction, cells were cultured as described in the presence of PDGF-BB and bFGF for 7 days to obtain immature pericytes. At this stage, cells reached confluency and the proportion of stem cells or undifferentiated cells was low, as shown in figures 3.23 and 3.24 describing the morphology of the cells during the differentiation.

With our optimised mesoderm induction, cells obtained after 4 days had a more homogeneous morphology than the ones obtained after sorting for CD31. The addition of bFGF in the medium allowed the cells to proliferate and reach confluency before the induction of pericyte differentiation. Although supplemented with FBS, the expansion immature PCs in commercial pericyte medium gave rise to a relatively pure population of cells with compact and elongated morphology in both PC1 and PC2 protocols. The morphological difference between both populations was low as observed in the original protocol and their phenotype required further investigation into pericyte-specific marker to evaluate their degree of maturation.
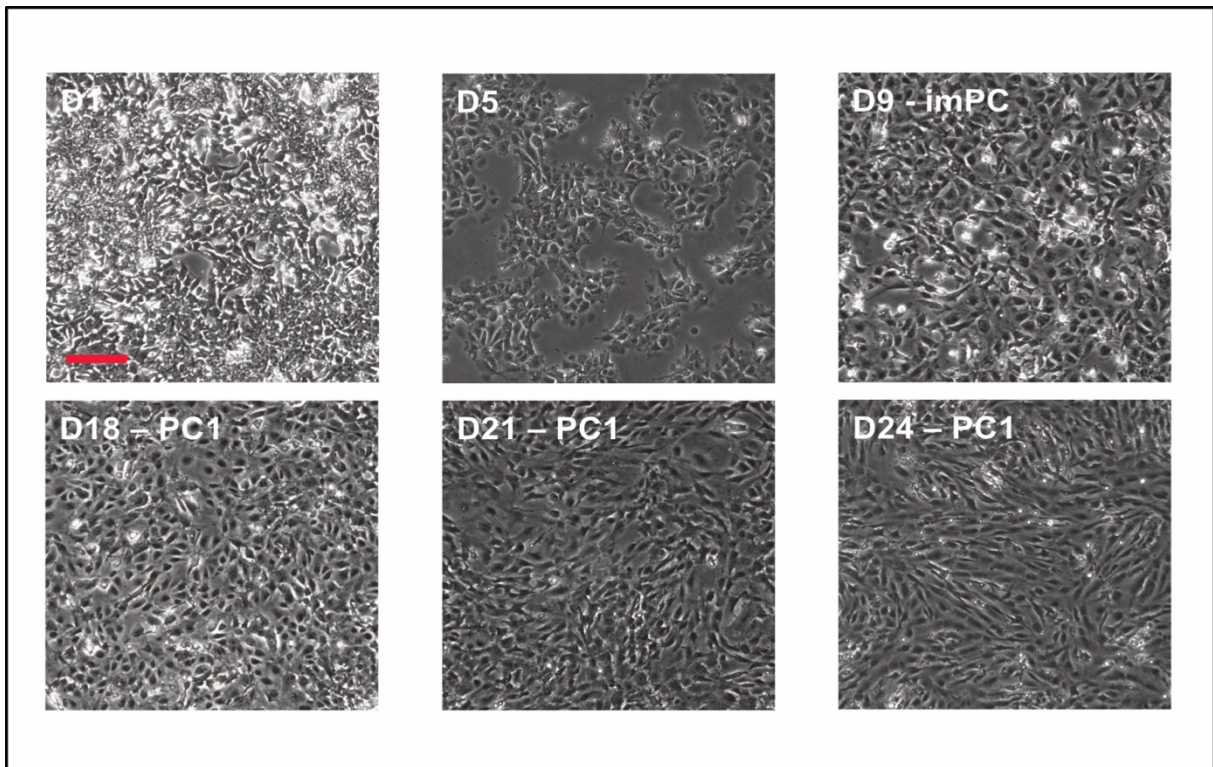
Figure 3.23: Cell morphology during the differentiation protocol of iPSCs towards pericytes type 1 (PC1) as described previously (Kumar et al., 2017). Cells were differentiated towards the mesodermal lineage as previously described and specialised towards pericyte type 1 for 24 days. Photographs were taken at different days during the protocol. Scale bar: 50μm.
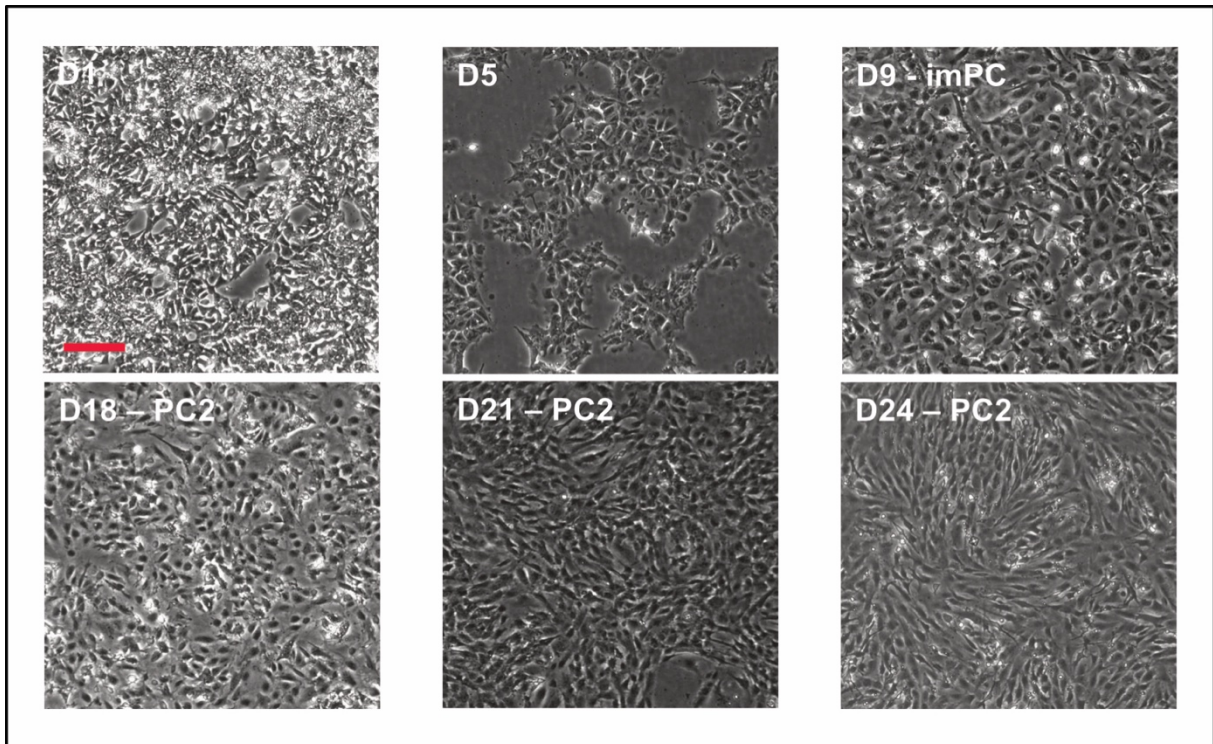
Figure 3.24: Cell morphology during the differentiation protocol of iPSCs towards pericytes type 2 (PC2) as described previously (Kumar et al., 2017). Cells were differentiated towards the mesodermal lineage as previously described and specialised towards pericyte type 2 for 24 days. Photographs were taken at different days during the protocol. Scale bar: 50μm.

ii. Cell sorting and phenotyping

As described earlier for EC differentiation, pericytes can be isolated from other cells in the population via magnetic activated cell sorting. Several surface markers have been reported in pericytes but markers such as PDGFR-β or CD146 are common markers shared with other blood vessel cell types (Hellstrom et al., 1999; Wang and Yan, 2013, p. 146) or mesenchymal progenitors (Xue-yi et al., 1998). One of the pericyte-specific markers used to differentiate them from other blood vessel cell types is NG2. This protein is only expressed by pericytes and other cells for the central nervous system (Ozerdem et al., 2001), making it a good candidate to purify pericyte populations obtained from stem cell differentiation.

Unfortunately, out of 3 attempts for both differentiation into PC1 and PC2, NG2-positive cells were found in culture after 21 days only for 1 differentiation each. Around 10% of cells were positive in the PC1 differentiation ($3.52.10^5$ out of $3.67.10^6$ cells) and 6% for the PC2 differentiation ($1.91.10^5$ out of $3.12.10^6$ cells). These cells were seeded on a collagen/fibronectin mix as described in the paper but did not proliferate further.

To assess the differentiation of the cells before the sorting and determine if these cells expressed pericytes markers, we evaluated the gene expression profile for few pericytes genes as seen in figure 3.25. The cells after 21 days of differentiation and several splits showed a

decrease in NANOG expression attesting of their loss of pluripotency. However, iPSC-derived pericytes (iPSC-PC) did not show any clear expression of pericytes markers such as PDGFR-β, desmin or NG2. Unfortunately, the placental pericytes used in the study showed little to no expression of these markers as shown by the higher expression of these genes by the pluripotent stem cells. The expression of generic mesenchymal markers PDGFR-α and NT5E in the primary pericytes could explain their low expression of pericytes markers due to a dedifferentiation in culture towards other mesenchymal lineages.

Nevertheless, few cells obtained after the successful sorting were immunostained for NG2, CD44 and actin cytoskeleton in comparison to primary pericytes, as shown in figure 3.26.

Pericytes obtained from iPSC did not show any NG2 expression, which was also quite low in primary pericytes. The same observation was true for the expression of CD44, an adhesion molecule expressed by vascular cell progenitors (Klein et al., 2011), with a very low expression in both types compared to primary pericytes. Furthermore, the morphology of the cells obtained after sorting was very different from primary pericyte morphology as demonstrated by actin staining. iPSC-PC were smaller and grew in clusters while primary pericytes adopt a large morphology and grow separately.
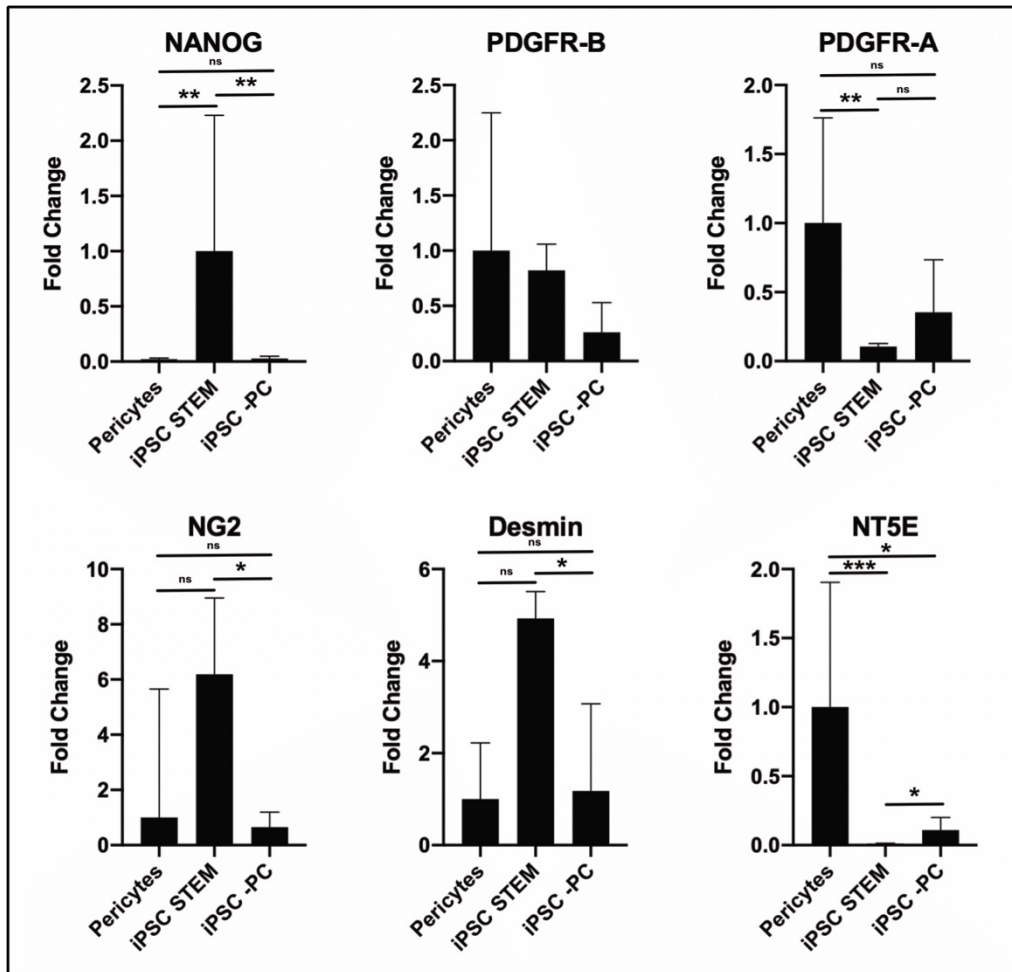
Figure 3.25: Gene expression analysis confirms the poor differentiation of iPSC derived pericytes. Gene expression profile for primary Pericytes, iPSCs and iPSC-PC after 21 days of differentiation for NANOG, PDGFR-β, PDGFR-α, NG2, Desmin and NT5E. n=3. ns: non-significant, *p<0.05, **p<0.01, ***p<0.001.

Overall, the differentiation of pericytes from iPSCs in preliminary experiments (n=3) attempting at implementing a previously published protocol did not yield a satisfactory population of pericytes. Further optimisation will be needed in order to obtain a scalable source of pericytes from stem cells for future purposes.
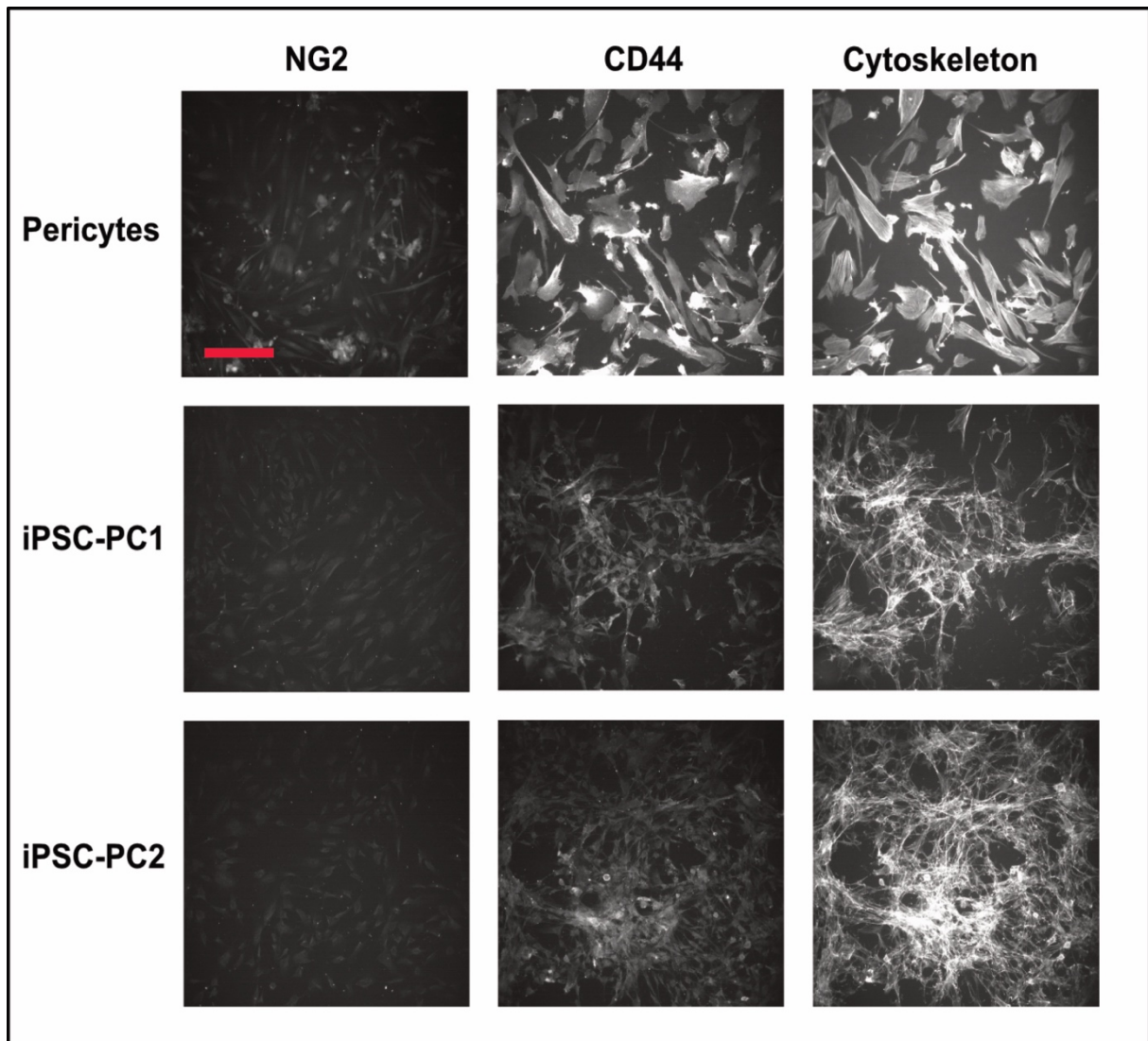
Figure 3.26: Immunostaining of pericytes, iPSC-PC1 and iPSC-PC2 after NG2 sorting for NG2, CD44 and actin cytoskeleton. Scale bar: 100μm.

b. Fibroblast differentiation

Fibroblasts also have a mesenchymal origin but are not classified as perivascular or mural cells. They are indispensable for the formation of organs and the connective tissues with the secretion of extracellular matrix proteins such as collagens. Their shared markers with other mesenchymal progenitors also makes their study difficult. Their close relationship with perivascular cells has led to several studies attributing fibroblasts phenotypes to vascular cells and the contrary (Göritz et al., 2011; Soderblom et al., 2013; Vanlandewijck et al., 2018). Recently, single-cell RNA sequencing of pericytes, SMCs and fibroblasts demonstrated specific markers of fibroblasts to discriminate them from mural cells and also uncovered fibroblast organ-specificity (Muhl et al., 2020).

With the aim of creating a complex model of blood vessel *in vitro* as described in the following chapter, we decided to adapt protocols to differentiate fibroblasts from PSCs. Similar to the protocol used for pericytes, we differentiated PSCs in 2D through directed differentiation as described previously (Fig. 3.27A)(Kim et al., 2018).
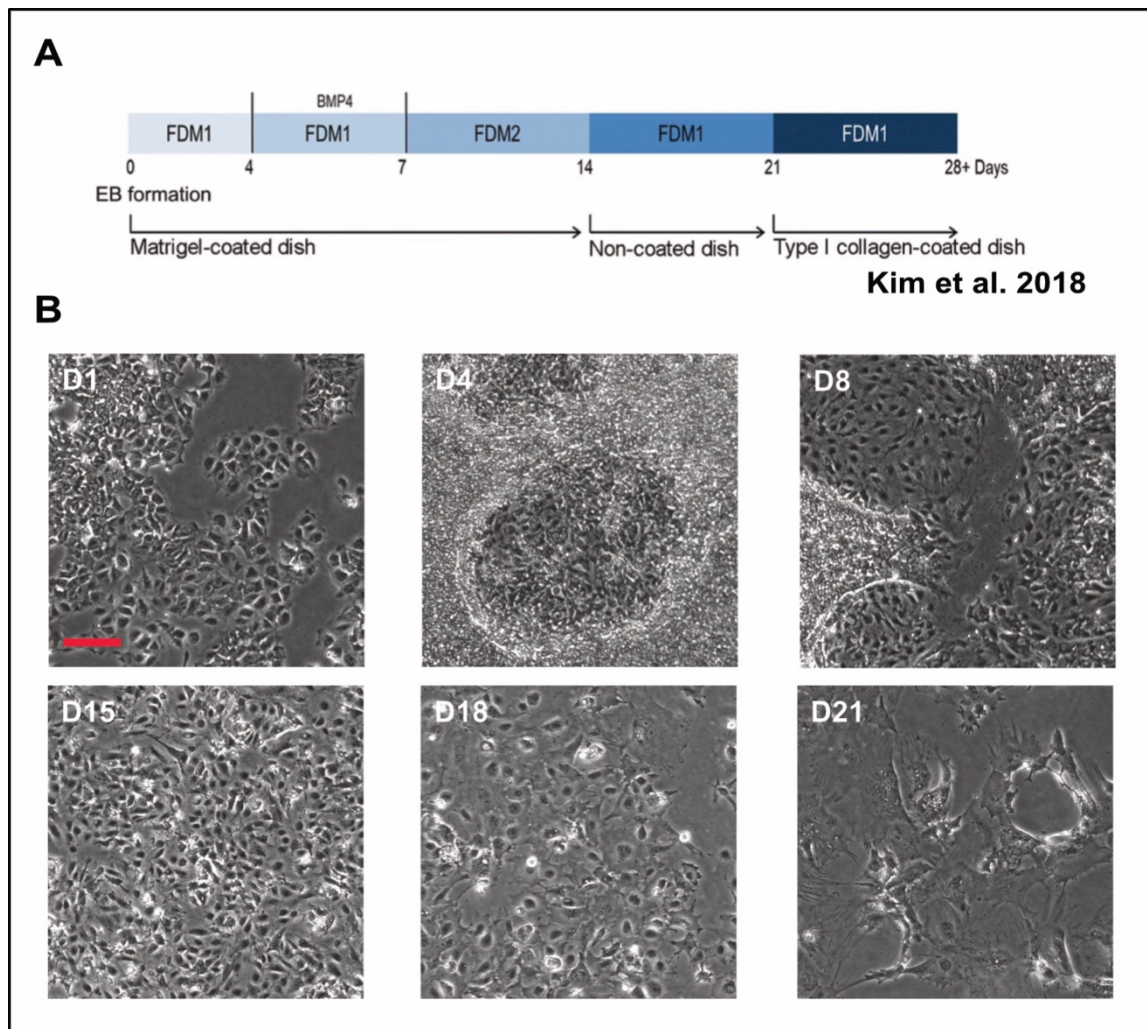
Figure 3.27: Stem cell differentiation towards fibroblasts. A) Schematics of the differentiation protocol as previously described (Kim et al., 2018). B) Photographs of the cells at different days during the differentiation for 21 days. Scale bar: 100μm.

Unfortunately, preliminary experiments using this protocol did not yield a satisfactory population of fibroblasts after 21 days of differentiation. As seen in figure 3.27B, the cells obtained also stopped proliferating after three to four passages and adopted a very large morphology. Like the pericyte differentiation, we decided to characterise the expression of some known fibroblasts markers to observe if some of the cells were differentiated before they stopped proliferating (Figure 3.28).

The differentiation of fibroblasts as described showed a significant decrease in NANOG expression for iPSC-derived fibroblasts after 21 days of culture, confirming the loss of pluripotency and a low percentage of stem cells left after few splits. The population of cells

obtained after the differentiation for 4 independent differentiations had a very high expression of fibroblasts specific markers such as ECM component fibronectin (Fibronectin 1 gene) or intermediate filament protein vimentin. Moreover, the expression of genes involved in synthesis of collagen I COL1A1 and COL1A2 as well as the gene for collagen type 3 alpha 1 chain COL3A1 was similar for both primary fibroblasts and iPSC-derived fibroblasts. Overall, the differentiation protocol adapted in this study (Kim et al., 2018) gave rise to a population of cells expressing high levels of fibroblasts markers but could not be expanded further than 3 to four passages as observed in the pericyte differentiation.
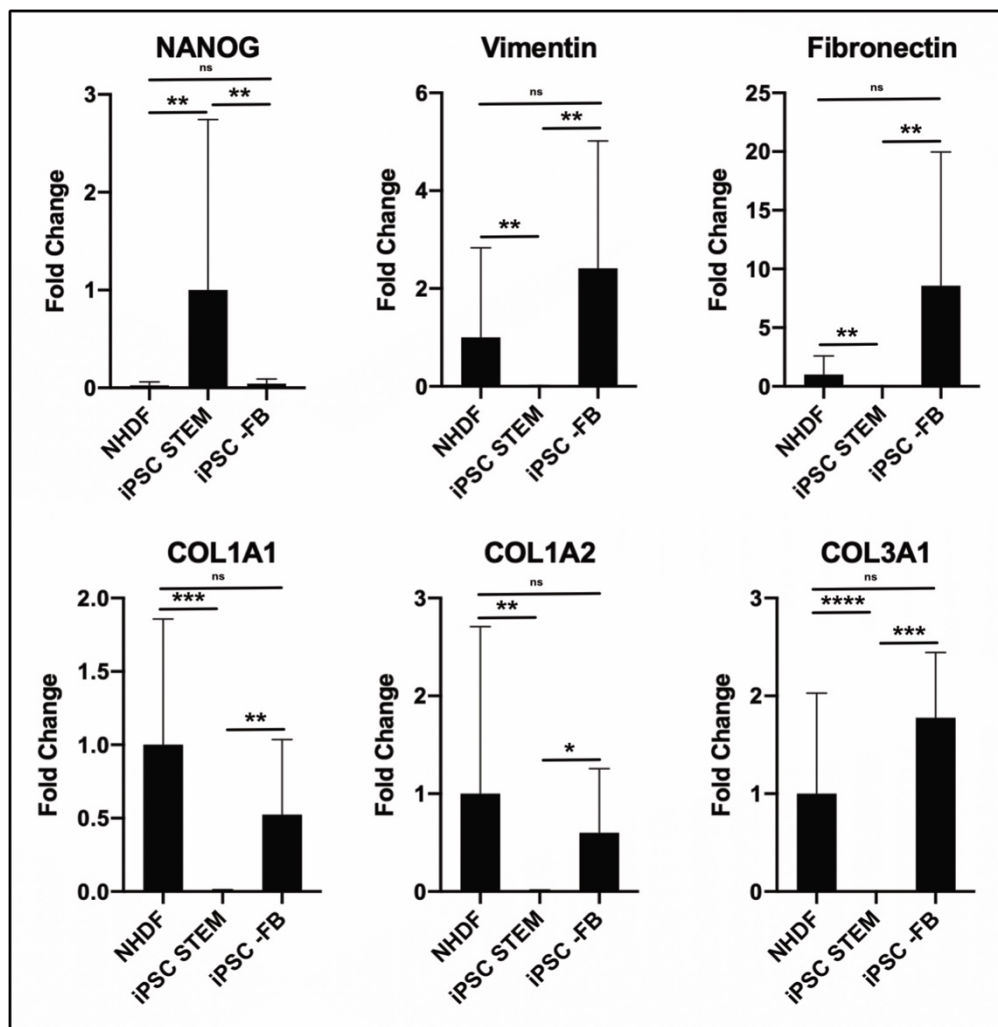
Figure 3.28: Gene expression analysis confirms the differentiation of iPSC-derived fibroblasts. Gene expression profile for normal human dermal fibroblasts (NHDF), iPSCs and iPSC-FB after 21 days of differentiation for NANOG, Vimentin, Fibronectin 1, COL1A1, COL1A2 and COL3A1. n=4. ns: non-significant, *p<0.05, **p<0.01, ***p<0.001, ****p<0.0001.

To conclude, the differentiation of perivascular and stromal cells from PSCs requires a precise optimisation of protocols to obtain mature and functional populations of cells. As variations occurs in between differentiations and technical biases can be introduced between labs, further effort will be needed to differentiate these cells and use them for tissue engineering strategies.

5- **Discussion**

Engineering vascularised tissues *in vitro* represents a major bottleneck in the field due to the complexity of the vasculature system, the organ-specific heterogeneity and the loss of phenotype in cultured primary cells *in vitro*. Creating models of blood vessels with mature phenotype and able to withstand mechanical stress experienced *in vivo* will be key to meet the need for vascular grafts, tissue engineering purposes, disease modelling and developmental studies (Song et al., 2018). Studies have demonstrated the use of primary vascular cells to create vascular grafts (Gui et al., 2014) and many *in vitro* models currently make use of such cells to study vascular biology (Chesnais et al., 2022a), organ development or regeneration (Marcu et al., 2018). However, these cells have a limited availability, do not recapitulate early vascular developmental processes and can lose their phenotypic integrity upon culturing.

The discovery of pluripotent stem cells and the induction of pluripotency from somatic human cells allowed a broad use of pluripotent stem cells in the last decade. This potentially unlimited source of (autologous) cells could allow the creation of *in vitro* blood vessels and vascular cells via the differentiation of these cells using developmental knowledge. The use of pluripotent stem cells has revealed useful for the derivation of endothelial cells (ECs)(Palpant et al., 2017; Prasain et al., 2014; Zhang et al., 2017) and perivascular cells such as pericytes, smooth muscle cells or other stromal cells (Biel et al., 2015; Faal et al., 2019; Kim et al., 2018; Kumar et al., 2017). This allowed the fabrication of tissue engineered vascular grafts (J. Luo et al., 2020; Sundaram et al., 2013), microvascular networks *in vitro* to model organ physiology (Campisi et al., 2018; Linville et al., 2019; Natividad-Diaz et al., 2019), or patient-specific models of disease (Kelleher et al., 2019; Vatine et al., 2019).

Creating vascular *in vitro* models necessitates the integration of different cell types. ECs represent the most inner layer of every blood vessel and have a central role in blood vessel physiology as they integrate signals from the blood and surrounding organs. Their broad heterogeneity within the body in terms of phenotype, function and development implies the integration of several signalling pathways in the differentiation of pluripotent stem cells to generate relevant ECs. Here, we decided to adapt a protocol using a xenogeneic-free direct differentiation to obtain ECs from different iPSC lines. The removal of animal-based products such as foetal bovine serum or Matrigel™ from iPSC differentiations reduces the variation in between independent differentiations due to the batch-to-batch differences in these products. The short-term differentiation protocol gave rise to population of ECs that could be further specified into venous or arterial phenotype following a purification step by CD31-sorting. Cells

obtained after 6 days expressed EC-specific markers such as KDR or VE-Cadherin and possessed an EC-specific morphology.

Unfortunately, the iPSC-derived EC obtained, although showing expression of VE-Cadherin and ERG at the protein level and an arterial specification, did not successfully recapitulate EC functions *in vitro*. The cells obtained poorly formed vascular networks when cultured on Matrigel™ and failed to sprout in a fibrin bead assay in fibrin hydrogels. This was accompanied by a rapid loss in proliferation observed after three passages in culture. Overall, the cells obtained with this 6-day protocol were not mature enough in comparison with primary ECs. This phenotype could be explained by the very fast differentiation with only 2 days of mesodermal differentiation and a low yield of CD31-positive cells at the term of the differentiation. As shown by the expression of arterial-specific marker EFNB2 in both population of venous and arterial ECs as well as the high expression of DLL4, these cells had a high Notch signalling activation. It is well known that Notch signalling plays a central role in EC development and arterial specification, but it is also closely linked to cell cycle arrest (Fang et al., 2017; W. Luo et al., 2021; Kathrina L. Marcelo et al., 2013). The culture of cells with a high concentration of VEGF (up to 50ng/mL for aECs) could be the origin of this activated Notch pathway and the decrease in proliferation. At the same time, VEGF-A is crucial for the differentiation and phenotype maintenance of these cells to not reverse their phenotype. Furthermore, the failure to replicate vascular function in functional assays also reflects a low level of maturation. The inability of iPSC-EC to adhere to beads coated in collagen and generate angiogenic sprout like primary ECs could imply their lack of expression of adhesion proteins as well as metalloproteases, indispensable for matrix remodelling. Further studies will be needed to characterise the role of high Notch signalling in iPSC-EC proliferation and explore other pathways and mechanisms involved in EC specification such as Wnt signalling, metabolism or the importance of hypoxic conditions in the generation of functional ECs.

With the aim of obtaining more mature ECs from PSCs, we used a genetically engineered PSC line with an inducible transcription factor central to EC development, ETV2. ETV2/ER71 is a pioneer factor involved in hematoendothelial specification and acts upstream of BMP and Notch signalling in the mesoderm to induce the formation of KDR-positive mesoderm (Koyano-Nakagawa and Garry, 2017, p. 2; Lee et al., 2008; Rasmussen et al., 2011). The overexpression of ETV2 via a doxycycline-inducible cassette in a PSC line allowed the rapid differentiation of EC progenitors as described previously (De Smedt et al., 2021). The protocol yielded a very high number of CD31-positive cells (around 60%) compared to the directed

differentiation (around 12%). After optimisation of the conditions to culture these cells, we obtained a very pure population of ECs expressing mature EC-specific markers.

Unfortunately, as observed with the iPSC-derived vECs and aECs, the ETV2-ECs also started to detach and rapidly stopped proliferating after few passages. Their high Notch signalling in comparison to primary ECs is reminiscent of the high Notch activation in iPSC-ECs. In a similar manner, although Notch signalling is crucial for EC differentiation, it might induce a cell cycle arrest in the population of PSC-derived ECs. However, the culture of these ETV2-EC in the same medium used to culture primary ECs, with very low VEGF-A concentration did not rescue this phenotype and induced a decreased proliferation of cell death. Interestingly, as observed after few days in culture and with a decrease in proliferation, cells acquired a migratory and elongated phenotype. This phenomenon was also present in culture with low concentration of VEGF-A and could indicate the need for early EC progenitors to form vascular networks and not be kept in 2D culture. Overall, this phenotype indicates that the cells obtained from PSCs lack a degree of maturation that allows primary ECs to proliferate for further passages when cultured *in vitro*.

However, it also raises a question on the origin of this proliferation rate for primary ECs and their ability to replenish EC population after injuries. The existence of an "endothelial stem cell" population has been defended by the finding of resident CD157-positive cells in big vessels *in vivo* (Wakabayashi et al., 2018). These cells have been able to generate blood vessels after injury and replenish EC populations. Future studies will have to investigate the expression of such markers in early EC development and study the role and degree of EC proliferation in the early phases of vascular development. As mentioned earlier, we can hypothesize the idea that early angioblasts and vascular progenitors in the embryo need specific conditions to proliferate and invade the different organs, conditions that are not recapitulated in normoxic conditions *in vitro*. Furthermore, the culture of isolated ECs cannot recapitulate the very close interaction of ECs with stromal cells and perivascular cells, indispensable for blood vessel formation and maturation.

To solve this issue, we also decided to adapt protocols to differentiate perivascular cells from stem cells. Pericytes plays a major role in vessel function, maturation and stabilisation and are the main source of perivascular cells in microvascular networks. To obtain pericytes (PCs) from stem cells, we first started by culturing cells obtained from CD31-negative population of iPSC derived towards ECs, but these cells did not show a satisfactory proliferation rate to be used for experiments. We then decided to reproduce a published protocol used to directly differentiate pericytes (Kumar et al., 2017). In the body, PCs origin varies depending on the

blood vessel of interest, but we implemented a protocol using a mesodermal intermediate to obtain pericytes with either a contractile phenotype (arteriolar PCs) or an anti-inflammatory phenotype (capillary PCs). The 21-day protocol used common growth factors known to play a role in PC differentiation such as FGF2 or PDGF-BB and gave rise to cells with a mesenchymal phenotype like the one observed in cultured primary pericytes. However, the analysis of their gene expression for few experiments revealed a very poor maturation of these cells. This was also comforted by the low yield of NG2-positive cells at the end of the differentiation and their low expression of pericyte markers at the protein level. Overall, the differentiation of PCs from PSCs was unsuccessful after implementation of this protocol, but this was relatively preliminary results with only few experiments done to reproduce this differentiation. Further repeats will be needed to conclude on the efficacy of this directed differentiation and obtain a robust population of mature pericytes from stem cells.

Finally, we also implemented a directed differentiation to obtain fibroblasts from stem cells. Fibroblasts have a major role in the formation of connective tissues, secretion of extracellular matrix (ECM) and in the maintenance of organ structure. We decided to differentiate fibroblasts to use in later experiments as they are a valuable source of ECM, needed for later tissue engineering experiments in this project. As for ECs and some perivascular cells, fibroblasts arise from the mesoderm and we decided to implement our mesoderm differentiation to start a directed differentiation in 2D and then implement a previously published protocol (Kim et al., 2018). Preliminary experiments reproducing this protocol showed very promising results with the generation of cells with a fibroblasts morphology and the expression of ECM genes and fibroblasts-specific markers. The use of these cells in functional assays and the optimisation of the protocol with a step of purification could yield to a mature population of fibroblasts as a valuable source of ECM-producing cells for future use in creation of tissue engineered constructs *in vitro*.

Overall, this chapter focused on the creation of vascular cells from stem cells. We report the differentiation of ECs, pericytes and fibroblasts from stem cells and compare their ability to fully recapitulate crucial functions in vascular development. Although further work is needed to obtain fully mature cells from stem cells, this work creates a base to explore mechanisms involved in blood vessel development, formation and maturation and validates the potential use of pluripotent stem cells to reproduce blood vessel heterogeneity and function.

Chapter 4: A new 3D printing-based workflow for rational manufacturing of custom Lab-on-chip (LOC) to study EC heterogeneity in 3D and flow-dependant maturation.

1- Introduction

Creating functional human tissues *in vitro* is a current major challenge in both regenerative medicine and basic cell and developmental biology. In the regenerative field the hope is to create stem cell- derived organ's functional units as an unlimited source of tissues for transplantation. In the cell and developmental fields, bottom-up creation of tissues is an appealing way to investigate the molecular details of cell differentiation and organogenesis and to reduce/replace animal experimentation. Creating functional tissues *in vitro* requires recapitulating the tissue microenvironment including specific vascular supply which is a currently unmet challenge. Addressing such challenge requires resolving a host of cell biology and engineering problems.

Blood vessels form a spread-out network *in vivo*, supplying organs with nutrients and oxygen, removing waste and enabling a permanent immune surveillance (Potente et al., 2011). Most cells in animal tissues reside within 100 μm from a blood capillary, and angiogenic/angiocrine signalling is key to proper development and homeostasis of an organ's functional units (Rafii et al., 2016). The cardiovascular system (CVS) is formed by the heart and a hierarchical network of blood vessels from large arteries and veins to tiny capillaries. Engineering such complex system *in vitro* requires taking into account both the differences in cell composition and the biophysical microenvironment experienced by different vessels in the body (Song et al., 2018).

Among all the key factors towards blood vessel maturation and function, flow-generated mechanical forces are essential (Fang et al., 2019; Obi et al., 2009). Applying appropriate mechanical forces *in vitro* requires precisely controlling and regulating the flow of medium or blood substitute entering engineered vessels.

Microphysiological systems have been recently developed to generate and perfuse primitive vascular networks resembling that observable during initial phases of wound healing (M. B. Chen et al., 2017; Hasan et al., 2014; Shin et al., 2012; van Dijk et al., 2020). These systems leverage spontaneous or guided endothelial cells (EC) self-assembly within 3D matrices like fibrin or collagen. One advantage of these systems is that perfusable vascular-like tubes or even

networks can be easily created in 2-3 days, however these networks are not reminiscent of mature, fully functional capillaries because hydrogels cannot support vessel maturation and remodelling in absence of matrix producing cells. Furthermore, continuous perfusion (> 24h) has not been extensively demonstrated due to limitations in creating secure connections between the vasculature and the flow generator (e.g., peristaltic or syringe pumps). In fact, perfusion has been mostly demonstrated using gravity-driven flow which is scarcely controllable and not maintainable for periods longer than a few hours. Finally, current systems manufactured by SU- 8 photolithography (M. B. Chen et al., 2017; Hasan et al., 2014; Song et al., 2018; Wang et al., 2016; Zheng et al., 2012) are relatively fixed in design and expensive to manufacture thus, they are not amenable to fast-prototyping of multicomponent systems which are key for future development of multiple connected organs on chip (Ronaldson-Bouchard et al., 2022).

In this chapter, we start by implementing existing protocols to create LOC devices and assess their use for the creation of complex vasculature-on-chip models. Then, with the aim of developing more advanced manufacturing workflows, we adapt 3D printing techniques and soft lithography to create inexpensive and custom microfluidic devices. This protocol is optimised and adapted to create a model of vasculature-on-chip via several design modifications and computational flow dynamics simulation (CFD). Furthermore, we develop a fully 3D-printed cell culture platform and adapt it to include a microfluidic system with the aim of introducing continuous perfusion in the vasculature-on-chip. This system is then validated with the perfusion of self-assembled vessels in hydrogel for several days. To create more complex vascularised systems, we adapt a matrix-free co-culture protocol and validate it with different organ-specific ECs and a model of iPSC-derived pancreatic islets. Finally, we combine our unique LOC device and organotypic matrix-free system to culture and continuously perfuse an advanced model of vasculature *in vitro* and assess the effect of long-term perfusion on the blood vessel maturation.

Overall, we present for the first time a scalable and customisable microphysiological system to grow biomimetic, vascularised and perfusable microtissues as a key initial step to enable growing mature and functional tissues *in vitro*.

2- <u>**Materials and methods**</u>

Microfluidic chip fabrication with SU-8 wafers

The first microfluidic device used has been made using a previously published protocol (M. B. Chen et al., 2017). A photomask with microfeatures is used to fabricate a mould with the epoxy resin SU-8. The mould is treated with Trichloro(1H,1H,2H,2H-perfluorooctyl) silane (Thermo) for 1h. PDMS (Sylgard^{TM} 184 Silicone Elastomer Kit**)** at 1:10 ratio is poured on the mould and baked for 1h at 60°C. The PDMS chip is peeled off the mould, inlet and outlet ports are punched using biopsy punches and the chip is bonded to a glass slide after plasma treatment (3min at 100% intensity). The fibrin gel is formed by mixing 8μL of a 6mg/mL solution of fibrinogen containing 12.10^6 HUVEC/mL and 8μL of a thrombin solution in EGM2 medium. 10μL of the mixture is inserted in the central channel and left 15 min at 37 °C, for the clot formation before the reservoirs are filled with medium. The chip is cultured in a humidity chamber for a week with medium changed every 2 days.

Computer assisted design (CAD)

The LOC device moulds, the plate containing the LOC device, and the cassette for the microfluidic pump were designed using AutoDesk Fusion 360 (Autodesk, California, USA). Once created, the 3D objects were exported in STL format (a format to represent 3D geometrical objects to allow the software to slice it) and sent to print on the different 3D printers or used for Computational Flow Dynamics (CFD) experiments.

Computational flow dynamics simulations

All CFD simulations were performed using SimScale (SimScale GmbH, Germany). For all simulations we employed the incompressible flow formalism including the k-omega SST turbulence model**,** which allows estimating the dynamics of medium flow through our chips. The parameters used where seawater 3.5 pc saline for the material of choice, 100 or 1000 μl/min for the velocity inlet and outlet values and mm for the model units. At the scales (channels sections 100-250x100-250 μm) and flow rates (FR) considered flow of medium containing 10% serum is in principle laminar throughout the chip (Reynolds number $<10^2$ estimated by considering linear square section pipes with side length = 100- 250 μm and 100 or 1000 μl/min fixed flow rate). CFD results were visualised using the Simscale data post-processing tool including cut-plane, particle trace analyses and corresponding statistics. We repeated all

simulations at least three times and all our simulation converged to stable flow after 500s (all simulations were run for 1000s with 1s steps).

Mould printing via stereolithography and post-processing

The moulds were printed using UV-curable resin with a DLP (Digital Light Processing) 3D printer (MiiCraft ultra series 125) using transparent resin BV-007. After printing the mould is detached from the platform and washed extensively to remove remaining resin. Briefly, it is rinsed in isopropanol then sonicated twice in isopropanol for 5 minutes. The mould is then sonicated 5 minutes in acetone before being dried and post-cured in a UV chamber for 1h at 60°C. This process is repeated twice, followed by vapour phase deposition of Trichloro (1H, 1H, 2H, 2H-perfluroctyl) silane 97% in a desiccator for 60 minutes.

PDMS preparation, tube embedding and casting

The LOC devices are manufactured by soft lithography on 3D printed moulds using silicon elastomer (Sylgard 184, Corning) and fixed on glass slides including silicon tubing (1.5mm ID, sourcing map) for world-to-LOC connections. For the creation of the LOC device, polydimethylsiloxane (PDMS, Sylgard™ 184 Silicone Elastomer) cast is prepared at a 1:10 base/curing agent ratio. The mixture is poured on the mould after placing the silicone tubing on the pillars to embed the tubing in the LOC device. Bubbles are removed from the silicone by a vacuum system before the mould is put to cure in the oven at 60°C for minimum 3h.

LoC assembly and sterilisation

Once the silicone is cured, the PDMS can be peeled off the mould using the walls and cut using cutting guides to create individual LOC devices. LOCs are bonded to a glass slide upon activation of the PDMS and glass surface via plasma treatment with a corona discharge device (piezobrush® PZ2, Relyon plasma, Germany). To create a medium reservoir, rectangular walls of ABS (Acrylonitrile butadiene styrene) are printed with a FDM 3D printer (Cubicon Single Plus, Cubicon, Republic of Korea) and glued on top of the PDMS with liquid PDMS for 1h in the oven. After ensuring that the LOC is properly assembled and sealed, the chip is autoclaved for sterilisation.

3D printed cassette with fused deposition modelling

The LOC device cassette is printed in ABS (Cubicon Single Plus, Cubicon, Republic of Korea). It is designed to keep the LOC device sterile therefore has standard cell culture plate dimension, can fit a cell culture plate lid for imaging, has a transparent bottom for imaging and wells to create a humidity chamber with slots to host the microfluidic tubing.

Microfluidic pump assembly and system sterilisation

After the LOC is assembled and sterile, it can be used to culture cells in a normal cell culture petri dish or the 3DP cassette and linked to the microfluidic system. For the culture of ECs, the chip is coated with bovine fibronectin solution (1mg/mL, Promocell) for at least 3h before cell seeding.

The microfluidic system used was the mpSmart-Lowdosing (Bartels mikrotechnik, Germany) including a microfluidic peristaltic pump (0.005-1mL/min), a filter (average 0.45μm pore size) and a flow sensor (Sensirion SLF3s-0600F) linked to a laptop via a controller driver for controllable FR. Before LOC perfusion, the system including tubing is sterilised by perfusing 1% sodium hypochlorite for 10min then rinsed thoroughly with distilled water.

Cell culture

Human Umbilical Vein Endothelial Cells (HUVEC, PromoCell), Human Aortic Endothelial Cells (HAoEC, Promocell), Human Pulmonary Microvascular Endothelial Cells (HPMEC, Promocell), Human Cardiac Microvascular Endothelial Cells (HCMEC, Promocell), Human Dermal Microvascular Endothelial Cells (HDMEC, Promocell), iPSC-ECFC (Axol) and Red Fluorescent Protein-tagged HUVEC (RFP-HUVEC, 2Bscientific, UK) were cultured on fibronectin- coated (PromoCell) plates up to passage 7 and maintained in Endothelial Growth Medium 2 (EGM2; Promocell). Normal Human Dermal Fibroblasts (NHDF, Promocell) were cultured in Fibroblast Growth Medium (Microvascular, MV) 2 (Promocell) up to passage 7. Human Mesenchymal Stem Cells (MSC, PromoCell) were cultured in Mesenchymal Growth medium 2 (PromoCell) up to passage 7. Cells were routinely passaged using Accutase[TM] (Thermo). The cell line THP-1 (ATCC, UK) was cultured in suspension in DMEM (Gibco) supplemented with 10% FBS (Thermo).

Fibrin gel vasculogenesis assay

The fibrin gel was formed by mixing an 8mg/mL solution of fibrinogen (Sigma) containing 15.10^6 EC/mL and a 4U/mL thrombin solution (Sigma) and 10μM Aprotinin (Thermo) in EGM2 medium (Promocell). 20μL of the mixture was pipetted in the central well of the LOC device and left 30 min at 37°C for hydrogel setting, before the reservoir and channels were filled with medium. The chip was cultured in a petri dish in presence of distilled water to create a humidity chamber and prevent medium evaporation before connection to the microfluidic system in the 3D-printed cassette.

Bead Fibrin gel assay

The bead fibrin gel assay (or Cytodex assay) was performed following a protocol previously published (Nakatsu et al., 2007). The day before the assay, cells are detached and mixed with Cytodex beads (Amersham) at a ratio of 400 cells per bead and incubated overnight for coating. The next day, beads are washed and resuspended in a 2mg/mL fibrinogen solution. The bead/fibrinogen solution is mixed with a 0.625 unit/mL thrombin solution and incubated 15min at 37°C to form the clot before the medium is added on top.

OVAA in static conditions

The method used is an optimised version of previously published one (Hetheridge et al., 2011). Briefly, $7.5 \times 10^3 / cm^2$ Red Fluorescent Protein-tagged HUVEC (RFP-HUVEC, 2Bscientific, UK) are mixed and seeded with $1.5 \times 10^5 / cm^2$ Normal Human Dermal Fibroblasts (NHDF, Promocell) and left in culture for 14 days to allow EC vasculogenesis with medium change (supplemented or not with 50ng/mL VEGFA, Peprotech, UK) every two days. Cultures are monitored daily to assess generation of microvascular structures which start to form around day 5 and can be maintained in culture for more than 30 days under static conditions. After 14 days of culture, cells are fixed and immunostained for CD31 (ab9498, 1μg/mL, Abcam) and revealed with fluorescently labelled secondary antibody goat anti-mouse (A- 21127, 1μg/mL, ThermoFisher). Images were obtained using an Operetta CLS system (PerkinElmer, Waltham, MA) equipped with a 10X objective for full well scans and 40X and 63X immersion objective for high resolution images. Images were quantified using the ImageJ AngioAnalyser plugin (Carpentier et al., 2020).

iPSC-derived pancreatic organoids culture and co-culture with endothelial cells

iPSC-derived pancreatic organoids were cultured and differentiated in the lab of Dr. Rocio Sancho as described previously (Cujba et al., 2022; Pedraza-Arevalo et al., 2022). Differentiated organoids were cultured in Matrigel™ and transferred in the co-culture system after formation of capillaries (after 14 days of culture in static conditions). After seeding, cells were co-cultured in EGMV2 (Promocell) and expansion medium (Advanced DMEM/F-12 with 1× hepes, 1× glutamax, 1× penicillin-streptomycin, 1× B-27, 0.5 nM A83-01, 50 ng/mL EGF, 100 ng/mL FGF10, 10 nM GastrinI, 1× Noggin, 1× R-Spondin, 1.25 mM N-Acetylcysteine and 10 mM Nicotinamide) at a 1:1 ratio. For differentiation, cells were cultured in EGMV2 (Promocell) and differentiation medium (Day 1 and 2: DMEM 25 mM Glucose with 0.5× B-27, 50 ng/mL EGF, 1 µM retinoic acid. Day 3 and 4: DMEM 25 mM Glucose with 0.5× B-27, 50 ng/mL EGF, 50 ng/mL FGF7. Day 5 and 6: DMEM 25 mM Glucose with 1× B27, 500 nM LDN-193189, 30 nM TBP, 1 µM ALKi II, 25 ng/mL FGF7. From day 7: DMEM 2.8 mM Glucose, 1× Glutamax, 1× non-essential amino acids.) at a 1:1 ratio for 21 days. The viability of cells was assessed using the LIVE/DEAD™ Viability/Cytotoxicity Kit (ThermoFisher).

Vasculature-on-chip (VOC) culture and continuous perfusion

The VOC is first cultured in static conditions in a 75cm^2 petri dish (Greiner bio-one) before perfusion in the 3D-printed cassette. HUVEC-RFP are first cultured in monolayers in the LOC device in the channels after fibronectin coating (PromoCell) for 3 to 5 days. Then, a co-culture of 7.5×10^3 Red Fluorescent Protein-tagged HUVEC (RFP-HUVEC, 2Bscientific, UK) and 1×10^5 Normal Human Dermal Fibroblasts (NHDF, Promocell) or Human Mesenchymal Stem cells (MSC, PromoCell) are seeded in the central well of the device. Cells are kept in static culture for 7 days and maintained in EGMV2 (PromoCell) changed every other day from the top of the device. After monitoring of vascular network formation, the device is transferred in the 3D-printed cassette and linked to the microfluidic pump device to be perfused continuously. Images from the vascular network and videos of the perfusion were obtained with a wide field inverted microscope (Olympus IX51, Biosystems, Munich, Germany). Confocal images were obtained with a Leica Sp8 confocal inverted microscope, from the RFP signal of the HUVEC-RFP or, after fixation, from the EC-specific VE-cadherin signal (Novusbio NB600-1409, 1µg/mL) counter-stained with a secondary Alexa Fluor 488 (A-21141, 1µg/mL, Thermo Fisher Scientific).

3- <u>Implementation of existing Lab-on-chip protocols</u>

Creating relevant vascular models *in vitro* is key to study vascular development, tissue engineering or the role of the vasculature in disease progression such as metastatic invasion. To model such processes, static cultures in two or three dimensions have been used for decades, but often lack a major component of a functional vasculature, the blood flow. The recent advances in microfabrication techniques and soft lithography have allowed the use and development of microfluidic devices in standard lab conditions. Among the most commonly used model to study blood vessel formation and development in 3D is the device created in the group of Prof. Kamm as described in the following section (Figure 4.1)(M. B. Chen et al., 2017; Shin et al., 2012).

As seen in figure 4.1A, the protocol uses traditional wafers created using SU-8 resin to obtain micro-features that will serve as negative to create the LOC device. It is created using PDMS that is poured and cured on top of the micro-features, before being peeled from the wafer, punched to create the inlets and outlets and bound to a glass slide. Once sterile, the device can be used to culture cells in the channels as the PDMS is transparent and inert.

To recreate a model of vasculature, Chen et al. (2017) used a exogenous fibrin hydrogel to embed HUVECs and fibroblasts and seed them in different parts of the design. The central channel contains the HUVECs in the fibrin hydrogel surrounded by 2 medium channels, and this design can also be supplemented with fibroblasts in two other side channels. Once polymerised and filled with culture medium, the device is cultured in a humidity chamber.

With the aim of recreating an *in vitro* model of blood vessel, we first decided to implement the exact same protocol and try to recreate the same blood vessel-like structures observed in the original manuscript. We obtained the design and manufactured the wafer with micro-features as described and used soft lithography to fabricate individual LOC devices. The fabrication of the wafer, although necessitating trained personal and expensive equipment, was very well documented and the devices were created in few days.
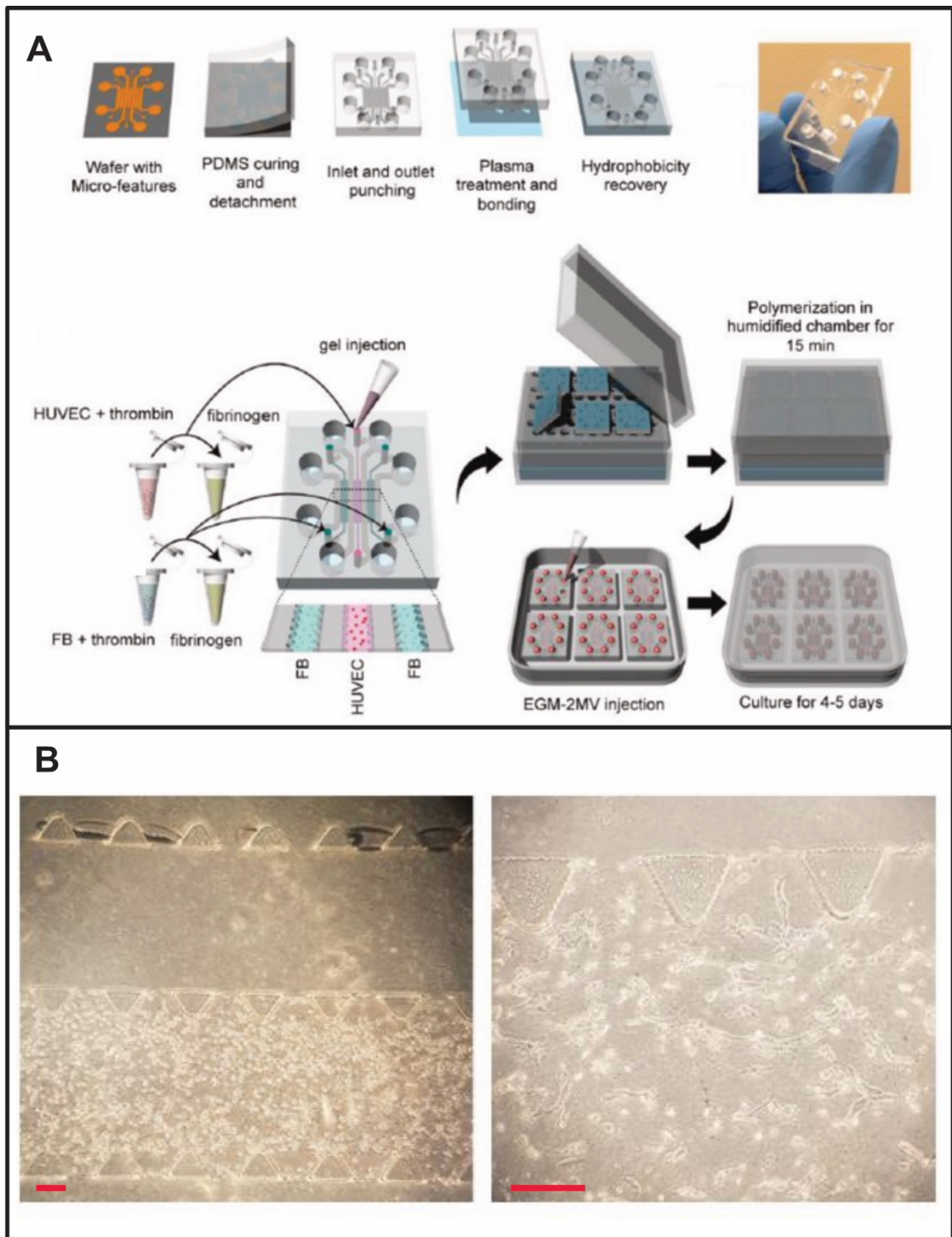
Figure 4.1: Implementation of soft lithography technique to create Lab-on-chip devices as described previously (M. B. Chen et al., 2017). A) Schematics of the soft lithography method to create PDMS Lab-on-chip device, followed by cell seeding and gel injection. B) Photographs of HUVEC seeded in a fibrin hydrogel in the Lab-on-chip device just after seeding and after 48h of culture. Scale bar: 50μm.

However, as seen in figure 4.1B, the implementation of cell culture in the device was not so successful. The creation of high-resolution features in the design was very interesting to create miniaturised models but also added a level of technical difficulties. First, the volumes used in

the device were very small, and the channels to culture the hydrogels were very narrow, building up pressure in the system. This coupled with the small openings between the hydrogel and medium channels often resulted in leakage of the fibrin gel in the medium channel and thus the obstruction of the chip. Furthermore, the small dimensions of the channels meant that any space for air bubbles or cell clumps caused clogging. Overall, the Lab-on-chip dimensions added a lot of complexity to reproduce microvasculature systems with consistency. Finally, the design presented did not contain any access to implement a pumping system any change in this design mean the creation of another expensive wafer (~£100 per wafer).

The use of PDMS devices created with soft lithography on wafers has been very useful for the creation of microvasculature in exogenous hydrogels as described in many studies (Campisi et al., 2018; M. B. Chen et al., 2017, p. 8; Hasan et al., 2014, p. 8; Shin et al., 2012; Wang et al., 2016). However, the implementation of this technique in a small laboratory with standard equipment is very expensive and results in devices that are fixed in design and technically challenging to work with. Finding new ways to create Lab-on-chip devices is key to a broader use of microfluidic systems in cell biology labs.

4- <u>3D printing allows inexpensive fabrication of multi-layered LOC devices</u>

3D printing has been used extensively for different applications in the manufacturing and constructions sectors but has also lately been developed for biomedical applications such as personalised biomedical implants (Liaw and Guvendiren, 2017). The rapid technical development of 3D printers also considerably reduced their cost in the last few years, with benchtop printers available for few hundreds of dollars. The low cost and efficiency of 3D printing to create objects at higher resolution allowed their use to fabricate microfluidic systems specifically designed for applications in cell biology (Amin et al., 2016; Au et al., 2016).

a. LOC design with computer assisted design (CAD) and 3D printing

To create an easier Lab-on-chip device to use and allow the creation of a more reproducible chip, we designed and created a simple custom microfluidic device (Fig. 4.2A). The design has bigger features than the one created previously with SU-8 silicon wafers, but the resolution of stereolithography (SLA) 3D printers (~100μm) stays satisfactory to create models of small calibre blood vessels. The creation of this custom design with computer assisted design (CAD), inspired by the previously available LOC devices allows a rapid modification and fabrication

of the moulds (Fig. 4.2B) that replace the wafers. Finally, the biggest advantage of this technique is the lowest cost of fabrication with each mould costing less than \$1.
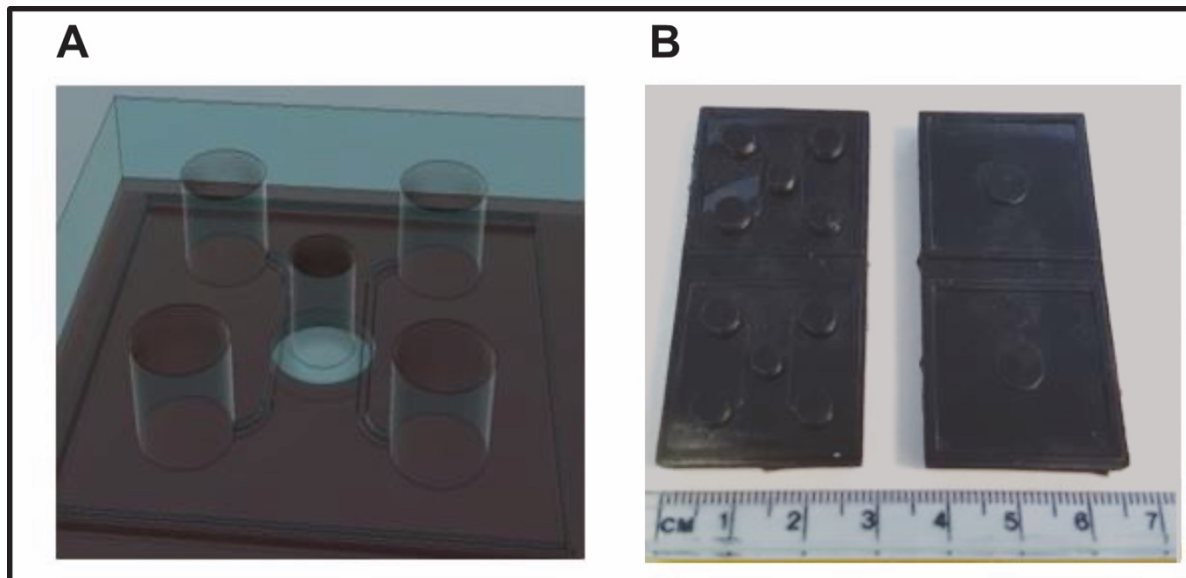
Figure 4.2: Computer assisted design and 3D printing as an alternative to traditional LOC fabrication. A) Picture of the design of a LOC device used in this study. B) 3D printed moulds using black resin. The right mould corresponds to the bottom layer of the LOC and the left one to the top layer of the chip.

The first device described here is composed of 2 different layers of PDMS. The bottom layer is created on a mould with a circular cutting aid (Fig. 4.2B right mould) and the top layer peeled from the mould with the design (Fig. 4.2B left mould). Apart from the creation of the moulds, the PDMS chip creation is the same as described earlier, with a coating of the 3D-printed moulds with Trichloro(1H,1H,2H,2H-perfluorooctyl) silane to prevent the PDMS to stick and a punching of the wells after peeling.

The original idea is to create two parallel channels coupled with reservoir that can be independently filled with medium as observed in the design presented earlier. These channels can be coated with ECs as a model of "big vessels" where ECs can cover the PDMS channels and experience flow. The second part is the central well, that will receive the hydrogel. The bottom layer created with the first mould is punched and will be filled with the hydrogel, at the lowest level. At the higher level, channels are filled with ECs and medium and another reservoir is punched on top of the circular hydrogel chamber to feed it from the top. The resulting assembled chip is presented in figure 4.3.
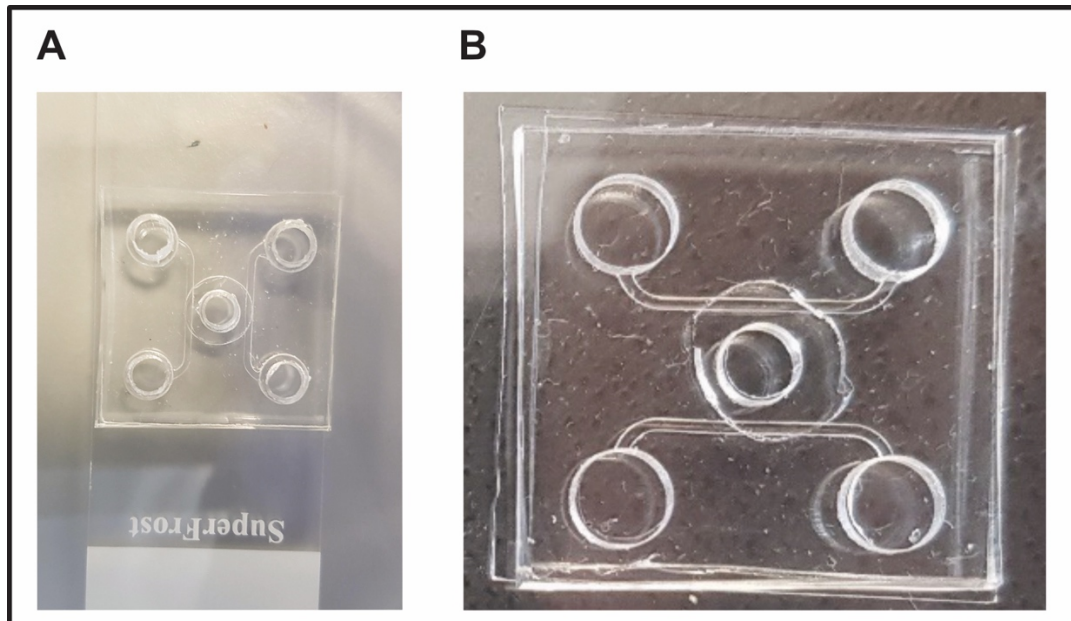
Figure 4.3 Assembled LOC device. A) Top view of the assembled device after binding the two layers of PDMS together and to a glass slide. B) Close view of the device with the bottom circular well for hydrogel and the top reservoirs and channels.

This design with bigger features described here allowed us to have more control on the following cell culture steps while keeping an easy fabrication, a transparent PDMS LOC device and the ability to easily modify the design. Overall, the implementation of 3D printing for the creation of microfluidic devices although resulting in lower resolution features, improved the scalability, ease of modification, and lowered the cost of fabrication.

b. Mould printing and optimisation

Several printers have been developed for different applications, from fused deposition modelling (FDM) printers melting polymers to SLA printers printing photopolymerised resin. During this project, we tested different printers and different materials to print our moulds. To decide on the appropriate material and printer, several variables must be considered.

First, the choice of 3D printer depends on the application. Here, the creation of moulds for microfluidic devices meant that we need a printer that had a good resolution of printing (<100µm) to create small features. This meant that FDM printers printing filaments could not be used, although they are the cheapest available, and the same for inkjet printers. Other printers using laser sintering or laminated manufacturing are less used and not available for broader use. Thus, we decided to use SLA 3D printers to create our moulds. The use of photopolymerised resin results in the creation of smooth surfaces, crucial for microfluidic moulds, and commercially available printers can print features down to ~25µm.

i. Resin compositions

Once the 3D printing process is decided, several resins can be used with different properties. Resin composition often differ from manufacturers and most printers can only be used with resins developed by the printer's manufacturer. The composition of these resins is also very heterogeneous between manufacturers, but the chemistry is often the same, a mix of photosensitive monomers and oligomers such as methacrylate. Unfortunately, the exact composition of SLA printer resins often remains unknown, with only a description of colour or toughness.

In this project, we have started by using the FormLabs2 printer with different resins available on the manufacturer's website, black resin or clear resin. Although, the Formlabs has a very high resolution down to 25μm in XY, both resins used resulted in the fabrication of moulds with an uneven surface. Furthermore, the surface was rough, leading to a PDMS layer that was not perfectly transparent after peeling off the mould.

We then decided to use the Miicraft series 125, with a lower resolution (down to 67μm in XY) but supplied with a microfluidic-specific clear resin. We tested this resin (Miicraft BV-007) and another supplied resin used for denture printing (Pro3dure generative GR-13) and listed their advantages in table 4.1.
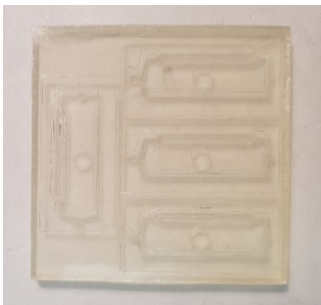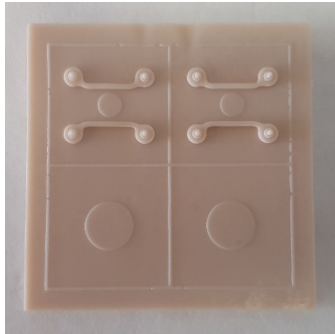
Printing resin	Visual observation of template	Advantages of use	Disadvantages of use
Miicraft BV-007 clear resin		-Smooth surface. -Template processing was quicker as the resin was less viscous.	-Supply difficulties. - Expensive.
Pro3dure generative GR-13 dental resin		- Easily supplied. -Cheaper	-Rougher surface. -High viscosity resulted in longer processing.

Table 4.1: Resins used with the Miicraft 125 series and their advantages.

As described, the BV-007 showed the best results and was used in the rest of the study.

ii. Printing settings

The success of the print also depends on the printer to reproduce exactly the design realised by CAD. Although it is defined by the manufacturer at the beginning, the lowest resolution of the print can be affected by many variables such as debris in the resin, scratches or dust in the resin tank or technical problems. These can lead to print defects in the design or in the structural integrity of the print. As shown in figure 4.4, defining adequate settings is important for each print and depending on the resin used.

In our specific application and for the example of the dental resin, a rapid fabrication allowing only 4 seconds of curating time (UV photopolymerization time) between layers (Fast) or 5 seconds (Normal) resulted in a defect in the layer attachment and a collapse of the structure. Slower process with longer curating time (6 seconds) was necessary for the proper fabrication of the mould.
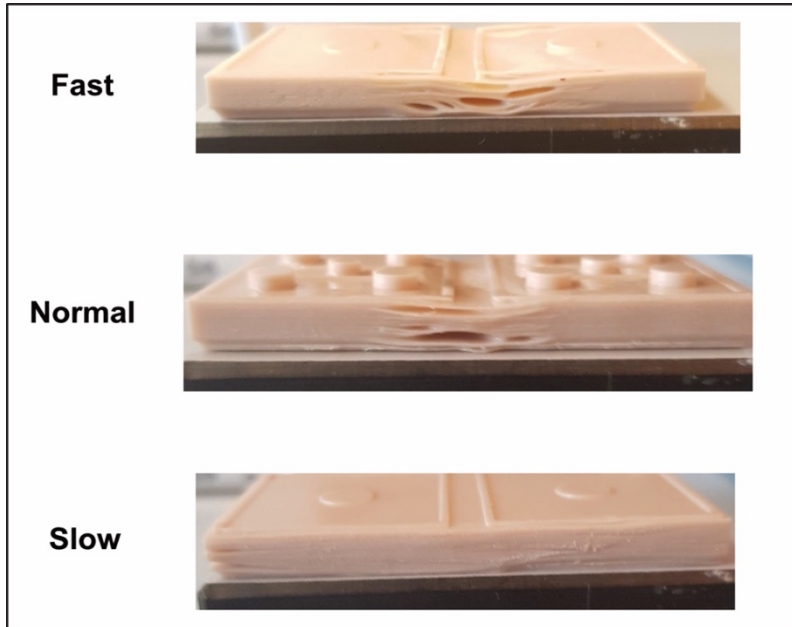
Figure 4.4: Print defect in the fabrication of the LOC device moulds caused by a fast manufacturing resulting in impaired layer attachment. The same design was printed using the Miicraft printer and the GR-13 dental resin with different speed settings and results in the differential attachment of layers.

Furthermore, it is important to understand how the 3D printer processes the design and how it is transformed to produce a 3D object. As the printer prints layer by layer, each layer is processed one by one with the layer divided into "pixels" of minimal resolution that are going to be illuminated or not. This is not a problem for structures that are higher than a single pixel resolution (in our case around 67μm in XY) but it can be problematic to define smaller structures as shown in figure 4.5.
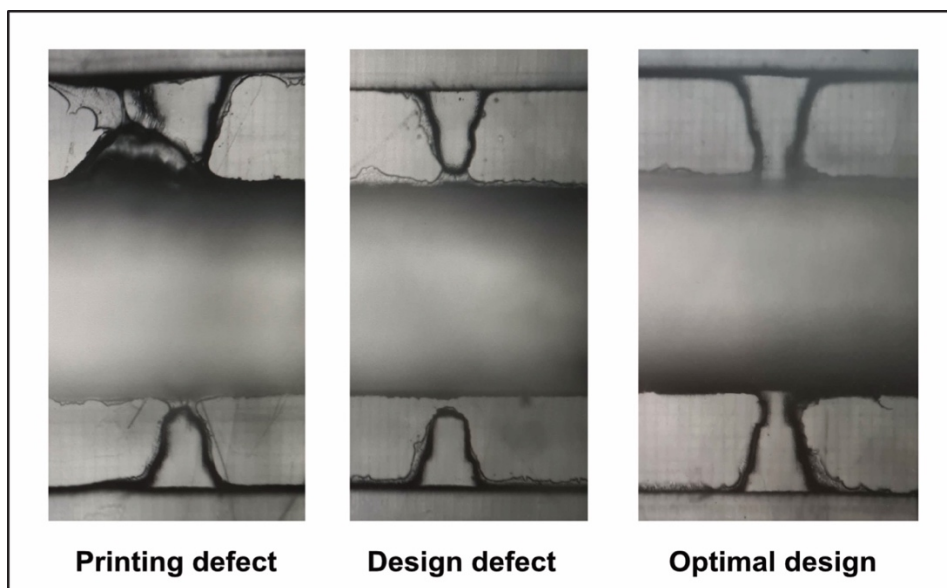
Figure 4.5: Examples of printing defects observed during the printing setting optimisation. Prints using the same design with the Miicraft printer and the BV-007 resin result in very different connections shapes. A debri in the resin bath can cause a printing defect and the merging of several parts or defects in the design such as the wrong dimensions in the junction between the channel and the central well leads to a gap between the different parts.

Lowering the resolution of the print to its minimal capacity often means that the print must be optimised to obtain satisfactory results. Apart from obvious printing defects due to debris or problems of illumination some design defects can affect the print. If the print contains very small structures down to 1 pixel and intersections as seen in figure 4.5, it can often fail to reproduce the design. Overall, going down to the highest resolution is not recommended but as seen in the optimised design, it can be done by removing smoothing of the design. This means that each pixel is either illuminated or not, and no surface smoothing is added to obtain curves, resulting in rougher designs but higher resolutions.

iii. Post-processing

Finally, after optimising the printing settings, we needed to make sure these moulds were compatible with soft lithography and the creation of PDMS devices. The 3D printing with SLA printers is done in a bath of resin, which means that the residual resin must be properly washed before use as a mould. Conventional washing procedures include a sonication in isopropanol to remove the uncured resin and a cycle of UV illumination at 60°C to finish the curing process for 30 minutes.

However, when we used this post-processing protocol with our resin, the PDMS poured and left to cure in the oven overnight was not cured and we could observe a layer of liquid PDMS at the interface with the mould. We hypothesized that this was due to residual monomers in the mould that were inhibiting the PDMS polymerisation.

To solve this issue, we extensively extended the post-processing time with two baths in isopropanol with sonication for 5 minutes followed by a rinse of the mould with acetone and an hour UV illumination at 60°C. After repeating this process twice and coating the mould with Trichloro(1H,1H,2H,2H-perfluorooctyl) silane to further avoid PDMS to stick to the mould, we managed to obtain a surface from which PDMS could be peeled off as described in figure 4.6.
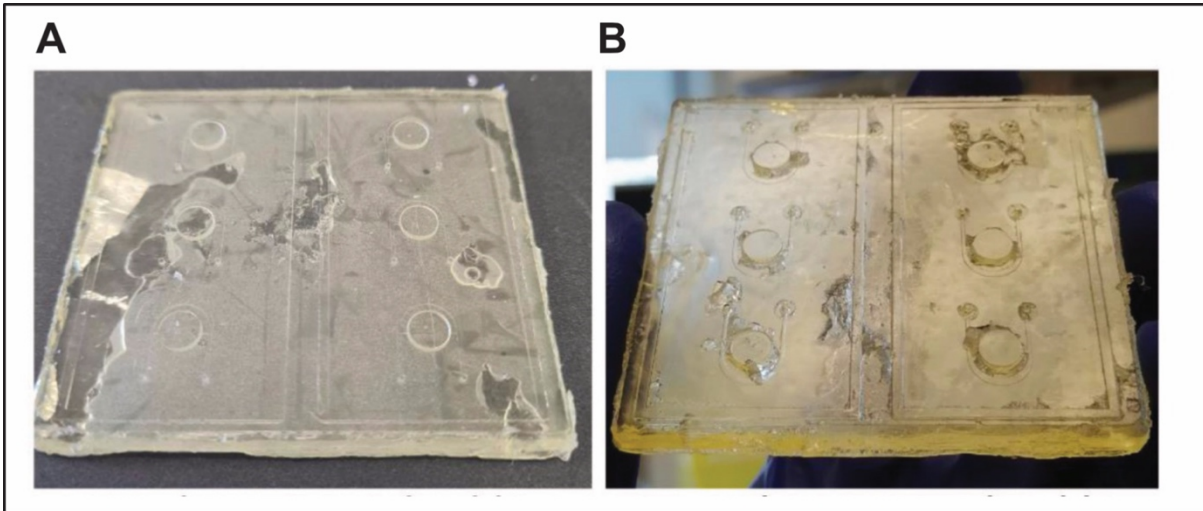
Figure 4.6: Importance of the post-processing for the fabrication of mould for microfluidic devices by soft lithography. A) Fully post-processed mould used for soft lithography. B) Incomplete post-processing led to PDMS to stay on the mould after peeling, affecting the result.

c. Creation of an assembly cassette to facilitate manufacturing

Traditional fabrication method using silicon wafers are used to create relatively thin PDMS LOC devices due to the inability to create tall microfeatures and the relative fragility of these structures. However, adapting the mould with 3D printing allowed us to increase the height of the print up to several centimetres if needed. This gave the advantage to create taller reservoirs and wells in the design and facilitate the punching of the PDMS chips. Unfortunately, this was also accompanied by a difficulty to keep the PDMS on the mould while pouring it in its liquid form, with the current flat mould design.

To solve this issue, we first fabricated walls with aluminium foil to contain the PDMS while it was curing in the oven overnight. However, this technique often resulted in leakage and the resulting LOC devices were not straight. We proceeded to design 3D printed walls to facilitate the LOC device assembly and obtain reproducible flat devices, as shown in figure 4.7.
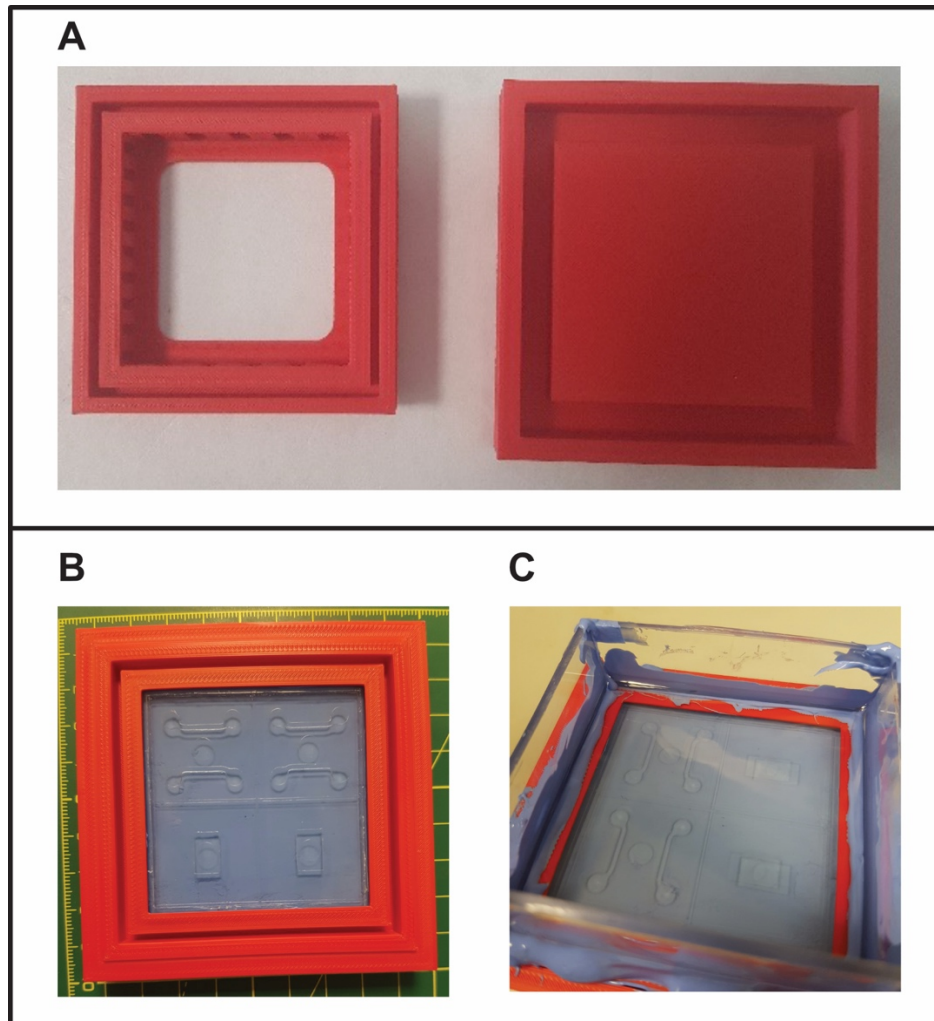
Figure 4.7: Assembly cassette to facilitate LOC device manufacturing. A) 3D printed cassette before fitting the mould. B) Assembled mould in the cassette. C) Assembled mould within the cassette and surrounded by polyvinyl chloride (PVC) walls bounds with silicone.

The assembly cassette consists in a 3D printed part printed in acrylonitrile butadiene styrene (ABS) that will contain the mould printed previously in resin to make sure it is kept flat. To allow an even height of the PDMS poured on the mould, we created walls in PVC that we glue to the printed cassette with silicone. This setup allows a reproducible fabrication of the LOC devices without loss of PDMS and facilitate the manufacturing by allowing the PDMS to cut directly on the mould and reused many times.

d. 3D printed LOC devices allow the culture of microvasculature in exogenous hydrogels.

After optimisation of the manufacturing, we wanted to validate the design with a hydrogel containing endothelial cells (ECs) as described earlier. To reproduce the microvasculature as seen in previous studies, we adapted the same protocol used in the manuscript detailing the

self-assembly of capillaries in a fibrin hydrogel inside the previously described LOC device (M. B. Chen et al., 2017).

As intended with the design, we seeded the fibrin hydrogel containing ECs in the central well of the lower layer in the LOC and left it to polymerise in a humidity chamber. As seen in figure 4.8, we tested two designs for the central well, one with a rectangular shape and one with a circular shape.
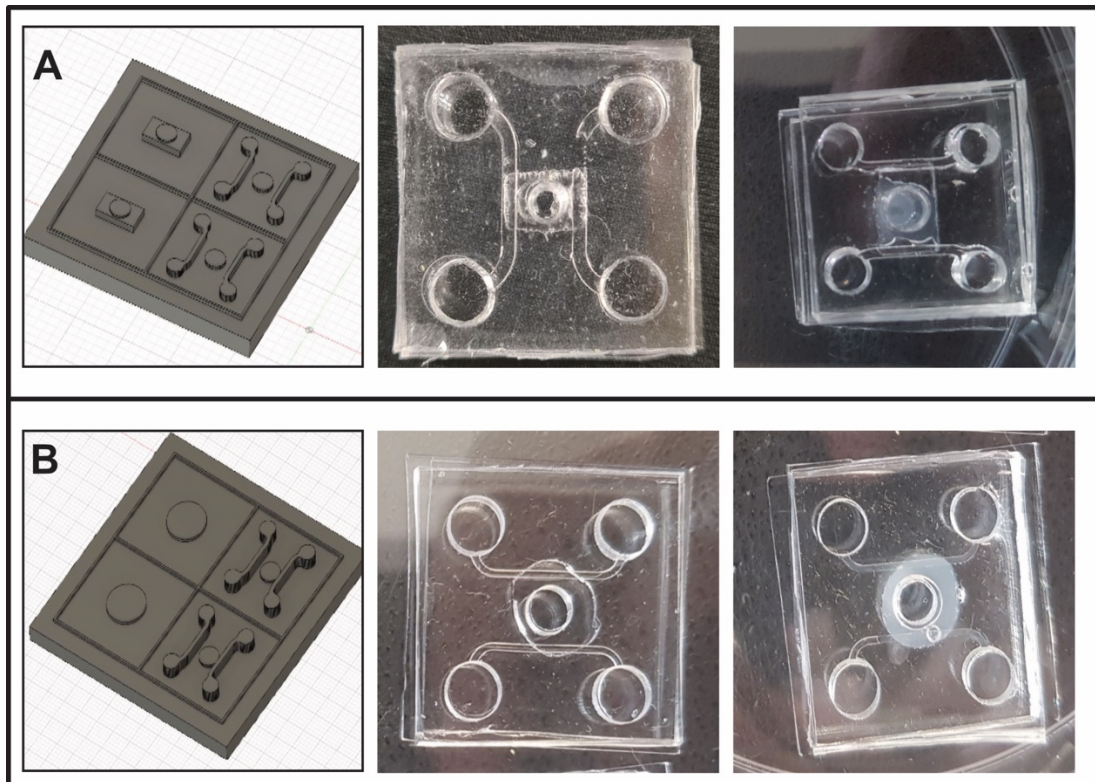
Figure 4.8: Design optimisation for the implementation of a hydrogel system. A) The LOC device can be modified to present a rectangular (A) or a circular central well (B) affecting the LOC assembly and seeding of hydrogels in the central well.

The introduction of a rectangular central well in the lower layer of the LOC facilitated the assembly of the two PDMS layer and created a longer overlap with the medium channels on the top layer. However, as seen in figure 4.8, the shape of the central well affected the proper distribution of the fibrin hydrogel. The 90° angles often trapped air bubbles and compromised the reproducibility of the system. The circular central well was easier to use for the seeding of the fibrin hydrogel and was kept for the later use of the device.

Following polymerisation of the hydrogel, ECs are kept in culture for several days until they form a self -assembled microvasculature as observed in figure 4.9.
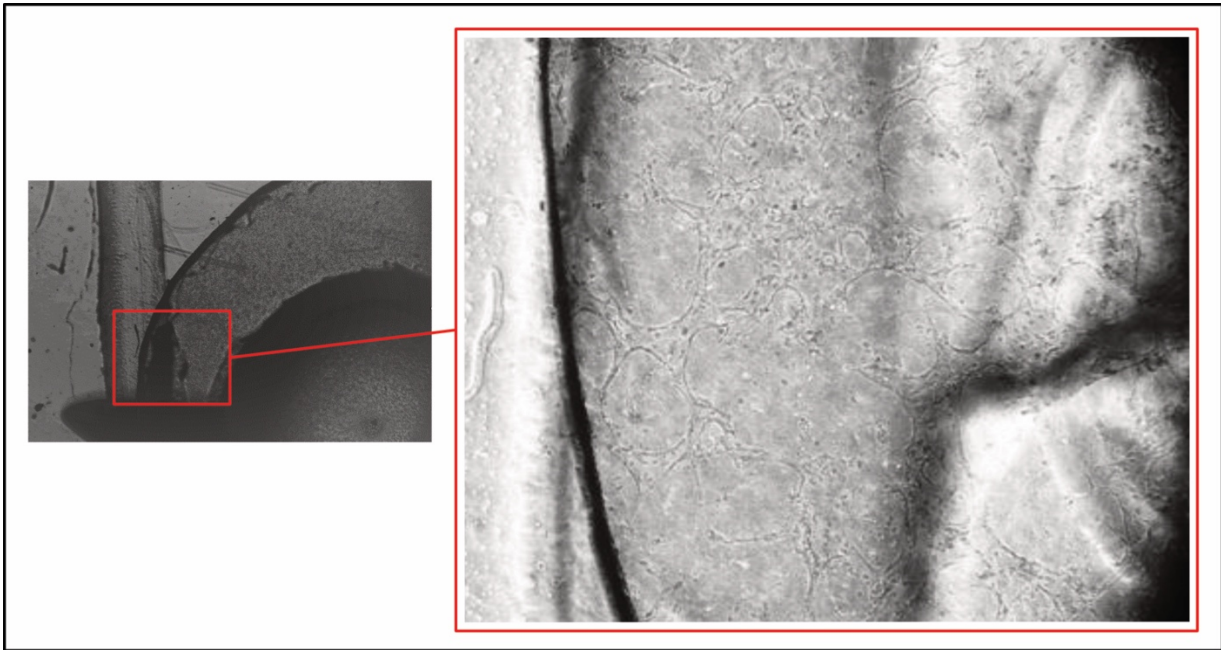
Figure 4.9: HUVECs form a self-assembled vascular network in fibrin hydrogel seeding in the custom LOC device after 72h of culture. A fibrin hydrogel containing embedded HUVECs has been seeded in the central well of the LOC device and cultured for 72h to promote the formation of self-assembled networks.

The fibrin hydrogel could be kept in culture for days while HUVECs formed an interconnected network in 72h. However, we quickly realised that the 2-layer system was not appropriate to try and perfuse these self-assembled capillaries due to the architecture and the dimensions of the LOC device. After formation of the network, we could not achieve any perfusion by gravity as observed in other studies (Campisi et al., 2018; M. B. Chen et al., 2017; Shin et al., 2012) because the flow was restricted to the channels. Moreover, the central well was too big to create a very well-connected network from one side to the other while keeping a pressure drop that would perfuse the whole network. Implementing perfusion in microfluidic devices of this size requires the connection of an active pumping system.

e. 3D printed moulds allow direct embedding of tubing and secure connection

Creation of vascularised tissues *in vitro* requires the introduction of blood flow. This can be achieved passively via gravity or actively with the introduction of a pumping system such as a syringe pump or a peristaltic pump as described earlier. Most systems used to create microvasculature in LOC devices use gravity-driven perfusion with medium reservoirs filled at different heights. This has shown efficient in the creation of lumenised microvasculature *in vitro* (Campisi et al., 2018; Chen et al., 2013; M. B. Chen et al., 2017; Marimuthu and Kim, 2013) but does not fully recapitulate the biomechanical cues experienced *in vivo*. Such systems often lack the ability to introduce active pumping systems because of the inability to connect

it to a close tubing system. The introduction of tubing for a pumping system necessitates a strong connection with the LOC device and an appropriate design flexibility to withstand the continuous perfusion.

To introduce a robust pumping system in our microfluidic device, we decided to directly modify the design of our mould to allow the direct embedding of silicone tubing during the manufacture, as seen in figure 4.10.
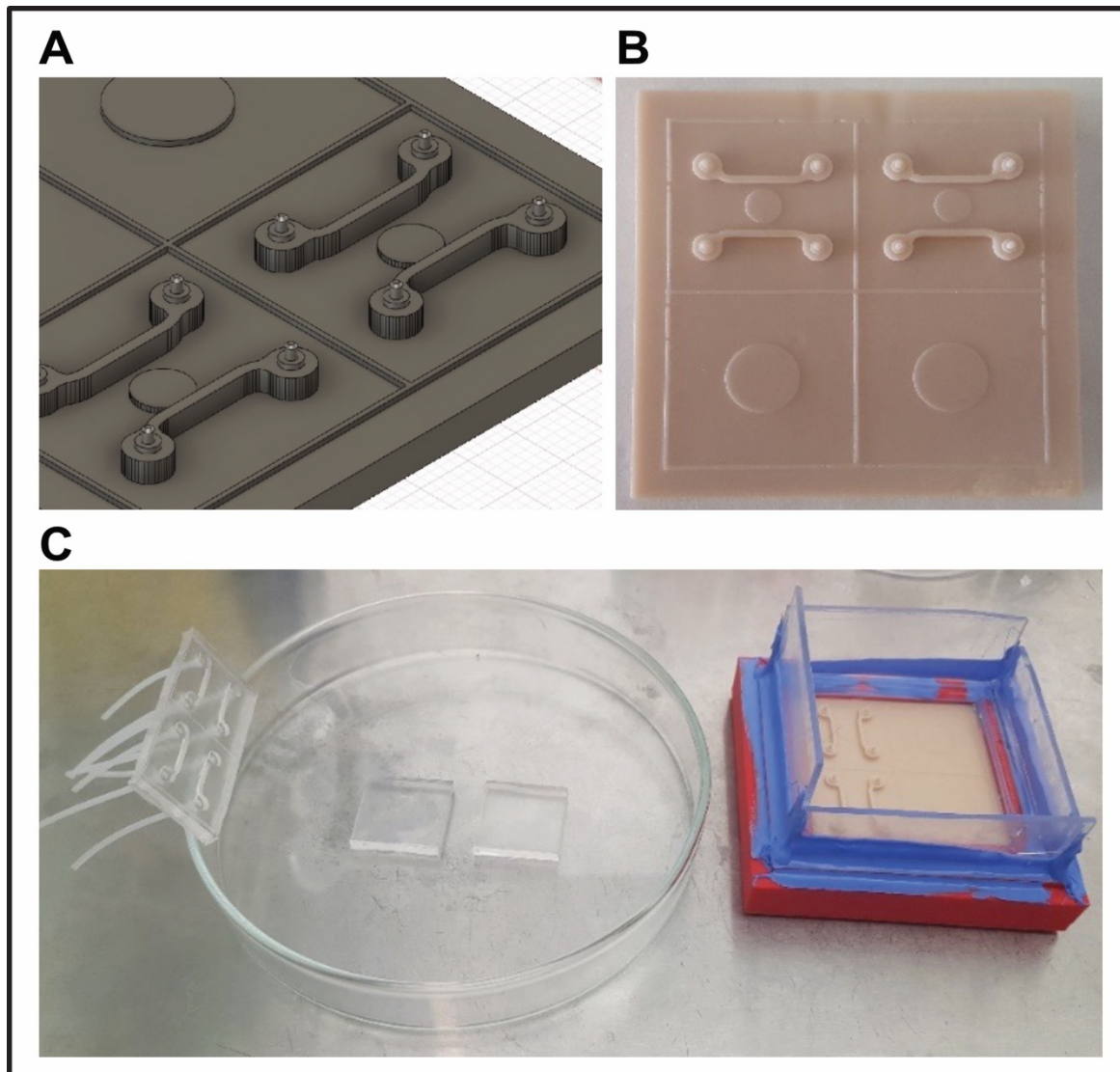
Figure 4.10: Direct embedding of tubing to allow secure connection. A) Design modification adding pillars to the mould to support the tubing. B) 3D printed mould after design modification. C) Embedded tubing in the PDMS chip after assembly.

This embedding before the PDMS cures created a seal between the PDMS and the silicon tubing and allowed a secure connection to a syringe or any other pumping system. To validate the system, we used a syringe to manually pump liquid between the inlet and the outlet of a closed LOC device and we could not observe any leakage up to several millilitres per minute

(SFig. 4.1). However, the introduction of this tubing in our current design with two layers did not solve the problem associated with the lack of perfusion of our vascular network.

5- <u>**Design optimisation and single layer LOC device**</u>

The design used with a single central well was not suitable for long term perfusion of vascular networks *in vitro*. However, the ease of modification caused by 3D printing of the mould allowed us to rapidly modify the LOC device and try several configurations to fit our purpose.

a. Creation of single layer and multi-well LOC device

To create an adequate model of microfluidic device that can withstand blood flow and allow an effortless perfusion of microvascular network, we decided to modify the design of our device. To reduce the effort for assembly and create a simpler model, we created a model of single-layer LOC where only a layer of PDMS is bound to a glass slide and the cells can be seeded directly on glass. We also decided to reduce the central well to 5mm to promote a faster network formation and perfusion. The first design created in single layer is presented in figure 4.11.
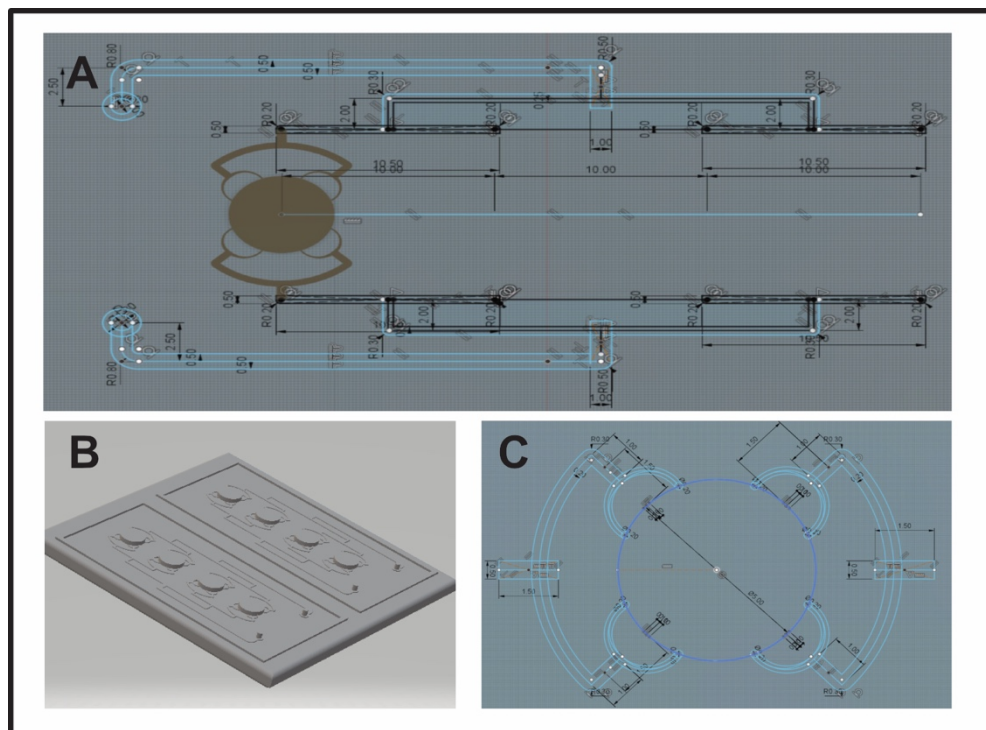
<u>Figure 4.11: Single layer design to create a multi-well LOC device. A) Design of the LOC device with 4 single central wells, an afferent and an efferent channel. B) 3D CAD model of the mould before printing. C) Design of the central well with 2 separate inlets and 2 separate outlets.</u>

The reduction of the central well allowed to put up to 4 wells in the device to have different cultures in parallel. The idea behind this design is to recapitulate the complex architecture of the vascular tree with different big arterioles that divide into small capillaries and capillary beds and the same for the venous part. These differences in size were recapitulated by different sizes in the channels, from the biggest channels straight after the inlet at 1mm of diameter to the junction between the channels and the central well down to 200µm. We validated the correct size and printability of the design as demonstrated in figure 4.12.
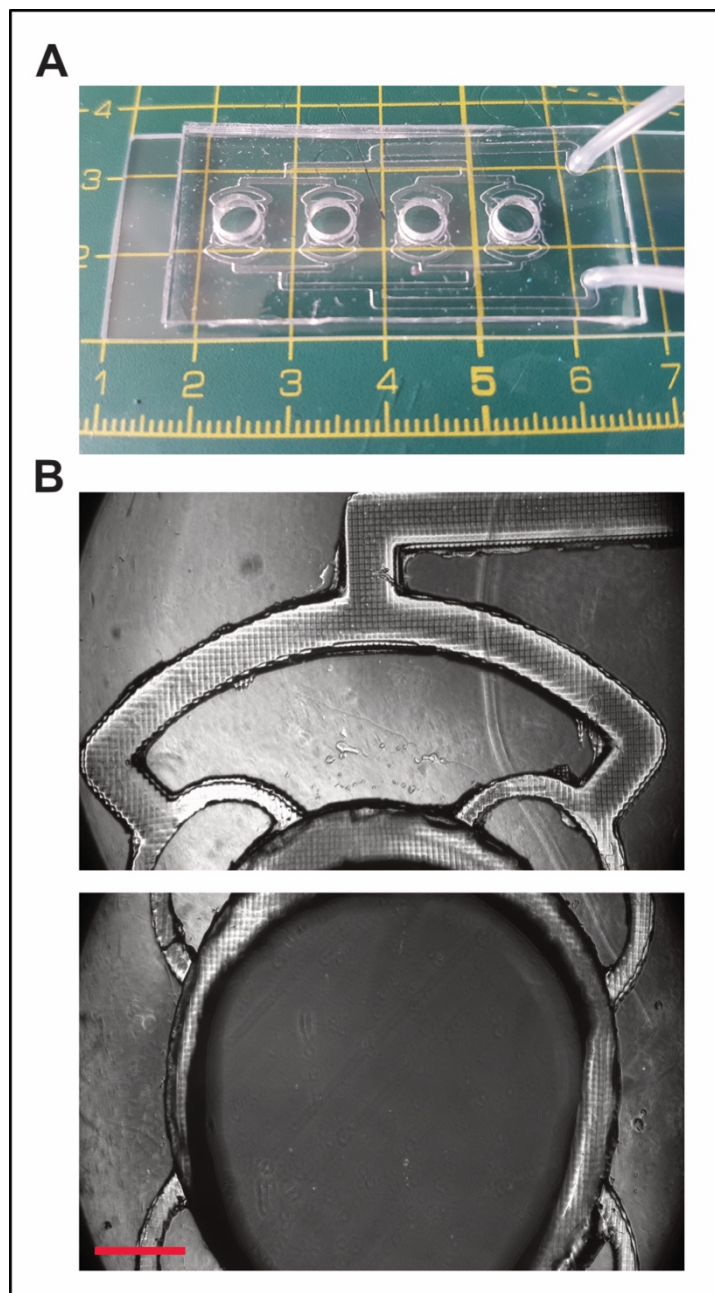
Figure 4.12: Single layer LOC device. A) LOC device assembled with embedded tubing on a glass slide. B) Photographs of the channels and central well after assembly of the chip. Scale bar: 1mm.

This design has everything at the same level, with the medium channels leading directly into the central well where the cells can be cultured. The reduction to a single inlet and a single outlet also created a closed loop where the inlet received higher pressure as a model of "arterial" side and the outlet only received the residual volume that passed through the "capillary bed" as a model of "venous" side.

b. 3D printed LOC device allows long term cell culture and the formation of blood vessel-like structures

With the introduction of the new LOC design, we started optimising a more complete model of microvasculature *in vitro*. To do so, we first seeded HUVEC-RFP in the chip to cover the side channels as a model of "big" vessel so that the flow could pass in their "lumen". As seen in figure 4.13, HUVEC-RFP nicely coated the bottom and sides of the channels and the central well after few days of culture.
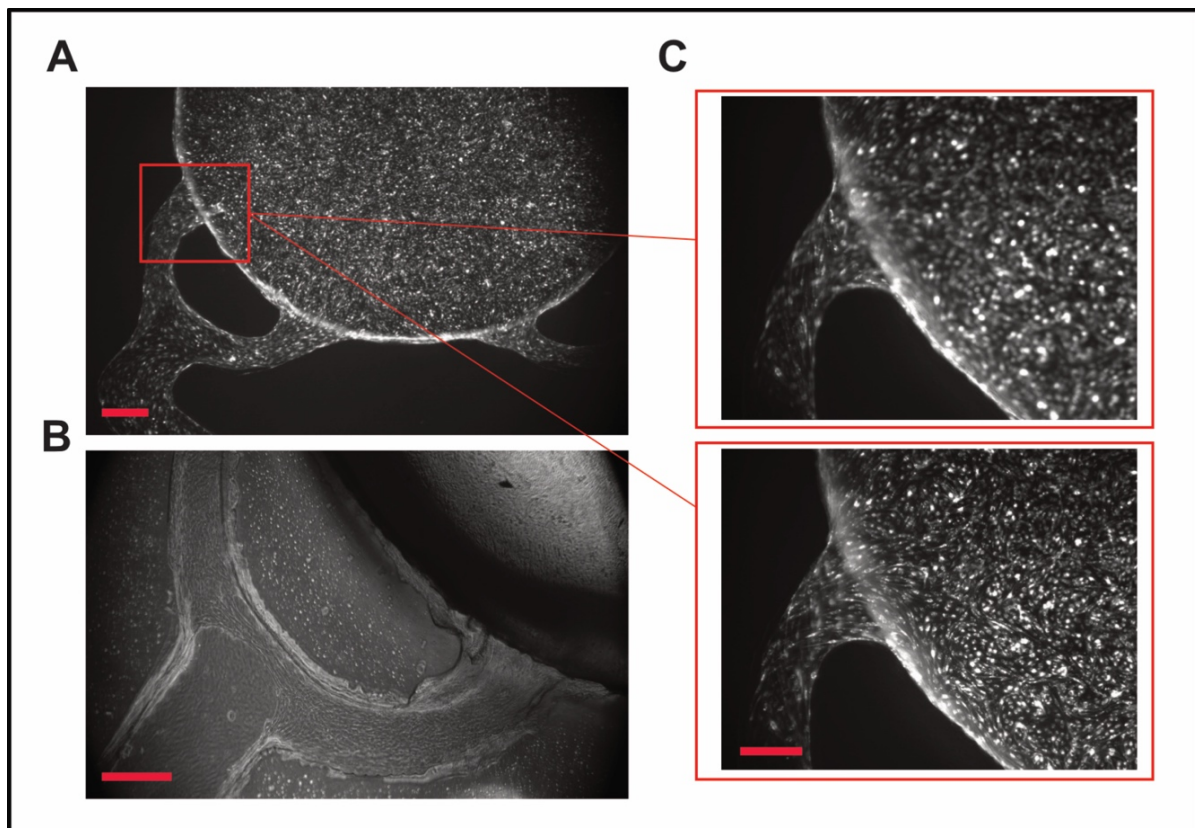
Figure 4.13: Long term culture in the new one-layer LOC. HUVEC-RFP were cultured for 10 days in the LOC device and could be seen via the RFP signal (A) or in brightfield (B). Scale bar: 200μm. After days of culture, HUVEC-RFP started coating the top surface of the side channels observed by photographs at different focuses (C). Scale bar: 100μm.

The coating of the LOC device with a mix of fibronectin and foetal bovine serum (FBS) overnight allowed a nice attachment of the HUVEC-RFP in the device. After several days, the HUVECs invaded the whole device including the central well and most of the side channels.

As observed in figure 4.13C, they also started coating all sides of the side channels creating an artificial vessel at the connection between the central well and the channels.

With this part of the microvasculature recapitulated, we moved to optimising the hydrogel system in the central well. The aim was to link both and obtain a model of "big vessel" connected with a capillary network formed in the central well in a hydrogel. To do so, we used the fibrin hydrogel system used previously and seeded it in the central well prior to HUVEC-RFP seeding in the channels in order to avoid leakage of the gel in the channels. As seen in figure 4.14A, the HUVEC-RFP embedded in a fibrin hydrogel in the central formed a nicely interconnected microvascular network.
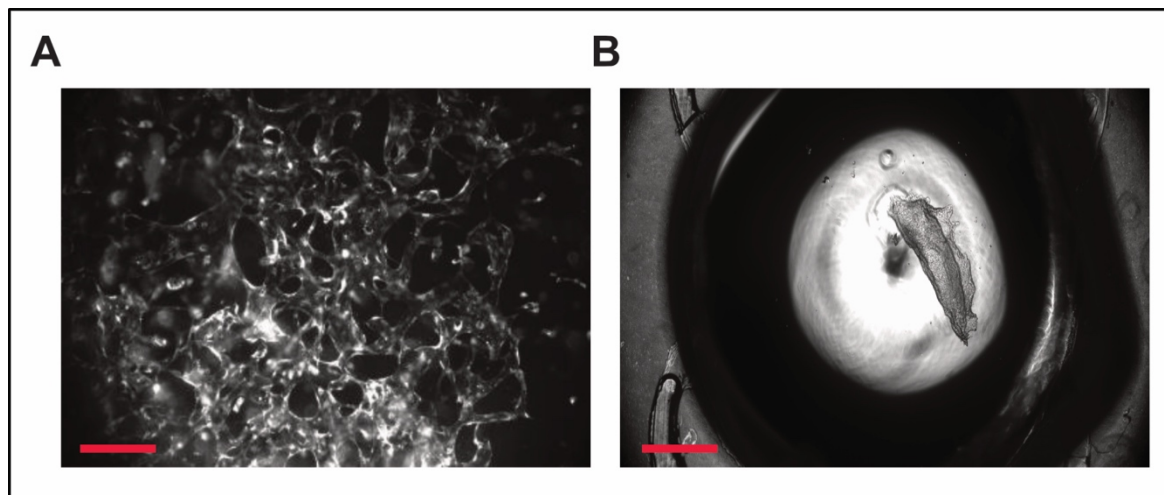
Figure 4.14: Self-assembled vascular network in the LOC device. A) HUVEC-RFP forming self-assembled microvascular network after 3 days of culture in a fibrin hydrogel. B) Cells detached in the central well after perfusion through the channels.

The coupling of the fibrin hydrogel and the channels coated with ECs allowed the creation of a model of closed vasculature in static conditions. However, as shown in figure 4.14B, the introduction of flow by adding medium with a syringe through the inlet resulted in the disruption of the hydrogel and the cell monolayer in the channels. Indeed, the design with one layer and the direct link between the side channels and the central wells allowed a strong link between the hydrogel and the cells in the channels but it did not withstand the flow. With this design, the whole flow is going into the central well (as shown in Sfig. 4.2) and if the vascular network is not properly opened, the build-up of pressure destroys the structures formed in the device.

Overall, this design including embedded tubing, side channels recapitulating the vascular hierarchy and a central well as a model of capillary bed resulted in the creation of a relevant model of microvasculature in static conditions. However, the introduction of flow in the device disturbed the system and could not result in the perfusion of the vasculature. Future designs will have to consider the importance of the flow distribution to create appropriate microfluidic devices allowing the perfusion of vascular networks.

6- ## CAD and 3DP allow effortless and inexpensive modifications of LOC devices

Manufacturing adequate LOC devices to recapitulate vasculature-on-chip requires considering several aspects of the fabrication. As previously described, the LOC device needs to fit dimensions of blood vessels as found *in vivo*, with the possibility to create capillary beds, bigger vessels and the ability to mature over time. Furthermore, the architecture of the chip needs to consider the physical forces inherent with the introduction of the flow, so as not to create disturbance in the system. Finally, the system needs to be easy to handle for daily cell culture, allow imaging to track of the evolution of the system and be robust for the long-term culture in sterile conditions under perfusion.

a. Design considerations to create a vasculature-on-chip

As described earlier, the design of the mould to create our LOC device has been at the centre of this project to optimise the creation of our vasculature-on-chip. Throughout the development of the LOC device, we tested and validated several designs as illustrated in figure 4.15

The first model used did not allow the perfusion of our microvasculature due to the direct flow into the central well. To avoid the cell disruption by the flow, we introduced a T-junction to restrict most of the flow into a U-shaped channel as seen in model 3 and 4. This allows only a portion of the flow to go into the central well and with a reduced velocity, to avoid destruction of the structures in the central well. To dampen the flow, we also tested designs including a derivation as seen in model 3, to further reduce the volume going to the central well. Finally, we also lengthen the channels to reduce the velocity of the flow coming through the junction in models such as the model 6.

.
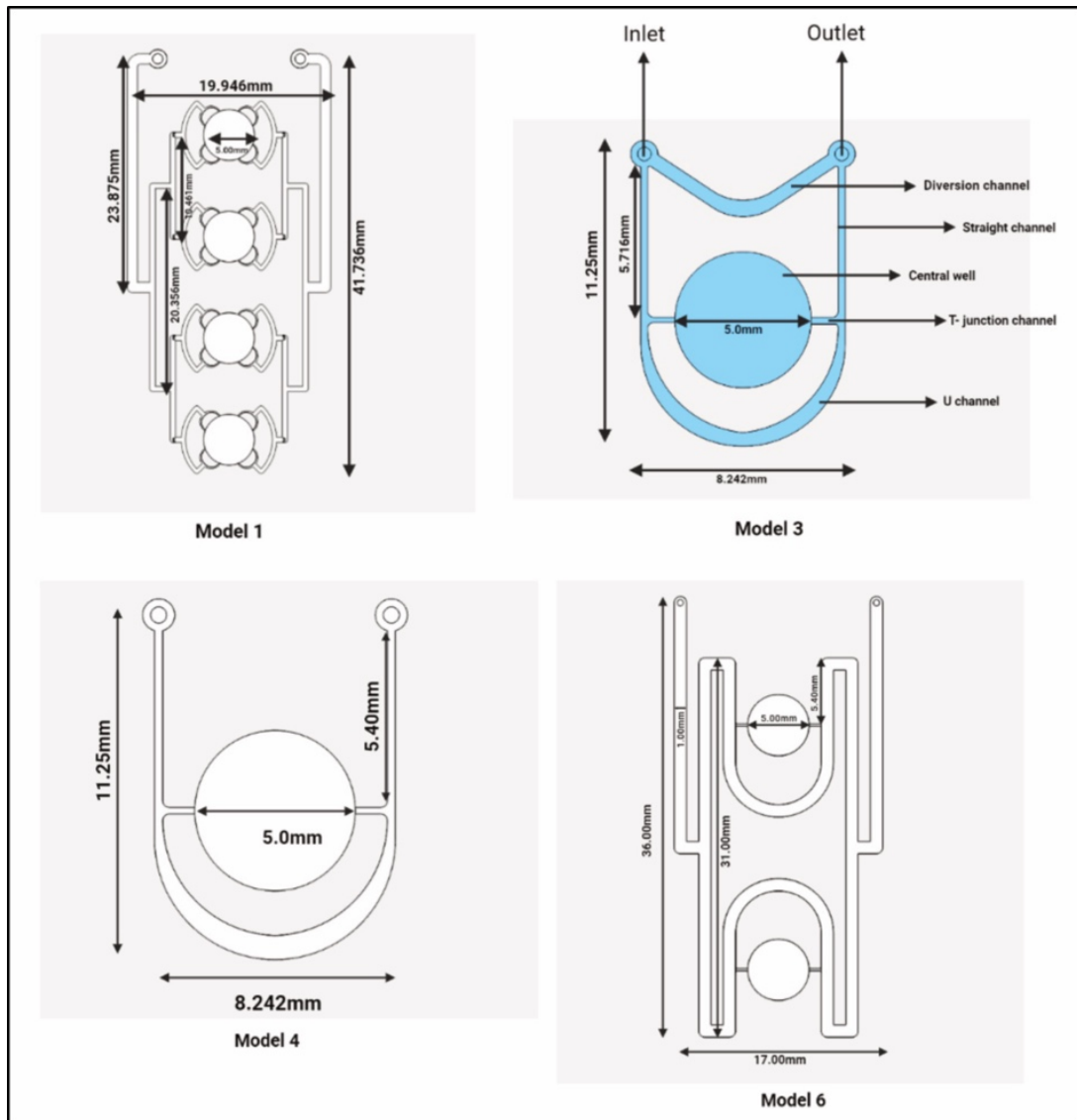
Figure 4.15: Several LOC device designs used during the study. Model 1 represents the first complex design with multiple central wells. Further designs include Model 3 and 4 that incorporate a U-shaped closed channel system and that can be doubled as seen in model 6.

During the development of the optimised design, we also introduced walls in the mould to facilitate the manufacture of the LOC device and replace the assembly cassette (Fig. 4.16A-B, SFig. 4.3). This allowed us to fabricate LOC devices with just the mould and removed the need to create a 3D-printed assembling walls for each mould.
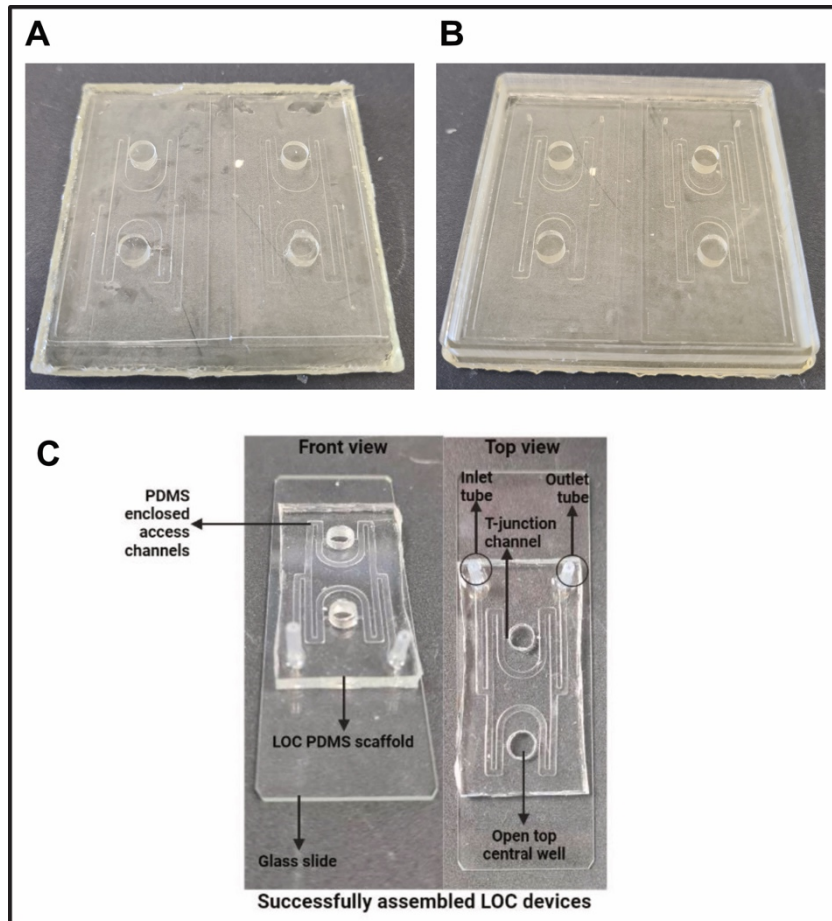
Figure 4.16: Design optimisation to include walls on the 3D printed mould and create more reproducible devices. A) 3D printed mould of the model 6. B) 3D printed mould of the model 7. C) Assembled chip with the design of the model 7.

b. Design optimisation for the introduction of perfusion

The introduction of continuous perfusion in the LOC device necessitates to consider small changes in the design such as the shape and dimensions of the different compartments. The central well dimensions and shape gave satisfactory results to culture cells and allowed an adequate imaging and dynamic culture. However, the connection between the side channel and the central well revealed to be a crucial point to allow the correct perfusion of the microvasculature in the central well. Indeed, the flow rate and volume of medium that reaches the microvasculature will determine the success of perfusion. To obtain a smooth transition between the side channels and the central well and reduce the disruption of the cells, we also modified the junction as described in figure 4.17.
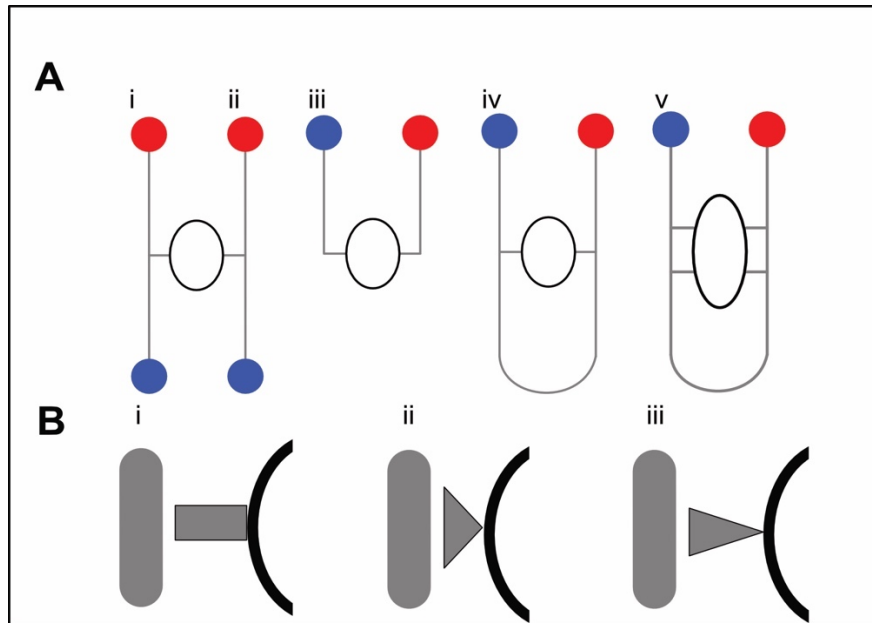
Figure 4.17: A) Different design of the side channel length and configuration. Designs that were considered include: independent (i-ii) afferent arteriole (aA) and efferent venule (eV), direct total perfusion (iii) in the central well, or partially divided (iv, v) flow into the central well. B) The junction between aA and eV can be designed to have a 90° angle (i), a bigger angle (ii) to receive more flow or a longer length (iii).

As seen in model 3, 4 and 6, we started with different models of connections, with either separate or joined medium channels (Fig. 4.17A). The preliminary experiments with cells using these designs showed encouraging perfusion but the 90° angle of the T-junction did not allow enough medium to enter the central well and was not ideal for the perfusion of vascular structures. Indeed, when cultured in the LOC fabricated with the mould model 6, cells could withstand the flow but very few vascular structures were formed in the central well as seen in supplementary figure 4.4. The dimensions of the central well (5mm in diameter) also necessitated that the vascular structures formed were perfectly perfused for both sides to be connected, which was often not the case before the start of the perfusion.

We reasoned that the low volume of flow going into the central well could be due to the structure of the junction, and that changing the angle between the side channels and the junction could increase the proportion of the flow available for perfusion of the structures in the well (Fig. 4.17B). Furthermore, modifying the junction into a V-shaped connection would recreate an architecture closer the shape of blood vessel connections in the body. To test these hypotheses without the need of recreating different moulds for each experiment, we needed to introduce an unbiased way to measure the effect of the flow in our system.

7- **Computational fluid dynamics (CFD) to validate design specifications**

The facilitated modification of our mould via 3D printing allowed us to rapidly test different LOC designs. However, these modifications still required time and several experiments to answer our questions on the ability of the chip to withstand the continuous perfusion. Computational fluid dynamics (CFD) has been used to predict the behaviour of fluids in fields such as engineering or aerodynamics to anticipate the interaction of fluids with predefined surfaces. Several open-source software have been created to use CFD with custom designs and allow the simulation of fluid dynamics in microscale systems such as LOC devices.

a. CFD to achieve *in vivo*-scale perfusion

To optimise the design of our VOC, we examined our candidates (Fig. 4.17, SFig. 4.5) by CFD and iteratively refined our design aiming to achieve balanced flow between inlet and outlet (in-flow = out-flow) as well as a pressure drop between afferent arteriole (aA) and efferent venule (eV). In this way, the total volume of medium in the system remains fixed while creating flow across the open-top central chamber. Figure 4.18 shows CFD analysis of our the most suitable design after optimisation and the design used for the rest of the study (analysis parameters are listed in methods).

Figure 4.18A demonstrates that CFD particle analysis predicts establishment of stable flow without turbulences in the system at the indicated FR. Particle speed analysis (FR=100 µl/min) predicted values of ~10 mm/s within the central chamber and ~ 100 mm/s in the aV and eV sections. These values are compatible with that observed for red blood cells in brain capillaries and arterioles (4-10 mm/s and 20-30 mm/s respectively)(Chaigneau et al., 2019). Simulations using FR of 1000 µl/min predicted formation of vortices in the LOC outlet, as turbulence could create bubbles in the medium, in experiments we employed maximum FR of 500 µl/min. Figure 4.18B shows cut plane analysis (plane at 50 µm distance from the chip base, corresponding to lines in figure 4.18D i-iii) displaying pressure in the different sections of the chip and demonstrating a pressure drop between the aA and eV sides (red and blue respectively) under both FR tested. Figure 4.18C shows a zoomed-in representation of the cut-plane analysis (corresponding to the red box in Fig. 4.18B) including predicted flow speed and directions across a section of the central well. Figure 4.18D shows a cut-plane analysis across planes perpendicular to points indicated in the 3D diagram (cross-section of the channels at

corresponding points, FR=100µl/min). The colour scale indicates flow speed in different points of the cross-section and the corresponding total volumetric flow rates (VFR).

Overall, our CFD analysis demonstrates that the design of our LOC produces desired biomimetic flow rates and directions. In our intended experimental workflow described later, the flow is constrained differently at different phases of the experiment. Especially, during the first phases, the central chamber is not accessible to flow because the connections are purposedly closed by cells. To assess the behaviour of our design in these conditions, further simulations were performed where the flow access to the central chamber was blocked. Figure 4.18E shows CFD analysis of our design under these conditions, demonstrating variation in the flow directions creating an interstitial-like flow at the interfaces between channels and cells. Under these conditions the flow velocity in the central chamber and most of the connection was ~0.
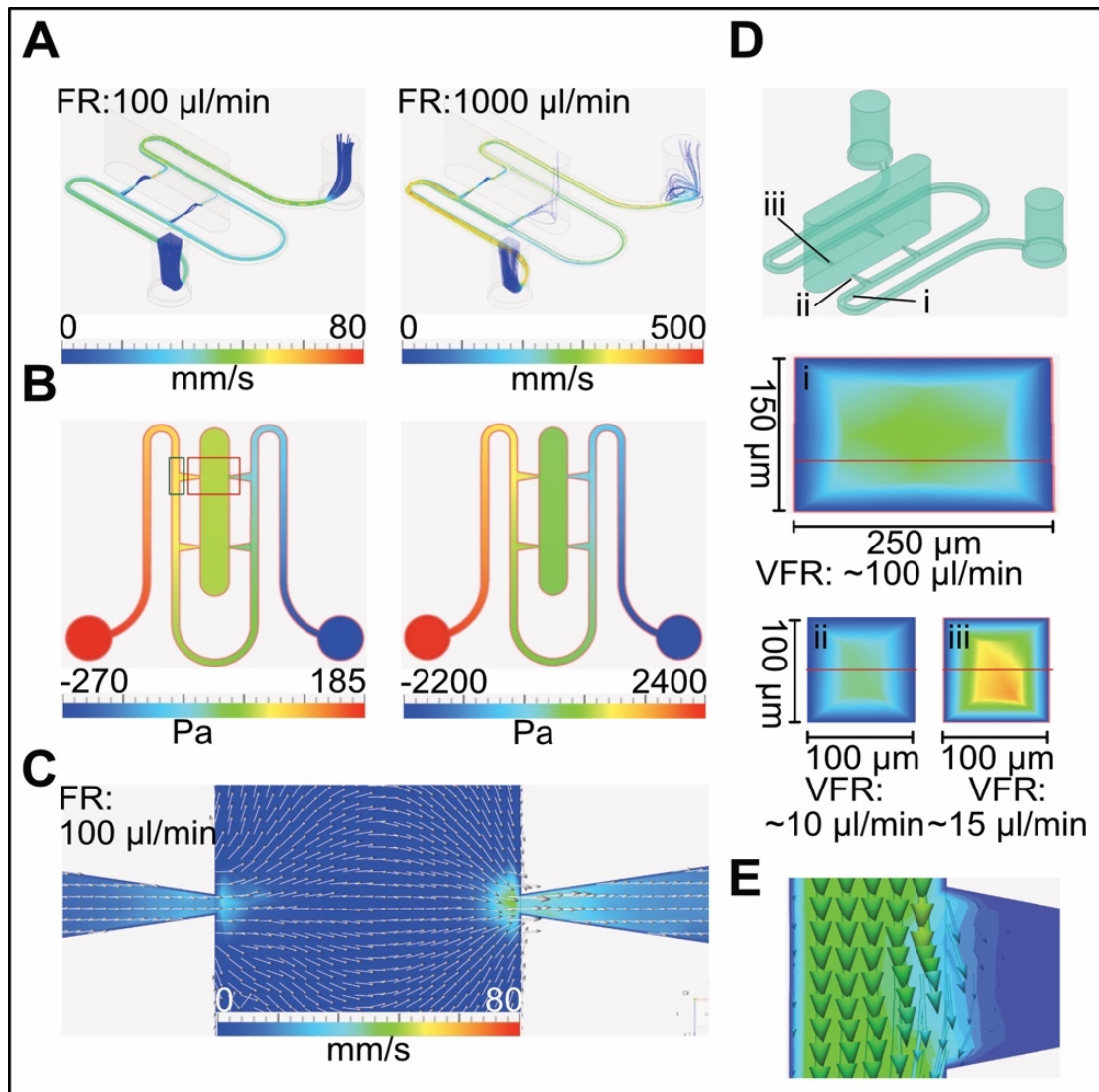
Figure 4.18: CFD analysis of the VOC design. A) Particle speed analysis at indicated flowrate (FR). Particles trajectories are indicated by coloured cylinders, colour scale indicates particle speed at each point. B) Cut plane analysis across the X/Y plane indicated in D i-iii and at indicated FR, colour scale indicates pressure at each point in the chip. Pressure in the central chamber is ~0 (atmospheric pressure, green colour). Red and green coloured boxes indicate locations of analyses illustrated in C and E respectively. C) Vector analysis across the X/Y plane indicated in D i-iii and at indicated FR. Colour scale indicates flow speed at each point, vectors indicate relative speed (intensity) and direction of the flow in a grid of points in the chip section. D) 3D rendering of the VOC geometry indicating regions highlighted in i-iii. D i-iii are cut plane sections at indicated points and with direction X/Z (i) and Y/Z (ii and iii). Colour code indicates flow speed at each point in the cross-sections (colour scale equivalent to A and C). Total Volumetric Flow Rate (VFR) across the sections is as indicated. E) Vector analysis of a simulation where flow through the central chamber was blocked. Analysis corresponds to a section of the chip indicated in B (green box) and across the X/Y plane indicated in D. Colour scale (both vectors and background) correspond to flow speed in the section. Vectors directions correspond to flow direction in a grid of points in the section.

8- **Creation of a 3D-printed cassette to introduce long-term continuous perfusion**

After optimisation of the design and fabrication of our custom LOC device, we needed to introduce a system to allow long-term cell culture. Commercially available platforms to perfuse LOC devices are tailored for their specific designs and could not be adapted for our device. For the introduction of a continuous perfusion system, we needed to consider several parameters. First, the perfusion system needed to fit our LOC device assembled with the tubing and reservoir. Then, the dimensions of the device needed to be standardised to fit in microscopes and allow imaging with a transparent bottom. Finally, the complete system needed to create a sterile environment and fit in standard cell culture incubators for a long period of time.

a. 3D printed custom cassette for sterile cell culture

The assembly of our LOC device on a glass slide required to create a vessel enabling long term cell culture in an incubator. To create a custom cell culture plate, we started with the dimensions of standard cell culture plates and modified it to be able to receive our LOC device. Using 3D printing, we manufactured a custom cassette with plate dimensions that could be used to keep our LOC in culture and in sterile conditions (Fig. 4.19)
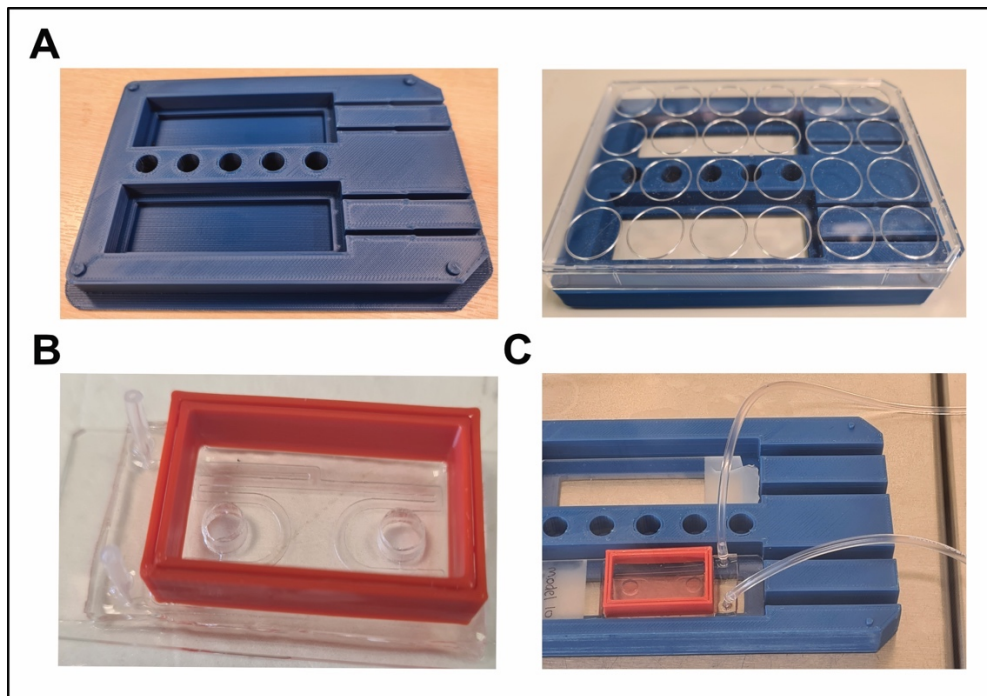
Figure 4.19: 3D printed cassette for the long-term culture of our LOC device. A) 3D printed cassette with plate dimensions to allow adaptation of cell culture lids. B) Assembled LOC device with embedded tubing and a 3D printed reservoir on top of the central wells. C) LOC device fitted in the cassette and filled with medium, linked to the perfusion system.

The design (Fig. 4.19A) includes small pillars to keep the lid elevated and allow gas exchanges as seen in standard cell culture plates. It also includes small wells to create a humidity chamber, slots for the tubing and a transparent bottom to allow imaging without removing the LOC from the cassette. Although the wells allowed the creation of a humidity chamber, the long-term culture and the relatively small volume in the central wells could lead to a volume reduction in the system. To avoid this problem and as seen in figure 4.19B, we added a 3D printed reservoir on top of the chip to create a bigger volume of medium available for the cells in the LOC. The whole setup (Fig. 4.19C), once linked to the perfusion system with the tubing, could be incubated in standard cell culture incubators.

b. Creation of a portable, sterile and waterproof setup including microfluidic pump, filter and flow sensor to introduce controlled LOC perfusion

As discussed above, commercially available perfusion systems often lack the ability to adapt custom designs to their setup. We also concluded with the introduction of CFD that the perfusion rates that was needed for our system were relatively low (<1mL/min), which required specific microfluidic perfusion systems tailored for small volumes. To introduce continuous perfusion in our system, we assembled a microfluidic system tailored for our specific vasculature-on-chip (VOC) system as described in figure 4.20.

As seen in figure 4.20A, our LOC device is comprised of two crucial components related to the introduction of the flow. First, the connection between the channel and the central well, the anastomosis channel (AC) where the flow will be separated from the side channel into the central well. This part is important because the perfusion of the whole system relies on the proper connection of the flow at this location. Then, the "LOC to World" (LWC) connection where the silicone tubing embedded in the PDMS chip received the flow from the pump. This is also a part that needs to be perfectly manufactured to avoid any leakage and a long-term perfusion without disturbing flow behaviour or introduction of air bubbles that could cause damage.

With the aim of perfusing this system, we introduced a custom perfusion system composed of a filter, a microfluidic pump, a flow dampener and a flow sensor as seen in figure 4.20B. The microfluidic pump can be set to deliver a flow rate between 5 and 1000uL/min, with a direct feedback loop from the sensor to a laptop connected via USB cable. As seen in figure 4.20C, the whole system has also been adapted to fit into a 3D-printed cassette and can be installed in the incubator next to the LOC device. This allows the continuous perfusion of the LOC in a

fully defined environment without any change in temperature, with only an external cable for the connection to a laptop to modify the flow without touching the setup.
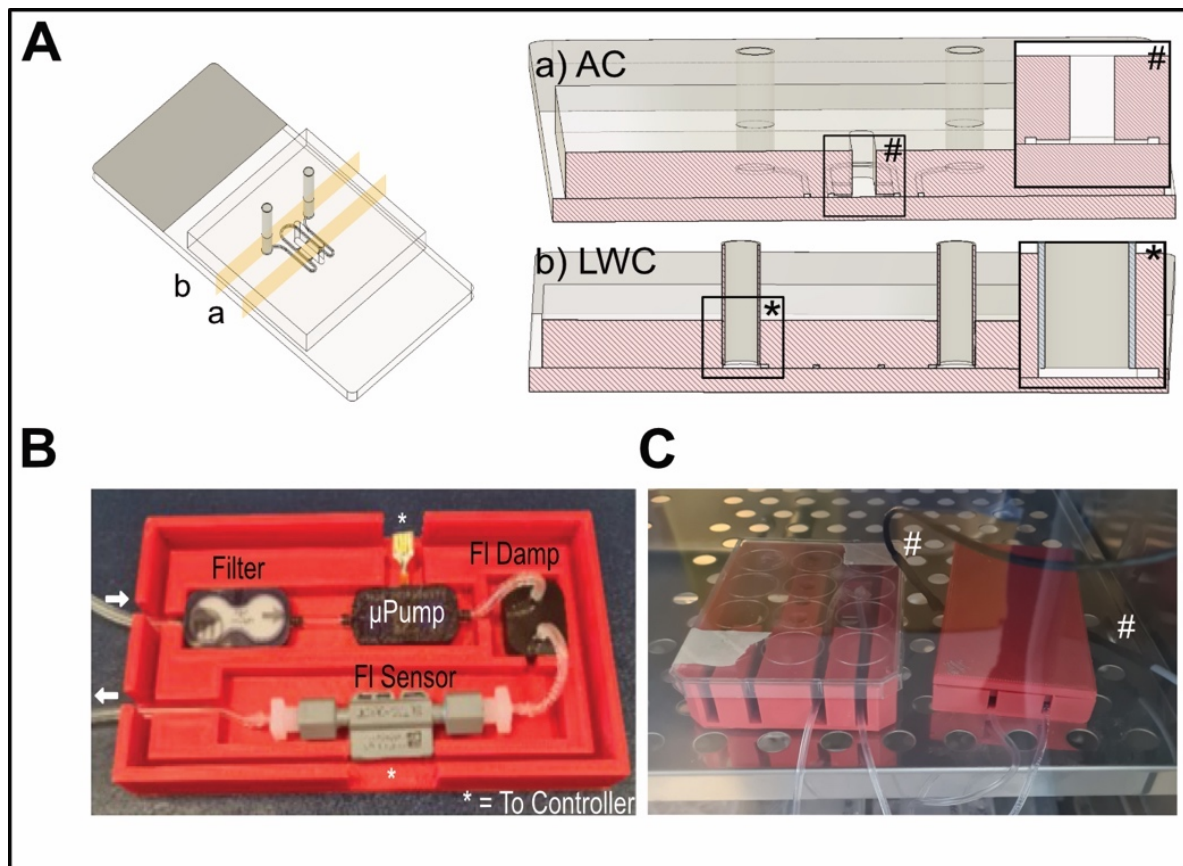
Figure 4.20: VOC design. A) 3D rendering of the VOC design and corresponding cut-plane analysis at indicated locations (a, b). Cut plane across the Anastomosis Channel (AC, a) highlights the smaller section of the AC in comparison to the main channels. Cut plane across the LOC to World Connection (b, LWC) channel highlights the tight coupling between the chip and the silicone tubing (blue shading in inset) which prevents creation of dead volume and allows predictable flow throughout the chip. B) Pocket-size microfluidic drive in its 3D printed cassette illustrating assembly of the system. C) Microfluidic driver (right) connected to the culture cassette (and chip, left) and positioned in a standard cell culture incubator. The black/grey cables visible on the right (# sign) are the only connection outside the incubator, therefore all medium circulating in the system is exposed to a constant environment.

9- **Introduction of flow into the LOC device allows stable and continuous perfusion**

With our final design validated with CFD, we wanted to validate the LOC with a system to allow continuous perfusion of microvascular networks. The most used system as described before is the fibrin hydrogels that allow rapid formation of self-assembled capillaries in 3D and form structures with a lumen that can be perfused.

a. Implementation of a hydrogel system to validate the design

To validate our system for continuous perfusion we performed preliminary experiments using perfusable vascular networks created in fibrin hydrogels. We encapsulated endothelial cells in fibrin hydrogels where ECs self-assemble to form perfusable structures in approximately 72h (Fig. 4.21). In this setup, we only use the central well as a recipient for a "capillary bed" created by the ECs in a 3D hydrogel. By introducing the hydrogel in the central well and the connection (Fig 4.21A), we create a rapidly perfusable vascular network formed by lumenised capillaries in around 72h as shown by the RFP signal of the HUVEC-RFP used in this experiment (Fig. 4.21C).
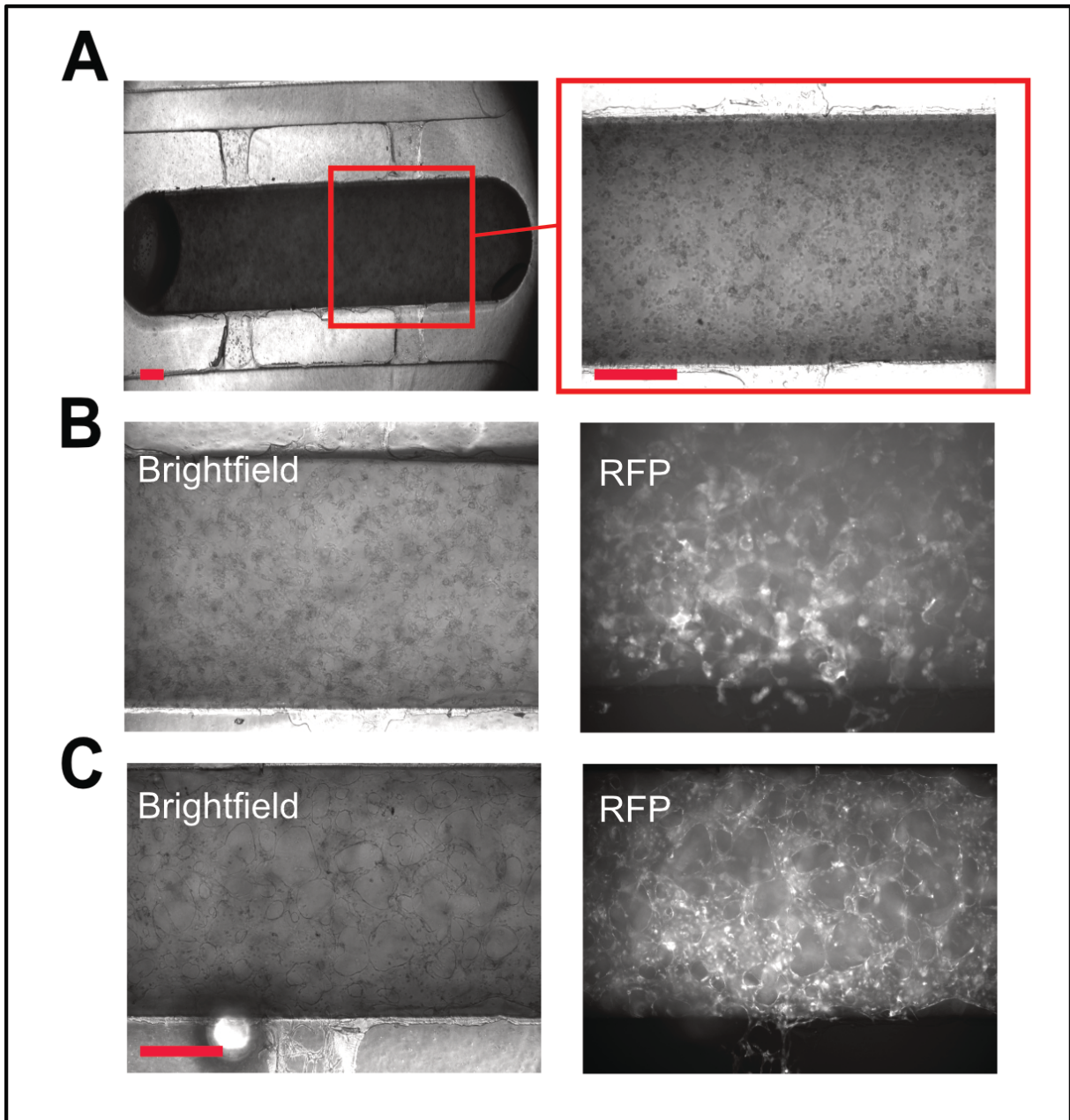
Figure 4.21: Self-assembled vasculature formed in fibrin hydrogel in the LOC device. A) HUVEC-RFP embedded in a fibrin hydrogel just after seeding in the central well. B) HUVEC-RFP after 24h of culture in the hydrogel. C) HUVEC-RFP embedded in the fibrin hydrogel and cultured for 72h forming an interconnected network of capillaries. Scale bar: 150µm.

b. Organ-specific heterogeneity in the formation of capillaries

As discussed in previous chapters, the heterogeneity of ECs and blood vessels is key for their organ-specific function. While ECs exhibit different junctional status, Notch pathway activation or cell proliferation, their inherent ability to form functional capillaries in 3D has been poorly documented. To create the best microvascular networks *in vitro* and study the impact of the organ of interest on the ability of ECs to form functional capillaries, we decided to characterise their vasculogenic and angiogenic potential in different 3D environments.

i. Bead fibrin gel assay

First, we decided to evaluate the ability of different organ-specific ECs to perform angiogenic sprouting with a fibrin bead assay (Fig. 4.22).
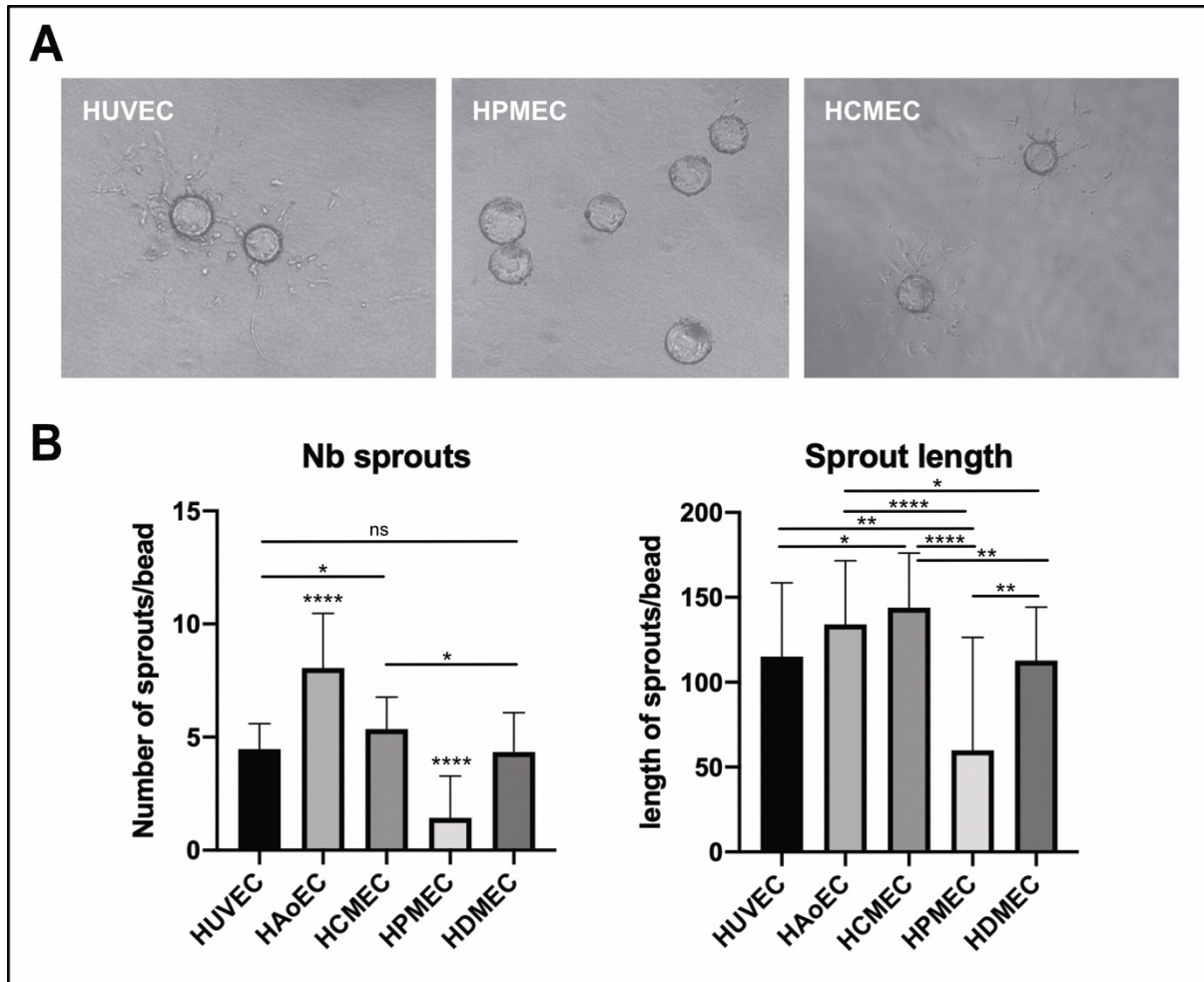
Figure 4.22: Organ-specific ECs have different angiogenic sprouting capacity. A) Photographs of different ECs on beads, embedded in a fibrin hydrogel and cultured for 48h. B) Quantification of the number and length of sprouts after 48h of culture for HUVEC (n=17 beads), HAoEC (n=32 beads), HCMEC (n=33 beads), HPMEC (n=47 beads) and HDMEC (n=20 beads). ns: non-significant: $p > 0.05$, $*p < 0.05$, $**p < 0.01$, $***p < 0,001****p < 0.0001$.

As seen by the photographs in figure 4.22A, organ-specific ECs had very different behaviours in fibrin hydrogels. We characterised the angiogenic potential of a venous EC (Human umbilical vein EC, HUVEC), an arterial EC (Human Aortic EC, HAoEC) and three microvascular ECs (Human cardiac microvascular, HCMEC, pulmonary microvascular, HPMEC, and dermal microvascular, HDMEC). All EC tested had a good adhesion to the collagen-coated beads but their angiogenic sprouting capacity was very heterogeneous. Although the number of sprouts per bead was relatively similar (around 5 to 6) for HUVEC, HCMEC and HDMEC, HAoEC exhibited a higher number of sprouts per bead, attesting an increased migratory phenotype for the arterial ECs. However, HPMECs showed very little

angiogenesis potential, with most beads without any sprouts at all. This was also correlated with a very low length of these sprouts. Overall, the different ECs had slightly different sprout length after 48h of culture, with HCMEC and HAoEC observed as the most angiogenic of the 4 other organ-specific ECs. Considering the right cell type for the creation of vascularised *in vitro* model also requires investigating the potential of these cells to create accurate 3D models of capillaries.

ii. Self-assembled networks in fibrin hydrogels within the LOC device

To further investigate their potential in creating perfusable vascular networks in our LOC device, we seeded the same cells in a fibrin hydrogel but in single cells to observe their ability to form capillaries as described previously. We seeded 3.10^5 EC in 20µL (15.10^6 cells/mL) of fibrin hydrogel in the central well and cultured the cells for several days to allow them to self-assemble into capillary structures as observed in figure 4.23.

Embedded in a degradable 3D environment such a fibrin hydrogel, ECs spontaneously form capillary structures via vasculogenesis in approximately 48 to 72h. As observed for the fibrin bead assay, organotypic ECs formed very heterogeneous vascular networks in fibrin hydrogels. While HUVEC-RFP formed tightly interconnected structures within 48h, ECs from big arteries such as the aorta (HAoEC) or the coronary artery (HCAEC) failed to form a closed capillary network. Although HAoEC formed some capillaries that could be perfused, their vasculogenic potential was lower than HUVECs. Interestingly, HCMECs, that had a very high angiogenic potential, created a very chaotic network of capillary-like structures with a lot of very small blood vessels.

We also wanted to compare the ability of stem cell-derived ECs to form blood vessels in the same environment than primary ECs. As seen in figure 4.23, both commercially available iPSC-ECFC and ECs derived from our genetically engineered H9-ETV2 line performed very well. The interconnected network of capillaries formed by the cells was very similar to the one observed with HUVEC and was stable for few days. Furthermore, we observed a very fast formation of these structures in the ETV2-ECs that formed these blood vessel networks in 24h while other ECs required 48h minimum.

The culture of these organ-specific ECs in hydrogel also gave us an indication of their potential to degrade ECM. Indeed, after the formation of the vascular network via vasculogenesis and without introduction of flow, the blood vessels rapidly started to collapse. On average 4 to 5 days after the creation of the hydrogel, the network could not be observed anymore, and some parts of the hydrogel were digested by the cells. This observation confirmed the need for the introduction of a perfusion system to keep these vascular networks viable over time.
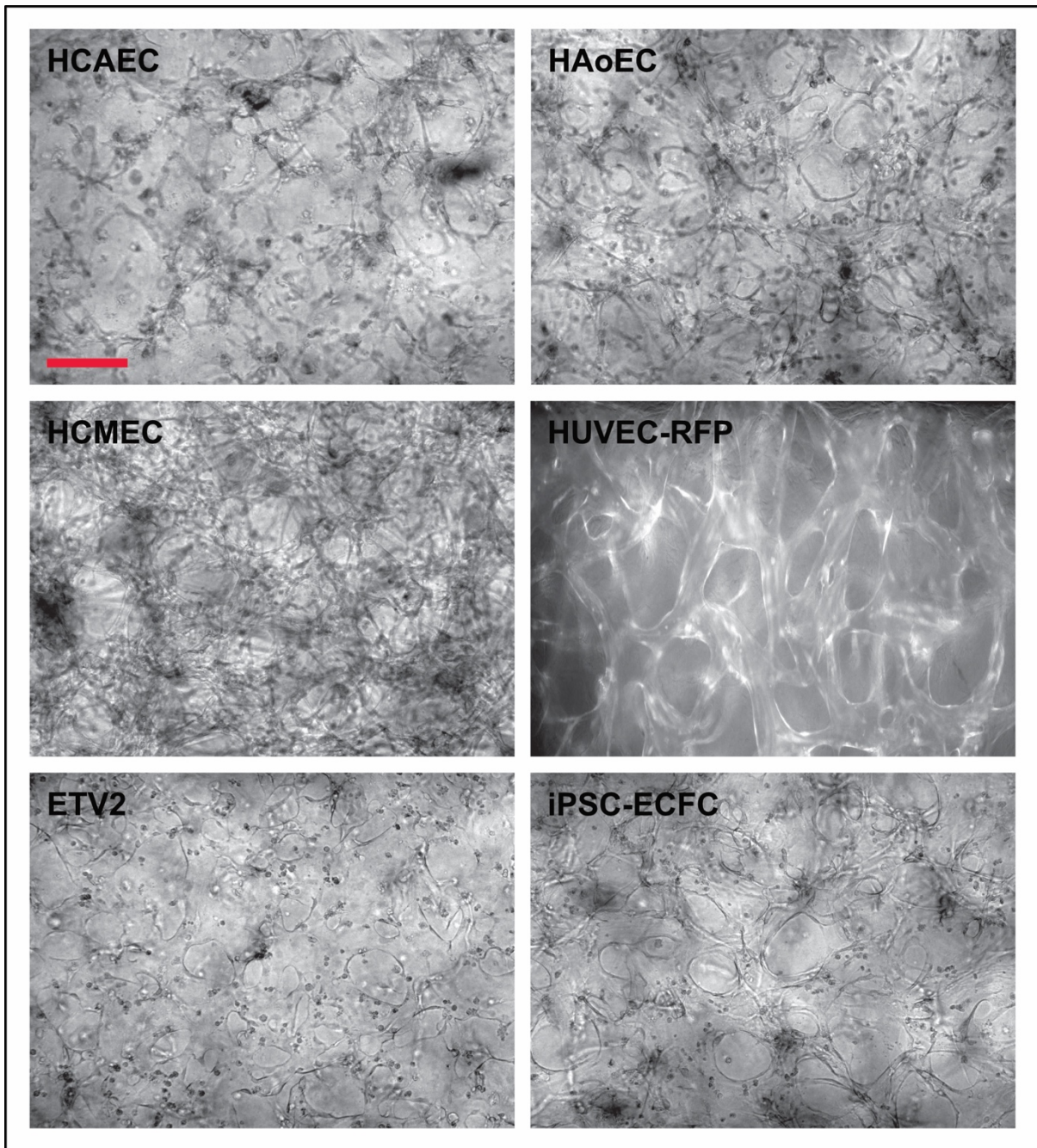
Figure 4.23: Vasculogenesis potential of organ-specific ECs. Photographs of HCAEC, HAoEC, HCMEC, HUVEC-RFP, ETV2-EC and iPSC-ECFC embedded in a fibrin hydrogel (15.10^6 cells/mL) and cultured in the LOC device for 48h. Scale bar: 100µm.

c. Continuous perfusion of self-assembled vasculature and their use for immune cell/EC interaction

With the ability of our VOC platform to plug on and off the perfusion system, we could validate the presence of a perfusable lumen in the self-assembled capillary networks in fibrin hydrogels.

To demonstrate perfusion of the vascular structures in our VOC, we inoculated a bolus of fluorescently labelled (Alexa 647) secondary anti mouse-specific antibody (mAb-647). Figure 4.24A shows fluorescence images relative to a representative experiment 1s after the mAb-647 has flowed through the main channels (FR =150uL/min). The top panel corresponds to an RFP signal of RFP-tagged HUVEC, the lower panel corresponds to signal from the mAb-647 demonstrating that the vascular-like structures are fully perfused. The same microscopic field returned to very low signal after 5s of perfusion demonstrating that the mAb didn't leak through the network in the timeframe of this experiment (60s).
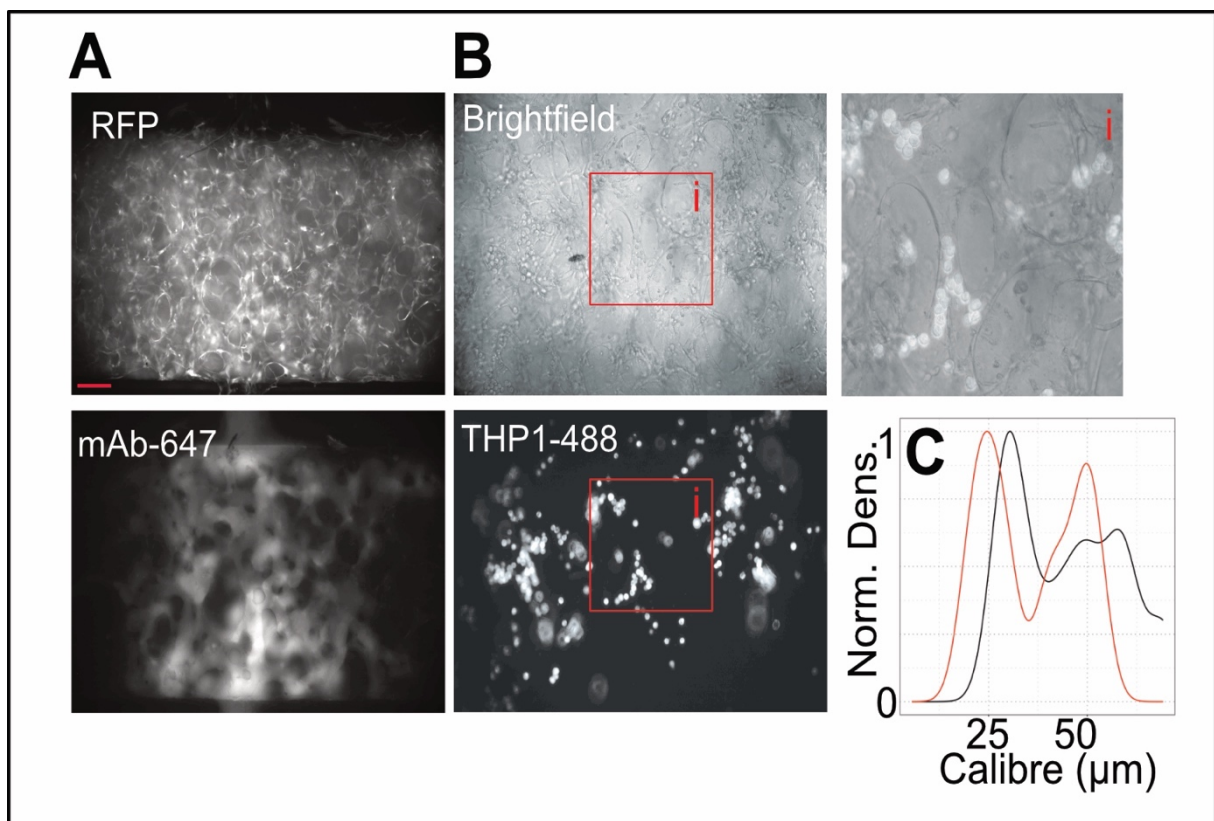
Figure 4.24: Perfusion of self-assembled network in hydrogels. A) Photograph of the vascular network formed in a fibrin hydrogel by HUVEC-RFP after 72h in culture. Images represent a snapshot of the HUVEC-RFP signal on top and the mAb-647 signal on the bottom during continuous perfusion of the antibody at 150μL/min. Scale bar: 200μm B) Photograph of the vascular network formed in a fibrin hydrogel by HUVEC after 72h of culture. The network was perfused with THP-1 monocytes stained with CellBrite Cytoplasmic Membrane dye Green (Biotium, UK) and a snapshot was taken for brightfield signal and green, fluorescent signal. A crop (i) shows the close interaction of THP-1 in perfused capillaries. C) Quantification of microvessel width (in μm) formed in fibrin hydrogels before (red trace) or after perfusion (black trace).

Inspection of the lumen of the structures as highlighted by the mAb-647 perfusion demonstrates that they lack hierarchical organisation and that they are reminiscent of sinusoidal/immature vasculature as that found during early phases of wound healing. To further demonstrate effective perfusion, we performed an experiment where we inoculated a bolus of THP-1 monocytes, reasoning that monocyte should adhere to activated EC such as those in engineered vascular networks. As expected, THP-1 monocytes entered the engineered vascular network and several adhered to the ECs (Fig. 4.24B main and zoomed in view, i). Finally, to estimate the structure of these networks we measured the calibre of several structures in independent experiments (Fig. 4.24C). Quantification of structures with or without active perfusion demonstrates that 1) in average vascular-like structures in fibrin hydrogels have calibres of 25-80μm (5-10 times bigger than small capillaries observed *in vivo*) and 2) that perfusion further enlarges these structures demonstrating creation of positive pressure within the network.

Overall, this experiment demonstrates the ability of our system to continuously perfuse hydrogels systems with self-assembled vasculature and will allow the implementation of different experiments requiring perfusion such as immune cell/EC interaction. However, blood vessels formed in this setup do not resemble appropriately capillaries found *in vivo* and further complexification of the system is needed.

10- **A new matrix-free model of vasculature-on-chip**

a. **Optimisation of a co-culture system to create a gel-free vasculature and study organ-specific heterogeneity**
i. **Implementation with organ-specific ECs**

To overcome the limitation of hydrogel-based systems, we have refined an existing organotypic co- culture assay (Organotypic Vasculo-/Angio-genesis Assay, OVAA)(Bishop, 1999; Wei et al., 2021) to create biomimetic vascularised microtissues. This co-culture assay combines the creation of vascular networks from ECs seeded in single cells and their maturation via sprouting angiogenesis. The long-term culture (weeks) of ECs and stromal cells such as fibroblasts allows the creation of vascular networks without use of exogenous matrix.

Previous work has shown the value of the OVAA to create patent capillary networks using HUVEC and human dermal fibroblast (HDF) in a two-week timeframe. Here we have optimised the OVAA to generate capillary networks using different organ-specific EC. Figure 4.25A shows representative low magnification images of our optimised OVAA employing

different endothelial cells in control conditions or under VEGF-A stimulation (after CD31 staining). Qualitative and quantitative analyses of microvascular networks generated by the OVAA demonstrate that the system faithfully recapitulates the reported effect of VEGF-A on angiogenesis and highlights striking differences in the intrinsic angiogenic potential of EC from different vascular beds. Figure 4.25B shows high-resolution images of the same capillary-like structures highlighting how the OVAA allows investigating key angiogenic processes such as tip cell selection, vascular branching, intussusceptive angiogenesis, and generation of filopodia.

As we previously reported (Chesnais et al., 2022a), ECs isolated from different vascular beds are highly heterogeneous at the population and at the single cell level. To analyse the complexity of the vascular networks in an unbiased way, we used previously published protocol using a Fiji plug-in, Angioanalyser (Carpentier et al., 2020). This allowed the segmentation of the vessels and the analysis of their composition to highlight differences in length of the network, branches of the vessels or number of junctions as detailed in supplementary figure 4.6. This analysis revealed appreciable differences in organ-specific EC angiogenic potential as highlighted in figure 4.25C. Although all 3 lines responded to VEGF-A treatment as expected (i.e., an increase of the network complexity), they had different intrinsic angiogenic potential under similar experimental conditions. HUVEC and HAoEC had a high proliferative and angiogenic phenotype, forming a highly interconnected network whereas the HPMEC only formed few thin vascular structures composed mainly of thin branches with a low number of big vessels, a small length of the network and only few junctions between capillaries.
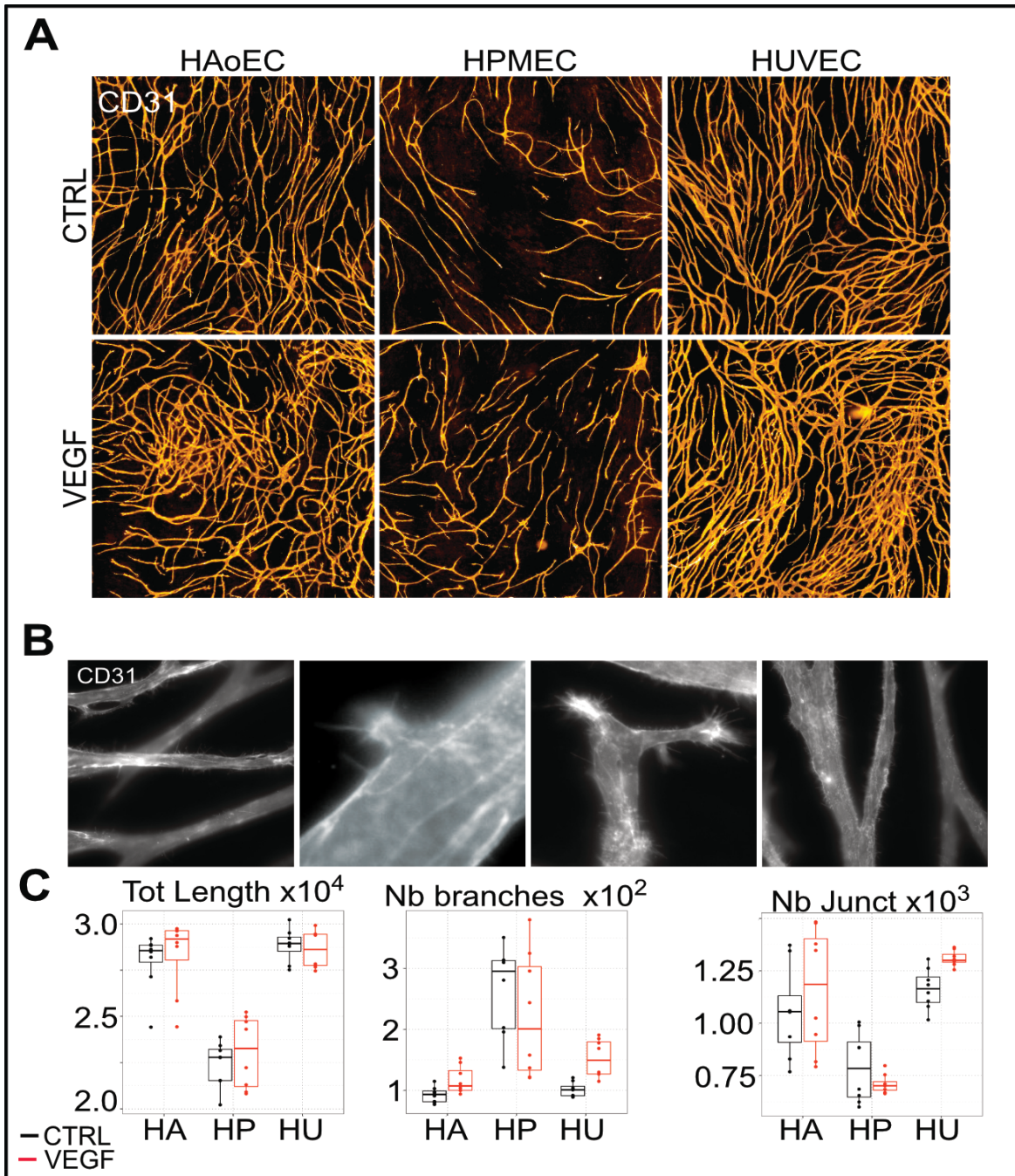
Figure 4.25: Endothelial/fibroblast co-culture vasculogenesis/angiogenesis assay (OVAA). A) Photographs of vascular networks formed by human aortic endothelial cells (HAoEC), human pulmonary endothelial cells (HPMEC) and human umbilical vein endothelial cells (HUVEC) in co-culture with human dermal fibroblasts (HDF) for 14 days and immunostained for CD31 (PECAM1). Panels show representative images of the different EC lines angiogenic potential in control conditions (EGMV2 medium) or after treatment with 50ng/mL VEGF-A. Scale bar: 200μm B) Representative images of vascular processes such as tip cell selection, vascular branching, intussusceptive angiogenesis and filopodia in the vascular networks formed by HUVECs in OVAA, stained for CD31 after 14 days and images at 63X magnification. Scale bar: 50μm C) Quantification of the vascular network complexity in the OVAA with FIJI and the AngioAnalyser plugin. Parameters such as total network length, number of branches and number of junctions have been quantified in control conditions (black) or upon VEGF treatment (red) for the 3 different EC lines in 4 separate experiments and for 2 donors for each EC line.

ii. Adaptation to culture stem cell-derived ECs

Following the adaptation of the system with primary ECs, we wanted to characterise the ability of our stem cell-derived ECs to form vascular networks and compare it to other ECs. As seen in figure 4.26, the ETV2-ECs obtained as described in chapter 3 were able to form complex vascular networks in co-culture with fibroblasts. After 2 splits and the generation of a homogeneous population of ECs, we cultured the cells on top of a fibroblast monolayer for 14 days under different treatments. To compare their ability to perform vasculogenesis and angiogenesis with the other EC types, we cultured the ETV2-ECs in EGMV2 either with or without doxycycline. As seen in figure 4.26A, cells in control conditions without doxycycline formed a very nicely interconnected network of capillaries that resembled the networks formed by HUVECs (Fig. 4.26F). However, the addition of VEGF-A or bFGF seemed to fragilize the vessels and reduce their angiogenic ability as seen in figure 4.26B-C. This phenotype was rescued by the addition of doxycycline (Fig. 4.26D) but also seen when VEGF-A and doxycycline were added to the medium (Fig. 4.26E). The quantification of the network complexity confirmed these results with the lower number of nodes and junctions in cells with or without doxycycline (Fig. 4.26G). The vessels formed appear to be thinner and mainly produce branches and extremities, with an overall less complex network.
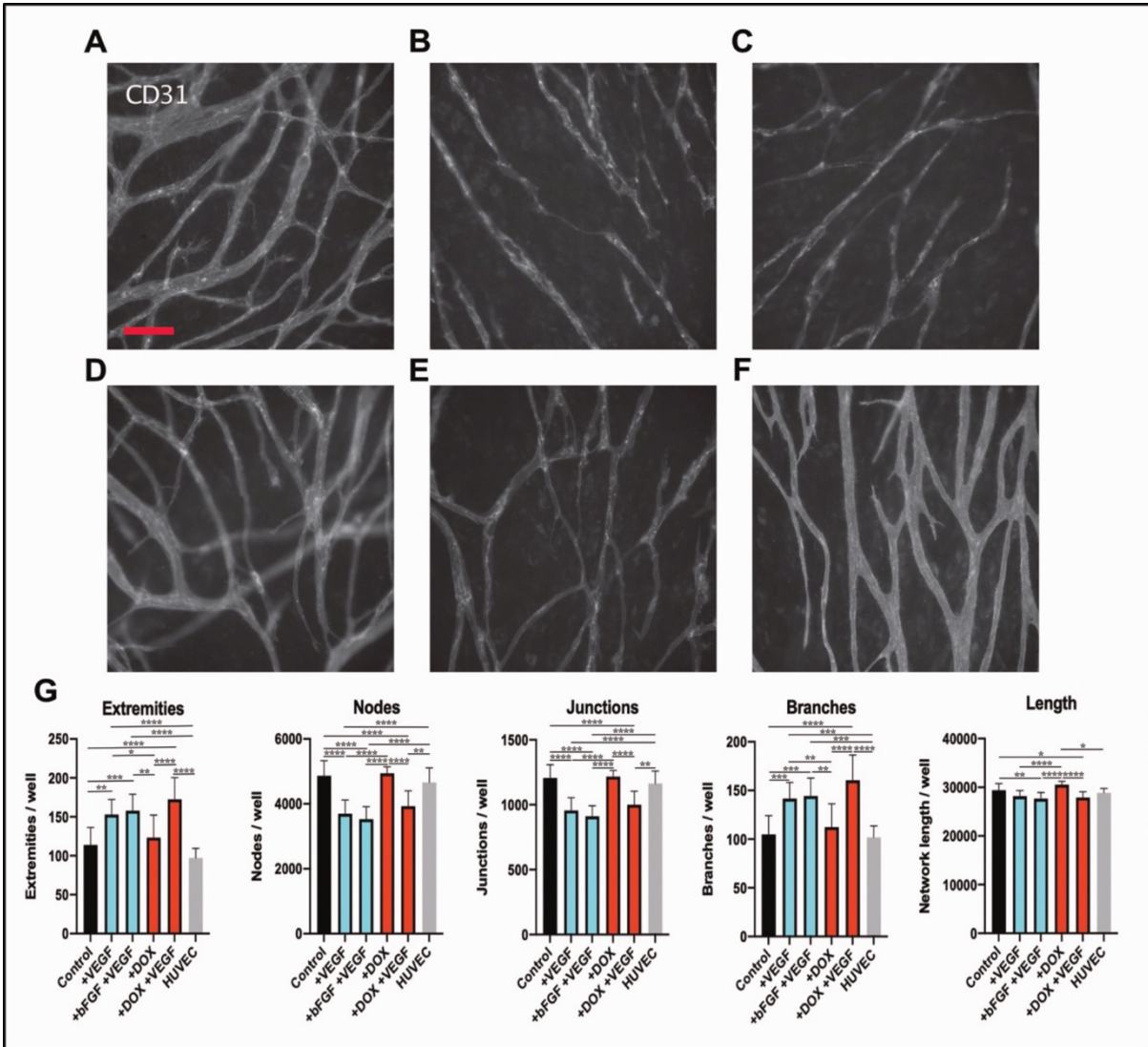
Figure 4.26: OVAA system with stem cell-derived ECs. ECs obtained from H9-ETV2 were co-cultured with HDFs for 14 days on stained for CD31. Cells were cultured in without doxycycline in control conditions (EGMV2)(A) or treated with VEGF-A (B), bFGF and VEGF-A (C) or with doxycycline (D) and VEGF-A (E). F) HUVEC co-cultured with HDFs in control conditions after 14 days in culture. G) Quantification of the vascular network complexity using the Angioanalyser pipeline. n=8. Scale bar: 50µm.

Interestingly, although the ETV2-ECs needed a constant activation of ETV2 as described in the previous chapter, their angiogenic potential was very similar to HUVECs cultured in control conditions.

Overall, using our optimised OVAA, we were able to grow capillaries using combinations of different ECs (HUVEC, HPMEC, HAoEC, ETV2-EC) and ECM secreting cells such as HDFs; thus, OVAA enables recapitulating different vascularised tissue microenvironments.

b. Implementation of the co-culture to study EC angiocrine signalling

Apart from the capacity to form different vascular networks, we hypothesized that organ-specific ECs could be heterogeneous angiocrine signalling. As reported previously, ECs have a crucial role in the development and regeneration of several organs such as the liver, pancreas or long bones (Ding et al., 2010; Kusumbe et al., 2014; Lammert et al., 2001). To validate this hypothesis, we decided to adapt our co-culture system to study the effect of ECs on the maturation of iPSCs.

i. Optimisation of the system to introduce iPSC-derived pancreatic islets

Standard methods to culture and differentiate organoids from stem cells often use exogenous matrix components such as Matrigel™, natural or exogenous hydrogels to create a 3D environment suitable for the expansion of organoids. However, these microenvironments do not fully recapitulate the stiffness and protein components found *in vivo* and products such as Matrigel™ often have a batch-to-batch variation leading to different yields in stem cell differentiation. With the aim of studying the effect of ECs on pancreatic organoids differentiation and possibly replace Matrigel™ culture, we decided to adapt our co-culture protocol to embed pancreatic organoids.

In collaboration with the lab of Dr. Rocio Sancho, we first attempted to optimise the culture of the organoids under different conditions. Since the organoids need an ECM component to grow, we decided to add them to the co-culture on after enough matrix was produced, at the end of the protocol after 14 days of EC culture. Figure 4.27A shows a snapshot of the morphology of the organoids 4 days after seeding. After 21 days in culture (Fig. 4.27B), we can observe the growth of organoids from small organoids observable at day 4 but also from "single cell" organoids that were not visible at the beginning of the culture, attesting of the growth of pancreatic organoids in our co-culture system.

To decide the optimal timing for the introduction of the organoids and observe their behaviour and proliferation, we performed different seeding experiments. We decided to seed the organoids either as "single cells" obtained from organoids grown in Matrigel™ or as small organoids. Figure 4.27C and D represent the vasculature after 21 days of co-culture of the OVAA with the pancreatic organoids. We did not observe any difference in the growth of the vasculature in between the two different seeding condition but observed that the seeding of

organoids already formed gave rise to bigger organoids at the end of the experiment and decided to perform the next experiments with this setting.

Figure 4.27E shows the viability of the cells in culture as attested by the number of "live" cells that are stained with calcein. The channel used for dead cells overlapped with the signal of the HUVEC-RFP used in this specific experiment but very few dead cells could be observed in the culture, with a viable cell percentage >99%.

Finally, a qualitative observation of the organoid morphology as observed in figure 4.27F revealed differences between the organoids in the different conditions. Organoids grown in Matrigel^{TM} often grow a hypoxic core as observed in the picture showing organoids in culture after 21 days. This was rarely the case for the organoids grown in our OVAA system or in culture with fibroblasts only. Overall, the pancreatic organoids could be cultured in our system, keep their organoid shape with a lumen as observed in the live/dead assay, kept proliferating and did not form hypoxic parts. Although these organoids seemed to proliferate in our system without exogenous matrix, we still needed to confirm that they were able to differentiate in this setup.
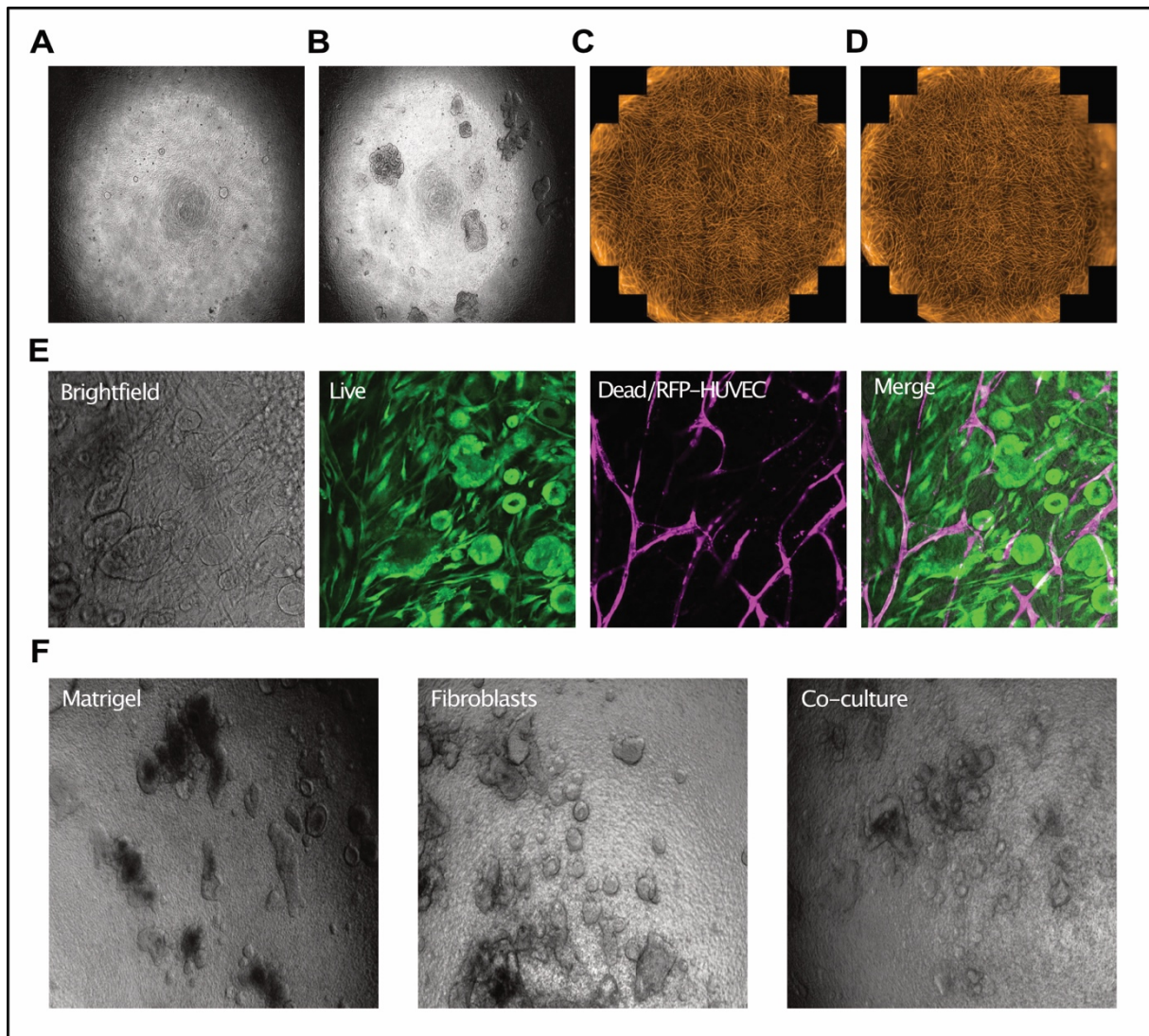
Figure 4.27: Implementation of the culture of iPSC-derived pancreatic organoids in the OVAA. A) Photograph of the morphology of iPSC-derived pancreatic organoids after 4 days in culture in the OVAA. B) Organoids after 21 days in culture in the same well. C) Whole well image of the vascular network immunostained for CD31 after 14 days of culture and 21 days of co-culture with organoids seeded as single cells. D) Vasculature immunostained for CD31 after co-culture with organoids seeded as small organoids. E) Live/dead assay of the organoids in co-culture in the OVAA after 21 days of culture. Images represent the brightfield signal, the green signal corresponding the live cells, the red signal corresponding to dead cells and the RFP signal of HUVEC-RFP and the merges channels. F) Morphology of the different organoids cultured for 21 days in Matrigel™, in co-culture with fibroblasts only or in co-culture in the OVAA with HUVECs.

ii. Long term culture and differentiation of pancreatic organoids in co-culture with self-assembled capillaries without exogenous matrix

The culture in Matrigel™ domes allows an easy maintenance and differentiation of the pancreatic organoids by switching between different media containing growth factors and cytokines as described previously (Cujba et al., 2022; Pedraza-Arevalo et al., 2022). Adapting the protocol for our co-culture system meant that we had to change the medium composition to allow both the pancreatic progenitors, fibroblasts and ECs to survive, proliferate and

differentiate. To do so, we mixed both media in which cells are normally cultured in the same ratio but kept the same final concentration of growth factors and cytokines. To observe if the organoids kept their pancreatic fate in the co-culture and observe the interaction with ECs, we first stained the organoids for PDX1, a pan-pancreatic marker and CD31 as an EC-specific marker (Fig. 4.28).
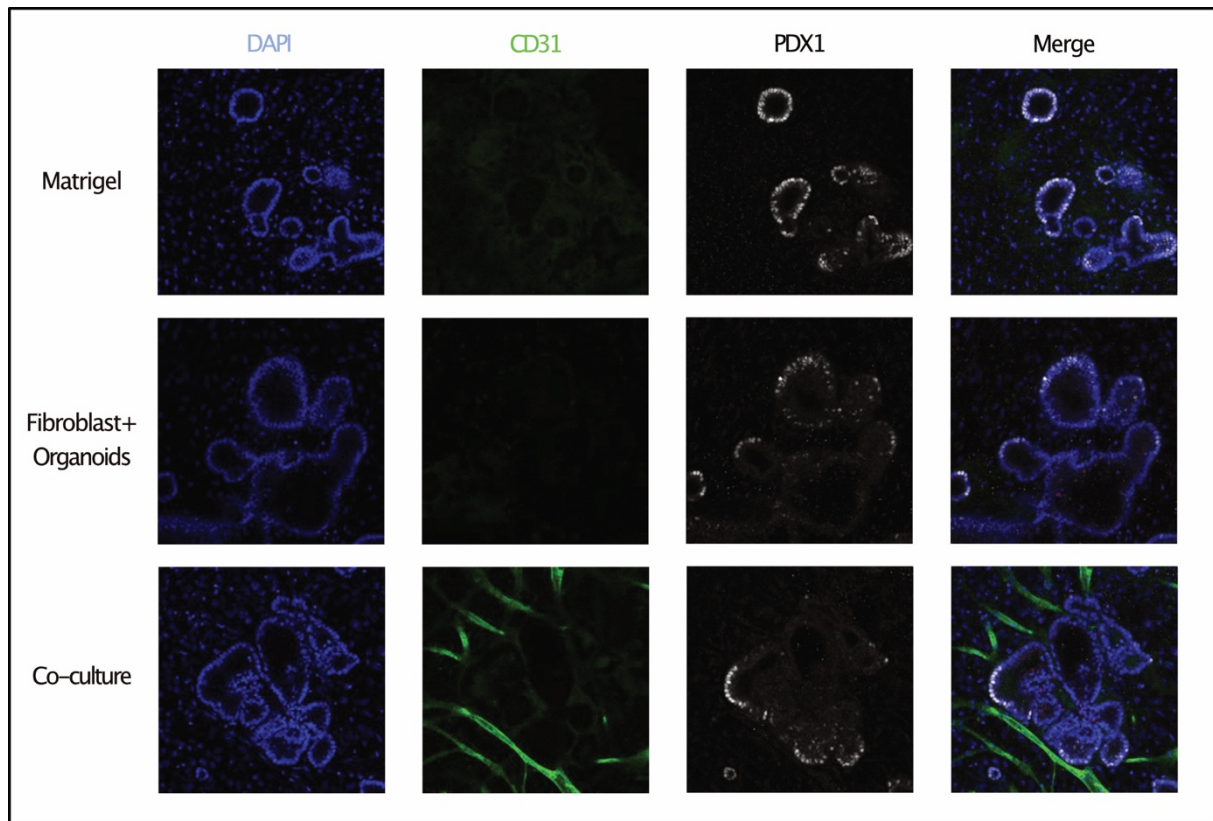
Figure 4.28: Immunostaining of iPSC-derived pancreatic organoids in expansion. Organoids were cultured in Matrigel™, in co-culture with fibroblasts only or in co-culture in the OVAA with HUVEC for 16 days and immunostained for CD31 and PDX1.

The protocol to culture iPSC-derived pancreatic organoids contains a step of expansion to allow the organoids to proliferate before the differentiation of the pancreatic progenitors to mature beta cells. (Cujba et al., 2022; Pedraza-Arevalo et al., 2022). As observed in figure 4.28, the organoids cultured in Matrigel™, in co-culture with fibroblasts or in the OVAA all proliferated and kept their shape with a distinct lumen as demonstrated by the images taken at a specific confocal layer. Cells kept their expression of PDX1 in all conditions, but qualitative observation revealed a lower expression of the pancreatic marker in the co-culture with fibroblasts only and OVAA compared to the Matrigel™ control. However, we could observe an interaction between the organoids and capillaries in our co-culture system, although the vessels did not directly penetrate the organoids. This could be due to the fact that the organoids

were seeded on top of the co-culture and did not have time to penetrate the matrix. We also did not observe any formation of hypoxic core in the organoids, that could explain why the vessels did not penetrate the "normoxic" organoids.

To determine if the co-culture system has an impact on the differentiation of the organoids, we proceeded to differentiate the pancreatic organoids further into beta cells. This implied the daily change of medium with different cytokines and growth factors as described in methods. The immunostaining for mature beta cells markers such as insulin and somatostatin is revealed in figure 4.29.
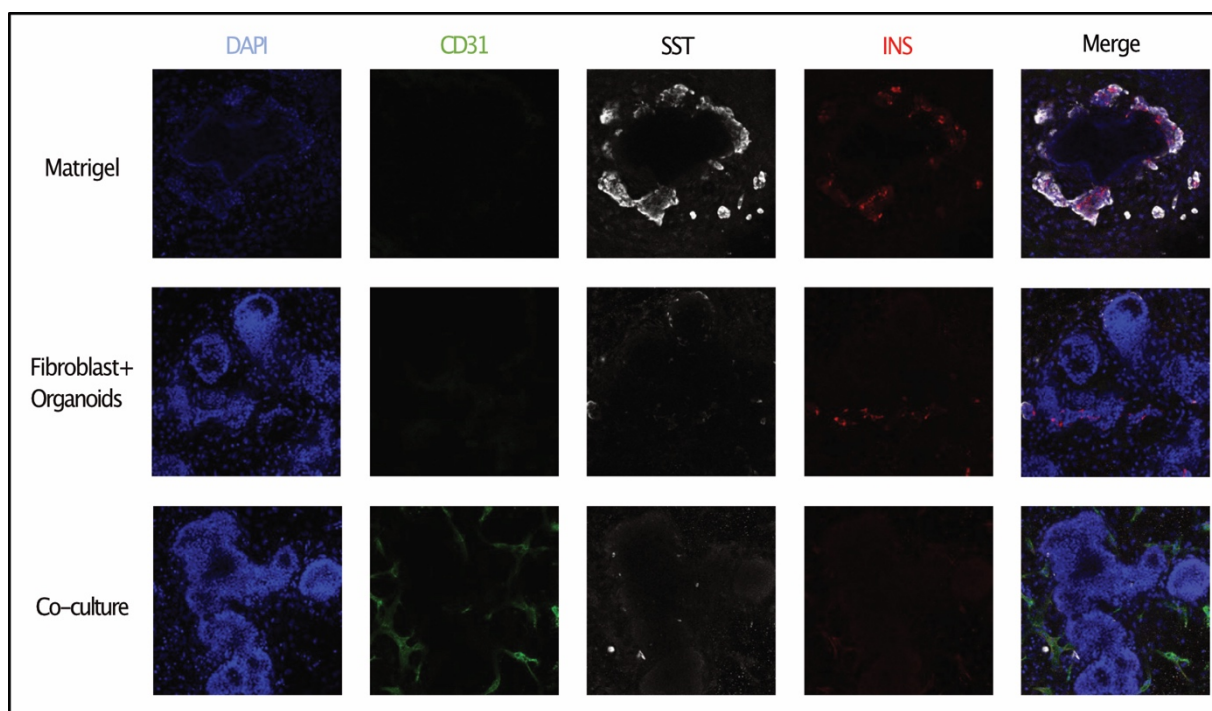
Figure 4.29: Immunostaining of iPSC-derived pancreatic organoids after differentiation. Organoids were cultured in Matrigel^{TM}, in co-culture with fibroblasts only or in co-culture in the OVAA with HUVEC for 21 days and immunostained for CD31, somatostatin (SST) and Insulin (INS).

As shown by the expression of somatostatin and insulin by the organoids cultured in Matrigel^{TM}, the differentiation is successful in creating mature beta cells. However, the culture of the same organoids in the layer of matrix secreted by fibroblasts only or in co-culture in our OVAA system with HUVECs almost totally inhibited their differentiation. We could observe the capillaries being formed as demonstrated by the CD31 staining, but only few cells per organoid were seen expressing somatostatin or insulin.

With the knowledge that only a certain population of EC promoted the differentiation of pancreatic progenitors in the developing pancreas (Lammert et al., 2001), we hypothesized that the angiocrine signalling of appropriate ECs could be needed to enhance the differentiation of pancreatic cells. To test, this hypothesis, we performed a preliminary screen on several organ-specific ECs as described in figure 4.30.

The OVAA was adapted to create capillaries with HUVEC, HAoEC or human pancreatic microvascular ECs (HPaEC) and the pancreatic organoids were cultured and differentiated for 21 days. We can observe that the 3 different EC populations created capillaries, but the HPaEC had a lower angiogenic potential, like the HPMEC described previously (Fig. 4. 25).
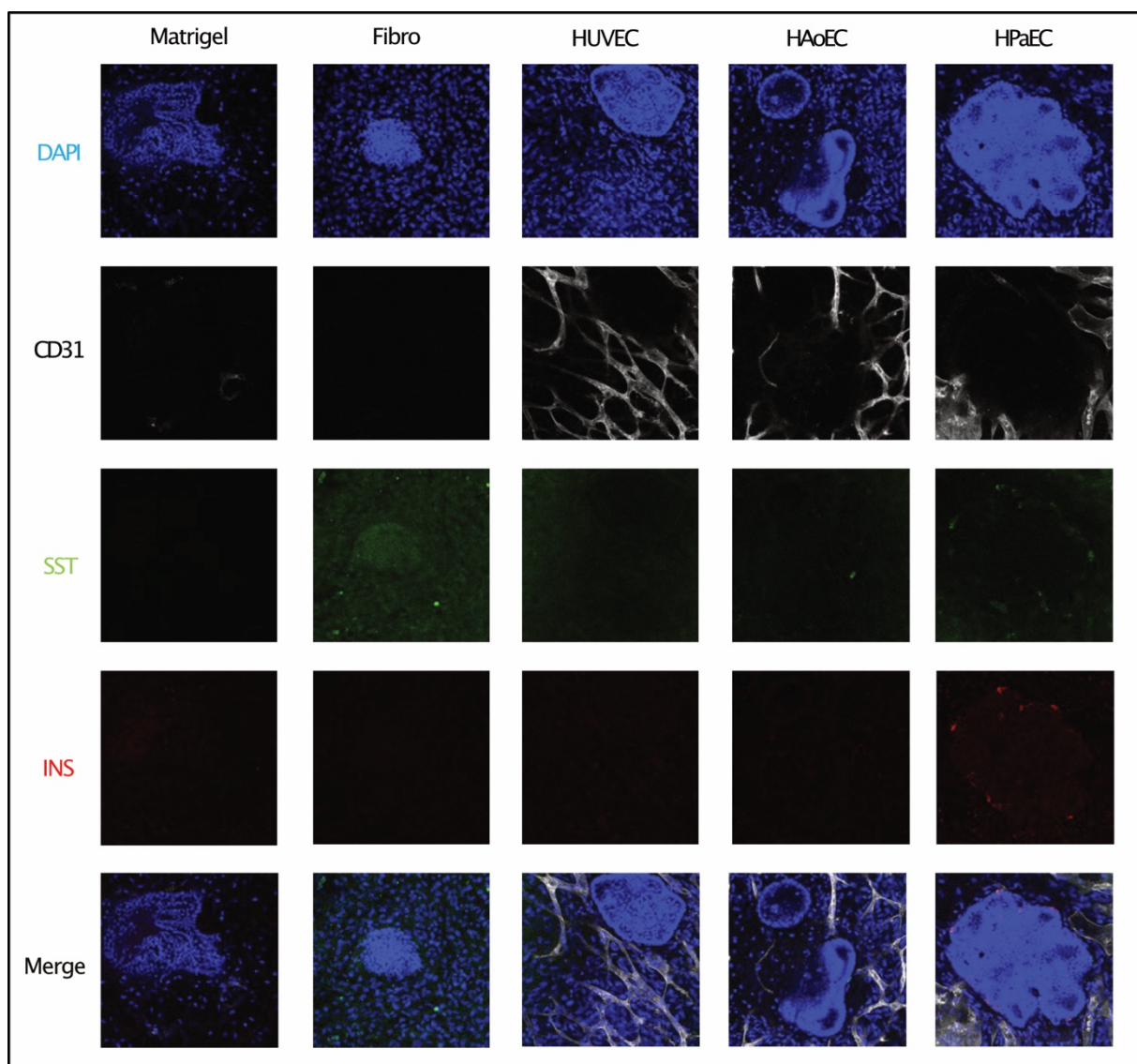
Figure 4.30: Immunostaining of iPSC-derived pancreatic organoids after differentiation with different organ-specific ECs. Organoids were cultured in Matrigel[TM], in co-culture with fibroblasts only or in co-culture in the OVAA with HUVEC, HAoEC or HPaEC for 21 days and immunostained for CD31, somatostatin (SST) and Insulin (INS).

Unfortunately, in this experiment we could not observe a successful differentiation of the pancreatic progenitors, even in the Matrigel™ domes used as control. However, qualitative observations of several organoids in the different conditions showed an encouraging number of cells expressing insulin and somatostatin in organoids co-cultured with pancreatic ECs as observed in figure 4.30. Overall, the implementation of iPSC-derived pancreatic organoids in our OVAA system allowed us to validate its use for the culture, proliferation and differentiation of stem cell-derived organoids. This technology could be optimised to replace the culture of organoids in Matrigel™ and be exploited for the creation of more complex vascularised tissues.

11- **Implementation of the co-culture system allows continuous perfusion and maturation of the vasculature-on-chip system**

As shown above, hydrogel systems are convenient to create and perfuse self-assembled vascular networks, however, they do not allow vascular maturation and remodelling. To overcome this key issue, we combined our OVAA and VOC perfusion system as detailed in methods to generate biomimetic vascular networks which can remodel over time in response to flow.

a. Optimisation of the system in the LOC device

The implementation of the co-culture system required to be adapted for the VOC device. In static conditions, fibroblasts or stromal cells are seeded first to secrete matrix and ECs are seeded later and cultured for 14 days. However, with the introduction of the cells in the LOC device, the surface properties and environment for the cell seeding are very different than the ones in standard cell culture plates. First, cells are seeded on glass that has not been treated for cell attachment and the walls of the LOC are made with PDMS. In the first attempt to seed cells within the VOC device, we observed a very low cell adhesion and a retraction of the cells after few days. To increase cell adhesion, we introduced a coating step with a mix of FBS and fibronectin. This allowed the ECs to adhere in the channels and help with the adhesion of fibroblasts in the central well. To increase the adhesion properties of the glass, we also introduced a step to etch the glass in the central well to create a rougher surface and increase fibroblast adhesion.

With the surface properties optimised for cell culture, we focused on the optimisation of the VOC system without the need of exogenous matrix. The aim of this system was to create a

complete model of vasculature comprised of side channels (aA and eV) and a central well that can be filled with cells creating a capillary bed. To do so, we optimised the co-culture protocol used previously in static conditions and adapted it for the LOC device. Figure 4.31A shows the timeline for the creation of a perfused vasculature-on-chip created only with cells.
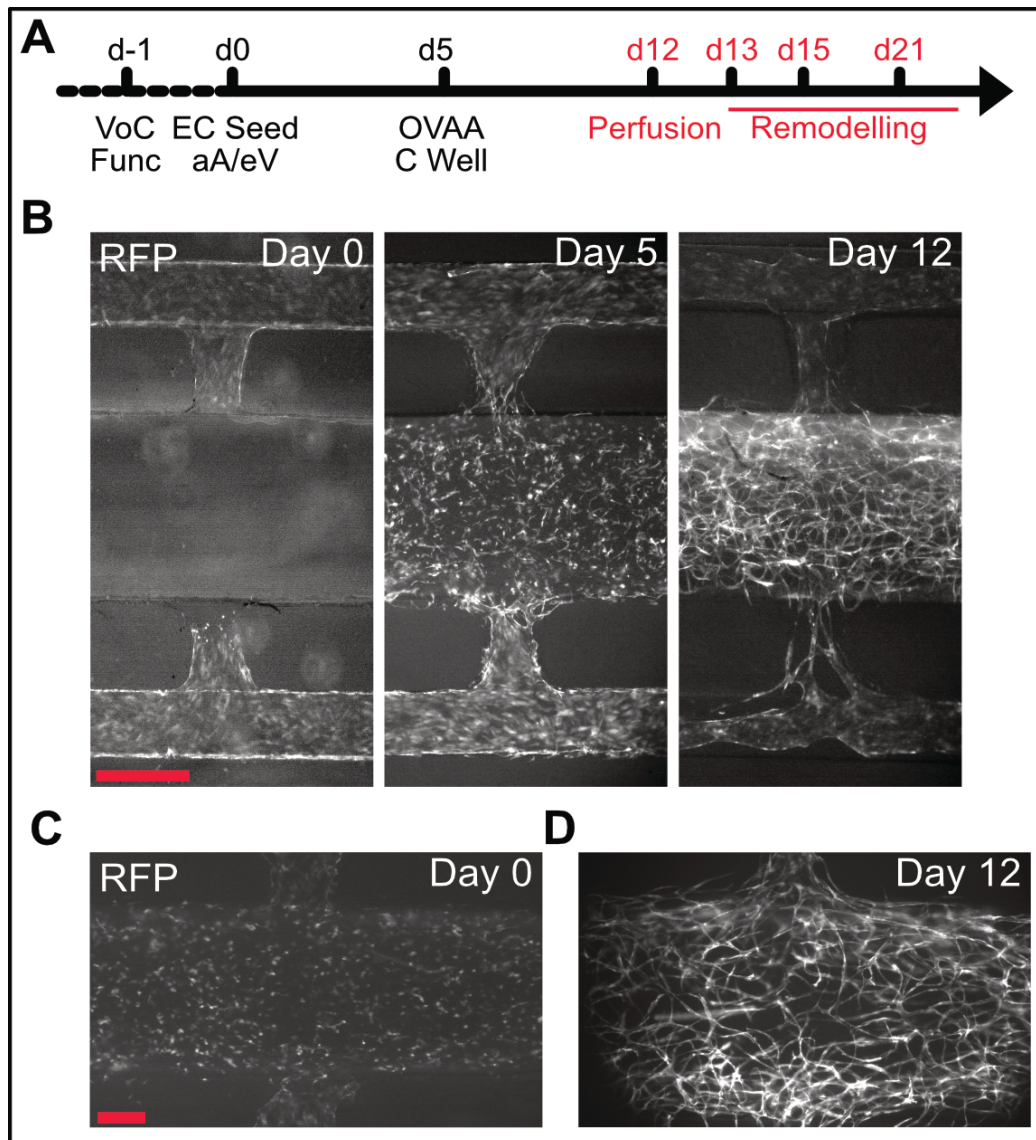
Figure 4.31: VOC timeline and versatility. A) Timeline for the creation of perfused vasculature-on-chip. The VOC is first coated with fibronectin to promote the adhesion of ECs in the side channels. At day 0, ECs are seeded in the side channels (aA and eV) and left in culture for 5 days to coat the channels on all sides. At day 5, the co-culture of ECs and FBs is seeded in the central well and cultured in static conditions for 7 days to promote capillary network formation. At day 12, the VOC can be linked to the microfluidic system and continuously perfused. B) Photographs of the VOC system with HUVEC-RFP at day 0, 5 and 12 of culture in co- culture with HDF. Scale bar: 500μm. C) Photographs of the VOC system with HUVEC-RFP at day 0 and 12 of culture in co-culture with MSCs. Scale bar: 250μm.

The first step of the matrix-free VOC is the seeding of ECs in the side channels to create the model of blood vessels with the coating of the PDMS channels with ECs. The channels are coated with fibronectin overnight and ECs are seeded and left to adhere to the bottom, sides

and top of the channels for 5 days as described in figure 4.31B (Day 0). After 5 days of culture, a mix of fibroblasts and ECs is seeded in the central well as observed by the RFP signal in figure 4.31B (Day 5). To accelerate the process of capillary network formation, we increased the FB and EC cell number in the LOC device compared to the co-culture in static conditions, from 1.10^4 FB and $2.5.10^3$ ECs in static to 1.10^5 FB and 5.10^3 ECs. This allowed the formation of an interconnected vascular network in 7 days of culture as observed in figure 4.31B (Day 12). After a week of co-culture, the capillary network formed only in the matrix secreted by the fibroblasts is ready to be perfused. Interestingly, this method could also be reproduced with other cells producing matrix such as mesenchymal stem cells (MSCs) as shown in figure 4.31C.

b. Introduction of a continuous flow

To introduce an active flow into the system, we used our microfluidic perfusion system that was connected directly to the VOC device. The first attempts to perfuse the capillary network in the central well while keeping the structures intact in the side channels required optimising the flow rates in the system as described previously. Before the onset of the flow, it was necessary to achieve formation of a perfusable network of capillaries in the central well with lumenised structures able to withstand the flow and perfuse through the whole central well to avoid a build-up of pressure. As described in figure 4.32A and supplementary video 4.1, the networks formed in the central well appeared suitable for perfusion after 12 days of culture. The use of HUVEC-RFP allowed us to monitor in detail the formation of these structures and adapt the day at which we started actively perfusing. The immunostaining for VE-Cadherin also revealed the opening of the blood vessels towards the entrance of the side channel and into the junction. The existence of the T-junction between the central well and the side channels was crucial for the creation of a perfusable network. Indeed, the EC lining the side channels allowed a complete anastomosis with the capillaries formed in the central well. In the first days of perfusion, we observed that these structures formed in the connection facilitated the perfusion of the capillaries in the central well by creating a preferential path for the flow. However, as observed in figure 4.32A, these connections were fragile in some experiments and could be detached from the capillaries in the central well.
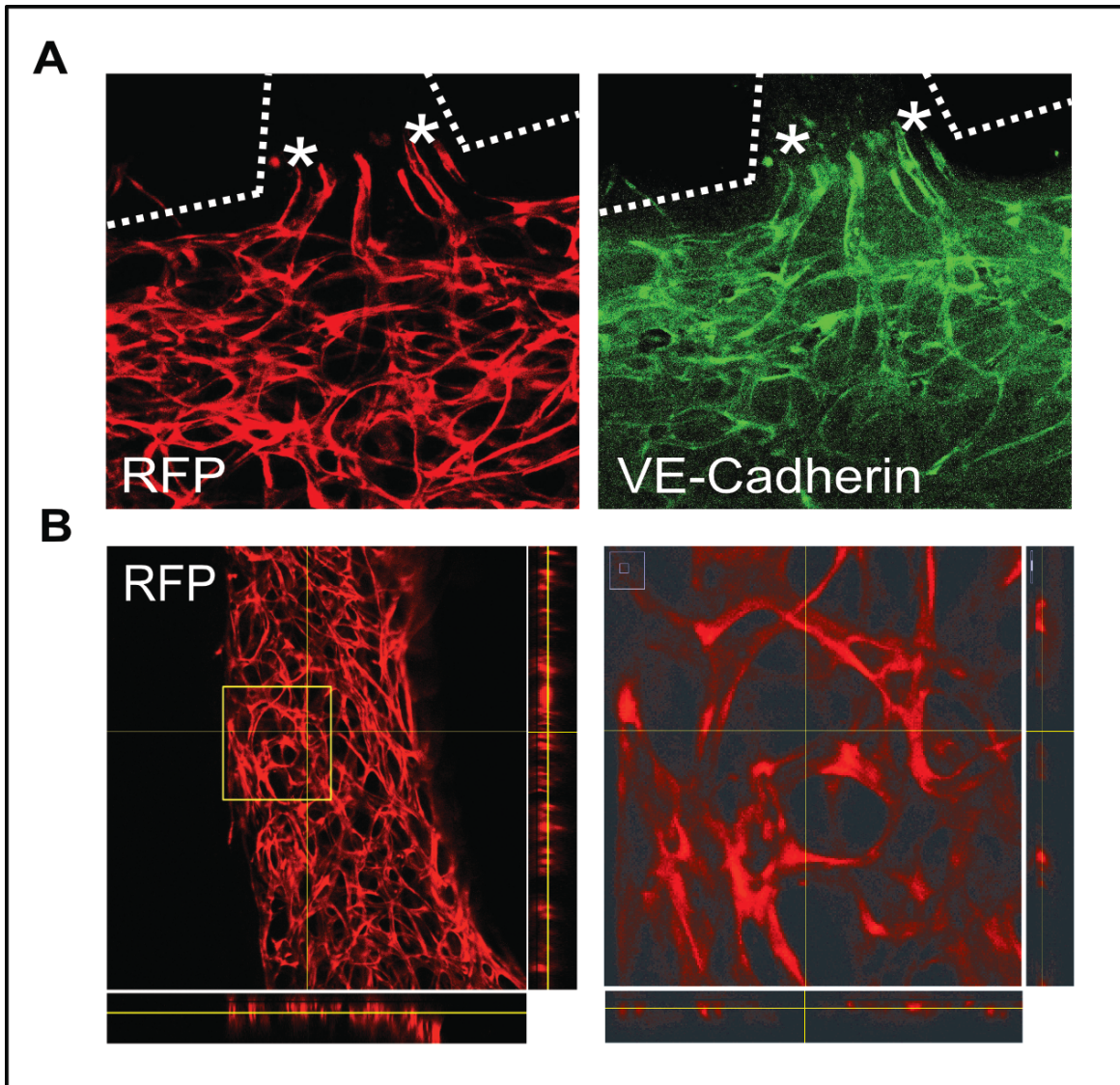
Figure 4.32: Matrix-free formation of perfusable vascular networks. A) Photographs of HUVEC-RFP signal and VE-cadherin staining in the VOC device after 3 days of perfusion, at the junction between the central well and the side channels. B) Confocal images of HUVEC-RFP vascular networks formed in the VOC after 7 days of culture. The 3D-projection shows the complexity of the network and the lumen formed by ECs in the micro-tissue.

The complexity of the vascular network formed in the central well is described in figure 4.32B and supplementary video 4.1. As highlighted by the RFP signal from the HUVEC-RFP, these cells formed an interconnected network of blood vessels in 3D and a confocal stack of these microtissues revealed the presence of lumenised structures.

To demonstrate that our microvascular structures are perfused, we inoculated a bolus of mAb-647 (FR = 500 µl/min) and recorded fluorescence images of the central chamber of our VOC.

Figure 4.33A shows the network formed by HUVEC-RFP in the OVAA-VOC after 10 days of perfusion. We can observe after introduction of the flow a change in morphology of the vessels compared to the capillaries formed in static conditions. Figure 4.33B shows a representative

time-series sequence of recordings demonstrating the mAb-647 bolus can transit through the capillaries in ~10s, differently from parallel experiments using fibrin gels (Fig. 4.24) where the mAb transited completely in less than 5s (and under lower FR = 150µl/min). Further inspection of the time-lapse recording and the capillary structures highlighted by the A647 fluorescence clearly suggests establishment of preferential flow directions through the networks (the central portion of the network is perfused and emptied faster than the lateral portions) and absence of leakage.
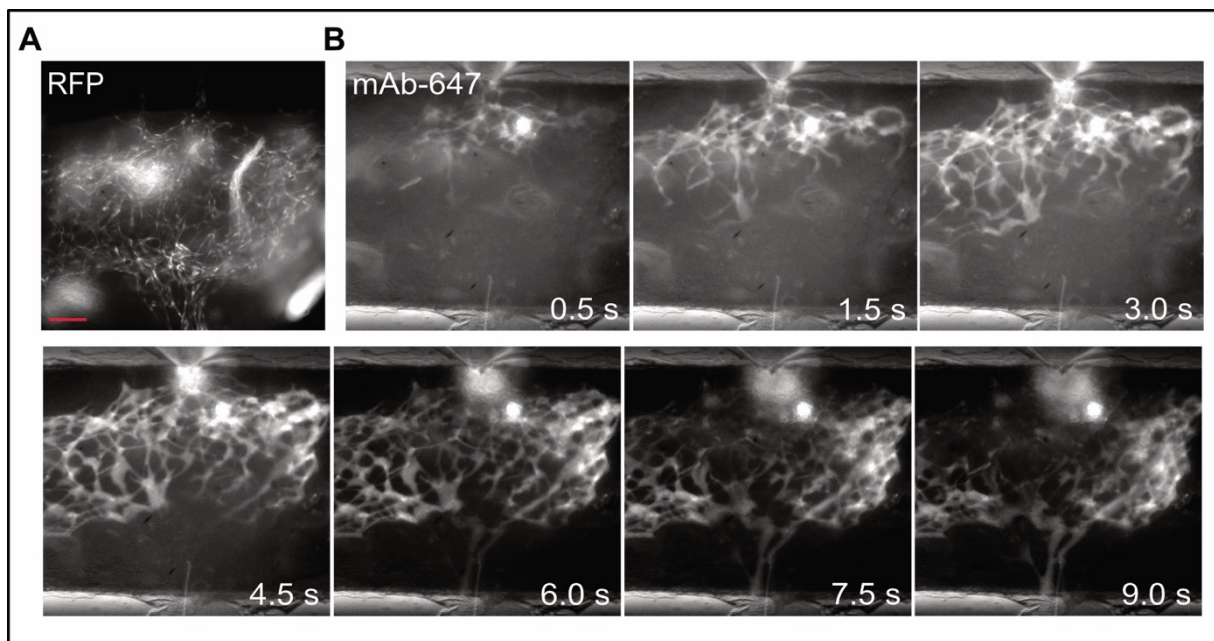
Figure 4.33: Continuous perfusion of the matrix-free vasculature. A) Snapshot of the vascular network formed by HUVEC-RFP in culture in the right side of the VOC system and perfused for 10 days. Scale bar: 200µm B) Time series of the same network perfused with mAb-647 (10µg/mL) at a flow rate of 500µL/min with images taken every second. Scale bar: 200µm.

Furthermore, OVAA-VOC generated capillary networks with a clear hierarchical structure in comparison to enlarged sinusoidal ones observed in the fibrin system. Overall, these data demonstrate that our OVAA-VOC combination enables the creation of vascularised and continuously perfusable microtissues.

c. Flow-dependant maturation of self-assembled vasculature

We qualitatively observed that OVAA-VOC networks under long-term perfusion remodelled over time creating organised structures as observed *in vivo*. Figure 4.34A shows representative images of the same portion of an OVAA-VOC network after one or ten days of perfusion clearly demonstrating remodelling and maturation of the capillary structures in response to continuous flow.
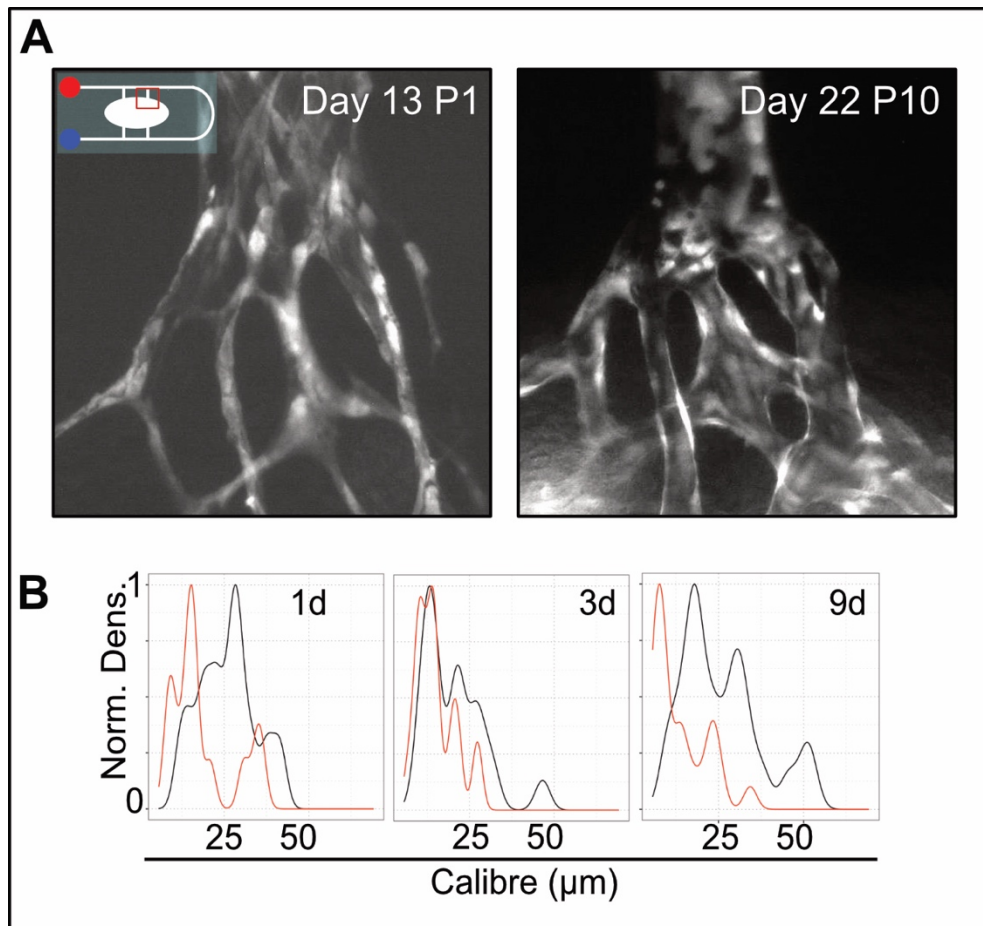
Figure 4.34: Vascular network remodelling over time in response to flow. A) Photographs of HUVEC-RFP microvessels formed in the VOC corresponding to the region highlighted in red box in schematics, after 13 days of culture (1 day of perfusion) and after 22 days of culture (10 days of perfusion) at 500µL/min. Scale bar: 50µm B) Quantification of the blood vessel structure's calibre in the VOC system after 1, 3 or 9 days of perfusion (black line) or without perfusion (red line) for 3 distinct experiments.

To quantify this effect, we measured the calibre of several randomly chosen capillaries at one, three and nine days upon perfusion in three independent experiments. Results of this analysis (Fig. 4.34B) showed that the capillaries created with OVAA-VOC are smaller than those generated in fibrin (red trace in Fig. 4.34A and 4.24C, ~5-40 µm vs 25-80 µm respectively) and that their size increases in response to positive pressure generated by flow. Density distributions of vessel calibre counts also highlighted that over time the network remodelled in such way to progressively generate a hierarchy of larger, medium sized and smaller vessels as highlighted by the three distinct peaks in figure 4.34B panels 3d and especially 9d. Since parallel experiments in absence of perfusion did not show similar reorganisation of the capillary structures, we hypothesize that mechanical forces due to perfusive flow in our system are necessary and sufficient to induce initial network remodelling and establishment of a hierarchical architecture.

Our optimised OVAA-VOC system creates a relatively thick (5-10 cells) tissue in the central well. We observed that when we stopped perfusion in a fully perfused OVAA-VOC the small calibre vessels collapsed (red trace Fig. 4.34B) suggesting presence of elastic forces within the tissue. This observation is also compatible with the need of high FR (in comparison to fibrin) to achieve perfusion and with the observed enlargement of vessels under perfusion (black traces Fig. 4.34B). Supplementary video 4.2 shows changes in microtissue morphology under low FR (~200μl/min, like that used in fibrin systems) suggesting that at this FR the tissue is perfused only during the peak of pressure due to the peristaltic cycle of the pump and that elastic return of the microtissue might cause oscillating flow in the capillaries. Higher FR (> 400μL/min) did not produce this effect, with the medium flowing linearly through the network without evident oscillations.

12- **Discussion**

Creating biomimetic, tissue specific and vascularised microenvironments is a current challenge in tissue engineering. Overcoming this challenge can help addressing greater ones in basic cell biology, regenerative medicine and cancer research. Examples span from the potential to generate functional stem cells derived microtissues *in vitro* for regenerative medicine, or to create predictive disease models (e.g., cancer-on-chip) for drug testing and development. Overall, creating healthy and pathologic microtissues *in vitro* from primary cells or stem cells is revolutionising the way we conduct basic investigations in health and disease and creating appropriate vasculature in these tissues is a major bottleneck to further progression. Here we have addressed this challenge by creating a perfusable, scalable, customisable, and low-cost Vessel on Chip (VOC) platform.

Barriers to adoption of microfluidic-based lab on chip (LOC) are high as commercially available LOC and perfusion drivers are usually expensive and relatively fixed in design. In this work, we first started by implementing a widely used protocol to create LOC devices for the perfusion of microvasculature. Although the fabrication of the device was well-documented, the implementation of the hydrogel system to create perfused microvascular system introduced a lot of technical difficulties. The microfeatures of the design complicated the seeding of the hydrogel and reproducibility of the system. We had technical difficulties in recreating the vessels observed in the protocol and the complex fabrication process did not allow any easy modification of the design, making the manufacture not scalable and expensive.

To solve this fabrication problems, we demonstrated a workflow to fabricate inexpensive, custom and scalable LOC devices. The workflow in the current research is based upon 3D printing and includes validation steps to engineer and manufacture low-cost LOC which can be rapidly modified and tailored to specific applications. By integrating tubing directly into our mould and creating a strong link between the tubing and the silicon used in the chip we introduced a secure connection to introduce perfusion in the system. This small modification allowed us to further implement active perfusion systems needed for the creation of stable perfused microtissues.

The implementation of 3D printing and computer assisted design for our workflow significantly decreased the cost and difficulty linked with the creation of LOC devices. Here, we tested several designs aimed at reproducing a complete model of microvasculature *in vitro*.

Starting from a very complex design with several central wells and branched side channels, we tailored and simplified our LOC design through repeated experiments with vascular cells as summarised in table 4.2.
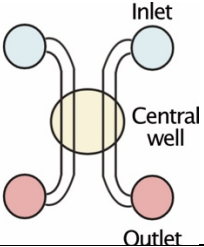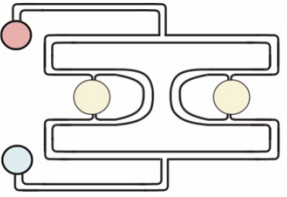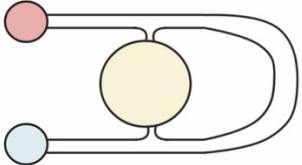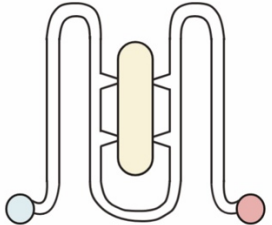
Design	Details	Advantages	Disadvantages
Model 1 	-Double PDMS layer with the central well under the channels. -Double inlet and double outlet	-Already existing design -Big perfusion channels allow easy of perfusion and cell culture	-2-level PDMS complicates the fabrication -No direct link with the tubing allows only passive perfusion
Model 2 	-Single inlet and outlet to create fully closed system. -4 central wells directly linked to the perfusion channels	-Direct embedding of the tubing. -Small channels can be covered by endothelial cells -Closed circuit with single inlet and outlet	-100% of the flow going in the central well disturbs the cell -Design too complex and too many wells
Model 3 	-Central wells reduced to two -T-junction between the perfusion channels and the central well -Creation of a diversion to reduce the amount of flow going in the central well	-T-junction allows the diversion of the flow and an easier perfusion of the central well.	-The presence of two central wells allows to perform parallel experiments but causes a dissymmetry in the flow.
Model 4 	-Reduced central well to one	-The single well and simplified design facilitates the cell seeding and perfusion	-The flow coming straight from the side channels can be too strong and inhibits the creation of a connection with the central well.
Model 5 	-Creation of two connections per side between the central well and side channels. Modification of the T-junction shape to allow a better connection to the channels.	- U-shaped channels allow the flow the properly enter the T-junctions. -Double connections with the central well multiplies the chances of vessel anastomosis with the perfusion channels	-Best device to date but could be optimised for the seeding of the gel-free co-culture.

Table 4.2: Comparison of the devices used in the study with their advantages and disadvantages and the reason for the change in design. The main five devices used are listed in the chronological order as they appeared in the study and the schematics show the different parts of the LOC with the inlet in blue, central well in yellow and outlet in red. Details, advantages and disadvantages of each model are listed to justify the changes in design.

The first design used in the study (model 1 in table 4.2) was inspired by the designs in the literature and created using 2 PDMS layers punched and assembled. As seen in the design, it has 2 inlets and 2 outlets and big side channels on the top layer and a big central well on the bottom layer. However, the attempt at creating perfused fibrin hydrogels with ECs within the LOC design were unsuccessful due to the difficult connections between the side channels and the central well and the presence of only big wells to allow a passive perfusion of the device as shown in the literature (M. B. Chen et al., 2017; Shin et al., 2012). The following complex model was reduced to a single inlet and outlet to allows the creation of a closed circulation but revealed to be too difficult to perfuse due to the direct flow in the central well that could cause a build-up in pressure if the system was not perfused properly. Following models 3 and 4 resolved this problem by creating a T-junction that diverted part of the flow in a U-shaped channel and could allow a control over the velocity in the side channels. Finally, the latest model 5 shown in table 4.2 is the LOC design used in the experiments with perfusion reported throughout the study. It is composed of a single inlet and outlet for the creation of a closed circuit, a single central well that is only 5mm in width to allow an easier formation and connection of vascular networks between the channels and two T-junctions on each side to multiply the chances of anastomosis between the side channels and the central well.

To accelerate LOC system design, we leveraged on the capabilities of Computational Flow Dynamics (CFD) as preliminary validation which has been invaluable during the dev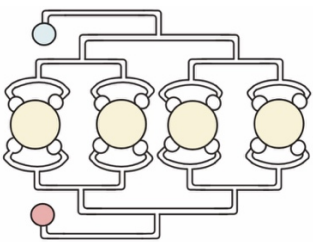elopment of our VOC (Vasculature on chip) prototype. CFD allowed us to conduct a preliminary *in silico* screening of possible designs and to rule out non-viable candidates. Furthermore, CFD allowed us to fine tune many parameters of our VOC design and optimise it for both functionality and easy assembly. Overall, the use of CFD enormously sped up and reduced the costs of VOC prototype development. As shown in the CFD simulations, different compartments receive distinct flow, experiencing a net pressure drop between the aA and eV sides, essential for the creation of functional and hierarchical vasculature. Our design allowed creating laminar flow into the central well to reduce biomechanical stresses in the first days of perfusion when the vasculature is still fragile. Overall, we believe that parallel integration of 3D CAD, 3DP and CFD offers great potential and will be of particular interest for future implementation of multi-organ chips and the study of vascular dynamics in engineered vascular beds.

One of the major challenges in the design of LOC/VOC systems is introducing continuous and controlled perfusion. By integrating a low-cost and compact flow driver in our design and by

using 3DP to facilitate assembly, we report the creation and validation of a perfusion system that can be integrated in any lab with standard cell culture incubators. Once again, the use of 3D printing and customised systems can be adapted for specific use and different LOC designs or microfluidic systems.

For initial validation of our VOC, we used a fibrin gel vasculogenesis assay and showed that our VOC and perfusion system enables continuous long term (>15 days) perfusion of engineered vascular networks. This system revealed to be particularly useful for the rapid creation of microvascular networks in just few days and could be used to study processes such as vascular cell/immune cell interaction. However, vascular networks formed in hydrogels cannot recapitulate vascular maturation because the cellular components enabling matrix remodelling (e.g., macrophages and matrix producing stromal cells) are absent in such systems. The inspection of these vessels demonstrated a lack of vascular hierarchy and dimensions that did not match capillary formation *in vivo*.

To develop a more biomimetic model of microvasculature *in vitro*, we adapted an organotypic co-culture system of matrix secreting stromal and endothelial cells (OVAA). OVAA exploits the ability of stromal cells like HDF (Human Dermal Fibroblasts) to secrete the ECM necessary to embed ECs and form a capillary network with patent microvessels resembling *in vivo* counterparts. We have shown that OVAA can be used with different EC and stromal cells enabling the creation of tissue specific microenvironments. The use of this assay also revealed intrinsic differences in angiogenic potential of the different organ-specific ECs used in this study. As described in the chapter 2 of this work, organ-specific ECs demonstrated heterogeneous behaviour at the population level. Here, we show that these differences are also relevant in the creation of capillary networks. The poor capacity of HPMEC to form vessels is in correlation with their slower proliferation rate and phenotype observed in 2D compared to HUVEC and HAoEC. Adaptation of the OVAA system with stem cell-derived ECs also revealed their ability to form capillary networks in 3D. ETV2-ECs showed an angiogenic potential similar to HUVECs, even with the removal of doxycycline to mimic transient ETV2 expression in the embryo. However, addition of VEGF-A and/or bFGF had the opposite effect than expected. Indeed, the vascular networks formed had lower junctions, nodes and overall complexity. The phenotype of ETV2-ECs observed in chapter 3 with a very high Notch signalling could explain this behaviour. High Notch activation could decrease cell proliferation and cause the network to regress. However, the co-culture of stem cell-derived ECs and stromal

cells revealed the high potential for these cells to form blood vessels that could be matured in 3D. Overall, the combined use of 2D and 3D assays as well as *in silico* simulations (Chesnais et al., 2022b) on the EC behaviour could be useful to predict angiogenic potential and EC behaviour in different tissues.

Creating relevant *in vitro* models to recapitulate developmental processes is key for the creation of tissue engineered constructs or to model diseases. This includes the development of complex *in vitro* models including several types of cells and relevant microenvironment. With the aim of creating a biomimetic environment resembling the developing pancreas, we adapted our OVAA protocol for the culture of iPSC-derived pancreatic organoids without the use of exogenous matrices. We show that introducing pancreatic organoids on the layer of matrix secreted by cells such as fibroblasts can replace the use of 3D exogenous matrices. We report that these organoids survive, proliferate and differentiate in this environment. The co-culture with ECs also create a very relevant microtissue with fully human proteins and ECM components and capillaries formed in close contact with the pancreatic organoids as described in early stages in the embryo (Lammert et al., 2001). Preliminary experiments to differentiate these organoids in our co-culture model showed that pancreatic cells keep their fate with expression of PDX1 but the culture in the OVAA system has a negative effect on the generation of mature beta cells. Further experiments will be needed to determine if this phenotype is due to the angiocrine signalling from fibroblasts, ECs, organ-specific ECs or if the composition and stiffness of the environment prevents the proper maturation of these cells.

Finally, we combined and optimised our platforms to create an integrated VOC-OVAA platform for the perfusion of microtissues. After 7-10 days of culture, ECs from the side channels and the central well assembled into a continuous vascular tree that could be perfused. To the best of our knowledge, this is the first reported platform enabling continuous and long-term perfusion of vascularised tissues. A key advantage of VOC-OVAA is the physiological biomechanical forces and flow experienced by the cell as observed by the stiff microtissue formed and its elastic properties. As reported, continuously perfused capillary networks remodel in response to these forces over time. Therefore, our platform paves the way to generating tissue-specific microenvironments surpassing current hydrogel-based strategies and allows creating vascularised tissues which are easy to image, possess physiological biomechanical properties and are highly customisable.

Overall, the LOC device presented in this study has several advantages compared to already published micro physiological systems. First, the use of 3D printing allows a fast prototyping of the device that can be adapted in any laboratory with standard equipment and training. The fabrication of our PDMS-based chip requires only 3 days of work and can be easily modified and adapted to different uses. The embedded tubing also allows the creation of a closed perfusion system that mimics the blood circulation and can be left in continuous perfusion for several days. The system described here using 3D printing for the design of both the LOC device and the perfusion system can easily be customised for the creation of other perfused systems or organ-on-chip models. However, the main advantage of the system and novelty of the work presented here is the development of our gel-free co-culture model (VOC-OVAA) allowing the perfusion of a self-assembled vascular networks without the use of exogenous hydrogels. The combination of out custom LOC device with a co-culture system allowed us to continuously perfuse ECs that self-assembled in matrix secreted entirely by cells to create a perfusable microtissue. This is, to the best of our knowledge, the first report of perfusion of a vascular network entirely created with cells. This system not only recreated the exact conditions found in the body where cells secrete matrix and closely interact to form perfusable vessels but also reproduce the biomechanical properties of a soft organ. Indeed, the perfused microtissue showed elastic properties unequalled in hydrogels and allowed the maturation of vessels to over time and under continuous perfusion for several days. In comparison to other published protocols to create perfusable vascular networks (Campisi et al., 2018; M. B. Chen et al., 2017; Hachey et al., 2021; Ronaldson-Bouchard et al., 2022; Sobrino et al., 2016; Song et al., 2018; Wang et al., 2016; Whisler et al., 2014), it allows a better maturation of the cells due to the continuous perfusion and the lack of a hydrogel to degrade or replace but we only describe the use of primary cells to form the vascular networks and this will need to be expanded to the use of stem cell derived cells and organ-specific ECs. Furthermore, although the system can be customised, the perfused microtissue described is still small (5mm) compared to the size needed to perfuse small organs and further effort will be needed to increase the robustness of the system and apply the technique for the creation of perfused organ-on-chip.

Our VOC-OVAA will enable investigating a variety of key mechanisms in vascular biology which have physio-pathologic implications. For example, cancer-associated signalling and extracellular matrix stiffening has been associated with impaired vascular maturation and reduced oxygenation of cancer tissue (Wu et al., 2021). Vascular abnormalities are also

associated with impaired delivery of chemotherapies and immunotherapies with overall worse prognosis, and vascular normalisation therapy represents a very promising avenue to improve therapy outcome (Jain, 2005). Our VOC-OVAA system is by design able to model several of these aspects allowing to investigate in fine detail the molecular dynamics underpinning physiologic or impaired vascular maturation opening the way to more precise drug targeting. In this sense, another interesting potential application of our VOC-OVAA is extensive culture of tissue slice which can be derived from healthy and pathologic human tissue (Nogueira et al., 2022; Pitoulis et al., 2020) cultured into a VOC and used for example for drug sensitivity assays. Our VOC-OVAA can be easily adapted to create interconnected multi-organ chips by creating multichambered VOC each containing separate microenvironments interconnected by a common circulation system (Ronaldson-Bouchard et al., 2022).

Finally, the VOC-OVAA platform presented here opens the way to develop models of vascularised organoids of stem cell-based systems where stem cell derived-EC, perivascular and stromal cells as well as tissue parenchyma can be cultured or co/differentiated to create functional microtissues. Such pursuit will not only immensely improve our knowledge over cellular and molecular mechanisms of vasculogenesis, angiogenesis and organogenesis but also deliver new animal-free platforms for regenerative medicine, disease modelling and drug discovery.

Chapter 5: Conclusion and future work

Creating biomimetic models of human vasculature is a key steppingstone towards generating functional microtissues *in vitro*. In turn, such functional microtissues have numerous applications for regenerative medicine, disease modelling, molecular targets identification and drug screenings.

For example, there is a high demand to develop efficient protocols to generate stem cells-derived pancreatic islets to cure diabetes, Vascularised lab-on-chip platforms have the potential to address this need from both the technological standpoint (developing appropriate bioreactors) and the biological side (reproducing developmental processes to generate fully mature tissue).

Another example is disease modelling of pathologies involving the development of diseased vasculature such as cancer. The development of dynamic platforms integrating tumour vasculature will greatly help modelling patient-specific treatments with the creation of vascularised patient-specific organoids (Hachey et al., 2021; Ingber, 2022).

Producing tissue-specific Vasculature on Chip (VOC) systems presents a host of engineering and biological problems.

First, recreating physiologic vascularised microenvironments *in vitro* remains challenging. Many efforts in the past 20 years have led to developing matrix-based systems to create patent micro-vessels, however engineered matrices cannot support appropriate tissue development in absence of stromal, matrix-producing cells. Exogenous matrices are invariably simplified versions of the natural ECM and although they can support initial assembly of the vasculature (as it happens during skin wound healing), they cannot support further maturation lacking yet unidentified molecular cues.

To address this problem, we adapted a protocol to create capillary networks in co-culture with stromal cells. The formation of self-assembled capillaries in a matrix exclusively secreted by stromal cells such as fibroblasts or mesenchymal stem cells increased the complexity and biomimetic properties of *in vitro* vasculature. Creating tailored models of organ-specific environments, as shown in this work, containing unique ECM, stiffness and blood vessels will be paramount for the development of functional organs. This system demonstrates the ability of ECs and stromal cells to spontaneously create perfusable microtissues with *in vivo*-like elastic properties and will be useful for the fabrication of complex organ-on-chip models. We demonstrated the versatility of the platform by introducing and culturing iPSC-derived

pancreatic organoids in the matrix-free system. We hypothesize that it can be adapted for the perfusion of serially vascularised organ-on-chip system as previously described (Ronaldson-Bouchard et al., 2022) but with the added complexity of directly perfusing the tissues. In this context, the rapid design modification could allow tailored manufacture of miniature organs linked by a closed continuously perfused vasculature.

Then, the generation of tissue-specific vasculature requires integrating both vasculature and stromal cells to recapitulate appropriate tissues, Efforts to reproduce mature cells from stem cells for the modelling of different organ-specific diseases or creation of engineered tissues will fail to produce relevant models without an integrated functional and perfused vasculature. It is now established, by us and others, that blood vessels not only bring blood to organs but have specific phenotypes and function depending on their location, crucial for the development and regeneration of tissues (Chesnais et al., 2022a; Ding et al., 2010; Itkin et al., 2016; Rafii et al., 2016). We have shown how different primary EC generate structurally different capillaries in vitro and their differences in angiocrine signalling, highlighting the necessity to choose appropriate ECs for the generation of engineered tissues in the future. The generation of stem cell-derived EC and perivascular cells is still challenging but we can generate functional ECs, pericytes and fibroblasts that will require further maturation to recapitulate physiological functions. We showed that by modulating the environment and choosing the right ECs and stromal cells (such as the integration of mesenchymal stem cells and specific fibroblasts to create biomimetic environments) we can increase the resemblance between *in vitro* models and *in vivo* counterparts. Furthermore, the platform presented in this work remains highly flexible for the creation of single or interconnected organ-on-chip models with the ability to integrate organotypic vasculature and study the effect or tailored microenvironments on organ development.

Another key issue encountered in the creation of *in vitro* microvasculature was the inability to scale up the manufacture due to the fixed prototyping and fabrication of LOC devices via traditional methods. To overcome these key challenges, we developed an integrated workflow to manufacture custom Lab-on-chip devices. By incorporating 3D printing, computer assisted design, computational fluid dynamics and soft lithography, we describe a protocol to create fast, scalable and inexpensive devices. This custom system easily adaptable and containing secure connection to a perfusion system can be adapted and modified for tailored applications. As it is still unclear which specifics will be required to generate tissue specific reactors in the future, we engineered the platform to be able to host several individual microenvironments

than can be coupled by a common vasculature. Our platform relies on 3D printing which still suffers from the inability to reach high resolution of features, down to 1µm or less for silicon wafers. However, it allows an extreme flexibility with the design with a rapid manufacture, a very low cost and does not require training or expensive equipment. The workflow we present in this work for the manufacture of custom LOC devices is very well adapted for the creation of microfluidic devices and low-cost devices for dynamic cell culture.

Integrating a continuous perfusion *in vitro* with the ability to perfuse microvascular networks for a long period has also been challenging. Implementing a controlled continuous perfusion into microfluidic devices comes with a set of engineering problems such as the need for temperature and gas exchange, the need for a sterile environment and the ability to adapt the system for standard lab equipment. Here, we addressed these issues by developing a custom perfusion system that is ergonomic and fits standard cell culture incubators and imaging systems by creating a platform with plate dimensions. Moreover, we used 3D printing to manufactures cassettes for both the LOC device and the microfluidic system so that they can be integrated in an incubator and control the temperature, humidity level and allow gas exchange. Finally, the connection to a laptop outside the incubator allows the control over the continuous perfusion of the system without any manipulation. This integrated continuous perfusion is a key feature of out vasculature-on-chip system. The ability to continuously perfuse tissues for weeks is fundamental for the creation of functional organs. Previous attempts at perfusing microvasculature *in vitro* could only achieve a partial passive gravity-driven perfusion (Chen et al., 2013; M. B. Chen et al., 2017; Wang et al., 2016) or the introduction of active perfusion systems such as syringe pumps were hardly controllable (Salmon et al., 2022). Introducing an easy way to continuously perfuse organ-on-chip models is the first step to solve the common development of hypoxic regions in organoids and tissues cultured in exogenous matrices.

The work presented here for the creation of tailored LOC systems paves the way for the creation of miniaturised systems allowing in-depth study of developmental processes or disease modelling. Extracting information from such dynamic systems will be key for their standardised use in labs and industry. To do so, it is necessary to adapt these devices for the creation of (semi) automated data analysis such as the work presented here on EC heterogeneity. We integrated the ability to image the system dynamically through a transparent

cell culture plate and demonstrate the ability to image our system with confocal imaging and live imaging. We envisage that the use of open-source software such as the ones described here for the single cell analysis of EC behaviour, or the blood vessel quantification will be crucial to extract maximal information from experiments.

Overall, the work presented paves the way to creating *in vitro* complex system including a functional microvasculature. The development of this flexible platform solved existing problems such as the implementation of a continuous and controlled perfusion of capillary networks in biomimetic environments. The platform described has several potential applications as discussed previously, from the study of tumour-associated vasculature and the role of vascularisation on organ developments to the vascularisation of stem cell-derived organoids. Future use of this system could also include the study of vascularisation and perfusion on engineered tissues from stem cells, organ slices such as commonly used liver or brain slices (Nogueira et al., 2022), development of multi organ-on-chip or implantation platform for the vascularisation of recently discovered embryo models from stem cells (Amadei et al., 2022; Tarazi et al., 2022).

Creating complex *in vitro* models of human development and disease has been of great interest in the last decades. The discovery of human stem cells and their global use allowed for better understanding of human physiology, but *in vitro* models still lack a degree of complexity. The development of microfluidic devices allowed tissue vascularisation and perfusion, representing an exciting challenge to further close the gap between *in vitro* models and *in vivo* experimentation. However, key components of human physiology remain to be integrated *in vitro* such as the creation of thick vascularised tissues, recirculation of immune cells, integration of organoids within stiff environments, culture under dynamic conditions for months or innervation of tissue engineered constructs.

The next step in the development of complete models, following the introduction of vascularisation and perfusion, will be to scale up tissue engineered constructs to recapitulate organ-level functions and use them for transplantation purposes or appropriate disease modelling. Challenges will need to be addressed such as the need for a long-term dynamics culture (several months) to create mature organs including mature vasculature, the need for scalable stem cell derived organs or the increased scalability of the systems to answer the transplantation needs worldwide. However, the recent interest in microfluidic devices is encouraging for the global effort in creating more and more complex *in vitro* models and reduce

animal testing. We envisage that the broad use of microfluidic system and lab-on-chip devices will improve our knowledge on organogenesis and deliver new platforms for the use of animal-free drug discovery and regenerative medicine.

References

Abu Taha, A., Taha, M., Seebach, J., Schnittler, H.-J., 2014. ARP2/3-mediated junction-associated lamellipodia control VE-cadherin-based cell junction dynamics and maintain monolayer integrity. Mol. Biol. Cell 25, 245–256. https://doi.org/10.1091/mbc.E13-07-0404

Adams, R.H., Alitalo, K., 2007. Molecular regulation of angiogenesis and lymphangiogenesis. Nat. Rev. Mol. Cell Biol. 8, 464–478. https://doi.org/10.1038/nrm2183

Adams, R.H., Wilkinson, G.A., Weiss, C., Diella, F., Gale, N.W., Deutsch, U., Risau, W., Klein, R., 1999. Roles of ephrinB ligands and EphB receptors in cardiovascular development: demarcation of arterial/venous domains, vascular morphogenesis, and sprouting angiogenesis. Genes Dev. 13, 295–306. https://doi.org/10.1101/gad.13.3.295

Adams, W.J., Zhang, Y., Cloutier, J., Kuchimanchi, P., Newton, G., Sehrawat, S., Aird, W.C., Mayadas, T.N., Luscinskas, F.W., García-Cardeña, G., 2013. Functional Vascular Endothelium Derived from Human Induced Pluripotent Stem Cells. Stem Cell Rep. 1, 105–113. https://doi.org/10.1016/j.stemcr.2013.06.007

Adil, M.S., Somanath, P.R., 2020. Endothelial Permeability Assays In Vitro, in: Turksen, K. (Ed.), Permeability Barrier, Methods in Molecular Biology. Springer US, New York, NY, pp. 177–191. https://doi.org/10.1007/7651_2020_309

Aird, W.C., 2007a. Phenotypic Heterogeneity of the Endothelium: I. Structure, Function, and Mechanisms. Circ. Res. 100, 158–173. https://doi.org/10.1161/01.RES.0000255691.76142.4a

Aird, W.C., 2007b. Phenotypic Heterogeneity of the Endothelium: II. Representative Vascular Beds. Circ. Res. 100, 174–190. https://doi.org/10.1161/01.RES.0000255690.03436.ae

Aird, W.C., Edelberg, J.M., Weiler-Guettler, H., Simmons, W.W., Smith, T.W., Rosenberg, R.D., 1997. Vascular Bed–specific Expression of an Endothelial Cell Gene Is Programmed by the Tissue Microenvironment. J. Cell Biol. 138, 1117–1124. https://doi.org/10.1083/jcb.138.5.1117

Aisenbrey, E.A., Torr, E., Johnson, H., Soref, C., Daly, W., Murphy, W.L., 2021. A protocol for rapid pericyte differentiation of human induced pluripotent stem cells. STAR Protoc. 2, 100261. https://doi.org/10.1016/j.xpro.2020.100261

Alarcon-Martinez, L., Yilmaz-Ozcan, S., Yemisci, M., Schallek, J., Kılıç, K., Can, A., Di Polo, A., Dalkara, T., 2018. Capillary pericytes express α-smooth muscle actin, which requires prevention of filamentous-actin depolymerization for detection. eLife 7, e34861. https://doi.org/10.7554/eLife.34861

Albelda, S.M., Oliver, P.D., Romer, L.H., Buck, C.A., 1990. EndoCAM: a novel endothelial cell-cell adhesion molecule. J. Cell Biol. 110, 1227–1237. https://doi.org/10.1083/jcb.110.4.1227

Amadei, G., Handford, C.E., Qiu, C., De Jonghe, J., Greenfeld, H., Tran, M., Martin, B.K., Chen, D.-Y., Aguilera-Castrejon, A., Hanna, J.H., Elowitz, M., Hollfelder, F., Shendure, J., Glover, D.M., Zernicka-Goetz, M., 2022. Synthetic embryos complete gastrulation to neurulation and organogenesis. Nature. https://doi.org/10.1038/s41586-022-05246-3

Ambati, B.K., Nozaki, M., Singh, N., Takeda, A., Jani, P.D., Suthar, T., Albuquerque, R.J.C., Richter, E., Sakurai, E., Newcomb, M.T., Kleinman, M.E., Caldwell, R.B., Lin, Q., Ogura, Y., Orecchia, A., Samuelson, D.A., Agnew, D.W., St. Leger, J., Green, W.R., Mahasreshti, P.J., Curiel, D.T., Kwan, D., Marsh, H., Ikeda, S., Leiper, L.J., Collinson, J.M., Bogdanovich, S., Khurana, T.S., Shibuya, M., Baldwin, M.E., Ferrara, N., Gerber, H.-P., De Falco, S., Witta, J., Baffi, J.Z., Raisler, B.J., Ambati, J., 2006. Corneal avascularity is due to soluble VEGF receptor-1. Nature 443, 993–997. https://doi.org/10.1038/nature05249

Amin, R., Knowlton, S., Hart, A., Yenilmez, B., Ghaderinezhad, F., Katebifar, S., Messina, M., Khademhosseini, A., Tasoglu, S., 2016. 3D-printed microfluidic devices. Biofabrication 8, 022001. https://doi.org/10.1088/1758-5090/8/2/022001

Ando, J., Yamamoto, K., 2022. Hemodynamic Forces, Endothelial Mechanotransduction, and Vascular Diseases. Magn. Reson. Med. Sci. 21, 258–266. https://doi.org/10.2463/mrms.rev.2021-0018

Andriopoulou, P., Navarro, P., Zanetti, A., Lampugnani, M.G., Dejana, E., 1999. Histamine induces tyrosine phosphorylation of endothelial cell-to-cell adherens junctions. Arterioscler. Thromb. Vasc. Biol. 19, 2286–2297. https://doi.org/10.1161/01.atv.19.10.2286

Aranguren, X.L., Beerens, M., Coppiello, G., Wiese, C., Vandersmissen, I., Lo Nigro, A., Verfaillie, C.M., Gessler, M., Luttun, A., 2013. COUP-TFII orchestrates venous and lymphatic endothelial identity by homo- or hetero-dimerisation with PROX1. J. Cell Sci. 126, 1164–1175. https://doi.org/10.1242/jcs.116293

Arif, N., Zinnhardt, M., Nyamay'Antu, A., Teber, D., Brückner, R., Schaefer, K., Li, Y., Trappmann, B., Grashoff, C., Vestweber, D., 2021. PECAM-1 supports leukocyte diapedesis by tension-dependent dephosphorylation of VE-cadherin. EMBO J. 40. https://doi.org/10.15252/embj.2020106113

Armulik, A., Genové, G., Betsholtz, C., 2011. Pericytes: Developmental, Physiological, and Pathological Perspectives, Problems, and Promises. Dev. Cell 21, 193–215. https://doi.org/10.1016/j.devcel.2011.07.001

Armulik, A., Genové, G., Mäe, M., Nisancioglu, M.H., Wallgard, E., Niaudet, C., He, L., Norlin, J., Lindblom, P., Strittmatter, K., Johansson, B.R., Betsholtz, C., 2010. Pericytes regulate the blood–brain barrier. Nature 468, 557–561. https://doi.org/10.1038/nature09522

Arora, S., Yim, E.K.F., Toh, Y.-C., 2019. Environmental Specification of Pluripotent Stem Cell Derived Endothelial Cells Toward Arterial and Venous Subtypes. Front. Bioeng. Biotechnol. 7, 143. https://doi.org/10.3389/fbioe.2019.00143

Asahina, K., Zhou, B., Pu, W.T., Tsukamoto, H., 2011. Septum transversum-derived mesothelium gives rise to hepatic stellate cells and perivascular mesenchymal cells in developing mouse liver. Hepatology 53, 983–995. https://doi.org/10.1002/hep.24119

Au, A.K., Huynh, W., Horowitz, L.F., Folch, A., 2016. 3D-Printed Microfluidics. Angew. Chem. Int. Ed. 55, 3862–3881. https://doi.org/10.1002/anie.201504382

Augustin, H.G., Koh, G.Y., 2017. Organotypic vasculature: From descriptive heterogeneity to functional pathophysiology. Science 357, eaal2379. https://doi.org/10.1126/science.aal2379

Ayuso-Íñigo, B., Méndez-García, L., Pericacho, M., Muñoz-Félix, J.M., 2021. The Dual Effect of the BMP9–ALK1 Pathway in Blood Vessels: An Opportunity for Cancer Therapy Improvement? Cancers 13, 5412. https://doi.org/10.3390/cancers13215412

Baeyens, N., Larrivée, B., Ola, R., Hayward-Piatkowskyi, B., Dubrac, A., Huang, B., Ross, T.D., Coon, B.G., Min, E., Tsarfati, M., Tong, H., Eichmann, A., Schwartz, M.A., 2016. Defective fluid shear stress mechanotransduction mediates hereditary hemorrhagic telangiectasia. J. Cell Biol. 214, 807–816. https://doi.org/10.1083/jcb.201603106

Ballermann, B.J., Dardik, A., Eng, E., Liu, A., 1998. Shear stress and the endothelium. Kidney Int. 54, S100–S108. https://doi.org/10.1046/j.1523-1755.1998.06720.x

Bazzoni, G., Dejana, E., 2004. Endothelial Cell-to-Cell Junctions: Molecular Organization and Role in Vascular Homeostasis. Physiol. Rev. 84, 869–901. https://doi.org/10.1152/physrev.00035.2003

Bendayan, M., 2002. Morphological and cytochemical aspects of capillary permeability. Microsc. Res. Tech. 57, 327–349. https://doi.org/10.1002/jemt.10088

Benjamin, L.E., Hemo, I., Keshet, E., 1998. A plasticity window for blood vessel remodelling is defined by pericyte coverage of the preformed endothelial network and is regulated by PDGF-B and VEGF. Development 125, 1591–1598. https://doi.org/10.1242/dev.125.9.1591

Bentley, K., Franco, C.A., Philippides, A., Blanco, R., Dierkes, M., Gebala, V., Stanchi, F., Jones, M., Aspalter, I.M., Cagna, G., Weström, S., Claesson-Welsh, L., Vestweber, D., Gerhardt, H., 2014. The role of differential VE-cadherin dynamics in cell rearrangement during angiogenesis. Nat. Cell Biol. 16, 309–321. https://doi.org/10.1038/ncb2926

Ben-Zvi, A., Lacoste, B., Kur, E., Andreone, B.J., Mayshar, Y., Yan, H., Gu, C., 2014. Mfsd2a is critical for the formation and function of the blood–brain barrier. Nature 509, 507–511. https://doi.org/10.1038/nature13324

Bernier-Latmani, J., Mauri, C., Marcone, R., Renevey, F., Durot, S., He, L., Vanlandewijck, M., Maclachlan, C., Davanture, S., Zamboni, N., Knott, G.W., Luther, S.A., Betsholtz, C., Delorenzi, M., Brisken, C., Petrova, T.V., 2022. ADAMTS18+ villus tip telocytes maintain a

polarized VEGFA signaling domain and fenestrations in nutrient-absorbing intestinal blood vessels. Nat. Commun. 13, 3983. https://doi.org/10.1038/s41467-022-31571-2

Bertassoni, L.E., Cecconi, M., Manoharan, V., Nikkhah, M., Hjortnaes, J., Cristino, A.L., Barabaschi, G., Demarchi, D., Dokmeci, M.R., Yang, Y., Khademhosseini, A., 2014. Hydrogel bioprinted microchannel networks for vascularization of tissue engineering constructs. Lab Chip 14, 2202–2211. https://doi.org/10.1039/C4LC00030G

Biel, N.M., Santostefano, K.E., DiVita, B.B., El Rouby, N., Carrasquilla, S.D., Simmons, C., Nakanishi, M., Cooper-DeHoff, R.M., Johnson, J.A., Terada, N., 2015. Vascular Smooth Muscle Cells From Hypertensive Patient-Derived Induced Pluripotent Stem Cells to Advance Hypertension Pharmacogenomics. Stem Cells Transl. Med. 4, 1380–1390. https://doi.org/10.5966/sctm.2015-0126

Bishop, E.T., 1999. An in vitro model of angiogenesis: Basic features. Angiogenesis 3, 335–344. https://doi.org/10.1023/A:1026546219962

Blanchard, J.W., Bula, M., Davila-Velderrain, J., Akay, L.A., Zhu, L., Frank, A., Victor, M.B., Bonner, J.M., Mathys, H., Lin, Y.-T., Ko, T., Bennett, D.A., Cam, H.P., Kellis, M., Tsai, L.-H., 2020. Reconstruction of the human blood–brain barrier in vitro reveals a pathogenic mechanism of APOE4 in pericytes. Nat. Med. 26, 952–963. https://doi.org/10.1038/s41591-020-0886-4

Blanco, R., Gerhardt, H., 2013. VEGF and Notch in Tip and Stalk Cell Selection. Cold Spring Harb. Perspect. Med. 3, a006569–a006569. https://doi.org/10.1101/cshperspect.a006569

Boareto, M., Jolly, M.K., Goldman, A., Pietilä, M., Mani, S.A., Sengupta, S., Ben-Jacob, E., Levine, H., Onuchic, J.N., 2016. Notch-Jagged signalling can give rise to clusters of cells exhibiting a hybrid epithelial/mesenchymal phenotype. J. R. Soc. Interface 13, 20151106. https://doi.org/10.1098/rsif.2015.1106

Boareto, M., Jolly, M.K., Lu, M., Onuchic, J.N., Clementi, C., Ben-Jacob, E., 2015. Jagged-Delta asymmetry in Notch signaling can give rise to a Sender/Receiver hybrid phenotype. Proc. Natl. Acad. Sci. U. S. A. 112, E402-409. https://doi.org/10.1073/pnas.1416287112

Bolmont, C., Lilienbaum, A., Paulin, D., Grimaud, J.A., 1990. Expression of desmin gene in skeletal and smooth muscle by in situ hybridization using a human desmin gene probe. J. Submicrosc. Cytol. Pathol. 22, 117–122.

Boon, R., Kumar, M., Tricot, T., Elia, I., Ordovas, L., Jacobs, F., One, J., De Smedt, J., Eelen, G., Bird, M., Roelandt, P., Doglioni, G., Vriens, K., Rossi, M., Vazquez, M.A., Vanwelden, T., Chesnais, F., El Taghdouini, A., Najimi, M., Sokal, E., Cassiman, D., Snoeys, J., Monshouwer, M., Hu, W.-S., Lange, C., Carmeliet, P., Fendt, S.-M., Verfaillie, C.M., 2020. Amino acid levels determine metabolism and CYP450 function of hepatocytes and hepatoma cell lines. Nat. Commun. 11, 1393. https://doi.org/10.1038/s41467-020-15058-6

Borenstein, J.T., Terai, H., King, K.R., Weinberg, E.J., Kaazempur-Mofrad, M.R., Vacanti, J.P., 2002. Microfabrication Technology for Vascularized Tissue Engineering. Biomed. Microdevices 4, 167–175. https://doi.org/10.1023/A:1016040212127

Brissova, M., Shostak, A., Shiota, M., Wiebe, P.O., Poffenberger, G., Kantz, J., Chen, Z., Carr, C., Jerome, W.G., Chen, J., Baldwin, H.S., Nicholson, W., Bader, D.M., Jetton, T., Gannon, M., Powers, A.C., 2006. Pancreatic Islet Production of Vascular Endothelial Growth Factor-A Is Essential for Islet Vascularization, Revascularization, and Function. Diabetes 55, 2974–2985. https://doi.org/10.2337/db06-0690

Browne, S., Gill, E.L., Schultheiss, P., Goswami, I., Healy, K.E., 2021. Stem cell-based vascularization of microphysiological systems. Stem Cell Rep. 16, 2058–2075. https://doi.org/10.1016/j.stemcr.2021.03.015

Bussmann, J., Wolfe, S.A., Siekmann, A.F., 2011. Arterial-venous network formation during brain vascularization involves hemodynamic regulation of chemokine signaling. Development 138, 1717–1726. https://doi.org/10.1242/dev.059881

Butcher, E.C., 1991. Leukocyte-endothelial cell recognition: Three (or more) steps to specificity and diversity. Cell 67, 1033–1036. https://doi.org/10.1016/0092-8674(91)90279-8

Byun, C.K., Abi-Samra, K., Cho, Y.-K., Takayama, S., 2014. Pumps for microfluidic cell culture: Microfluidics and Miniaturization. ELECTROPHORESIS 35, 245–257. https://doi.org/10.1002/elps.201300205

Caicedo, J.C., Cooper, S., Heigwer, F., Warchal, S., Qiu, P., Molnar, C., Vasilevich, A.S., Barry, J.D., Bansal, H.S., Kraus, O., Wawer, M., Paavolainen, L., Herrmann, M.D., Rohban, M., Hung, J., Hennig, H., Concannon, J., Smith, I., Clemons, P.A., Singh, S., Rees, P., Horvath, P., Linington, R.G., Carpenter, A.E., 2017. Data-analysis strategies for image-based cell profiling. Nat. Methods 14, 849–863. https://doi.org/10.1038/nmeth.4397

Cakir, B., Xiang, Y., Tanaka, Y., Kural, M.H., Parent, M., Kang, Y.-J., Chapeton, K., Patterson, B., Yuan, Y., He, C.-S., Raredon, M.S.B., Dengelegi, J., Kim, K.-Y., Sun, P., Zhong, M., Lee, S., Patra, P., Hyder, F., Niklason, L.E., Lee, S.-H., Yoon, Y.-S., Park, I.-H., 2019. Engineering of human brain organoids with a functional vascular-like system. Nat. Methods 16, 1169–1175. https://doi.org/10.1038/s41592-019-0586-5

Campbell, S.B., Wu, Q., Yazbeck, J., Liu, C., Okhovatian, S., Radisic, M., 2021. Beyond Polydimethylsiloxane: Alternative Materials for Fabrication of Organ-on-a-Chip Devices and Microphysiological Systems. ACS Biomater. Sci. Eng. 7, 2880–2899. https://doi.org/10.1021/acsbiomaterials.0c00640

Campisi, M., Shin, Y., Osaki, T., Hajal, C., Chiono, V., Kamm, R.D., 2018. 3D self-organized microvascular model of the human blood-brain barrier with endothelial cells, pericytes and astrocytes. Biomaterials 180, 117–129. https://doi.org/10.1016/j.biomaterials.2018.07.014

Cao, J., Ehling, M., März, S., Seebach, J., Tarbashevich, K., Sixta, T., Pitulescu, M.E., Werner, A.-C., Flach, B., Montanez, E., Raz, E., Adams, R.H., Schnittler, H., 2017. Polarized actin and VE-cadherin dynamics regulate junctional remodelling and cell migration during sprouting angiogenesis. Nat. Commun. 8, 2210. https://doi.org/10.1038/s41467-017-02373-8

Carmeliet, P., 2003. Angiogenesis in health and disease. Nat. Med. 9, 653–660. https://doi.org/10.1038/nm0603-653

Carmeliet, P., 2000. Mechanisms of angiogenesis and arteriogenesis. Nat. Med. 6, 389–395. https://doi.org/10.1038/74651

Carmeliet, P., Ferreira, V., Breier, G., Pollefeyt, S., Kieckens, L., Gertsenstein, M., Fahrig, M., Vandenhoeck, A., Harpal, K., Eberhardt, C., Declercq, C., Pawling, J., Moons, L., Collen, D., Risau, W., Nagy, A., 1996. Abnormal blood vessel development and lethality in embryos lacking a single VEGF allele. Nature 380, 435–439. https://doi.org/10.1038/380435a0

Carpenter, A.E., Jones, T.R., Lamprecht, M.R., Clarke, C., Kang, I.H., Friman, O., Guertin, D.A., Chang, J.H., Lindquist, R.A., Moffat, J., Golland, P., Sabatini, D.M., 2006. CellProfiler: image analysis software for identifying and quantifying cell phenotypes. Genome Biol. 7, R100. https://doi.org/10.1186/gb-2006-7-10-r100

Carpenter, B., Lin, Y., Stoll, S., Raffai, R.L., McCuskey, R., Wang, R., 2005. VEGF is crucial for the hepatic vascular development required for lipoprotein uptake. Development 132, 3293–3303. https://doi.org/10.1242/dev.01902

Carpentier, G., Berndt, S., Ferratge, S., Rasband, W., Cuendet, M., Uzan, G., Albanese, P., 2020. Angiogenesis Analyzer for ImageJ — A comparative morphometric analysis of "Endothelial Tube Formation Assay" and "Fibrin Bead Assay." Sci. Rep. 10, 11568. https://doi.org/10.1038/s41598-020-67289-8

Chaigneau, E., Roche, M., Charpak, S., 2019. Unbiased Analysis Method for Measurement of Red Blood Cell Size and Velocity With Laser Scanning Microscopy. Front. Neurosci. 13, 644. https://doi.org/10.3389/fnins.2019.00644

Chan, X.Y., Elliott, M.B., Macklin, B., Gerecht, S., 2017. Human Pluripotent Stem Cells to Engineer Blood Vessels, in: Martin, U., Zweigerdt, R., Gruh, I. (Eds.), Engineering and Application of Pluripotent Stem Cells, Advances in Biochemical Engineering/Biotechnology. Springer International Publishing, Cham, pp. 147–168. https://doi.org/10.1007/10_2017_28

Chanda, B., Ditadi, A., Iscove, N.N., Keller, G., 2013. Retinoic Acid Signaling Is Essential for Embryonic Hematopoietic Stem Cell Development. Cell 155, 215–227. https://doi.org/10.1016/j.cell.2013.08.055

Chavkin, N.W., Hirschi, K.K., 2020. Single Cell Analysis in Vascular Biology. Front. Cardiovasc. Med. 7, 42. https://doi.org/10.3389/fcvm.2020.00042

Chen, C.-Y., Bertozzi, C., Zou, Z., Yuan, L., Lee, J.S., Lu, M., Stachelek, S.J., Srinivasan, S., Guo, L., Vincente, A., Mericko, P., Levy, R.J., Makinen, T., Oliver, G., Kahn, M.L., 2012. Blood flow

reprograms lymphatic vessels to blood vessels. J. Clin. Invest. 122, 2006–2017. https://doi.org/10.1172/JCI57513

Chen, J., Luo, Y., Hui, H., Cai, T., Huang, H., Yang, F., Feng, J., Zhang, J., Yan, X., 2017. CD146 coordinates brain endothelial cell–pericyte communication for blood–brain barrier development. Proc. Natl. Acad. Sci. 114, E7622–E7631. https://doi.org/10.1073/pnas.1710848114

Chen, M.B., Whisler, J.A., Fröse, J., Yu, C., Shin, Y., Kamm, R.D., 2017. On-chip human microvasculature assay for visualization and quantification of tumor cell extravasation dynamics. Nat. Protoc. 12, 865–880. https://doi.org/10.1038/nprot.2017.018

Chen, M.B., Whisler, J.A., Jeon, J.S., Kamm, R.D., 2013. Mechanisms of tumor cell extravasation in an in vitro microvascular network platform. Integr. Biol. 5, 1262. https://doi.org/10.1039/c3ib40149a

Chen, Q., Zhang, H., Liu, Y., Adams, S., Eilken, H., Stehling, M., Corada, M., Dejana, E., Zhou, B., Adams, R.H., 2016. Endothelial cells are progenitors of cardiac pericytes and vascular smooth muscle cells. Nat. Commun. 7, 12422. https://doi.org/10.1038/ncomms12422

Chen, Y.-C., Lin, R.-Z., Qi, H., Yang, Y., Bae, H., Melero-Martin, J.M., Khademhosseini, A., 2012. Functional Human Vascular Network Generated in Photocrosslinkable Gelatin Methacrylate Hydrogels. Adv. Funct. Mater. 22, 2027–2039. https://doi.org/10.1002/adfm.201101662

Chesnais, F., Hue, J., Roy, E., Branco, M., Stokes, R., Pellon, A., Le Caillec, J., Elbahtety, E., Battilocchi, M., Danovi, D., Veschini, L., 2022a. High-content image analysis to study phenotypic heterogeneity in endothelial cell monolayers. J. Cell Sci. 135, jcs259104. https://doi.org/10.1242/jcs.259104

Chesnais, F., Sego, T.J., Engstler, E., Battilocchi, M., Danovi, D., Glazier, J.A., Veschini, L., 2022b. A spatialised agent-based model of NOTCH signalling pathway in Endothelial Cells predicts emergent heterogeneity due to continual dynamic phenotypic adjustments (preprint). Cell Biology. https://doi.org/10.1101/2022.08.06.503043

Cheung, C., Bernardo, A.S., Trotter, M.W.B., Pedersen, R.A., Sinha, S., 2012. Generation of human vascular smooth muscle subtypes provides insight into embryological origin–dependent disease susceptibility. Nat. Biotechnol. 30, 165–173. https://doi.org/10.1038/nbt.2107

Chi, J.-T., Chang, H.Y., Haraldsen, G., Jahnsen, F.L., Troyanskaya, O.G., Chang, D.S., Wang, Z., Rockson, S.G., van de Rijn, M., Botstein, D., Brown, P.O., 2003. Endothelial cell diversity revealed by global expression profiling. Proc. Natl. Acad. Sci. U. S. A. 100, 10623–10628. https://doi.org/10.1073/pnas.1434429100

Chiang, I.K.-N., Fritzsche, M., Pichol-Thievend, C., Neal, A., Holmes, K., Lagendijk, A., Overman, J., D'Angelo, D., Omini, A., Hermkens, D., Lesieur, E., Liu, K., Ratnayaka, I., Corada, M., Bou-Gharios, G., Carroll, J., Dejana, E., Schulte-Merker, S., Hogan, B., Beltrame, M., De Val, S., Francois, M., 2017. SoxF factors induce Notch1 expression via direct transcriptional regulation during early arterial development. Development dev.146241. https://doi.org/10.1242/dev.146241

Chiu, J.-J., Chien, S., 2011. Effects of Disturbed Flow on Vascular Endothelium: Pathophysiological Basis and Clinical Perspectives. Physiol. Rev. 91, 327–387. https://doi.org/10.1152/physrev.00047.2009

Choi, K.-D., Yu, J., Smuga-Otto, K., Salvagiotto, G., Rehrauer, W., Vodyanik, M., Thomson, J., Slukvin, I., 2009. Hematopoietic and Endothelial Differentiation of Human Induced Pluripotent Stem Cells. Stem Cells 27, 559–567. https://doi.org/10.1634/stemcells.2008-0922

Cleaver, O., Melton, D.A., 2003. Endothelial signaling during development. Nat. Med. 9, 661–668. https://doi.org/10.1038/nm0603-661

Cleuren, A.C.A., van der Ent, M.A., Jiang, H., Hunker, K.L., Yee, A., Siemieniak, D.R., Molema, G., Aird, W.C., Ganesh, S.K., Ginsburg, D., 2019. The in vivo endothelial cell translatome is highly heterogeneous across vascular beds. Proc. Natl. Acad. Sci. 116, 23618–23624. https://doi.org/10.1073/pnas.1912409116

Cokelet, G.R., Soave, R., Pugh, G., Rathbun, L., 1993. Fabrication of in Vitro Microvascular Blood Flow Systems by Photolithography. Microvasc. Res. 46, 394–400. https://doi.org/10.1006/mvre.1993.1062

Comina, G., Suska, A., Filippini, D., 2014. PDMS lab-on-a-chip fabrication using 3D printed templates. Lab Chip 14, 424–430. https://doi.org/10.1039/C3LC50956G

Corada, M., Nyqvist, D., Orsenigo, F., Caprini, A., Giampietro, C., Taketo, M.M., Iruela-Arispe, M.L., Adams, R.H., Dejana, E., 2010. The Wnt/β-Catenin Pathway Modulates Vascular Remodeling and Specification by Upregulating Dll4/Notch Signaling. Dev. Cell 18, 938–949. https://doi.org/10.1016/j.devcel.2010.05.006

Cox, C.M., Poole, T.J., 2000. Angioblast differentiation is influenced by the local environment: FGF-2 induces angioblasts and patterns vessel formation in the quail embryo. Dev. Dyn. 218, 371–382. https://doi.org/10.1002/(SICI)1097-0177(200006)218:2<371::AID-DVDY10>3.0.CO;2-Z

Crawford, Y., Ferrara, N., 2009. VEGF inhibition: insights from preclinical and clinical studies. Cell Tissue Res. 335, 261–269. https://doi.org/10.1007/s00441-008-0675-8

Crisan, M., Yap, S., Casteilla, L., Chen, C.-W., Corselli, M., Park, T.S., Andriolo, G., Sun, B., Zheng, B., Zhang, L., Norotte, C., Teng, P.-N., Traas, J., Schugar, R., Deasy, B.M., Badylak, S., Bűhring, H.-J., Giacobino, J.-P., Lazzari, L., Huard, J., Péault, B., 2008. A Perivascular Origin for Mesenchymal Stem Cells in Multiple Human Organs. Cell Stem Cell 3, 301–313. https://doi.org/10.1016/j.stem.2008.07.003

Cujba, A.-M., Alvarez-Fallas, M.E., Pedraza-Arevalo, S., Laddach, A., Shepherd, M.H., Hattersley, A.T., Watt, F.M., Sancho, R., 2022. An HNF1α truncation associated with maturity-onset diabetes of the young impairs pancreatic progenitor differentiation by antagonizing HNF1β function. Cell Rep. 38, 110425. https://doi.org/10.1016/j.celrep.2022.110425

Cunningham, K.S., Gotlieb, A.I., 2005. The role of shear stress in the pathogenesis of atherosclerosis. Lab. Invest. 85, 9–23. https://doi.org/10.1038/labinvest.3700215

Cybulsky, M.I., Gimbrone, M.A., 1991. Endothelial Expression of a Mononuclear Leukocyte Adhesion Molecule During Atherogenesis. Science 251, 788–791. https://doi.org/10.1126/science.1990440

Dar, A., Domev, H., Ben-Yosef, O., Tzukerman, M., Zeevi-Levin, N., Novak, A., Germanguz, I., Amit, M., Itskovitz-Eldor, J., 2012. Multipotent Vasculogenic Pericytes From Human Pluripotent Stem Cells Promote Recovery of Murine Ischemic Limb. Circulation 125, 87–99. https://doi.org/10.1161/CIRCULATIONAHA.111.048264

Das, R.N., Tevet, Y., Safriel, S., Han, Y., Moshe, N., Lambiase, G., Bassi, I., Nicenboim, J., Brückner, M., Hirsch, D., Eilam-Altstadter, R., Herzog, W., Avraham, R., Poss, K.D., Yaniv, K., 2022. Generation of specialized blood vessels via lymphatic transdifferentiation. Nature 606, 570–575. https://doi.org/10.1038/s41586-022-04766-2

Davenport Huyer, L., Bannerman, A.D., Wang, Y., Savoji, H., Knee-Walden, E.J., Brissenden, A., Yee, B., Shoaib, M., Bobicki, E., Amsden, B.G., Radisic, M., 2019. One-Pot Synthesis of Unsaturated Polyester Bioelastomer with Controllable Material Curing for Microscale Designs. Adv. Healthc. Mater. 8, 1900245. https://doi.org/10.1002/adhm.201900245

David, L., Mallet, C., Keramidas, M., Lamandé, N., Gasc, J.-M., Dupuis-Girod, S., Plauchu, H., Feige, J.-J., Bailly, S., 2008. Bone Morphogenetic Protein-9 Is a Circulating Vascular Quiescence Factor. Circ. Res. 102, 914–922. https://doi.org/10.1161/CIRCRESAHA.107.165530

David, L., Mallet, C., Mazerbourg, S., Feige, J.-J., Bailly, S., 2007. Identification of BMP9 and BMP10 as functional activators of the orphan activin receptor-like kinase 1 (ALK1) in endothelial cells. Blood 109, 1953–1961. https://doi.org/10.1182/blood-2006-07-034124

Davis, G.E., Senger, D.R., 2005. Endothelial Extracellular Matrix: Biosynthesis, Remodeling, and Functions During Vascular Morphogenesis and Neovessel Stabilization. Circ. Res. 97, 1093–1107. https://doi.org/10.1161/01.RES.0000191547.64391.e3

De Smedt, J., van Os, E.A., Talon, I., Ghosh, S., Toprakhisar, B., Furtado Madeiro Da Costa, R., Zaunz, S., Vazquez, M.A., Boon, R., Baatsen, P., Smout, A., Verhulst, S., van Grunsven, L.A., Verfaillie, C.M., 2021. PU.1 drives specification of pluripotent stem cell-derived endothelial cells to LSEC-like cells. Cell Death Dis. 12, 84. https://doi.org/10.1038/s41419-020-03356-2

De Val, S., Black, B.L., 2009. Transcriptional Control of Endothelial Cell Development. Dev. Cell 16, 180–195. https://doi.org/10.1016/j.devcel.2009.01.014

De Val, S., Chi, N.C., Meadows, S.M., Minovitsky, S., Anderson, J.P., Harris, I.S., Ehlers, M.L., Agarwal, P., Visel, A., Xu, S.-M., Pennacchio, L.A., Dubchak, I., Krieg, P.A., Stainier, D.Y.R., Black, B.L., 2008. Combinatorial Regulation of Endothelial Gene Expression by Ets and Forkhead Transcription Factors. Cell 135, 1053–1064. https://doi.org/10.1016/j.cell.2008.10.049

de Vries, M.R., Simons, K.H., Jukema, J.W., Braun, J., Quax, P.H.A., 2016. Vein graft failure: from pathophysiology to clinical outcomes. Nat. Rev. Cardiol. 13, 451–470. https://doi.org/10.1038/nrcardio.2016.76

Dejana, E., Hirschi, K.K., Simons, M., 2017. The molecular basis of endothelial cell plasticity. Nat. Commun. 8, 14361. https://doi.org/10.1038/ncomms14361

Dellavalle, A., Sampaolesi, M., Tonlorenzi, R., Tagliafico, E., Sacchetti, B., Perani, L., Innocenzi, A., Galvez, B.G., Messina, G., Morosetti, R., Li, S., Belicchi, M., Peretti, G., Chamberlain, J.S., Wright, W.E., Torrente, Y., Ferrari, S., Bianco, P., Cossu, G., 2007. Pericytes of human skeletal muscle are myogenic precursors distinct from satellite cells. Nat. Cell Biol. 9, 255–267. https://doi.org/10.1038/ncb1542

Dickson, M.C., Martin, J.S., Cousins, F.M., Kulkarni, A.B., Karlsson, S., Akhurst, R.J., 1995. Defective haematopoiesis and vasculogenesis in transforming growth factor-beta 1 knock out mice. Development 121, 1845–1854. https://doi.org/10.1242/dev.121.6.1845

Ding, B.-S., Nolan, D.J., Butler, J.M., James, D., Babazadeh, A.O., Rosenwaks, Z., Mittal, V., Kobayashi, H., Shido, K., Lyden, D., Sato, T.N., Rabbany, S.Y., Rafii, S., 2010. Inductive angiocrine signals from sinusoidal endothelium are required for liver regeneration. Nature 468, 310–315. https://doi.org/10.1038/nature09493

Drake, C.J., Fleming, P.A., 2000. Vasculogenesis in the day 6.5 to 9.5 mouse embryo. Blood 95, 1671–1679.

Drakhlis, L., Biswanath, S., Farr, C.-M., Lupanow, V., Teske, J., Ritzenhoff, K., Franke, A., Manstein, F., Bolesani, E., Kempf, H., Liebscher, S., Schenke-Layland, K., Hegermann, J., Nolte, L., Meyer, H., de la Roche, J., Thiemann, S., Wahl-Schott, C., Martin, U., Zweigerdt, R., 2021. Human heart-forming organoids recapitulate early heart and foregut development. Nat. Biotechnol. 39, 737–746. https://doi.org/10.1038/s41587-021-00815-9

Du, Y., Lo, E., Ali, S., Khademhosseini, A., 2008. Directed assembly of cell-laden microgels for fabrication of 3D tissue constructs. Proc. Natl. Acad. Sci. 105, 9522–9527. https://doi.org/10.1073/pnas.0801866105

Duband, J.-L., Gimona, M., Scatena, M., Sartore, S., Small, J.V., 1993. Calponin and SM22 as differentiation markers of smooth muscle: spatiotemporal distribution during avian embryonic development. Differentiation 55, 1–11. https://doi.org/10.1111/j.1432-0436.1993.tb00027.x

Ebos, J.M.L., Kerbel, R.S., 2011. Antiangiogenic therapy: impact on invasion, disease progression, and metastasis. Nat. Rev. Clin. Oncol. 8, 210–221. https://doi.org/10.1038/nrclinonc.2011.21

Eelen, G., de Zeeuw, P., Simons, M., Carmeliet, P., 2015. Endothelial Cell Metabolism in Normal and Diseased Vasculature. Circ. Res. 116, 1231–1244. https://doi.org/10.1161/CIRCRESAHA.116.302855

Eelen, G., Treps, L., Li, X., Carmeliet, P., 2020. Basic and Therapeutic Aspects of Angiogenesis Updated. Circ. Res. 127, 310–329. https://doi.org/10.1161/CIRCRESAHA.120.316851

Ehebauer, M., Hayward, P., Arias, A.M., 2006. Notch, a Universal Arbiter of Cell Fate Decisions. Science 314, 1414–1415. https://doi.org/10.1126/science.1134042

Eilken, H.M., Diéguez-Hurtado, R., Schmidt, I., Nakayama, M., Jeong, H.-W., Arf, H., Adams, S., Ferrara, N., Adams, R.H., 2017. Pericytes regulate VEGF-induced endothelial sprouting through VEGFR1. Nat. Commun. 8, 1574. https://doi.org/10.1038/s41467-017-01738-3

Esser, J.S., Rahner, S., Deckler, M., Bode, C., Patterson, C., Moser, M., 2015. Fibroblast Growth Factor Signaling Pathway in Endothelial Cells Is Activated by BMPER to Promote Angiogenesis. Arterioscler. Thromb. Vasc. Biol. 35, 358–367. https://doi.org/10.1161/ATVBAHA.114.304345

Evensen, L., Micklem, D.R., Blois, A., Berge, S.V., Aarsæther, N., Littlewood-Evans, A., Wood, J., Lorens, J.B., 2009. Mural Cell Associated VEGF Is Required for Organotypic Vessel Formation. PLoS ONE 4, e5798. https://doi.org/10.1371/journal.pone.0005798

Faal, T., Phan, D.T.T., Davtyan, H., Scarfone, V.M., Varady, E., Blurton-Jones, M., Hughes, C.C.W., Inlay, M.A., 2019. Induction of Mesoderm and Neural Crest-Derived Pericytes from Human Pluripotent Stem Cells to Study Blood-Brain Barrier Interactions. Stem Cell Rep. 12, 451–460. https://doi.org/10.1016/j.stemcr.2019.01.005

Fang, J.S., Coon, B.G., Gillis, N., Chen, Z., Qiu, J., Chittenden, T.W., Burt, J.M., Schwartz, M.A., Hirschi, K.K., 2017. Shear-induced Notch-Cx37-p27 axis arrests endothelial cell cycle to enable arterial specification. Nat. Commun. 8, 2149. https://doi.org/10.1038/s41467-017-01742-7

Fang, Y., Wu, D., Birukov, K.G., 2019. Mechanosensing and Mechanoregulation of Endothelial Cell Functions, in: Terjung, R. (Ed.), Comprehensive Physiology. Wiley, pp. 873–904. https://doi.org/10.1002/cphy.c180020

Feil, S., Hofmann, F., Feil, R., 2004. SM22α Modulates Vascular Smooth Muscle Cell Phenotype During Atherogenesis. Circ. Res. 94, 863–865. https://doi.org/10.1161/01.RES.0000126417.38728.F6

Ferdous, A., Caprioli, A., Iacovino, M., Martin, C.M., Morris, J., Richardson, J.A., Latif, S., Hammer, R.E., Harvey, R.P., Olson, E.N., Kyba, M., Garry, D.J., 2009. Nkx2–5 transactivates the *Ets-related protein 71* gene and specifies an endothelial/endocardial fate in the developing embryo. Proc. Natl. Acad. Sci. 106, 814–819. https://doi.org/10.1073/pnas.0807583106

Fernández-Chacón, M., García-González, I., Mühleder, S., Benedito, R., 2021. Role of Notch in endothelial biology. Angiogenesis 24, 237–250. https://doi.org/10.1007/s10456-021-09793-7

Fernández-Klett, F., Offenhauser, N., Dirnagl, U., Priller, J., Lindauer, U., 2010. Pericytes in capillaries are contractile in vivo, but arterioles mediate functional hyperemia in the mouse brain. Proc. Natl. Acad. Sci. U. S. A. 107, 22290–22295. https://doi.org/10.1073/pnas.1011321108

Ferrara, N., 2002. Role of vascular endothelial growth factor in physiologic and pathologic angiogenesis: Therapeutic implications. Semin. Oncol. 29, 10–14. https://doi.org/10.1053/sonc.2002.37264

Filippi, M.-D., 2019. Neutrophil transendothelial migration: updates and new perspectives. Blood 133, 2149–2158. https://doi.org/10.1182/blood-2018-12-844605

Fish, J.E., Wythe, J.D., 2015. The molecular regulation of arteriovenous specification and maintenance. Dev. Dyn. Off. Publ. Am. Assoc. Anat. 244, 391–409. https://doi.org/10.1002/dvdy.24252

Furuse, M., Hirase, T., Itoh, M., Nagafuchi, A., Yonemura, S., Tsukita, S., Tsukita, S., 1993. Occludin: a novel integral membrane protein localizing at tight junctions. J. Cell Biol. 123, 1777–1788. https://doi.org/10.1083/jcb.123.6.1777

Gabbiani, G., Schmid, E., Winter, S., Chaponnier, C., de Ckhastonay, C., Vandekerckhove, J., Weber, K., Franke, W.W., 1981. Vascular smooth muscle cells differ from other smooth muscle cells: predominance of vimentin filaments and a specific alpha-type actin. Proc. Natl. Acad. Sci. 78, 298–302. https://doi.org/10.1073/pnas.78.1.298

Gabe, I.T., Gault, J.H., Ross, J., Mason, D.T., Mills, C.J., Schillingford, J.P., Braunwald, E., 1969. Measurement of Instantaneous Blood Flow Velocity and Pressure in Conscious Man with a Catheter-Tip Velocity Probe. Circulation 40, 603–614. https://doi.org/10.1161/01.CIR.40.5.603

Gage, B.K., Liu, J.C., Innes, B.T., MacParland, S.A., McGilvray, I.D., Bader, G.D., Keller, G.M., 2020. Generation of Functional Liver Sinusoidal Endothelial Cells from Human Pluripotent Stem-Cell-Derived Venous Angioblasts. Cell Stem Cell 27, 254-269.e9. https://doi.org/10.1016/j.stem.2020.06.007

Gama-Norton, L., Ferrando, E., Ruiz-Herguido, C., Liu, Z., Guiu, J., Islam, A.B.M.M.K., Lee, S.-U., Yan, M., Guidos, C.J., López-Bigas, N., Maeda, T., Espinosa, L., Kopan, R., Bigas, A., 2015. Notch signal strength controls cell fate in the haemogenic endothelium. Nat. Commun. 6, 8510. https://doi.org/10.1038/ncomms9510

Garcia-Gonzalo, F.R., Izpisúa Belmonte, J.C., 2008. Albumin-Associated Lipids Regulate Human Embryonic Stem Cell Self-Renewal. PLoS ONE 3, e1384. https://doi.org/10.1371/journal.pone.0001384

García-León, J.A., García-Díaz, B., Eggermont, K., Cáceres-Palomo, L., Neyrinck, K., Madeiro da Costa, R., Dávila, J.C., Baron-Van Evercooren, A., Gutiérrez, A., Verfaillie, C.M., 2020. Generation of oligodendrocytes and establishment of an all-human myelinating platform from human pluripotent stem cells. Nat. Protoc. 15, 3716–3744. https://doi.org/10.1038/s41596-020-0395-4

Gebb, S., Stevens, T., 2004. On lung endothelial cell heterogeneity. Microvasc. Res. 68, 1–12. https://doi.org/10.1016/j.mvr.2004.02.002

Geng, X., Cha, B., Mahamud, Md.R., Srinivasan, R.S., 2017. Intraluminal valves: development, function and disease. Dis. Model. Mech. 10, 1273–1287. https://doi.org/10.1242/dmm.030825

Géraud, C., Koch, P.-S., Zierow, J., Klapproth, K., Busch, K., Olsavszky, V., Leibing, T., Demory, A., Ulbrich, F., Diett, M., Singh, S., Sticht, C., Breitkopf-Heinlein, K., Richter, K., Karppinen, S.-M., Pihlajaniemi, T., Arnold, B., Rodewald, H.-R., Augustin, H.G., Schledzewski, K., Goerdt, S., 2017. GATA4-dependent organ-specific endothelial differentiation controls liver development and embryonic hematopoiesis. J. Clin. Invest. 127, 1099–1114. https://doi.org/10.1172/JCI90086

Gerhardt, H., Golding, M., Fruttiger, M., Ruhrberg, C., Lundkvist, A., Abramsson, A., Jeltsch, M., Mitchell, C., Alitalo, K., Shima, D., Betsholtz, C., 2003. VEGF guides angiogenic sprouting utilizing endothelial tip cell filopodia. J. Cell Biol. 161, 1163–1177. https://doi.org/10.1083/jcb.200302047

Ghaffari, S., Leask, R.L., Jones, E.A.V., 2015. Flow dynamics control the location of sprouting and direct elongation during developmental angiogenesis. Development dev.128058. https://doi.org/10.1242/dev.128058

Ghimire, K., Altmann, H.M., Straub, A.C., Isenberg, J.S., 2017. Nitric oxide: what's new to NO? Am. J. Physiol.-Cell Physiol. 312, C254–C262. https://doi.org/10.1152/ajpcell.00315.2016

Giacomelli, E., Bellin, M., Orlova, V.V., Mummery, C.L., 2017. Co-Differentiation of Human Pluripotent Stem Cells-Derived Cardiomyocytes and Endothelial Cells from Cardiac Mesoderm Provides a Three-Dimensional Model of Cardiac Microtissue. Curr. Protoc. Hum. Genet. 95. https://doi.org/10.1002/cphg.46

Ginsberg, M., James, D., Ding, B.-S., Nolan, D., Geng, F., Butler, J.M., Schachterle, W., Pulijaal, V.R., Mathew, S., Chasen, S.T., Xiang, J., Rosenwaks, Z., Shido, K., Elemento, O., Rabbany, S.Y., Rafii, S., 2012. Efficient Direct Reprogramming of Mature Amniotic Cells into Endothelial Cells by ETS Factors and TGFβ Suppression. Cell 151, 559–575. https://doi.org/10.1016/j.cell.2012.09.032

Glaser, D.E., Turner, W.S., Madfis, N., Wong, L., Zamora, J., White, N., Reyes, S., Burns, A.B., Gopinathan, A., McCloskey, K.E., 2016. Multifactorial Optimizations for Directing Endothelial Fate from Stem Cells. PLOS ONE 11, e0166663. https://doi.org/10.1371/journal.pone.0166663

Golden, A.P., Tien, J., 2007. Fabrication of microfluidic hydrogels using molded gelatin as a sacrificial element. Lab. Chip 7, 720. https://doi.org/10.1039/b618409j

Gómez-Salinero, J.M., Izzo, F., Lin, Y., Houghton, S., Itkin, T., Geng, F., Bram, Y., Adelson, R.P., Lu, T.M., Inghirami, G., Xiang, J.Z., Lis, R., Redmond, D., Schreiner, R., Rabbany, S.Y., Landau, D.A., Schwartz, R.E., Rafii, S., 2022. Specification of fetal liver endothelial progenitors to functional zonated adult sinusoids requires c-Maf induction. Cell Stem Cell 29, 593-609.e7. https://doi.org/10.1016/j.stem.2022.03.002

Gomez-Salinero, J.M., Rafii, S., 2018. Endothelial cell adaptation in regeneration. Science 362, 1116–1117. https://doi.org/10.1126/science.aar4800

Göritz, C., Dias, D.O., Tomilin, N., Barbacid, M., Shupliakov, O., Frisén, J., 2011. A Pericyte Origin of Spinal Cord Scar Tissue. Science 333, 238–242. https://doi.org/10.1126/science.1203165

Goveia, J., Rohlenova, K., Taverna, F., Treps, L., Conradi, L.-C., Pircher, A., Geldhof, V., de Rooij, L.P.M.H., Kalucka, J., Sokol, L., García-Caballero, M., Zheng, Y., Qian, J., Teuwen, L.-A., Khan, S., Boeckx, B., Wauters, E., Decaluwé, H., De Leyn, P., Vansteenkiste, J., Weynand, B., Sagaert, X., Verbeken, E., Wolthuis, A., Topal, B., Everaerts, W., Bohnenberger, H., Emmert, A., Panovska, D., De Smet, F., Staal, F.J.T., Mclaughlin, R.J., Impens, F., Lagani, V., Vinckier, S., Mazzone, M., Schoonjans, L., Dewerchin, M., Eelen, G., Karakach, T.K., Yang, H., Wang, J., Bolund, L., Lin, L., Thienpont, B., Li, X., Lambrechts, D., Luo, Y.,

Carmeliet, P., 2020. An Integrated Gene Expression Landscape Profiling Approach to Identify Lung Tumor Endothelial Cell Heterogeneity and Angiogenic Candidates. Cancer Cell 37, 21-36.e13. https://doi.org/10.1016/j.ccell.2019.12.001

Granata, A., Serrano, F., Bernard, W.G., McNamara, M., Low, L., Sastry, P., Sinha, S., 2017. An iPSC-derived vascular model of Marfan syndrome identifies key mediators of smooth muscle cell death. Nat. Genet. 49, 97–109. https://doi.org/10.1038/ng.3723

Grigoryan, B., Paulsen, S.J., Corbett, D.C., Sazer, D.W., Fortin, C.L., Zaita, A.J., Greenfield, P.T., Calafat, N.J., Gounley, J.P., Ta, A.H., Johansson, F., Randles, A., Rosenkrantz, J.E., Louis-Rosenberg, J.D., Galie, P.A., Stevens, K.R., Miller, J.S., 2019. Multivascular networks and functional intravascular topologies within biocompatible hydrogels. Science 364, 458–464. https://doi.org/10.1126/science.aav9750

Gritz, E., Hirschi, K.K., 2016. Specification and function of hemogenic endothelium during embryogenesis. Cell. Mol. Life Sci. 73, 1547–1567. https://doi.org/10.1007/s00018-016-2134-0

Gu, M., Shao, N.-Y., Sa, S., Li, D., Termglinchan, V., Ameen, M., Karakikes, I., Sosa, G., Grubert, F., Lee, J., Cao, A., Taylor, S., Ma, Y., Zhao, Z., Chappell, J., Hamid, R., Austin, E.D., Gold, J.D., Wu, J.C., Snyder, M.P., Rabinovitch, M., 2017. Patient-Specific iPSC-Derived Endothelial Cells Uncover Pathways that Protect against Pulmonary Hypertension in BMPR2 Mutation Carriers. Cell Stem Cell 20, 490-504.e5. https://doi.org/10.1016/j.stem.2016.08.019

Gui, L., Boyle, M.J., Kamin, Y.M., Huang, A.H., Starcher, B.C., Miller, C.A., Vishnevetsky, M.J., Niklason, L.E., 2014. Construction of Tissue-Engineered Small-Diameter Vascular Grafts in Fibrin Scaffolds in 30 Days. Tissue Eng. Part A 20, 1499–1507. https://doi.org/10.1089/ten.tea.2013.0263

Gui, L., Dash, B.C., Luo, J., Qin, L., Zhao, L., Yamamoto, K., Hashimoto, T., Wu, H., Dardik, A., Tellides, G., Niklason, L.E., Qyang, Y., 2016. Implantable tissue-engineered blood vessels from human induced pluripotent stem cells. Biomaterials 102, 120–129. https://doi.org/10.1016/j.biomaterials.2016.06.010

Guimarães-Camboa, N., Cattaneo, P., Sun, Y., Moore-Morris, T., Gu, Y., Dalton, N.D., Rockenstein, E., Masliah, E., Peterson, K.L., Stallcup, W.B., Chen, J., Evans, S.M., 2017. Pericytes of Multiple Organs Do Not Behave as Mesenchymal Stem Cells In Vivo. Cell Stem Cell 20, 345-359.e5. https://doi.org/10.1016/j.stem.2016.12.006

Haase, K., Kamm, R.D., 2017. Advances in on-chip vascularization. Regen. Med. 12, 285–302. https://doi.org/10.2217/rme-2016-0152

Hachey, S.J., Movsesyan, S., Nguyen, Q.H., Burton-Sojo, G., Tankazyan, A., Wu, J., Hoang, T., Zhao, D., Wang, S., Hatch, M.M., Celaya, E., Gomez, S., Chen, G.T., Davis, R.T., Nee, K., Pervolarakis, N., Lawson, D.A., Kessenbrock, K., Lee, A.P., Lowengrub, J., Waterman, M.L., Hughes, C.C.W., 2021. An in vitro vascularized micro-tumor model of human colorectal cancer recapitulates in vivo responses to standard-of-care therapy. Lab. Chip 21, 1333–1351. https://doi.org/10.1039/D0LC01216E

Hakanpaa, L., Sipila, T., Leppanen, V.-M., Gautam, P., Nurmi, H., Jacquemet, G., Eklund, L., Ivaska, J., Alitalo, K., Saharinen, P., 2015. Endothelial destabilization by angiopoietin-2 via integrin β1 activation. Nat. Commun. 6, 5962. https://doi.org/10.1038/ncomms6962

Hall, C.N., Reynell, C., Gesslein, B., Hamilton, N.B., Mishra, A., Sutherland, B.A., O'Farrell, F.M., Buchan, A.M., Lauritzen, M., Attwell, D., 2014. Capillary pericytes regulate cerebral blood flow in health and disease. Nature 508, 55–60. https://doi.org/10.1038/nature13165

Hamano, Y., Zeisberg, M., Sugimoto, H., Lively, J.C., Maeshima, Y., Yang, C., Hynes, R.O., Werb, Z., Sudhakar, A., Kalluri, R., 2003. Physiological levels of tumstatin, a fragment of collagen IV α3 chain, are generated by MMP-9 proteolysis and suppress angiogenesis via αVβ3 integrin. Cancer Cell 3, 589–601. https://doi.org/10.1016/S1535-6108(03)00133-8

Harink, B., Le Gac, S., Barata, D., van Blitterswijk, C., Habibovic, P., 2014. Microtiter plate-sized standalone chip holder for microenvironmental physiological control in gas-impermeable microfluidic devices. Lab Chip 14, 1816–1820. https://doi.org/10.1039/C4LC00190G

Hasan, A., Paul, A., Vrana, N.E., Zhao, X., Memic, A., Hwang, Y.-S., Dokmeci, M.R., Khademhosseini, A., 2014. Microfluidic techniques for development of 3D vascularized tissue. Biomaterials 35, 7308–7325. https://doi.org/10.1016/j.biomaterials.2014.04.091

Haudenschild, C.C., 1984. Morphology of vascular endothelial cells in culture, in: Jaffe, E.A. (Ed.), Biology of Endothelial Cells, Developments in Cardiovascular Medicine. Springer US, Boston, MA, pp. 129–140. https://doi.org/10.1007/978-1-4613-2825-4_13

Hellstrom, M., Kal n, M., Lindahl, P., Abramsson, A., Betsholtz, C., 1999. Role of PDGF-B and PDGFR-beta in recruitment of vascular smooth muscle cells and pericytes during embryonic blood vessel formation in the mouse. Development 126, 3047–3055. https://doi.org/10.1242/dev.126.14.3047

Hellström, M., Phng, L.-K., Hofmann, J.J., Wallgard, E., Coultas, L., Lindblom, P., Alva, J., Nilsson, A.-K., Karlsson, L., Gaiano, N., Yoon, K., Rossant, J., Iruela-Arispe, M.L., Kalén, M., Gerhardt, H., Betsholtz, C., 2007. Dll4 signalling through Notch1 regulates formation of tip cells during angiogenesis. Nature 445, 776–780. https://doi.org/10.1038/nature05571

Herbert, S.P., Stainier, D.Y.R., 2011. Molecular control of endothelial cell behaviour during blood vessel morphogenesis. Nat. Rev. Mol. Cell Biol. 12, 551–564. https://doi.org/10.1038/nrm3176

Hernández Vera, R., O'Callaghan, P., Fatsis-Kavalopoulos, N., Kreuger, J., 2019. Modular microfluidic systems cast from 3D-printed molds for imaging leukocyte adherence to differentially treated endothelial cultures. Sci. Rep. 9, 11321. https://doi.org/10.1038/s41598-019-47475-z

Herzog, Y., Kalcheim, C., Kahane, N., Reshef, R., Neufeld, G., 2001. Differential expression of neuropilin-1 and neuropilin-2 in arteries and veins. Mech. Dev. 109, 115–119. https://doi.org/10.1016/S0925-4773(01)00518-4

Hetheridge, C., Mavria, G., Mellor, H., 2011. Uses of the *in vitro* endothelial–fibroblast organotypic co-culture assay in angiogenesis research. Biochem. Soc. Trans. 39, 1597–1600. https://doi.org/10.1042/BST20110738

Hirama, H., Satoh, T., Sugiura, S., Shin, K., Onuki-Nagasaki, R., Kanamori, T., Inoue, T., 2019. Glass-based organ-on-a-chip device for restricting small molecular absorption. J. Biosci. Bioeng. 127, 641–646. https://doi.org/10.1016/j.jbiosc.2018.10.019

Hirota, A., Kamino, K., Komuro, H., Sakai, T., Yada, T., 1985. Early events in development of electrical activity and contraction in embryonic rat heart assessed by optical recording. J. Physiol. 369, 209–227. https://doi.org/10.1113/jphysiol.1985.sp015897

Holloway, E.M., Wu, J.H., Czerwinski, M., Sweet, C.W., Wu, A., Tsai, Y.-H., Huang, S., Stoddard, A.E., Capeling, M.M., Glass, I., Spence, J.R., 2020. Differentiation of Human Intestinal Organoids with Endogenous Vascular Endothelial Cells. Dev. Cell 54, 516-528.e7. https://doi.org/10.1016/j.devcel.2020.07.023

Hong, C.C., Peterson, Q.P., Hong, J.-Y., Peterson, R.T., 2006. Artery/Vein Specification Is Governed by Opposing Phosphatidylinositol-3 Kinase and MAP Kinase/ERK Signaling. Curr. Biol. 16, 1366–1372. https://doi.org/10.1016/j.cub.2006.05.046

Hsu, Y.-H., Moya, M.L., Abiri, P., Hughes, C.C.W., George, S.C., Lee, A.P., 2013. Full range physiological mass transport control in 3D tissue cultures. Lab. Chip 13, 81–89. https://doi.org/10.1039/c2lc40787f

Huber, T.L., Kouskoff, V., Joerg Fehling, H., Palis, J., Keller, G., 2004. Haemangioblast commitment is initiated in the primitive streak of the mouse embryo. Nature 432, 625–630. https://doi.org/10.1038/nature03122

Ingber, D.E., 2022. Human organs-on-chips for disease modelling, drug development and personalized medicine. Nat. Rev. Genet. 23, 467–491. https://doi.org/10.1038/s41576-022-00466-9

Itkin, T., Gur-Cohen, S., Spencer, J.A., Schajnovitz, A., Ramasamy, S.K., Kusumbe, A.P., Ledergor, G., Jung, Y., Milo, I., Poulos, M.G., Kalinkovich, A., Ludin, A., Kollet, O., Shakhar, G., Butler, J.M., Rafii, S., Adams, R.H., Scadden, D.T., Lin, C.P., Lapidot, T., 2016. Distinct bone marrow blood vessels differentially regulate haematopoiesis. Nature 532, 323–328. https://doi.org/10.1038/nature17624

Jaffe, E.A., Nachman, R.L., Becker, C.G., Minick, C.R., 1973. Culture of Human Endothelial Cells Derived from Umbilical Veins. IDENTIFICATION BY MORPHOLOGIC AND IMMUNOLOGIC CRITERIA. J. Clin. Invest. 52, 2745–2756. https://doi.org/10.1172/JCI107470

Jain, R.K., 2005. Normalization of Tumor Vasculature: An Emerging Concept in Antiangiogenic Therapy. Science 307, 58–62. https://doi.org/10.1126/science.1104819

Jain, R.K., 2003. Molecular regulation of vessel maturation. Nat. Med. 9, 685–693. https://doi.org/10.1038/nm0603-685

Jakobsson, L., Bentley, K., Gerhardt, H., 2009. VEGFRs and Notch: a dynamic collaboration in vascular patterning. Biochem. Soc. Trans. 37, 1233–1236. https://doi.org/10.1042/BST0371233

Jakobsson, L., Franco, C.A., Bentley, K., Collins, R.T., Ponsioen, B., Aspalter, I.M., Rosewell, I., Busse, M., Thurston, G., Medvinsky, A., Schulte-Merker, S., Gerhardt, H., 2010. Endothelial cells dynamically compete for the tip cell position during angiogenic sprouting. Nat. Cell Biol. 12, 943–953. https://doi.org/10.1038/ncb2103

Jamieson, J.J., Linville, R.M., Ding, Y.Y., Gerecht, S., Searson, P.C., 2019. Role of iPSC-derived pericytes on barrier function of iPSC-derived brain microvascular endothelial cells in 2D and 3D. Fluids Barriers CNS 16, 15. https://doi.org/10.1186/s12987-019-0136-7

Jarad, M., Kuczynski, E.A., Morrison, J., Viloria-Petit, A.M., Coomber, B.L., 2017. Release of endothelial cell associated VEGFR2 during TGF-β modulated angiogenesis in vitro. BMC Cell Biol. 18, 10. https://doi.org/10.1186/s12860-017-0127-y

Jeske, R., Albo, J., Marzano, M., Bejoy, J., Li, Y., 2020. Engineering Brain-Specific Pericytes from Human Pluripotent Stem Cells. Tissue Eng. Part B Rev. 26, 367–382. https://doi.org/10.1089/ten.teb.2020.0091

Ji, R.P., Phoon, C.K.L., Aristizábal, O., McGrath, K.E., Palis, J., Turnbull, D.H., 2003. Onset of Cardiac Function During Early Mouse Embryogenesis Coincides With Entry of Primitive Erythroblasts Into the Embryo Proper. Circ. Res. 92, 133–135. https://doi.org/10.1161/01.RES.0000056532.18710.C0

Jia, W., Lu, R., Martin, T.A., Jiang, W.G., 2014. The role of claudin-5 in blood-brain barrier (BBB) and brain metastases (Review). Mol. Med. Rep. 9, 779–785. https://doi.org/10.3892/mmr.2013.1875

Jih, Y., Lien, W., Tsai, W., Yang, G., Li, C., Wu, L., 2001. Distinct regulation of genes by bFGF and VEGF-A in endothelial cells. Angiogenesis 4, 313–321. https://doi.org/10.1023/A:1016080321956

Jones, T.R., Kang, I.H., Wheeler, D.B., Lindquist, R.A., Papallo, A., Sabatini, D.M., Golland, P., Carpenter, A.E., 2008. CellProfiler Analyst: data exploration and analysis software for complex image-based screens. BMC Bioinformatics 9, 482. https://doi.org/10.1186/1471-2105-9-482

Joshi, R.S., Kanugula, S.S., Sudhir, S., Pereira, M.P., Jain, S., Aghi, M.K., 2021. The Role of Cancer-Associated Fibroblasts in Tumor Progression. Cancers 13, 1399. https://doi.org/10.3390/cancers13061399

Jourde-Chiche, N., Fakhouri, F., Dou, L., Bellien, J., Burtey, S., Frimat, M., Jarrot, P.-A., Kaplanski, G., Le Quintrec, M., Pernin, V., Rigothier, C., Sallée, M., Fremeaux-Bacchi, V., Guerrot, D., Roumenina, L.T., 2019. Endothelium structure and function in kidney health and disease. Nat. Rev. Nephrol. 15, 87–108. https://doi.org/10.1038/s41581-018-0098-z

Kalogeris, T.J., Kevil, C.G., Laroux, F.S., Coe, L.L., Phifer, T.J., Alexander, J.S., 1999. Differential monocyte adhesion and adhesion molecule expression in venous and arterial endothelial cells. Am. J. Physiol.-Lung Cell. Mol. Physiol. 276, L9–L19. https://doi.org/10.1152/ajplung.1999.276.1.L9

Kalucka, J., Bierhansl, L., Conchinha, N.V., Missiaen, R., Elia, I., Brüning, U., Scheinok, S., Treps, L., Cantelmo, A.R., Dubois, C., de Zeeuw, P., Goveia, J., Zecchin, A., Taverna, F., Morales-Rodriguez, F., Brajic, A., Conradi, L.-C., Schoors, S., Harjes, U., Vriens, K., Pilz, G.-A., Chen, R., Cubbon, R., Thienpont, B., Cruys, B., Wong, B.W., Ghesquière, B., Dewerchin, M., De Bock, K., Sagaert, X., Jessberger, S., Jones, E.A.V., Gallez, B., Lambrechts, D., Mazzone, M., Eelen, G., Li, X., Fendt, S.-M., Carmeliet, P., 2018. Quiescent Endothelial Cells Upregulate Fatty Acid β-Oxidation for Vasculoprotection via Redox Homeostasis. Cell Metab. 28, 881-894.e13. https://doi.org/10.1016/j.cmet.2018.07.016

Kalucka, J., de Rooij, L.P.M.H., Goveia, J., Rohlenova, K., Dumas, S.J., Meta, E., Conchinha, N.V., Taverna, F., Teuwen, L.-A., Veys, K., García-Caballero, M., Khan, S., Geldhof, V., Sokol, L.,

Chen, R., Treps, L., Borri, M., de Zeeuw, P., Dubois, C., Karakach, T.K., Falkenberg, K.D., Parys, M., Yin, X., Vinckier, S., Du, Y., Fenton, R.A., Schoonjans, L., Dewerchin, M., Eelen, G., Thienpont, B., Lin, L., Bolund, L., Li, X., Luo, Y., Carmeliet, P., 2020. Single-Cell Transcriptome Atlas of Murine Endothelial Cells. Cell 180, 764-779.e20. https://doi.org/10.1016/j.cell.2020.01.015

Kanki, Y., Nakaki, R., Shimamura, T., Matsunaga, T., Yamamizu, K., Katayama, S., Suehiro, J.-I., Osawa, T., Aburatani, H., Kodama, T., Wada, Y., Yamashita, J.K., Minami, T., 2017. Dynamically and epigenetically coordinated GATA/ETS/SOX transcription factor expression is indispensable for endothelial cell differentiation. Nucleic Acids Res. 45, 4344–4358. https://doi.org/10.1093/nar/gkx159

Karkkainen, M.J., Haiko, P., Sainio, K., Partanen, J., Taipale, J., Petrova, T.V., Jeltsch, M., Jackson, D.G., Talikka, M., Rauvala, H., Betsholtz, C., Alitalo, K., 2004. Vascular endothelial growth factor C is required for sprouting of the first lymphatic vessels from embryonic veins. Nat. Immunol. 5, 74–80. https://doi.org/10.1038/ni1013

Kawasaki, T., Kitsukawa, T., Bekku, Y., Matsuda, Y., Sanbo, M., Yagi, T., Fujisawa, H., 1999. A requirement for neuropilin-1 in embryonic vessel formation. Development 126, 4895–4902. https://doi.org/10.1242/dev.126.21.4895

Kelleher, J., Dickinson, A., Cain, S., Hu, Y., Bates, N., Harvey, A., Ren, J., Zhang, W., Moreton, F.C., Muir, K.W., Ward, C., Touyz, R.M., Sharma, P., Xu, Q., Kimber, S.J., Wang, T., 2019. Patient-Specific iPSC Model of a Genetic Vascular Dementia Syndrome Reveals Failure of Mural Cells to Stabilize Capillary Structures. Stem Cell Rep. 13, 817–831. https://doi.org/10.1016/j.stemcr.2019.10.004

Kim, J., Cooper, J.A., 2018. Septins regulate junctional integrity of endothelial monolayers. Mol. Biol. Cell 29, 1693–1703. https://doi.org/10.1091/mbc.E18-02-0136

Kim, S., Chung, M., Ahn, J., Lee, S., Jeon, N.L., 2016. Interstitial flow regulates the angiogenic response and phenotype of endothelial cells in a 3D culture model. Lab. Chip 16, 4189–4199. https://doi.org/10.1039/C6LC00910G

Kim, S., Lee, H., Chung, M., Jeon, N.L., 2013. Engineering of functional, perfusable 3D microvascular networks on a chip. Lab. Chip 13, 1489. https://doi.org/10.1039/c3lc41320a

Kim, Y., Park, N., Rim, Y.A., Nam, Y., Jung, H., Lee, K., Ju, J.H., 2018. Establishment of a complex skin structure via layered co-culture of keratinocytes and fibroblasts derived from induced pluripotent stem cells. Stem Cell Res. Ther. 9, 217. https://doi.org/10.1186/s13287-018-0958-2

King, K.R., Wang, C.C.J., Kaazempur-Mofrad, M.R., Vacanti, J.P., Borenstein, J.T., 2004. Biodegradable Microfluidics. Adv. Mater. 16, 2007–2012. https://doi.org/10.1002/adma.200306522

Klein, D., Weißhardt, P., Kleff, V., Jastrow, H., Jakob, H.G., Ergün, S., 2011. Vascular Wall-Resident CD44+ Multipotent Stem Cells Give Rise to Pericytes and Smooth Muscle Cells and Contribute to New Vessel Maturation. PLoS ONE 6, e20540. https://doi.org/10.1371/journal.pone.0020540

Kleinman, H.K., McGarvey, M.L., Hassell, J.R., Star, V.L., Cannon, F.B., Laurie, G.W., Martin, G.R., 1986. Basement membrane complexes with biological activity. Biochemistry 25, 312–318. https://doi.org/10.1021/bi00350a005

Knolle, P.A., Wohlleber, D., 2016. Immunological functions of liver sinusoidal endothelial cells. Cell. Mol. Immunol. 13, 347–353. https://doi.org/10.1038/cmi.2016.5

Kolesky, D.B., Homan, K.A., Skylar-Scott, M.A., Lewis, J.A., 2016. Three-dimensional bioprinting of thick vascularized tissues. Proc. Natl. Acad. Sci. 113, 3179–3184. https://doi.org/10.1073/pnas.1521342113

Kolesky, D.B., Truby, R.L., Gladman, A.S., Busbee, T.A., Homan, K.A., Lewis, J.A., 2014. 3D Bioprinting of Vascularized, Heterogeneous Cell-Laden Tissue Constructs. Adv. Mater. 26, 3124–3130. https://doi.org/10.1002/adma.201305506

Korn, J., Christ, B., Kurz, H., 2002. Neuroectodermal origin of brain pericytes and vascular smooth muscle cells. J. Comp. Neurol. 442, 78–88. https://doi.org/10.1002/cne.1423

Koyano-Nakagawa, N., Garry, D.J., 2017. Etv2 as an essential regulator of mesodermal lineage development. Cardiovasc. Res. 113, 1294–1306. https://doi.org/10.1093/cvr/cvx133

Kubota, Y., Kleinman, H.K., Martin, G.R., Lawley, T.J., 1988. Role of laminin and basement membrane in the morphological differentiation of human endothelial cells into capillary-like structures. J. Cell Biol. 107, 1589–1598. https://doi.org/10.1083/jcb.107.4.1589

Kumano, K., Chiba, S., Kunisato, A., Sata, M., Saito, T., Nakagami-Yamaguchi, E., Yamaguchi, T., Masuda, S., Shimizu, K., Takahashi, T., Ogawa, S., Hamada, Y., Hirai, H., 2003. Notch1 but Not Notch2 Is Essential for Generating Hematopoietic Stem Cells from Endothelial Cells. Immunity 18, 699–711. https://doi.org/10.1016/S1074-7613(03)00117-1

Kumar, A., D'Souza, S.S., Moskvin, O.V., Toh, H., Wang, B., Zhang, J., Swanson, S., Guo, L.-W., Thomson, J.A., Slukvin, I.I., 2017. Specification and Diversification of Pericytes and Smooth Muscle Cells from Mesenchymoangioblasts. Cell Rep. 19, 1902–1916. https://doi.org/10.1016/j.celrep.2017.05.019

Kumar, M., Toprakhisar, B., Van Haele, M., Antoranz, A., Boon, R., Chesnais, F., De Smedt, J., Tricot, T., Idoype, T.I., Canella, M., Tilliole, P., De Boeck, J., Bajaj, M., Ranga, A., Bosisio, F.M., Roskams, T., van Grunsven, L.A., Verfaillie, C.M., 2021. A fully defined matrix to support a pluripotent stem cell derived multi-cell-liver steatohepatitis and fibrosis model. Biomaterials 276, 121006. https://doi.org/10.1016/j.biomaterials.2021.121006

Kunz, J., Krause, D., Kremer, M., Dermietzel, R., 2008. The 140-kDa Protein of Blood-Brain Barrier-Associated Pericytes Is Identical to Aminopeptidase N. J. Neurochem. 62, 2375–2386. https://doi.org/10.1046/j.1471-4159.1994.62062375.x

Kusuma, S., Shen, Y.-I., Hanjaya-Putra, D., Mali, P., Cheng, L., Gerecht, S., 2013. Self-organized vascular networks from human pluripotent stem cells in a synthetic matrix. Proc. Natl. Acad. Sci. 110, 12601–12606. https://doi.org/10.1073/pnas.1306562110

Kusumbe, A.P., Ramasamy, S.K., Adams, R.H., 2014. Coupling of angiogenesis and osteogenesis by a specific vessel subtype in bone. Nature 507, 323–328. https://doi.org/10.1038/nature13145

Lammert, E., Cleaver, O., Melton, D., 2001. Induction of Pancreatic Differentiation by Signals from Blood Vessels. Science 294, 564–567. https://doi.org/10.1126/science.1064344

Lampugnani, M.G., Corada, M., Caveda, L., Breviario, F., Ayalon, O., Geiger, B., Dejana, E., 1995. The molecular organization of endothelial cell to cell junctions: differential association of plakoglobin, beta-catenin, and alpha-catenin with vascular endothelial cadherin (VE-cadherin). J. Cell Biol. 129, 203–217. https://doi.org/10.1083/jcb.129.1.203

Lampugnani, M.G., Dejana, E., Giampietro, C., 2018. Vascular Endothelial (VE)-Cadherin, Endothelial Adherens Junctions, and Vascular Disease. Cold Spring Harb. Perspect. Biol. 10, a029322. https://doi.org/10.1101/cshperspect.a029322

Lampugnani, M.G., Resnati, M., Raiteri, M., Pigott, R., Pisacane, A., Houen, G., Ruco, L.P., Dejana, E., 1992. A novel endothelial-specific membrane protein is a marker of cell-cell contacts. J. Cell Biol. 118, 1511–1522. https://doi.org/10.1083/jcb.118.6.1511

Lawson, N.D., Mugford, J.W., Diamond, B.A., Weinstein, B.M., 2003. *phospholipase C gamma-1* is required downstream of *vascular endothelial growth factor* during arterial development. Genes Dev. 17, 1346–1351. https://doi.org/10.1101/gad.1072203

Lazarus, A., Del-Moral, P.M., Ilovich, O., Mishani, E., Warburton, D., Keshet, E., 2011. A perfusion-independent role of blood vessels in determining branching stereotypy of lung airways. Development 138, 2359–2368. https://doi.org/10.1242/dev.060723

le Noble, F., Moyon, D., Pardanaud, L., Yuan, L., Djonov, V., Matthijsen, R., Bréant, C., Fleury, V., Eichmann, A., 2004. Flow regulates arterial-venous differentiation in the chick embryo yolk sac. Development 131, 361–375. https://doi.org/10.1242/dev.00929

LeCouter, J., Kowalski, J., Foster, J., Hass, P., Zhang, Z., Dillard-Telm, L., Frantz, G., Rangell, L., DeGuzman, L., Keller, G.-A., Peale, F., Gurney, A., Hillan, K.J., Ferrara, N., 2001. Identification of an angiogenic mitogen selective for endocrine gland endothelium. Nature 412, 877–884. https://doi.org/10.1038/35091000

Lee, D., Park, C., Lee, H., Lugus, J.J., Kim, S.H., Arentson, E., Chung, Y.S., Gomez, G., Kyba, M., Lin, S., Janknecht, R., Lim, D.-S., Choi, K., 2008. ER71 Acts Downstream of BMP, Notch, and Wnt Signaling in Blood and Vessel Progenitor Specification. Cell Stem Cell 2, 497–507. https://doi.org/10.1016/j.stem.2008.03.008

Lee, M.D., Buckley, C., Zhang, X., Louhivuori, L., Uhlén, P., Wilson, C., McCarron, J.G., 2022. Small-world connectivity dictates collective endothelial cell signaling. Proc. Natl. Acad. Sci. 119, e2118927119. https://doi.org/10.1073/pnas.2118927119

Lee, S.-J., Sohn, Y.-D., Andukuri, A., Kim, S., Byun, J., Han, J.W., Park, I.-H., Jun, H.-W., Yoon, Y., 2017. Enhanced Therapeutic and Long-Term Dynamic Vascularization Effects of Human Pluripotent Stem Cell–Derived Endothelial Cells Encapsulated in a Nanomatrix Gel. Circulation 136, 1939–1954. https://doi.org/10.1161/CIRCULATIONAHA.116.026329

Lertkiatmongkol, P., Liao, D., Mei, H., Hu, Y., Newman, P.J., 2016. Endothelial functions of platelet/endothelial cell adhesion molecule-1 (CD31): Curr. Opin. Hematol. 23, 253–259. https://doi.org/10.1097/MOH.0000000000000239

Levenberg, S., Golub, J.S., Amit, M., Itskovitz-Eldor, J., Langer, R., 2002. Endothelial cells derived from human embryonic stem cells. Proc. Natl. Acad. Sci. 99, 4391–4396. https://doi.org/10.1073/pnas.032074999

Liaw, C.-Y., Guvendiren, M., 2017. Current and emerging applications of 3D printing in medicine. Biofabrication 9, 024102. https://doi.org/10.1088/1758-5090/aa7279

Lin, K., Hsu, P.-P., Chen, B.P., Yuan, S., Usami, S., Shyy, J.Y.-J., Li, Y.-S., Chien, S., 2000. Molecular mechanism of endothelial growth arrest by laminar shear stress. Proc. Natl. Acad. Sci. 97, 9385–9389. https://doi.org/10.1073/pnas.170282597

Lindahl, P., Johansson, B.R., Levéen, P., Betsholtz, C., 1997. Pericyte Loss and Microaneurysm Formation in PDGF-B-Deficient Mice. Science 277, 242–245. https://doi.org/10.1126/science.277.5323.242

Lindgren, A.G., Veldman, M.B., Lin, S., 2015. ETV2 expression increases the efficiency of primitive endothelial cell derivation from human embryonic stem cells. Cell Regen. 4, 4:1. https://doi.org/10.1186/s13619-014-0014-3

Linville, R.M., DeStefano, J.G., Sklar, M.B., Xu, Z., Farrell, A.M., Bogorad, M.I., Chu, C., Walczak, P., Cheng, L., Mahairaki, V., Whartenby, K.A., Calabresi, P.A., Searson, P.C., 2019. Human iPSC-derived blood-brain barrier microvessels: validation of barrier function and endothelial cell behavior. Biomaterials 190–191, 24–37. https://doi.org/10.1016/j.biomaterials.2018.10.023

Lippmann, E.S., Azarin, S.M., Kay, J.E., Nessler, R.A., Wilson, H.K., Al-Ahmad, A., Palecek, S.P., Shusta, E.V., 2012. Derivation of blood-brain barrier endothelial cells from human pluripotent stem cells. Nat. Biotechnol. 30, 783–791. https://doi.org/10.1038/nbt.2247

Liu, G.-H., Barkho, B.Z., Ruiz, S., Diep, D., Qu, J., Yang, S.-L., Panopoulos, A.D., Suzuki, K., Kurian, L., Walsh, C., Thompson, J., Boue, S., Fung, H.L., Sancho-Martinez, I., Zhang, K., Iii, J.Y., Belmonte, J.C.I., 2011. Recapitulation of premature ageing with iPSCs from Hutchinson–Gilford progeria syndrome. Nature 472, 221–225. https://doi.org/10.1038/nature09879

Liu, H., Zhang, W., Kennard, S., Caldwell, R.B., Lilly, B., 2010. Notch3 Is Critical for Proper Angiogenesis and Mural Cell Investment. Circ. Res. 107, 860–870. https://doi.org/10.1161/CIRCRESAHA.110.218271

Low, J.H., Li, P., Chew, E.G.Y., Zhou, B., Suzuki, K., Zhang, T., Lian, M.M., Liu, M., Aizawa, E., Rodriguez Esteban, C., Yong, K.S.M., Chen, Q., Campistol, J.M., Fang, M., Khor, C.C., Foo, J.N., Izpisua Belmonte, J.C., Xia, Y., 2019. Generation of Human PSC-Derived Kidney Organoids with Patterned Nephron Segments and a De Novo Vascular Network. Cell Stem Cell 25, 373-387.e9. https://doi.org/10.1016/j.stem.2019.06.009

Lukowski, S.W., Patel, J., Andersen, S.B., Sim, S.-L., Wong, H.Y., Tay, J., Winkler, I., Powell, J.E., Khosrotehrani, K., 2019. Single-Cell Transcriptional Profiling of Aortic Endothelium Identifies a Hierarchy from Endovascular Progenitors to Differentiated Cells. Cell Rep. 27, 2748-2758.e3. https://doi.org/10.1016/j.celrep.2019.04.102

Luo, J., Lin, Y., Shi, X., Li, G., Kural, M.H., Anderson, C.W., Ellis, M.W., Riaz, M., Tellides, G., Niklason, L.E., Qyang, Y., 2021. Xenogeneic-free generation of vascular smooth muscle cells from human induced pluripotent stem cells for vascular tissue engineering. Acta Biomater. 119, 155–168. https://doi.org/10.1016/j.actbio.2020.10.042

Luo, J., Qin, L., Zhao, L., Gui, L., Ellis, M.W., Huang, Y., Kural, M.H., Clark, J.A., Ono, S., Wang, J., Yuan, Y., Zhang, S.-M., Cong, X., Li, G., Riaz, M., Lopez, C., Hotta, A., Campbell, S.,

Tellides, G., Dardik, A., Niklason, L.E., Qyang, Y., 2020. Tissue-Engineered Vascular Grafts with Advanced Mechanical Strength from Human iPSCs. Cell Stem Cell 26, 251-261.e8. https://doi.org/10.1016/j.stem.2019.12.012

Luo, W., Garcia-Gonzalez, I., Fernández-Chacón, M., Casquero-Garcia, V., Sanchez-Muñoz, M.S., Mühleder, S., Garcia-Ortega, L., Andrade, J., Potente, M., Benedito, R., 2021. Arterialization requires the timely suppression of cell growth. Nature 589, 437–441. https://doi.org/10.1038/s41586-020-3018-x

Luo, Z., Mu, L., Zheng, Y., Shen, W., Li, J., Xu, L., Zhong, B., Liu, Y., Zhou, Y., 2020. NUMB enhances Notch signaling by repressing ubiquitination of NOTCH1 intracellular domain. J. Mol. Cell Biol. 12, 345–358. https://doi.org/10.1093/jmcb/mjz088

Mack, J.J., Mosqueiro, T.S., Archer, B.J., Jones, W.M., Sunshine, H., Faas, G.C., Briot, A., Aragón, R.L., Su, T., Romay, M.C., McDonald, A.I., Kuo, C.-H., Lizama, C.O., Lane, T.F., Zovein, A.C., Fang, Y., Tarling, E.J., de Aguiar Vallim, T.Q., Navab, M., Fogelman, A.M., Bouchard, L.S., Iruela-Arispe, M.L., 2017. NOTCH1 is a mechanosensor in adult arteries. Nat. Commun. 8, 1620. https://doi.org/10.1038/s41467-017-01741-8

Malinda, K.M., 2009. In Vivo Matrigel Migration and Angiogenesis Assay, in: Murray, C., Martin, S. (Eds.), Angiogenesis Protocols, Methods in Molecular Biology. Humana Press, Totowa, NJ, pp. 287–294. https://doi.org/10.1007/978-1-59745-241-0_17

Manian, K.V., Galloway, C.A., Dalvi, S., Emanuel, A.A., Mereness, J.A., Black, W., Winschel, L., Soto, C., Li, Y., Song, Y., DeMaria, W., Kumar, A., Slukvin, I., Schwartz, M.P., Murphy, W.L., Anand-Apte, B., Chung, M., Benoit, D.S.W., Singh, R., 2021. 3D iPSC modeling of the retinal pigment epithelium-choriocapillaris complex identifies factors involved in the pathology of macular degeneration. Cell Stem Cell 28, 846-862.e8. https://doi.org/10.1016/j.stem.2021.02.006

Marcelo, Kathrina L., Goldie, L.C., Hirschi, K.K., 2013. Regulation of Endothelial Cell Differentiation and Specification. Circ. Res. 112, 1272–1287. https://doi.org/10.1161/CIRCRESAHA.113.300506

Marcelo, Kathrina L., Sills, T.M., Coskun, S., Vasavada, H., Sanglikar, S., Goldie, L.C., Hirschi, K.K., 2013. Hemogenic Endothelial Cell Specification Requires c-Kit, Notch Signaling, and p27-Mediated Cell-Cycle Control. Dev. Cell 27, 504–515. https://doi.org/10.1016/j.devcel.2013.11.004

Marcu, R., Choi, Y.J., Xue, J., Fortin, C.L., Wang, Y., Nagao, R.J., Xu, J., MacDonald, J.W., Bammler, T.K., Murry, C.E., Muczynski, K., Stevens, K.R., Himmelfarb, J., Schwartz, S.M., Zheng, Y., 2018. Human Organ-Specific Endothelial Cell Heterogeneity. iScience 4, 20–35. https://doi.org/10.1016/j.isci.2018.05.003

Marimuthu, M., Kim, S., 2013. Pumpless steady-flow microfluidic chip for cell culture. Anal. Biochem. 437, 161–163. https://doi.org/10.1016/j.ab.2013.02.007

Masedunskas, A., King, J.A., Tan, F., Cochran, R., Stevens, T., Sviridov, D., Ofori-Acquah, S.F., 2006. Activated leukocyte cell adhesion molecule is a component of the endothelial junction involved in transendothelial monocyte migration. FEBS Lett. 580, 2637–2645. https://doi.org/10.1016/j.febslet.2006.04.013

Mazzieri, R., Pucci, F., Moi, D., Zonari, E., Ranghetti, A., Berti, A., Politi, L.S., Gentner, B., Brown, J.L., Naldini, L., De Palma, M., 2011. Targeting the ANG2/TIE2 Axis Inhibits Tumor Growth and Metastasis by Impairing Angiogenesis and Disabling Rebounds of Proangiogenic Myeloid Cells. Cancer Cell 19, 512–526. https://doi.org/10.1016/j.ccr.2011.02.005

McCarron, J.G., Lee, M.D., Wilson, C., 2017. The Endothelium Solves Problems That Endothelial Cells Do Not Know Exist. Trends Pharmacol. Sci. 38, 322–338. https://doi.org/10.1016/j.tips.2017.01.008

McCarron, J.G., Wilson, C., Heathcote, H.R., Zhang, X., Buckley, C., Lee, M.D., 2019. Heterogeneity and emergent behaviour in the vascular endothelium. Curr. Opin. Pharmacol. 45, 23–32. https://doi.org/10.1016/j.coph.2019.03.008

McGrath, K.E., Koniski, A.D., Malik, J., Palis, J., 2003. Circulation is established in a stepwise pattern in the mammalian embryo. Blood 101, 1669–1675. https://doi.org/10.1182/blood-2002-08-2531

Miano, J.M., Cserjesi, P., Ligon, K.L., Periasamy, M., Olson, E.N., 1994. Smooth muscle myosin heavy chain exclusively marks the smooth muscle lineage during mouse embryogenesis. Circ. Res. 75, 803–812. https://doi.org/10.1161/01.RES.75.5.803

Millán, J., Cain, R.J., Reglero-Real, N., Bigarella, C., Marcos-Ramiro, B., Fernández-Martín, L., Correas, I., Ridley, A.J., 2010. Adherens junctions connect stress fibres between adjacent endothelial cells. BMC Biol. 8, 11. https://doi.org/10.1186/1741-7007-8-11

Miller, J.S., Stevens, K.R., Yang, M.T., Baker, B.M., Nguyen, D.-H.T., Cohen, D.M., Toro, E., Chen, A.A., Galie, P.A., Yu, X., Chaturvedi, R., Bhatia, S.N., Chen, C.S., 2012. Rapid casting of patterned vascular networks for perfusable engineered three-dimensional tissues. Nat. Mater. 11, 768–774. https://doi.org/10.1038/nmat3357

Milutinović, A., Šuput, D., Zorc-Pleskovič, R., 2019. Pathogenesis of atherosclerosis in the tunica intima, media, and adventitia of coronary arteries: An updated review. Bosn. J. Basic Med. Sci. https://doi.org/10.17305/bjbms.2019.4320

Minami, T., Aird, W.C., 2005. Endothelial Cell Gene Regulation. Trends Cardiovasc. Med. 15, 174.e1-174.e24. https://doi.org/10.1016/j.tcm.2005.06.002

Monk, N.A.M., 2003. Oscillatory expression of Hes1, p53, and NF-kappaB driven by transcriptional time delays. Curr. Biol. CB 13, 1409–1413. https://doi.org/10.1016/s0960-9822(03)00494-9

Moyon, D., Pardanaud, L., Yuan, L., Bréant, C., Eichmann, A., 2001. Plasticity of endothelial cells during arterial-venous differentiation in the avian embryo. Development 128, 3359–3370. https://doi.org/10.1242/dev.128.17.3359

Muhl, L., Genové, G., Leptidis, S., Liu, J., He, L., Mocci, G., Sun, Y., Gustafsson, S., Buyandelger, B., Chivukula, I.V., Segerstolpe, Å., Raschperger, E., Hansson, E.M., Björkegren, J.L.M., Peng, X.-R., Vanlandewijck, M., Lendahl, U., Betsholtz, C., 2020. Single-cell analysis uncovers fibroblast heterogeneity and criteria for fibroblast and mural cell identification and discrimination. Nat. Commun. 11, 3953. https://doi.org/10.1038/s41467-020-17740-1

Mukouyama, Y., Gerber, H.-P., Ferrara, N., Gu, C., Anderson, D.J., 2005. Peripheral nerve-derived VEGF promotes arterial differentiation via neuropilin 1-mediated positive feedback. Development 132, 941–952. https://doi.org/10.1242/dev.01675

Mulfaul, K., Giacalone, J.C., Voigt, A.P., Riker, M.J., Ochoa, D., Han, I.C., Stone, E.M., Mullins, R.F., Tucker, B.A., 2020. Stepwise differentiation and functional characterization of human induced pluripotent stem cell-derived choroidal endothelial cells. Stem Cell Res. Ther. 11, 409. https://doi.org/10.1186/s13287-020-01903-4

Muller, W.A., Weigl, S.A., Deng, X., Phillips, D.M., 1993. PECAM-1 is required for transendothelial migration of leukocytes. J. Exp. Med. 178, 449–460. https://doi.org/10.1084/jem.178.2.449

Nakajima, H., Mochizuki, N., 2017. Flow pattern-dependent endothelial cell responses through transcriptional regulation. Cell Cycle 16, 1893–1901. https://doi.org/10.1080/15384101.2017.1364324

Nakano, T., Kodama, H., Honjo, T., 1994. Generation of Lymphohematopoietic Cells from Embryonic Stem Cells in Culture. Science 265, 1098–1101. https://doi.org/10.1126/science.8066449

Nakatsu, M.N., Davis, J., Hughes, C.C.W., 2007. Optimized Fibrin Gel Bead Assay for the Study of Angiogenesis. J. Vis. Exp. 186. https://doi.org/10.3791/186

Nandagopal, N., Santat, L.A., Elowitz, M.B., 2019. Cis-activation in the Notch signaling pathway. eLife 8, e37880. https://doi.org/10.7554/eLife.37880

Natividad-Diaz, S.L., Browne, S., Jha, A.K., Ma, Z., Hossainy, S., Kurokawa, Y.K., George, S.C., Healy, K.E., 2019. A combined hiPSC-derived endothelial cell and in vitro microfluidic platform for assessing biomaterial-based angiogenesis. Biomaterials 194, 73–83. https://doi.org/10.1016/j.biomaterials.2018.11.032

Nedergaard, M., Goldman, S.A., 2020. Glymphatic failure as a final common pathway to dementia. Science 370, 50–56. https://doi.org/10.1126/science.abb8739

Nehls, V., Drenckhahn, D., 1991. Heterogeneity of microvascular pericytes for smooth muscle type alpha-actin. J. Cell Biol. 113, 147–154. https://doi.org/10.1083/jcb.113.1.147

Newman, P.J., Berndt, M.C., Gorski, J., White, G.C., Lyman, S., Paddock, C., Muller, W.A., 1990. PECAM-1 (CD31) Cloning and Relation to Adhesion Molecules of the Immunoglobulin Gene Superfamily. Science 247, 1219–1222. https://doi.org/10.1126/science.1690453

Nguyen, J., Lin, Y.-Y., Gerecht, S., 2021. The next generation of endothelial differentiation: Tissue-specific ECs. Cell Stem Cell 28, 1188–1204. https://doi.org/10.1016/j.stem.2021.05.002

Nikolova-Krstevski, V., Yuan, L., Le Bras, A., Vijayaraj, P., Kondo, M., Gebauer, I., Bhasin, M., Carman, C.V., Oettgen, P., 2009. ERG is required for the differentiation of embryonic stem cells along the endothelial lineage. BMC Dev. Biol. 9, 72. https://doi.org/10.1186/1471-213X-9-72

Nogueira, G.O., Garcez, P.P., Bardy, C., Cunningham, M.O., Sebollela, A., 2022. Modeling the Human Brain With ex vivo Slices and in vitro Organoids for Translational Neuroscience. Front. Neurosci. 16, 838594. https://doi.org/10.3389/fnins.2022.838594

Nolan, D.J., Ginsberg, M., Israely, E., Palikuqi, B., Poulos, M.G., James, D., Ding, B.-S., Schachterle, W., Liu, Y., Rosenwaks, Z., Butler, J.M., Xiang, J., Rafii, A., Shido, K., Rabbany, S.Y., Elemento, O., Rafii, S., 2013. Molecular Signatures of Tissue-Specific Microvascular Endothelial Cell Heterogeneity in Organ Maintenance and Regeneration. Dev. Cell 26, 204–219. https://doi.org/10.1016/j.devcel.2013.06.017

Nostro, M.C., Cheng, X., Keller, G.M., Gadue, P., 2008. Wnt, Activin, and BMP Signaling Regulate Distinct Stages in the Developmental Pathway from Embryonic Stem Cells to Blood. Cell Stem Cell 2, 60–71. https://doi.org/10.1016/j.stem.2007.10.011

Nowak-Sliwinska, P., Alitalo, K., Allen, E., Anisimov, A., Aplin, A.C., Auerbach, R., Augustin, H.G., Bates, D.O., van Beijnum, J.R., Bender, R.H.F., Bergers, G., Bikfalvi, A., Bischoff, J., Böck, B.C., Brooks, P.C., Bussolino, F., Cakir, B., Carmeliet, P., Castranova, D., Cimpean, A.M., Cleaver, O., Coukos, G., Davis, G.E., De Palma, M., Dimberg, A., Dings, R.P.M., Djonov, V., Dudley, A.C., Dufton, N.P., Fendt, S.-M., Ferrara, N., Fruttiger, M., Fukumura, D., Ghesquière, B., Gong, Y., Griffin, R.J., Harris, A.L., Hughes, C.C.W., Hultgren, N.W., Iruela-Arispe, M.L., Irving, M., Jain, R.K., Kalluri, R., Kalucka, J., Kerbel, R.S., Kitajewski, J., Klaassen, I., Kleinmann, H.K., Koolwijk, P., Kuczynski, E., Kwak, B.R., Marien, K., Melero-Martin, J.M., Munn, L.L., Nicosia, R.F., Noel, A., Nurro, J., Olsson, A.-K., Petrova, T.V., Pietras, K., Pili, R., Pollard, J.W., Post, M.J., Quax, P.H.A., Rabinovich, G.A., Raica, M., Randi, A.M., Ribatti, D., Ruegg, C., Schlingemann, R.O., Schulte-Merker, S., Smith, L.E.H., Song, J.W., Stacker, S.A., Stalin, J., Stratman, A.N., Van de Velde, M., van Hinsbergh, V.W.M., Vermeulen, P.B., Waltenberger, J., Weinstein, B.M., Xin, H., Yetkin-Arik, B., Yla-Herttuala, S., Yoder, M.C., Griffioen, A.W., 2018. Consensus guidelines for the use and interpretation of angiogenesis assays. Angiogenesis 21, 425–532. https://doi.org/10.1007/s10456-018-9613-x

Nyberg, P., 2008. Tumor microenvironment and angiogenesis. Front. Biosci. Volume, 6537. https://doi.org/10.2741/3173

Obermeier, B., Daneman, R., Ransohoff, R.M., 2013. Development, maintenance and disruption of the blood-brain barrier. Nat. Med. 19, 1584–1596. https://doi.org/10.1038/nm.3407

Obi, S., Yamamoto, K., Shimizu, N., Kumagaya, S., Masumura, T., Sokabe, T., Asahara, T., Ando, J., 2009. Fluid shear stress induces arterial differentiation of endothelial progenitor cells. J. Appl. Physiol. 106, 203–211. https://doi.org/10.1152/japplphysiol.00197.2008

Offeddu, G.S., Haase, K., Gillrie, M.R., Li, R., Morozova, O., Hickman, D., Knutson, C.G., Kamm, R.D., 2019. An on-chip model of protein paracellular and transcellular permeability in the microcirculation. Biomaterials 212, 115–125. https://doi.org/10.1016/j.biomaterials.2019.05.022

Ong, J., Serra, M.P., Segal, J., Cujba, A.-M., Ng, S.S., Butler, R., Millar, V., Hatch, S., Zimri, S., Koike, H., Chan, K., Bonham, A., Walk, M., Voss, T., Heaton, N., Mitry, R., Dhawan, A., Ebner, D., Danovi, D., Nakauchi, H., Rashid, S.T., 2018. Imaging-Based Screen Identifies Laminin 411 as a Physiologically Relevant Niche Factor with Importance for i-Hep Applications. Stem Cell Rep. 10, 693–702. https://doi.org/10.1016/j.stemcr.2018.01.025

Orlova, V.V., van den Hil, F.E., Petrus-Reurer, S., Drabsch, Y., ten Dijke, P., Mummery, C.L., 2014. Generation, expansion and functional analysis of endothelial cells and pericytes derived from human pluripotent stem cells. Nat. Protoc. 9, 1514–1531. https://doi.org/10.1038/nprot.2014.102

Ozerdem, U., Grako, K.A., Dahlin-Huppe, K., Monosov, E., Stallcup, W.B., 2001. NG2 proteoglycan is expressed exclusively by mural cells during vascular morphogenesis. Dev. Dyn. 222, 218–227. https://doi.org/10.1002/dvdy.1200

Padget, R.L., Mohite, S.S., Hoog, T.G., Justis, B.S., Green, B.E., Udan, R.S., 2019. Hemodynamic force is required for vascular smooth muscle cell recruitment to blood vessels during mouse embryonic development. Mech. Dev. 156, 8–19. https://doi.org/10.1016/j.mod.2019.02.002

Paik, D.T., Tian, L., Lee, J., Sayed, N., Chen, I.Y., Rhee, S., Rhee, J.-W., Kim, Y., Wirka, R.C., Buikema, J.W., Wu, S.M., Red-Horse, K., Quertermous, T., Wu, J.C., 2018. Large-Scale Single-Cell RNA-Seq Reveals Molecular Signatures of Heterogeneous Populations of Human Induced Pluripotent Stem Cell-Derived Endothelial Cells. Circ. Res. 123, 443–450. https://doi.org/10.1161/CIRCRESAHA.118.312913

Palis, J., Yoder, M.C., 2001. Yolk-sac hematopoiesis. Exp. Hematol. 29, 927–936. https://doi.org/10.1016/S0301-472X(01)00669-5

Palpant, N.J., Pabon, L., Friedman, C.E., Roberts, M., Hadland, B., Zaunbrecher, R.J., Bernstein, I., Zheng, Y., Murry, C.E., 2017. Generating high-purity cardiac and endothelial derivatives from patterned mesoderm using human pluripotent stem cells. Nat. Protoc. 12, 15–31. https://doi.org/10.1038/nprot.2016.153

Pappenheimer, J.R., Michel, C.C., 2003. Role of villus microcirculation in intestinal absorption of glucose: coupling of epithelial with endothelial transport. J. Physiol. 553, 561–574. https://doi.org/10.1113/jphysiol.2003.043257

Pardanaud, L., Pibouin-Fragner, L., Dubrac, A., Mathivet, T., English, I., Brunet, I., Simons, M., Eichmann, A., 2016. Sympathetic Innervation Promotes Arterial Fate by Enhancing Endothelial ERK Activity. Circ. Res. 119, 607–620. https://doi.org/10.1161/CIRCRESAHA.116.308473

Park, C., Lugus, J.J., Choi, K., 2005. Stepwise Commitment from Embryonic Stem to Hematopoietic and Endothelial Cells, in: Current Topics in Developmental Biology. Elsevier, pp. 1–36. https://doi.org/10.1016/S0070-2153(05)66001-2

Pasquale, E.B., 2005. Eph receptor signalling casts a wide net on cell behaviour. Nat. Rev. Mol. Cell Biol. 6, 462–475. https://doi.org/10.1038/nrm1662

Pasut, A., Becker, L.M., Cuypers, A., Carmeliet, P., 2021. Endothelial cell plasticity at the single-cell level. Angiogenesis 24, 311–326. https://doi.org/10.1007/s10456-021-09797-3

Patsch, C., Challet-Meylan, L., Thoma, E.C., Urich, E., Heckel, T., O'Sullivan, J.F., Grainger, S.J., Kapp, F.G., Sun, L., Christensen, K., Xia, Y., Florido, M.H.C., He, W., Pan, W., Prummer, M., Warren, C.R., Jakob-Roetne, R., Certa, U., Jagasia, R., Freskgård, P.-O., Adatto, I., Kling, D., Huang, P., Zon, L.I., Chaikof, E.L., Gerszten, R.E., Graf, M., Iacone, R., Cowan, C.A., 2015. Generation of vascular endothelial and smooth muscle cells from human pluripotent stem cells. Nat. Cell Biol. 17, 994–1003. https://doi.org/10.1038/ncb3205

Pedraza-Arevalo, S., Cujba, A.-M., Alvarez-Fallas, M.E., Sancho, R., 2022. Differentiation of beta-like cells from human induced pluripotent stem cell-derived pancreatic progenitor organoids. STAR Protoc. 3, 101656. https://doi.org/10.1016/j.xpro.2022.101656

Piera-Velazquez, S., Li, Z., Jimenez, S.A., 2011. Role of Endothelial-Mesenchymal Transition (EndoMT) in the Pathogenesis of Fibrotic Disorders. Am. J. Pathol. 179, 1074–1080. https://doi.org/10.1016/j.ajpath.2011.06.001

Pitoulis, F.G., Watson, S.A., Perbellini, F., Terracciano, C.M., 2020. Myocardial slices come to age: an intermediate complexity in vitro cardiac model for translational research. Cardiovasc. Res. 116, 1275–1287. https://doi.org/10.1093/cvr/cvz341

Pola, R., Ling, L.E., Silver, M., Corbley, M.J., Kearney, M., Blake Pepinsky, R., Shapiro, R., Taylor, F.R., Baker, D.P., Asahara, T., Isner, J.M., 2001. The morphogen Sonic hedgehog is an indirect angiogenic agent upregulating two families of angiogenic growth factors. Nat. Med. 7, 706–711. https://doi.org/10.1038/89083

Potente, M., Gerhardt, H., Carmeliet, P., 2011. Basic and therapeutic aspects of angiogenesis. Cell 146, 873–887. https://doi.org/10.1016/j.cell.2011.08.039

Potente, M., Mäkinen, T., 2017. Vascular heterogeneity and specialization in development and disease. Nat. Rev. Mol. Cell Biol. 18, 477–494. https://doi.org/10.1038/nrm.2017.36

Prasain, N., Lee, M.R., Vemula, S., Meador, J.L., Yoshimoto, M., Ferkowicz, M.J., Fett, A., Gupta, M., Rapp, B.M., Saadatzadeh, M.R., Ginsberg, M., Elemento, O., Lee, Y., Voytik-Harbin, S.L., Chung, H.M., Hong, K.S., Reid, E., O'Neill, C.L., Medina, R.J., Stitt, A.W., Murphy, M.P., Rafii, S., Broxmeyer, H.E., Yoder, M.C., 2014. Differentiation of human pluripotent stem cells to cells similar to cord-blood endothelial colony–forming cells. Nat. Biotechnol. 32, 1151–1157. https://doi.org/10.1038/nbt.3048

Que, J., Wilm, B., Hasegawa, H., Wang, F., Bader, D., Hogan, B.L.M., 2008. Mesothelium contributes to vascular smooth muscle and mesenchyme during lung development. Proc. Natl. Acad. Sci. 105, 16626–16630. https://doi.org/10.1073/pnas.0808649105

Rafii, S., Butler, J.M., Ding, B.-S., 2016. Angiocrine functions of organ-specific endothelial cells. Nature 529, 316–325. https://doi.org/10.1038/nature17040

Ramasamy, S.K., Kusumbe, A.P., Schiller, M., Zeuschner, D., Bixel, M.G., Milia, C., Gamrekelashvili, J., Limbourg, A., Medvinsky, A., Santoro, M.M., Limbourg, F.P., Adams, R.H., 2016. Blood flow controls bone vascular function and osteogenesis. Nat. Commun. 7, 13601. https://doi.org/10.1038/ncomms13601

Ramasamy, S.K., Kusumbe, A.P., Wang, L., Adams, R.H., 2014. Endothelial Notch activity promotes angiogenesis and osteogenesis in bone. Nature 507, 376–380. https://doi.org/10.1038/nature13146

Randi, A.M., Smith, K.E., Castaman, G., 2018. von Willebrand factor regulation of blood vessel formation. Blood 132, 132–140. https://doi.org/10.1182/blood-2018-01-769018

Rao, L., Qian, Y., Khodabukus, A., Ribar, T., Bursac, N., 2018. Engineering human pluripotent stem cells into a functional skeletal muscle tissue. Nat. Commun. 9, 126. https://doi.org/10.1038/s41467-017-02636-4

Rasmussen, T.L., Kweon, J., Diekmann, M.A., Belema-Bedada, F., Song, Q., Bowlin, K., Shi, X., Ferdous, A., Li, T., Kyba, M., Metzger, J.M., Koyano-Nakagawa, N., Garry, D.J., 2011. ER71 directs mesodermal fate decisions during embryogenesis. Development 138, 4801–4812. https://doi.org/10.1242/dev.070912

Ribatti, D., Annese, T., Ruggieri, S., Tamma, R., Crivellato, E., 2019. Limitations of Anti-Angiogenic Treatment of Tumors. Transl. Oncol. 12, 981–986. https://doi.org/10.1016/j.tranon.2019.04.022

Ribatti, D., Djonov, V., 2012. Intussusceptive microvascular growth in tumors. Cancer Lett. 316, 126–131. https://doi.org/10.1016/j.canlet.2011.10.040

Ricard, N., Bailly, S., Guignabert, C., Simons, M., 2021. The quiescent endothelium: signalling pathways regulating organ-specific endothelial normalcy. Nat. Rev. Cardiol. 18, 565–580. https://doi.org/10.1038/s41569-021-00517-4

Risau, W., Flamme, I., 1995. Vasculogenesis. Annu. Rev. Cell Dev. Biol. 11, 73–91. https://doi.org/10.1146/annurev.cb.11.110195.000445

Rocha, A.S., Vidal, V., Mertz, M., Kendall, T.J., Charlet, A., Okamoto, H., Schedl, A., 2015. The Angiocrine Factor Rspondin3 Is a Key Determinant of Liver Zonation. Cell Rep. 13, 1757–1764. https://doi.org/10.1016/j.celrep.2015.10.049

Rocha, S.F., Adams, R.H., 2009. Molecular differentiation and specialization of vascular beds. Angiogenesis 12, 139–147. https://doi.org/10.1007/s10456-009-9132-x

Ronaldson-Bouchard, K., Teles, D., Yeager, K., Tavakol, D.N., Zhao, Y., Chramiec, A., Tagore, S., Summers, M., Stylianos, S., Tamargo, M., Lee, B.M., Halligan, S.P., Abaci, E.H., Guo, Z., Jacków, J., Pappalardo, A., Shih, J., Soni, R.K., Sonar, S., German, C., Christiano, A.M., Califano, A., Hirschi, K.K., Chen, C.S., Przekwas, A., Vunjak-Novakovic, G., 2022. A multi-organ chip with matured tissue niches linked by vascular flow. Nat. Biomed. Eng. 6, 351–371. https://doi.org/10.1038/s41551-022-00882-6

Rosa, S., Praça, C., Pitrez, P.R., Gouveia, P.J., Aranguren, X.L., Ricotti, L., Ferreira, L.S., 2019. Functional characterization of iPSC-derived arterial- and venous-like endothelial cells. Sci. Rep. 9, 3826. https://doi.org/10.1038/s41598-019-40417-9

Ross, R., Glomset, J.A., 1973. Atherosclerosis and the Arterial Smooth Muscle Cell: Proliferation of smooth muscle is a key event in the genesis of the lesions of atherosclerosis. Science 180, 1332–1339. https://doi.org/10.1126/science.180.4093.1332

Roy, P., Orecchioni, M., Ley, K., 2022. How the immune system shapes atherosclerosis: roles of innate and adaptive immunity. Nat. Rev. Immunol. 22, 251–265. https://doi.org/10.1038/s41577-021-00584-1

Salmon, I., Grebenyuk, S., Abdel Fattah, A.R., Rustandi, G., Pilkington, T., Verfaillie, C., Ranga, A., 2022. Engineering neurovascular organoids with 3D printed microfluidic chips. Lab. Chip 22, 1615–1629. https://doi.org/10.1039/D1LC00535A

Samuel, R., Daheron, L., Liao, S., Vardam, T., Kamoun, W.S., Batista, A., Buecker, C., Schafer, R., Han, X., Au, P., Scadden, D.T., Duda, D.G., Fukumura, D., Jain, R.K., 2013. Generation of functionally competent and durable engineered blood vessels from human induced pluripotent stem cells. Proc. Natl. Acad. Sci. 110, 12774–12779. https://doi.org/10.1073/pnas.1310675110

Sanchez Noriega, J.L., Chartrand, N.A., Valdoz, J.C., Cribbs, C.G., Jacobs, D.A., Poulson, D., Viglione, M.S., Woolley, A.T., Van Ry, P.M., Christensen, K.A., Nordin, G.P., 2021. Spatially and optically tailored 3D printing for highly miniaturized and integrated microfluidics. Nat. Commun. 12, 5509. https://doi.org/10.1038/s41467-021-25788-w

Schindelin, J., Arganda-Carreras, I., Frise, E., Kaynig, V., Longair, M., Pietzsch, T., Preibisch, S., Rueden, C., Saalfeld, S., Schmid, B., Tinevez, J.-Y., White, D.J., Hartenstein, V., Eliceiri, K., Tomancak, P., Cardona, A., 2012. Fiji: an open-source platform for biological-image analysis. Nat. Methods 9, 676–682. https://doi.org/10.1038/nmeth.2019

Schlingemann, R.O., Oosterwijk, E., Wesseling, P., Rietveld, F.J.R., Ruiter, D.J., 1996. AMINOPEPTIDASE A IS A CONSTITUENT OF ACTIVATED PERICYTES IN ANGIOGENESIS. J. Pathol. 179, 436–442. https://doi.org/10.1002/(SICI)1096-9896(199608)179:4<436::AID-PATH611>3.0.CO;2-A

Seebach, J., Klusmeier, N., Schnittler, H., 2020. Autoregulatory "Multitasking" at Endothelial Cell Junctions by Junction-Associated Intermittent Lamellipodia Controls Barrier Properties. Front. Physiol. 11, 586921. https://doi.org/10.3389/fphys.2020.586921

Shah, A.V., Birdsey, G.M., Randi, A.M., 2016. Regulation of endothelial homeostasis, vascular development and angiogenesis by the transcription factor ERG. Vascul. Pharmacol. 86, 3–13. https://doi.org/10.1016/j.vph.2016.05.003

Shalaby, F., Ho, J., Stanford, W.L., Fischer, K.-D., Schuh, A.C., Schwartz, L., Bernstein, A., Rossant, J., 1997. A Requirement for Flk1 in Primitive and Definitive Hematopoiesis and Vasculogenesis. Cell 89, 981–990. https://doi.org/10.1016/S0092-8674(00)80283-4

Shemesh, J., Jalilian, I., Shi, A., Heng Yeoh, G., Knothe Tate, M.L., Ebrahimi Warkiani, M., 2015. Flow-induced stress on adherent cells in microfluidic devices. Lab. Chip 15, 4114–4127. https://doi.org/10.1039/C5LC00633C

Shi, Y., Patel, S., Davenpeck, K.L., Niculescu, R., Rodriguez, E., Magno, M.G., Ormont, M.L., Mannion, J.D., Zalewski, A., 2001. Oxidative Stress and Lipid Retention in Vascular Grafts: Comparison Between Venous and Arterial Conduits. Circulation 103, 2408–2413. https://doi.org/10.1161/01.CIR.103.19.2408

Shin, Y., Han, S., Jeon, J.S., Yamamoto, K., Zervantonakis, I.K., Sudo, R., Kamm, R.D., Chung, S., 2012. Microfluidic assay for simultaneous culture of multiple cell types on surfaces or within hydrogels. Nat. Protoc. 7, 1247–1259. https://doi.org/10.1038/nprot.2012.051

Simmons, C.A., Grant, G.R., Manduchi, E., Davies, P.F., 2005. Spatial heterogeneity of endothelial phenotypes correlates with side-specific vulnerability to calcification in normal porcine aortic valves. Circ. Res. 96, 792–799. https://doi.org/10.1161/01.RES.0000161998.92009.64

Sivarapatna, A., Ghaedi, M., Le, A.V., Mendez, J.J., Qyang, Y., Niklason, L.E., 2015. Arterial specification of endothelial cells derived from human induced pluripotent stem cells in a biomimetic flow bioreactor. Biomaterials 53, 621–633. https://doi.org/10.1016/j.biomaterials.2015.02.121

Smyth, L.C.D., Rustenhoven, J., Scotter, E.L., Schweder, P., Faull, R.L.M., Park, T.I.H., Dragunow, M., 2018. Markers for human brain pericytes and smooth muscle cells. J. Chem. Neuroanat. 92, 48–60. https://doi.org/10.1016/j.jchemneu.2018.06.001

Sobrino, A., Phan, D.T.T., Datta, R., Wang, X., Hachey, S.J., Romero-López, M., Gratton, E., Lee, A.P., George, S.C., Hughes, C.C.W., 2016. 3D microtumors in vitro supported by perfused vascular networks. Sci. Rep. 6, 31589. https://doi.org/10.1038/srep31589

Soderblom, C., Luo, X., Blumenthal, E., Bray, E., Lyapichev, K., Ramos, J., Krishnan, V., Lai-Hsu, C., Park, K.K., Tsoulfas, P., Lee, J.K., 2013. Perivascular Fibroblasts Form the Fibrotic Scar after Contusive Spinal Cord Injury. J. Neurosci. 33, 13882–13887. https://doi.org/10.1523/JNEUROSCI.2524-13.2013

Song, H.-H.G., Rumma, R.T., Ozaki, C.K., Edelman, E.R., Chen, C.S., 2018. Vascular Tissue Engineering: Progress, Challenges, and Clinical Promise. Cell Stem Cell 22, 340–354. https://doi.org/10.1016/j.stem.2018.02.009

Song, J.W., Munn, L.L., 2011. Fluid forces control endothelial sprouting. Proc. Natl. Acad. Sci. U. S. A. 108, 15342–15347. https://doi.org/10.1073/pnas.1105316108

Song, S., Ewald, A.J., Stallcup, W., Werb, Z., Bergers, G., 2005. PDGFRβ+ perivascular progenitor cells in tumours regulate pericyte differentiation and vascular survival. Nat. Cell Biol. 7, 870–879. https://doi.org/10.1038/ncb1288

Sørensen, K.K., McCourt, P., Berg, T., Crossley, C., Couteur, D.L., Wake, K., Smedsrød, B., 2012. The scavenger endothelial cell: a new player in homeostasis and immunity. Am. J. Physiol.-Regul. Integr. Comp. Physiol. 303, R1217–R1230. https://doi.org/10.1152/ajpregu.00686.2011

Srinivasan, R.S., Escobedo, N., Yang, Y., Interiano, A., Dillard, M.E., Finkelstein, D., Mukatira, S., Gil, H.J., Nurmi, H., Alitalo, K., Oliver, G., 2014. The Prox1–Vegfr3 feedback loop maintains the identity and the number of lymphatic endothelial cell progenitors. Genes Dev. 28, 2175–2187. https://doi.org/10.1101/gad.216226.113

Stark, K., Eckart, A., Haidari, S., Tirniceriu, A., Lorenz, M., von Brühl, M.-L., Gärtner, F., Khandoga, A.G., Legate, K.R., Pless, R., Hepper, I., Lauber, K., Walzog, B., Massberg, S., 2013. Capillary and arteriolar pericytes attract innate leukocytes exiting through venules and "instruct" them with pattern-recognition and motility programs. Nat. Immunol. 14, 41–51. https://doi.org/10.1038/ni.2477

Staton, C., Kumar, I., Reed, M., Brown, N., 2007. Neuropilins in physiological and pathological angiogenesis. J. Pathol. 212, 237–248. https://doi.org/10.1002/path.2182

Stebbins, M.J., Gastfriend, B.D., Canfield, S.G., Lee, M.-S., Richards, D., Faubion, M.G., Li, W.-J., Daneman, R., Palecek, S.P., Shusta, E.V., 2019. Human pluripotent stem cell–derived brain pericyte–like cells induce blood-brain barrier properties. Sci. Adv. 5, eaau7375. https://doi.org/10.1126/sciadv.aau7375

Stenman, J.M., Rajagopal, J., Carroll, T.J., Ishibashi, M., McMahon, J., McMahon, A.P., 2008. Canonical Wnt signaling regulates organ-specific assembly and differentiation of CNS vasculature. Science 322, 1247–1250. https://doi.org/10.1126/science.1164594

Stratman, A.N., Malotte, K.M., Mahan, R.D., Davis, M.J., Davis, G.E., 2009. Pericyte recruitment during vasculogenic tube assembly stimulates endothelial basement membrane matrix formation. Blood 114, 5091–5101. https://doi.org/10.1182/blood-2009-05-222364

Suburo, A.M., D'Amore, P.A., 2006. Development of the Endothelium, in: Moncada, S., Higgs, A. (Eds.), The Vascular Endothelium I, Handbook of Experimental Pharmacology. Springer Berlin Heidelberg, Berlin, Heidelberg, pp. 71–105. https://doi.org/10.1007/3-540-32967-6_3

Sundaram, S., Echter, A., Sivarapatna, A., Qiu, C., Niklason, L., 2013. Small diameter vascular graft engineered using human embryonic stem cell-derived mesenchymal cells. Tissue Eng. Part A 131015043635000. https://doi.org/10.1089/ten.TEA.2012.0738

Swift, M.R., Pham, V.N., Castranova, D., Bell, K., Poole, R.J., Weinstein, B.M., 2014. SoxF factors and Notch regulate nr2f2 gene expression during venous differentiation in zebrafish. Dev. Biol. 390, 116–125. https://doi.org/10.1016/j.ydbio.2014.03.018

Swift, M.R., Weinstein, B.M., 2009. Arterial–Venous Specification During Development. Circ. Res. 104, 576–588. https://doi.org/10.1161/CIRCRESAHA.108.188805

Takahashi, K., Yamanaka, S., 2006. Induction of Pluripotent Stem Cells from Mouse Embryonic and Adult Fibroblast Cultures by Defined Factors. Cell 126, 663–676. https://doi.org/10.1016/j.cell.2006.07.024

Tang, W., Zeve, D., Suh, J.M., Bosnakovski, D., Kyba, M., Hammer, R.E., Tallquist, M.D., Graff, J.M., 2008. White Fat Progenitor Cells Reside in the Adipose Vasculature. Science 322, 583–586. https://doi.org/10.1126/science.1156232

Tarazi, S., Aguilera-Castrejon, A., Joubran, C., Ghanem, N., Ashouokhi, S., Roncato, F., Wildschutz, E., Haddad, M., Oldak, B., Gomez-Cesar, E., Livnat, N., Viukov, S., Lokshtanov, D., Naveh-Tassa, S., Rose, M., Hanna, S., Raanan, C., Brenner, O., Kedmi, M., Keren-Shaul, H., Lapidot, T., Maza, I., Novershtern, N., Hanna, J.H., 2022. Post-gastrulation synthetic embryos generated ex utero from mouse naive ESCs. Cell 185, 3290-3306.e25. https://doi.org/10.1016/j.cell.2022.07.028

Tărlungeanu, D.C., Deliu, E., Dotter, C.P., Kara, M., Janiesch, P.C., Scalise, M., Galluccio, M., Tesulov, M., Morelli, E., Sonmez, F.M., Bilguvar, K., Ohgaki, R., Kanai, Y., Johansen, A., Esharif, S., Ben-Omran, T., Topcu, M., Schlessinger, A., Indiveri, C., Duncan, K.E., Caglayan, A.O., Gunel, M., Gleeson, J.G., Novarino, G., 2016. Impaired Amino Acid Transport at the Blood Brain Barrier Is a Cause of Autism Spectrum Disorder. Cell 167, 1481-1494.e18. https://doi.org/10.1016/j.cell.2016.11.013

Tatin, F., Taddei, A., Weston, A., Fuchs, E., Devenport, D., Tissir, F., Makinen, T., 2013. Planar Cell Polarity Protein Celsr1 Regulates Endothelial Adherens Junctions and Directed Cell Rearrangements during Valve Morphogenesis. Dev. Cell 26, 31–44. https://doi.org/10.1016/j.devcel.2013.05.015

Taura, D., Sone, M., Homma, K., Oyamada, N., Takahashi, K., Tamura, N., Yamanaka, S., Nakao, K., 2009. Induction and Isolation of Vascular Cells From Human Induced Pluripotent Stem Cells—Brief Report. Arterioscler. Thromb. Vasc. Biol. 29, 1100–1103. https://doi.org/10.1161/ATVBAHA.108.182162

Tefft, J.B., Bays, J.L., Lammers, A., Kim, S., Eyckmans, J., Chen, C.S., 2022. Notch1 and Notch3 coordinate for pericyte-induced stabilization of vasculature. Am. J. Physiol.-Cell Physiol. 322, C185–C196. https://doi.org/10.1152/ajpcell.00320.2021

Teichert, M., Milde, L., Holm, A., Stanicek, L., Gengenbacher, N., Savant, S., Ruckdeschel, T., Hasanov, Z., Srivastava, K., Hu, J., Hertel, S., Bartol, A., Schlereth, K., Augustin, H.G., 2017. Pericyte-expressed Tie2 controls angiogenesis and vessel maturation. Nat. Commun. 8, 16106. https://doi.org/10.1038/ncomms16106

Tellides, G., Pober, J.S., 2015. Inflammatory and Immune Responses in the Arterial Media. Circ. Res. 116, 312–322. https://doi.org/10.1161/CIRCRESAHA.116.301312

Teodoro, J.G., Parker, A.E., Zhu, X., Green, M.R., 2006. p53-Mediated Inhibition of Angiogenesis Through Up-Regulation of a Collagen Prolyl Hydroxylase. Science 313, 968–971. https://doi.org/10.1126/science.1126391

Terman, B.I., Dougher-Vermazen, M., Carrion, M.E., Dimitrov, D., Armellino, D.C., Gospodarowicz, D., Böhlen, P., 1992. Identification of the KDR tyrosine kinase as a receptor for vascular endothelial cell growth factor. Biochem. Biophys. Res. Commun. 187, 1579–1586. https://doi.org/10.1016/0006-291X(92)90483-2

Tiemeier, G.L., Wang, G., Dumas, S.J., Sol, W.M.P.J., Avramut, M.C., Karakach, T., Orlova, V.V., van den Berg, C.W., Mummery, C.L., Carmeliet, P., van den Berg, B.M., Rabelink, T.J., 2019. Closing the Mitochondrial Permeability Transition Pore in hiPSC-Derived Endothelial Cells Induces Glycocalyx Formation and Functional Maturation. Stem Cell Rep. 13, 803–816. https://doi.org/10.1016/j.stemcr.2019.10.005

Tousoulis, D., Kampoli, A.-M., Tentolouris Nikolaos Papageorgiou, C., Stefanadis, C., 2012. The Role of Nitric Oxide on Endothelial Function. Curr. Vasc. Pharmacol. 10, 4–18. https://doi.org/10.2174/157016112798829760

Travaglini, K.J., Nabhan, A.N., Penland, L., Sinha, R., Gillich, A., Sit, R.V., Chang, S., Conley, S.D., Mori, Y., Seita, J., Berry, G.J., Shrager, J.B., Metzger, R.J., Kuo, C.S., Neff, N., Weissman, I.L., Quake, S.R., Krasnow, M.A., 2020. A molecular cell atlas of the human lung from single-cell RNA sequencing. Nature 587, 619–625. https://doi.org/10.1038/s41586-020-2922-4

Tsang, K.M., Hyun, J.S., Cheng, K.T., Vargas, M., Mehta, D., Ushio-Fukai, M., Zou, L., Pajcini, K.V., Rehman, J., Malik, A.B., 2017. Embryonic Stem Cell Differentiation to Functional Arterial Endothelial Cells through Sequential Activation of ETV2 and NOTCH1 Signaling by HIF1α. Stem Cell Rep. 9, 796–806. https://doi.org/10.1016/j.stemcr.2017.07.001

van Dijk, C.G.M., Brandt, M.M., Poulis, N., Anten, J., van der Moolen, M., Kramer, L., Homburg, E.F.G.A., Louzao-Martinez, L., Pei, J., Krebber, M.M., van Balkom, B.W.M., de Graaf, P.,

Duncker, D.J., Verhaar, M.C., Luttge, R., Cheng, C., 2020. A new microfluidic model that allows monitoring of complex vascular structures and cell interactions in a 3D biological matrix. Lab. Chip 20, 1827–1844. https://doi.org/10.1039/d0lc00059k

Vanlandewijck, M., He, L., Mäe, M.A., Andrae, J., Ando, K., Del Gaudio, F., Nahar, K., Lebouvier, T., Laviña, B., Gouveia, L., Sun, Y., Raschperger, E., Räsänen, M., Zarb, Y., Mochizuki, N., Keller, A., Lendahl, U., Betsholtz, C., 2018. A molecular atlas of cell types and zonation in the brain vasculature. Nature 554, 475–480. https://doi.org/10.1038/nature25739

Vatine, G.D., Barrile, R., Workman, M.J., Sances, S., Barriga, B.K., Rahnama, M., Barthakur, S., Kasendra, M., Lucchesi, C., Kerns, J., Wen, N., Spivia, W.R., Chen, Z., Van Eyk, J., Svendsen, C.N., 2019. Human iPSC-Derived Blood-Brain Barrier Chips Enable Disease Modeling and Personalized Medicine Applications. Cell Stem Cell 24, 995-1005.e6. https://doi.org/10.1016/j.stem.2019.05.011

Vigilante, A., Laddach, A., Moens, N., Meleckyte, R., Leha, A., Ghahramani, A., Culley, O.J., Kathuria, A., Hurling, C., Vickers, A., Wiseman, E., Tewary, M., Zandstra, P.W., HipSci Consortium, Durbin, R., Fraternali, F., Stegle, O., Birney, E., Luscombe, N.M., Danovi, D., Watt, F.M., 2019. Identifying Extrinsic versus Intrinsic Drivers of Variation in Cell Behavior in Human iPSC Lines from Healthy Donors. Cell Rep. 26, 2078-2087.e3. https://doi.org/10.1016/j.celrep.2019.01.094

Vodyanik, M.A., Bork, J.A., Thomson, J.A., Slukvin, I.I., 2005. Human embryonic stem cell–derived CD34+ cells: efficient production in the coculture with OP9 stromal cells and analysis of lymphohematopoietic potential. Blood 105, 617–626. https://doi.org/10.1182/blood-2004-04-1649

Vokes, S.A., Yatskievych, T.A., Heimark, R.L., McMahon, J., McMahon, A.P., Antin, P.B., Krieg, P.A., 2004. Hedgehog signaling is essential for endothelial tube formation during vasculogenesis. Development 131, 4371–4380. https://doi.org/10.1242/dev.01304

Wakabayashi, T., Naito, H., Suehiro, J., Lin, Y., Kawaji, H., Iba, T., Kouno, T., Ishikawa-Kato, S., Furuno, M., Takara, K., Muramatsu, F., Weizhen, J., Kidoya, H., Ishihara, K., Hayashizaki, Y., Nishida, K., Yoder, M.C., Takakura, N., 2018. CD157 Marks Tissue-Resident Endothelial Stem Cells with Homeostatic and Regenerative Properties. Cell Stem Cell 22, 384-397.e6. https://doi.org/10.1016/j.stem.2018.01.010

Waller, B.F., Orr, C.M., Slack, J.D., Pinkerton, C.A., Van Tassel, J., Peters, T., 1992. Anatomy, histology, and pathology of coronary arteries: A review relevant to new interventional and imaging techniques-Part I. Clin. Cardiol. 15, 451–457. https://doi.org/10.1002/clc.4960150613

Walpola, P.L., Gotlieb, A.I., Cybulsky, M.I., Langille, B.L., 1995. Expression of ICAM-1 and VCAM-1 and Monocyte Adherence in Arteries Exposed to Altered Shear Stress. Arterioscler. Thromb. Vasc. Biol. 15, 2–10. https://doi.org/10.1161/01.ATV.15.1.2

Wang, B., Zhao, L., Fish, M., Logan, C.Y., Nusse, R., 2015. Self-renewing diploid Axin2(+) cells fuel homeostatic renewal of the liver. Nature 524, 180–185. https://doi.org/10.1038/nature14863

Wang, G., Jacquet, L., Karamariti, E., Xu, Q., 2015. Origin and differentiation of vascular smooth muscle cells: Smooth muscle cell origin and differentiation. J. Physiol. 593, 3013–3030. https://doi.org/10.1113/JP270033

Wang, H.U., Chen, Z.-F., Anderson, D.J., 1998. Molecular Distinction and Angiogenic Interaction between Embryonic Arteries and Veins Revealed by ephrin-B2 and Its Receptor Eph-B4. Cell 93, 741–753. https://doi.org/10.1016/S0092-8674(00)81436-1

Wang, R., Chadalavada, K., Wilshire, J., Kowalik, U., Hovinga, K.E., Geber, A., Fligelman, B., Leversha, M., Brennan, C., Tabar, V., 2010. Glioblastoma stem-like cells give rise to tumour endothelium. Nature 468, 829–833. https://doi.org/10.1038/nature09624

Wang, X., Phan, D.T.T., Sobrino, A., George, S.C., Hughes, C.C.W., Lee, A.P., 2016. Engineering anastomosis between living capillary networks and endothelial cell-lined microfluidic channels. Lab. Chip 16, 282–290. https://doi.org/10.1039/C5LC01050K

Wang, Z., Yan, X., 2013. CD146, a multi-functional molecule beyond adhesion. Cancer Lett. 330, 150–162. https://doi.org/10.1016/j.canlet.2012.11.049

Wanjare, M., Kuo, F., Gerecht, S., 2013. Derivation and maturation of synthetic and contractile vascular smooth muscle cells from human pluripotent stem cells. Cardiovasc. Res. 97, 321–330. https://doi.org/10.1093/cvr/cvs315

Wanjare, M., Kusuma, S., Gerecht, S., 2014. Defining Differences among Perivascular Cells Derived from Human Pluripotent Stem Cells. Stem Cell Rep. 2, 561–575. https://doi.org/10.1016/j.stemcr.2014.03.004

Wasteson, P., Johansson, B.R., Jukkola, T., Breuer, S., Akyürek, L.M., Partanen, J., Lindahl, P., 2008. Developmental origin of smooth muscle cells in the descending aorta in mice. Development 135, 1823–1832. https://doi.org/10.1242/dev.020958

Wei, H., Sundararaman, A., Truelsen, S.L.B., Gurevich, D., Thastrup, J., Mellor, H., 2021. In Vitro Coculture Assays of Angiogenesis. Methods Mol. Biol. Clifton NJ 2206, 39–46. https://doi.org/10.1007/978-1-0716-0916-3_4

Wettschureck, N., Strilic, B., Offermanns, S., 2019. Passing the Vascular Barrier: Endothelial Signaling Processes Controlling Extravasation. Physiol. Rev. 99, 1467–1525. https://doi.org/10.1152/physrev.00037.2018

Whisler, J.A., Chen, M.B., Kamm, R.D., 2014. Control of Perfusable Microvascular Network Morphology Using a Multiculture Microfluidic System. Tissue Eng. Part C Methods 20, 543–552. https://doi.org/10.1089/ten.tec.2013.0370

White, A.C., Lavine, K.J., Ornitz, D.M., 2007. FGF9 and SHH regulate mesenchymal *Vegfa* expression and development of the pulmonary capillary network. Development 134, 3743–3752. https://doi.org/10.1242/dev.004879

Whitesides, G.M., Ostuni, E., Takayama, S., Jiang, X., Ingber, D.E., 2001. Soft Lithography in Biology and Biochemistry. Annu. Rev. Biomed. Eng. 3, 335–373. https://doi.org/10.1146/annurev.bioeng.3.1.335

Wiese, C., Heisig, J., Gessler, M., 2010. Hey bHLH Factors in Cardiovascular Development. Pediatr. Cardiol. 31, 363–370. https://doi.org/10.1007/s00246-009-9609-9

Wigle, J.T., 2002. An essential role for Prox1 in the induction of the lymphatic endothelial cell phenotype. EMBO J. 21, 1505–1513. https://doi.org/10.1093/emboj/21.7.1505

Wigle, J.T., Oliver, G., 1999. Prox1 Function Is Required for the Development of the Murine Lymphatic System. Cell 98, 769–778. https://doi.org/10.1016/S0092-8674(00)81511-1

Wijelath, E.S., Rahman, S., Murray, J., Patel, Y., Savidge, G., Sobel, M., 2004. Fibronectin promotes VEGF-induced CD34+ cell differentiation into endothelial cells. J. Vasc. Surg. 39, 655–660. https://doi.org/10.1016/j.jvs.2003.10.042

Wilm, B., Ipenberg, A., Hastie, N.D., Burch, J.B.E., Bader, D.M., 2005. The serosal mesothelium is a major source of smooth muscle cells of the gut vasculature. Development 132, 5317–5328. https://doi.org/10.1242/dev.02141

Wimmer, R.A., Leopoldi, A., Aichinger, M., Wick, N., Hantusch, B., Novatchkova, M., Taubenschmid, J., Hämmerle, M., Esk, C., Bagley, J.A., Lindenhofer, D., Chen, G., Boehm, M., Agu, C.A., Yang, F., Fu, B., Zuber, J., Knoblich, J.A., Kerjaschki, D., Penninger, J.M., 2019. Human blood vessel organoids as a model of diabetic vasculopathy. Nature 565, 505–510. https://doi.org/10.1038/s41586-018-0858-8

Winneberger, J., Schöls, S., Lessmann, K., Rández-Garbayo, J., Bauer, A.T., Mohamud Yusuf, A., Hermann, D.M., Gunzer, M., Schneider, S.W., Fiehler, J., Gerloff, C., Gelderblom, M., Ludewig, P., Magnus, T., 2021. Platelet endothelial cell adhesion molecule-1 is a gatekeeper of neutrophil transendothelial migration in ischemic stroke. Brain. Behav. Immun. 93, 277–287. https://doi.org/10.1016/j.bbi.2020.12.026

Wiseman, E., Zamuner, A., Tang, Z., Rogers, J., Munir, S., Di Silvio, L., Danovi, D., Veschini, L., 2019. Integrated Multiparametric High-Content Profiling of Endothelial Cells. SLAS Discov. Adv. Life Sci. R D 24, 264–273. https://doi.org/10.1177/2472555218820848

Wu, L., Vasilijic, S., Sun, Y., Chen, J., Landegger, L.D., Zhang, Y., Zhou, W., Ren, J., Early, S., Yin, Z., Ho, W.W., Zhang, N., Gao, X., Lee, G.Y., Datta, M., Sagers, J.E., Brown, A., Muzikansky, A., Stemmer-Rachamimov, A., Zhang, L., Plotkin, S.R., Jain, R.K., Stankovic, K.M., Xu, L., 2021. Losartan prevents tumor-induced hearing loss and augments radiation efficacy in NF2 schwannoma rodent models. Sci. Transl. Med. 13, eabd4816. https://doi.org/10.1126/scitranslmed.abd4816

Xia, Y., Whitesides, G.M., 1998. Soft Lithography. Angew. Chem. Int. Ed. 37, 550–575. https://doi.org/10.1002/(SICI)1521-3773(19980316)37:5<550::AID-ANIE550>3.0.CO;2-G

Xie, W.-B., Li, Z., Shi, N., Guo, X., Tang, J., Ju, W., Han, J., Liu, T., Bottinger, E.P., Chai, Y., Jose, P.A., Chen, S.-Y., 2013. Smad2 and Myocardin-Related Transcription Factor B Cooperatively Regulate Vascular Smooth Muscle Differentiation From Neural Crest Cells. Circ. Res. 113. https://doi.org/10.1161/CIRCRESAHA.113.301921

Xu, J., Nie, X., Cai, X., Cai, C.-L., Xu, P.-X., 2014. Tbx18 is essential for normal development of vasculature network and glomerular mesangium in the mammalian kidney. Dev. Biol. 391, 17–31. https://doi.org/10.1016/j.ydbio.2014.04.006

Xue-yi, Z., Jian-zhong, Z., Ping, T., Sheng-qing, M., 1998. Expression of platelet-derived growth factor B-chain and platelet-derived growth factor β-receptor in fibroblasts of scleroderma. J. Dermatol. Sci. 18, 90–97. https://doi.org/10.1016/S0923-1811(98)00027-9

Yamashita, J., Itoh, H., Hirashima, M., Ogawa, M., Nishikawa, S., Yurugi, T., Naito, M., Nakao, K., Nishikawa, S.-I., 2000. Flk1-positive cells derived from embryonic stem cells serve as vascular progenitors. Nature 408, 92–96. https://doi.org/10.1038/35040568

Yamashita, J.K., 2007. Differentiation of Arterial, Venous, and Lymphatic Endothelial Cells From Vascular Progenitors. Trends Cardiovasc. Med. 17, 59–63. https://doi.org/10.1016/j.tcm.2007.01.001

Yamazaki, T., Mukouyama, Y., 2018. Tissue Specific Origin, Development, and Pathological Perspectives of Pericytes. Front. Cardiovasc. Med. 5, 78. https://doi.org/10.3389/fcvm.2018.00078

Yamazaki, T., Nalbandian, A., Uchida, Y., Li, W., Arnold, T.D., Kubota, Y., Yamamoto, S., Ema, M., Mukouyama, Y., 2017. Tissue Myeloid Progenitors Differentiate into Pericytes through TGF-β Signaling in Developing Skin Vasculature. Cell Rep. 18, 2991–3004. https://doi.org/10.1016/j.celrep.2017.02.069

Yang, A.C., Vest, R.T., Kern, F., Lee, D.P., Agam, M., Maat, C.A., Losada, P.M., Chen, M.B., Schaum, N., Khoury, N., Toland, A., Calcuttawala, K., Shin, H., Pálovics, R., Shin, A., Wang, E.Y., Luo, J., Gate, D., Schulz-Schaeffer, W.J., Chu, P., Siegenthaler, J.A., McNerney, M.W., Keller, A., Wyss-Coray, T., 2022. A human brain vascular atlas reveals diverse mediators of Alzheimer's risk. Nature. https://doi.org/10.1038/s41586-021-04369-3

Yang, Y., Oliver, G., 2014. Development of the mammalian lymphatic vasculature. J. Clin. Invest. 124, 888–897. https://doi.org/10.1172/JCI71609

Yoshida, T., Kaestner, K.H., Owens, G.K., 2008. Conditional Deletion of Krüppel-Like Factor 4 Delays Downregulation of Smooth Muscle Cell Differentiation Markers but Accelerates Neointimal Formation Following Vascular Injury. Circ. Res. 102, 1548–1557. https://doi.org/10.1161/CIRCRESAHA.108.176974

Yoshioka-Kobayashi, K., Matsumiya, M., Niino, Y., Isomura, A., Kori, H., Miyawaki, A., Kageyama, R., 2020. Coupling delay controls synchronized oscillation in the segmentation clock. Nature 580, 119–123. https://doi.org/10.1038/s41586-019-1882-z

You, L.-R., Lin, F.-J., Lee, C.T., DeMayo, F.J., Tsai, M.-J., Tsai, S.Y., 2005. Suppression of Notch signalling by the COUP-TFII transcription factor regulates vein identity. Nature 435, 98–104. https://doi.org/10.1038/nature03511

Zarins, C.K., Giddens, D.P., Bharadvaj, B.K., Sottiurai, V.S., Mabon, R.F., Glagov, S., 1983. Carotid bifurcation atherosclerosis. Quantitative correlation of plaque localization with flow velocity profiles and wall shear stress. Circ. Res. 53, 502–514. https://doi.org/10.1161/01.RES.53.4.502

Zhang, J., Chu, L.-F., Hou, Z., Schwartz, M.P., Hacker, T., Vickerman, V., Swanson, S., Leng, N., Nguyen, B.K., Elwell, A., Bolin, J., Brown, M.E., Stewart, R., Burlingham, W.J., Murphy, W.L., Thomson, J.A., 2017. Functional characterization of human pluripotent stem cell-derived arterial endothelial cells. Proc. Natl. Acad. Sci. U. S. A. 114, E6072–E6078. https://doi.org/10.1073/pnas.1702295114

Zheng, Y., Chen, J., Craven, M., Choi, N.W., Totorica, S., Diaz-Santana, A., Kermani, P., Hempstead, B., Fischbach-Teschl, C., López, J.A., Stroock, A.D., 2012. In vitro microvessels for the study of angiogenesis and thrombosis. Proc. Natl. Acad. Sci. 109, 9342–9347. https://doi.org/10.1073/pnas.1201240109

Zhong, T.P., Childs, S., Leu, J.P., Fishman, M.C., 2001. Gridlock signalling pathway fashions the first embryonic artery. Nature 414, 216–220. https://doi.org/10.1038/35102599

Zhou, Y., Nathans, J., 2014. Gpr124 Controls CNS Angiogenesis and Blood-Brain Barrier Integrity by Promoting Ligand-Specific Canonical Wnt Signaling. Dev. Cell 31, 248–256. https://doi.org/10.1016/j.devcel.2014.08.018

Supplementary information

| Antibody	Company	Catalog Number	Concentration
Anti-human VE-cadherin	Novusbio	NB600-1409	1μg/mL
NOTCH1	Abcam	ab194122	1μg/mL
Anti-human Hes1	Abcam	ab119776	1μg/mL
Anti-mouse VE-Cadherin	Thermo	#14-1441-82	5μg/mL
Anti-mouse Hes1	Thermo	#PA5-28802	5μg/mL
Rabbit Anti-Ephrin B2	Abcam	ab150411	1μg/mL
Rabbit Anti VE-Cadherin	Abcam	ab33168	1μg/mL
Rabbit Anti activated-Notch1	Abcam	ab8925	1μg/mL
Alexa Fluor 647 Anti-ERG	Abcam	ab196149	1μg/mL
CD31	Abcam	ab9498	1μg/mL
CD44	BD Biosciences	#550989	1μg/mL
NG2	Abcam	ab83178	1μg/mL
PDX1	Abcam	ab47308	1μg/mL
Somatostatin	Dako	#A0566	1μg/mL
Insulin	Dako	#A0564	1μg/mL
Goat Anti-rabbit Alexa Fluor 488	Thermo	A-11034	0.5 μg/mL
Goat Anti-rabbit Alexa Fluor 647	Thermo	A-21246	0.5 μg/mL
Goat Anti-mouse Alexa Fluor 555	Thermo	A-21127	0.5 μg/mL

Supplementary table 1: Antibodies used in the study.

| Primer	Forward sequence	Reverse sequence
RPL19	CAGAAGATACCGTGAATCTAAG	TGTTTTTGAACACATTCCCC
CDH5	CGCAATAGACAAGGACATAAC	TATCGTGATTATCCGTGAGG
LYVE1	AGGCTCTTTGCGTGCAGAA	GGTTCGCCTTTTTGCTCACAA
PROX1	AAAGGACGGTAGGGACAGCAT	CCTTGGGGATTCATGGCACTAA
DLL4	GTCTCCACGCCGGTATTGG	CAGGTGAAATTGAAGGGCAGT
KDR	GTACATAGTTGTCGTTGTAGG	TCAATCCCCACATTTAGTTC
HEY2	GGATTATAGAGAAAAGGCGTC	GTTTTTCAAAAGCAGTTGGC
NOTCH1	GAGGCGTGGCAGACTATGC	CTTGTACTCCGTCAGCGTGA
JAG1	GTCCATGCAGAACGTGAACG	GCGGGACTGATACTCCTTGA
HES1	TCAACACGACACCGGATAAAC	GCCGCGAGCTATCTTTCTTCA
COUP-TFII	GCTAGTGCCTACTTTTTATCAG	GCAAAACCATATTTGCCTTG
EFNB2	TATGCAGAACTGCGATTTCCAA	TGGGTATAGTACCAGTCCTTGTC
EPHB4	CGCACCTACGAAGTGTGTGA	GTCCGCATCGCTCTCATAGTA
NANOG	CCAGAACCAGAGAATGAAATC	TGGTGGTAGGAAGAGTAAAG
PDGFR-β	GGGAAGAGAAGTTTGAGATTC	TTCTTTTTGTAACCTTCGCC
PDGFR-α	TCAGTTCCTTCATCCATCC	CATCCACTCAATATCAGGAAG
NG2	CTTTGACCCTGACTATGTTGGC	TGCAGGCGTCCAGAGTAGA
NT5E	GCCTGGGAGCTTACGATTTTG	TAGTGCCCTGGTACTGGTCG
VIMENTIN	GACGCCATCAACACCGAGTT	CTTTGTCGTTGGTTAGCTGGT
FIBRONECTIN	CGGTGGCTGTCAGTCAAAG	AAACCTCGGCTTCCTCCATAA
COL1A1	GAGGGCCAAGACGAAGACATC	CAGATCACGTCATCGCACAAC
COL1A2	GTTGCTGCTTGCAGTAACCTT	AGGGCCAAGTCCAACTCCTT
COL3A1	GGAGCTGGCTACTTCTCGC	GGGAACATCCTCCTTCAACAG

Supplementary Table 2: Primer sequences used in qRT-PCR.
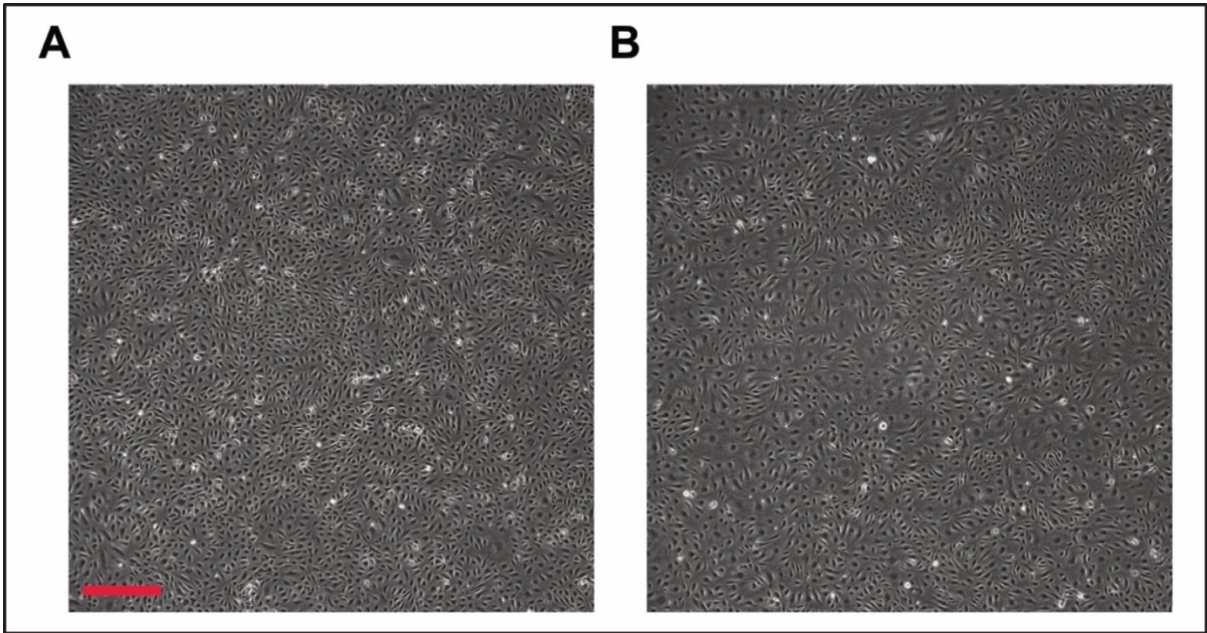
Supplementary Figure 2.1: HCAEC (A) and HDMEC (B) morphology in confluent monolayers. Scale bar: 250μm
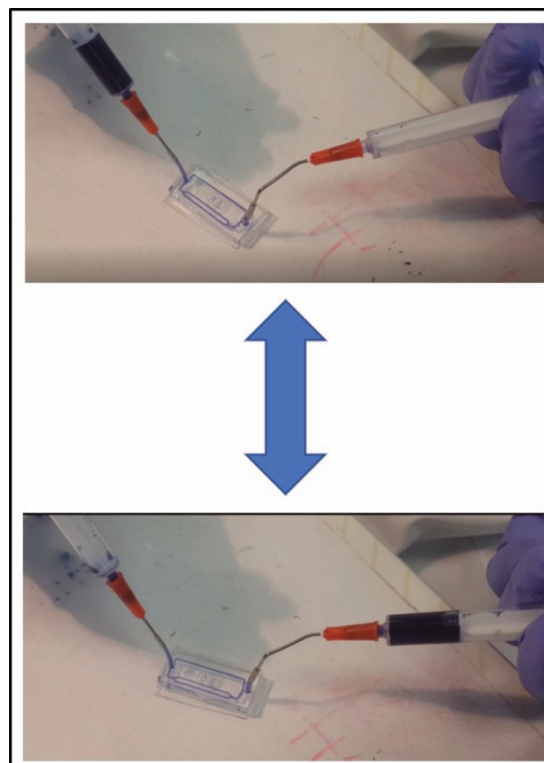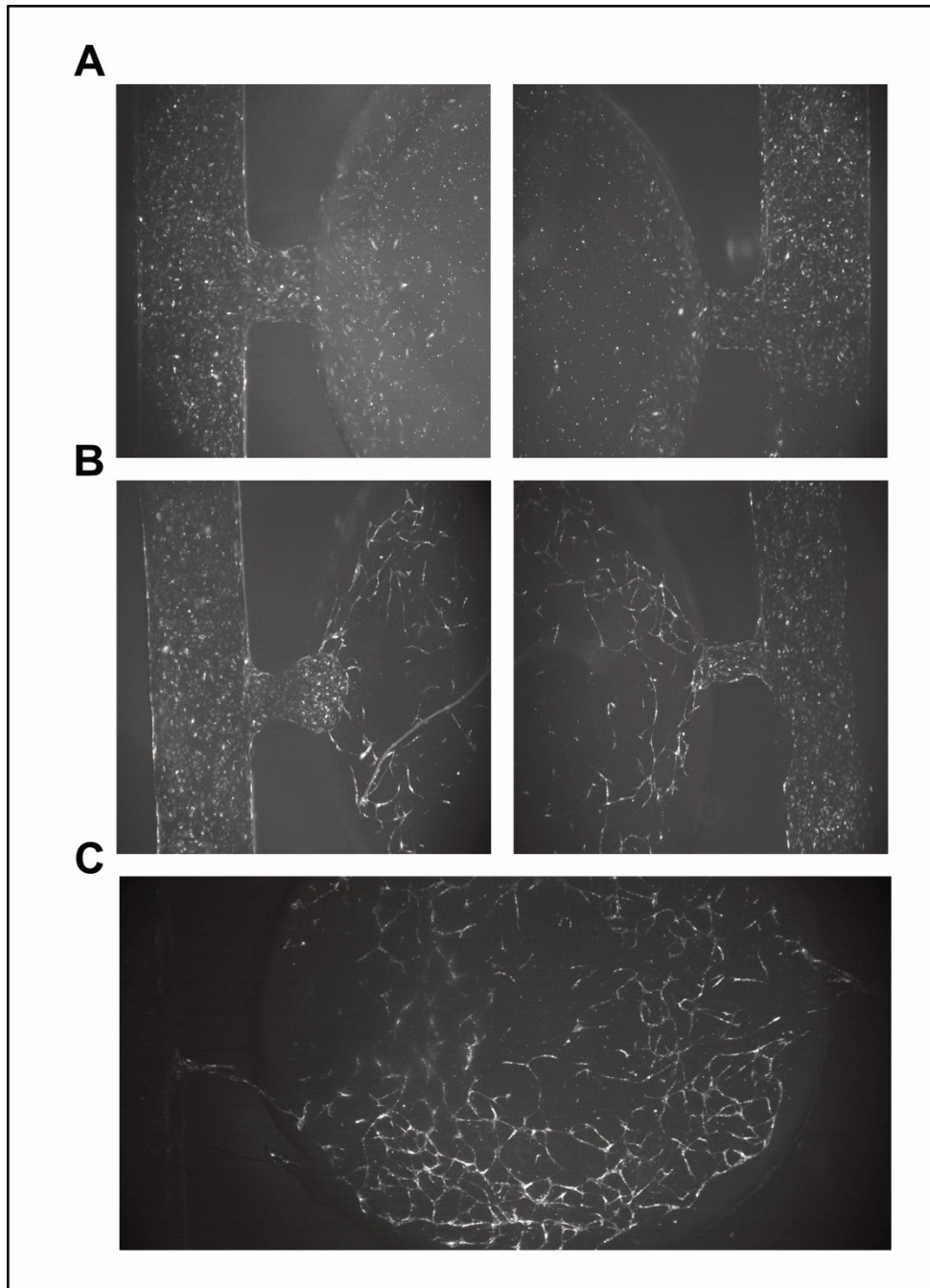

Supplementary figure 4.1: Tube embedding allows secure perfusion of the LOC device.
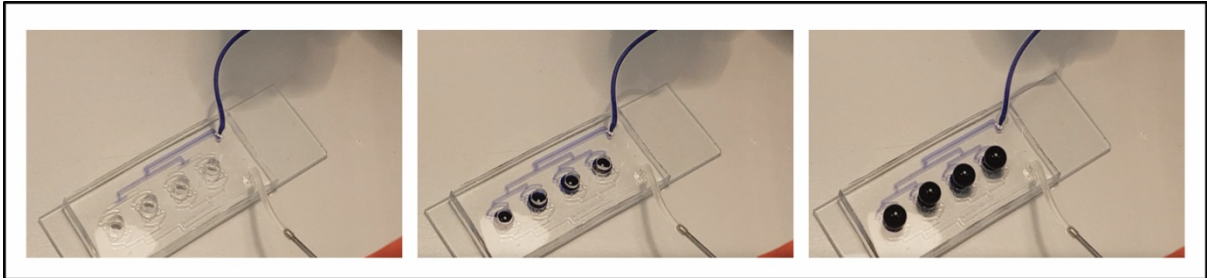
Supplementary figure 4.2: Unilateral perfusion of the LOC device causes overflow in the central wells.
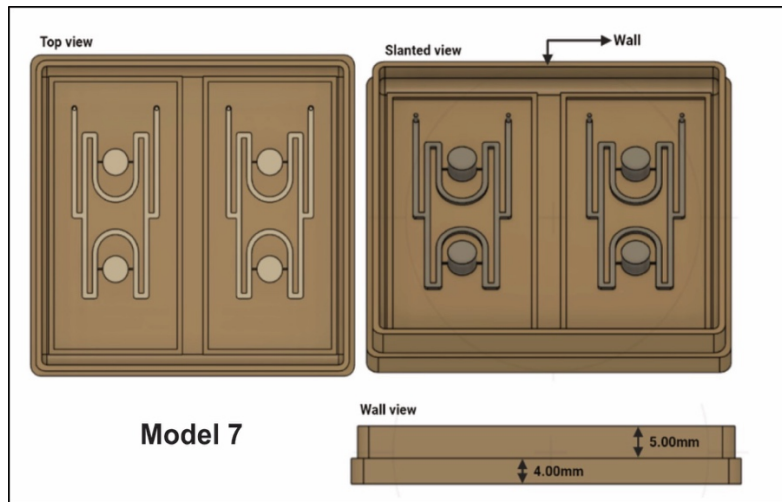
Supplementary figure 4.3: Computer assisted design of the mould with added walls and the model 7 of the LOC device.

Supplementary figure 4.4: Vasculature-on-chip with the model 6. A) HUVEC-RFP cultured for 3 days coat the side channels. B) After 3 days, HUVEC-RFP invaded the central well filled with a fibrin hydrogel. C) After 7 days of culture, few self-assembled blood vessels can be observed in the central well but did not get perfused.
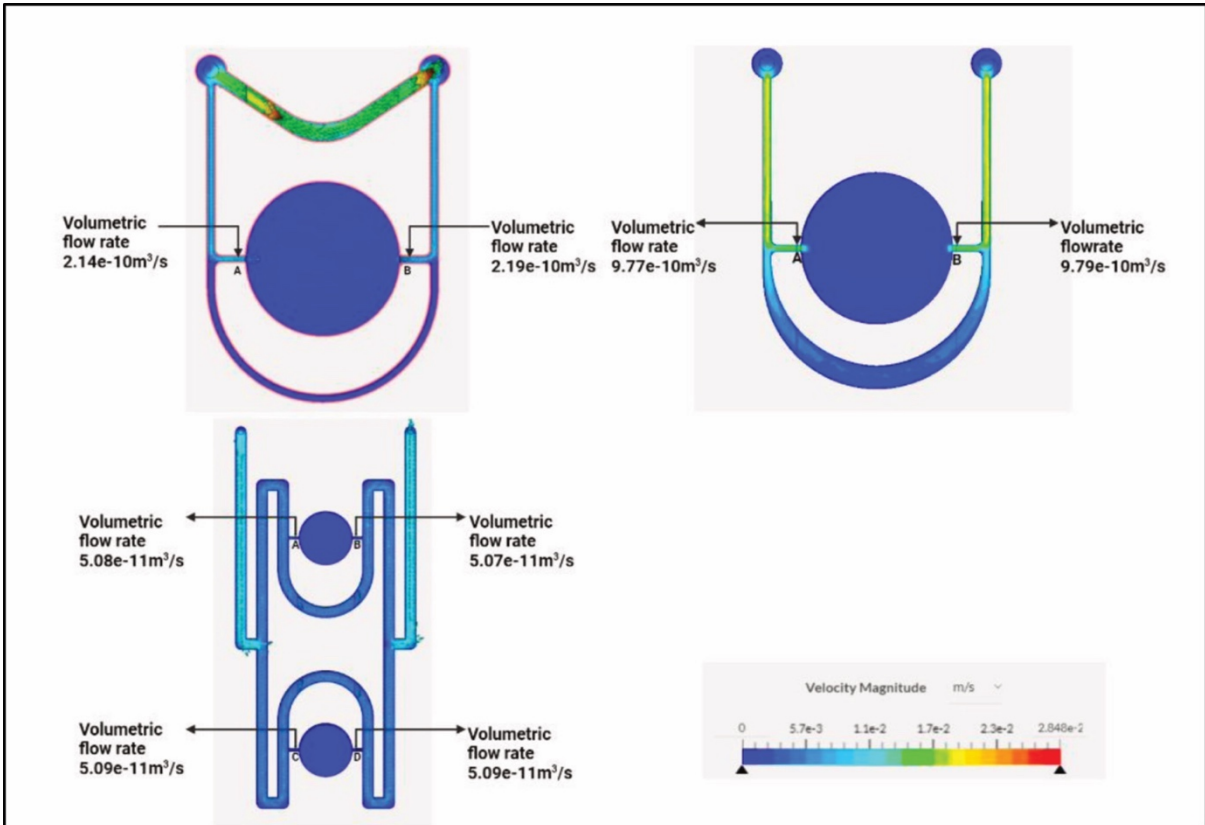
Supplementary figure 4.5: Computational fluid dynamics on the LOC devices. Flow dynamics was simulated on several of our designs (here models 3, 4 and 6) to predict the velocity of the flow in our system at different flow rate.
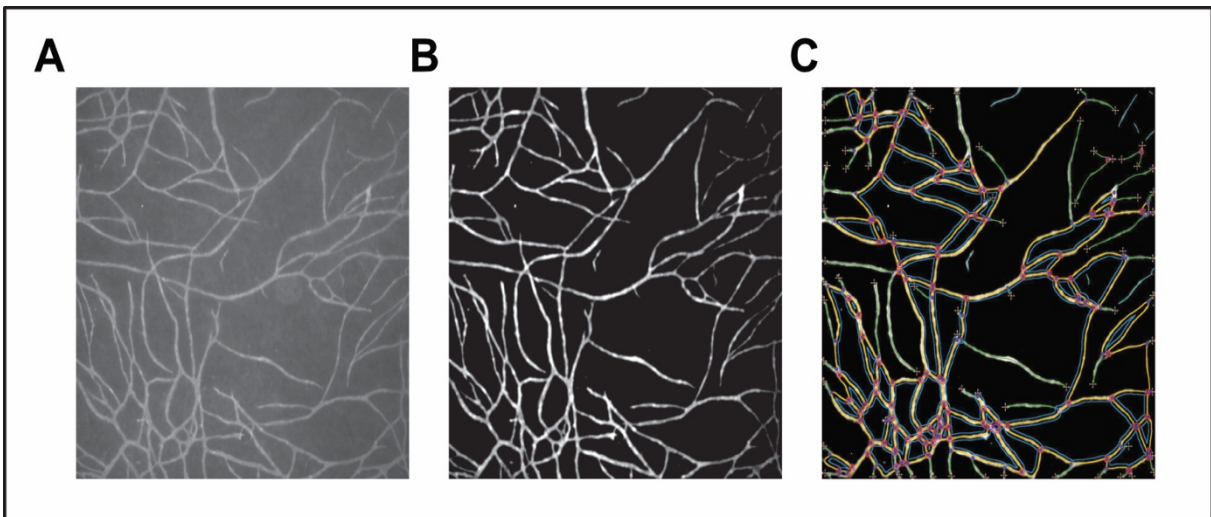
Supplementary figure 4.6: Analysis of blood vessel networks by the Angioanalyser plugin (Carpentier et al., 2020). A) Original image of a CD31-stained co-culture of EC and fibroblasts after 14 days of culture. B) Segmented image to facilitate the use of the plugin. C) Analysed network with Angioanalyser. Big blood vessel segments are highlighted in yellow, branches in green and junctions with a pink circle.

Supplementary video 4.1: 3D projection of the vascular network formed by HUVEC-RFP in the central well of the VOC after 7 days of culture, before perfusion.

Supplementary video 4.2: Video of the VOC system at one of the aA junctions after 4 days of perfusion at 200uL/min.